SUPPRESSION OF CA^{2+} SIGNALING ENHANCES MELANOMA PROGRESSION

A Dissertation Submitted to the Temple University Graduate Board

---

In Partial Fulfillment of the requirements for the Degree of DOCTOR OF PHILOSOPHY

By: Scott Gross
August 2022

Examining Committee Members:

Jonathan Soboloff, Advisory Chair, Fels Cancer Institute for Personalized Medicine
M. Raza Zaidi, Fels Cancer Institute for Personalized Medicine
Scott Shore, Fels Cancer Institute for Personalized Medicine
Brad Rothberg, Department of Medical Genetics and Molecular Biochemistry
J. Kevin Foskett, External Member University of Pennsylvania, Department of Physiology

ABSTRACT

Ca^{2+} is a ubiquitous and dynamic second messenger molecule that is induced by many factors including receptor activation, environmental factors, and voltage, leading to pleiotropic effects on cell function including changes in migration, metabolism and transcription. As such, it is not surprising that aberrant regulation of Ca^{2+} signals can lead to pathological phenotypes, including cancer progression. However, given the highly context-specific nature of Ca^{2+}-dependent changes in cell function, delineation of its role in cancer has been a challenge. Hence, the role of store-operated Ca^{2+} entry (SOCE) in melanoma metastasis is still not fully elucidated. To address this, we examined UV-dependent metastasis, revealing a critical role for SOCE suppression. As previous literature demonstrated a role for cholesterol (CHL) in melanoma progression, our investigations corroborate this revealing UV-induced CHL biosynthesis as a critical mediator for UV-induced SOCE suppression and subsequent metastasis. However, SOCE suppression alone was both necessary and sufficient for metastasis to occur. Further, SOCE suppression facilitated UV-dependent differences in gene expression associated with increased invasion through altered glucose utilization. Functional analyses further establish that increased glucose uptake leads to a metabolic shift towards biosynthetic pathways critical for melanoma metastasis. Finally, examination of fresh surgically isolated human melanoma explants revealed CHL dependent low SOCE. Invasiveness could be reversed with either CHL biosynthesis inhibitors, pharmacological inhibition of terminal glycosylation enzyme, OGT, or pharmacological SOCE potentiation. In parallel, we demonstrate that Geranylgeranylpyrophosphate (GGPP) can function as a novel SOCE inhibitor either by saturation or prevention of transfer to membrane proteins; both of which lead to GGPP accumulation in the cytosol. Collectively, we provide evidence

that Ca^{2+} signals can block invasive behavior, and suppression of these signals promotes invasion and metastasis.

ACKNOWLEDGMENTS

First and foremost, I would like to extend my unwavering gratitude and appreciation to Dr. Jonathan Soboloff for taking a chance on me and helping me develop as a student, scientist and person. These past 5 years have been a blessing and I am very grateful to have had the opportunity to work in this lab and complete my training as an independent scientist. Dr. Soboloff has been an unlimited source of guidance, critique and support that has allowed me to achieve my research goals and graduate school accomplishments. To this, I can't thank you enough and I am forever grateful.

In addition to my advisor, I would like to thank my advisory committee members Dr. M. Raza Zaidi, Dr. Brad Rothberg, and Dr. Scott Shore for their guidance and suggestions throughout my graduate work. Dr. Zaidi has been seemingly involved in my project on a daily basis providing invaluable support throughout my time in the lab. Dr. Rothberg has provided me with much appreciated guidance at Ion Channel Journal Clubs and committee meetings. Dr. Shore has provided me with much appreciated guidance as not only an initial interviewer when I applied to the program, but also for my IRP Candidacy Exam as well as committee meetings. I am very grateful to all of you for your continued support. I would also like to thank Dr. Dianne Soprano who has also been a very important mentor for me every step of the way. I would also like to thank my external thesis examiner, Dr. J. Kevin Foskett for taking the time to critique my thesis. I wish all of these individuals continued success with their research and other endeavors.

Following, I would like to thank all present and past members of the Soboloff lab. I am forever grateful to Dr. Robert Hooper for helping commence my thesis project and training me in a variety of lab techniques and concepts that have allowed me to

successfully generate data for my thesis project. I would also like to thank Dr. Christina Go and Mr. Bryant Schultz for their continued patience in teaching me lab concepts and techniques that have served as indispensable for my thesis work. I would also like to thank Mr. Alexander Armstead, Ms. Pranava Mallu, Mr. No'ad Shanas, Ms. Suravi Ray, Ms. Hinal Joshi, Mr. Gabriel Wingert, Mr. Jared McFerran, Ms. Rachel Blackman, Ms. Anuya Prubhdesai, Ms. Lauren Womer, and Ms. Kimberly Ferrero for all of their technical support throughout my time in the lab. I owe a great deal to all of these individuals for their guidance, support, and friendship. Further, I would like to thank all other collaborators on my thesis work including Dr. Dhanendra Tomar, Dr. Parkson Chong, Dr. Igor Astsaturov, Dr. Kathy Cai, and Dr. John Elrod of whom this work would not be possible without their instrumental guidance and expertise.

Also, I would like to thank my Masters of Science thesis advisor Dr. Dmitriy Markov at Rowan University School of Medicine for helping me find my passion for scientific research. Without you, I may have never considered becoming a research scientist.

Finally, I would like to thank my family for their encouragement and support. To my parents, Debbie and Daniel, who supported me throughout my educational journey and always encouraged me to be in the sciences. To my sister, Nicole, who always was always so supportive of me. Finally, to my beautiful wife, Morgan who has supported me through the ups and downs and always gave me the confidence and love needed to complete this thesis. I am forever grateful to all of you in completing this journey.

PREFACE:

Ca^{2+} is a ubiquitous and dynamic second messenger molecule that regulates a variety of cellular functions including proliferation, cell cycle control, focal adhesion and others (1). As such, it is perhaps not surprising that the contribution of Ca^{2+} signals to the genesis and progression of cancer has long been under investigation. Hence, dysregulation of Ca^{2+} signaling is now well established to modulate oncogenic signaling pathways and promote invasive behavior (1). The oldest record of the use of Ca^{2+} in cancer treatment is from 1896, when Calcium Carbide (CaC_2) was used as a clinical palliative treatment for uterine cancer (2), while the role of Calcium Chloride ($CaCl_2$) in cancer growth was proposed in 1918 (3). As of today, there are over 42,000 publications featuring both Ca^{2+} and cancer listed in pubmed, a number that has increased 4-fold over the last 20 years.

In considering the role of Ca^{2+} in cancer, it is important to recognize that the expression and function of Ca^{2+} permeable channels varies considerably between cell types, driving considerable heterogeneity across different forms of cancer. This results in what seems to be mutually exclusive roles in cancer biology; Ca^{2+} can drive proliferation, migration and invasion, but can also induce apoptosis. In conclusion, while it would appear that there is no relationship between Ca^{2+} and cancer, the reality is that Ca^{2+} signals serve distinct roles in different contexts, a point that we hope to clarify over the course of this work.

TABLE OF CONTENTS

LIST OF FIGURES/TABLES

I. List of Figures

II. List of Tables

CHAPTER 1

INTRODUCTION

Part 1: Calcium

I. Ca^{2+} signal generation:

Ca^{2+} signals are generated in response to a wide variety of autocrine, paracrine, hormonal, neurocrine and environmental factors. Here, we will briefly discuss some of the major underlying approaches that cells use to generate Ca^{2+} responses.

A. Receptor-mediated control of Ca^{2+} signals

G-Protein Coupled Receptor (GPCR) and Receptor Tyrosine Kinase (RTK) families are widely expressed and facilitate Ca^{2+} responses in virtually all cell types through phospholipase C (PLC). Briefly, as shown in Figure 1-1, when Gαq-coupled GPCRs (driving PLCβ activation) or RTKs with PLCγ docking sites are activated, PLC hydrolyzes phosphatidylinositol 4,5-bisphosphate (PIP_2) into Inositol Trisphosphate ($InsP_3$) and diacylglycerol (DAG). $InsP_3$ diffuses within the cell towards the ER where it encounters $InsP_3$ Receptors ($InsP_3Rs$), ER-localized Ca^{2+} channels that mediate ER Ca^{2+} release. The resultant ER Ca^{2+} depletion leads to a highly conserved process known as store-operated Ca^{2+} entry (SOCE) (4-7). SOCE is initiated by Stromal Interaction Molecule (STIM), a single pass membrane protein that acts as an Endoplasmic Reticulum (ER) Ca^{2+} sensor, responding to ER Ca^{2+} depletion by translocating within the ER towards the plasma membrane (PM) where it binds to and activates members of the Orai family of Ca^{2+}-selective channels (6, 8). STIM1 and Orai1 serve as the predominant mediators of SOCE in most cell types (8), although the other members of the STIM and Orai families can function analogously, although with distinct characteristics. For example, a decrease

in the Ca^{2+} affinity of STIM2's EF hand causes its activation at near-resting ER Ca^{2+} levels (9-11). Given that, it is perhaps not surprising that STIM2 also exhibits a decreased capacity to activate Orai1 (12) which has been attributed to the presence of a leucine in place of a key phenylalanine within the Orai-binding region of STIM-Orai Activating Region (SOAR) (13). Orai2 and Orai3 can each be activated by STIM proteins expressed heterologously (14, 15), although the roles of the endogenous proteins are less clear. Transformed cells can exhibit fundamental changes in the expression and activation of all components of these pathways (GPCRs, RTKs, STIM, and Orai) (16-18), making this an important current area in the investigation of Ca^{2+} signaling in cancer cells. As such, this will be discussed considerably below.

Although SOCE is a major source of Ca^{2+} entry, members of other classes of channels also mediate receptor-dependent Ca^{2+} signals. The Transient Receptor Potential (TRP) channel superfamily of non-selective cationic channels includes 28 different members organized into 6 families expressed in mammals: TRPA, TRPC, TRPM, TRPML, TRPP, and TRPV (19). The canonical TRP (TRPC) family is particularly relevant in this context since, similar to SOCE, they are activated downstream of PLC-coupled receptors (20), facilitating Ca^{2+} entry through SOCE-like mechanisms (21). Hence, DAG directly activates TRPC3/6/7 (22, 23) while TRPC1/4/5 activation is thought to be mediated by PIP_2 depletion (24, 25). TRPC2 is not expressed in higher mammals (20) in rodents, it is found primarily within the vemeronasal organ (26). As discussed below, many TRPC family members exhibit dysregulated expression in cancer, making this area of considerable potential interest.

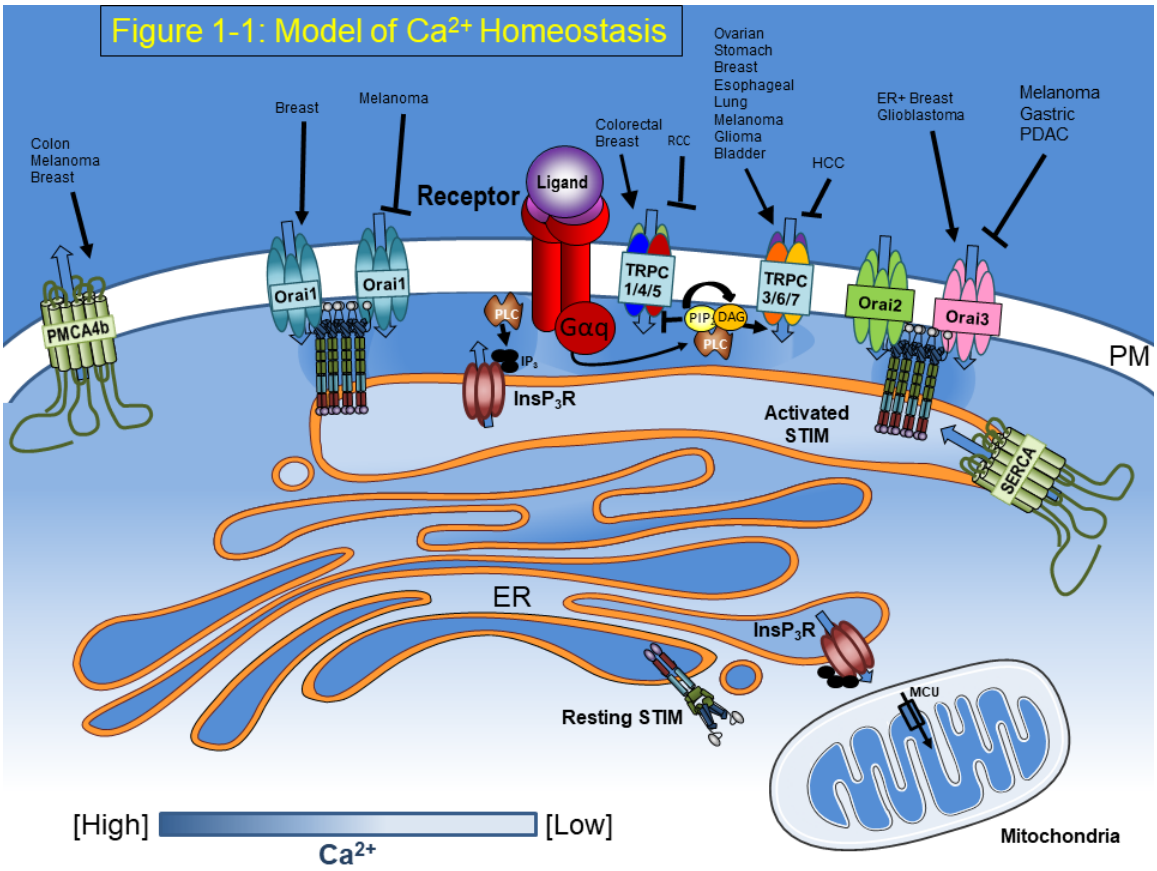
Figure 1-1: Model of Ca2+ Homeostasis
Colon
Melanoma
Breast
Breast
Melanoma
Receptor
Ligand
Colorectal
Breast
RCC
Ovarian
Stomach
Breast
Esophageal
Lung
Melanoma
Glioma
Bladder
HCC
ER+ Breast
Glioblastoma
Melanoma
Gastric
PDAC
PMCA4b
Orai1
Orai1
PLC
Gαq
TRPC
1/4/5
PIP2
DAG
PLC
TRPC
3/6/7
Orai2
Orai3
PM
IP3
InsP3R
Activated
STIM
SERCA
ER
InsP3R
MCU
Resting STIM
[High]
[Low]
Ca2+
Mitochondria

Figure 1-1. Model of Ca^{2+} Homeostasis. At rest Ca^{2+} levels are higher in Extracellular Matrix (ECM) and in the ER (darker blue), which functions as an intracellular Ca^{2+} store. Upon ligand binding to receptors, including GPCR and RTK, downstream effector PLC is activated which activates TRPC channels for Ca^{2+} entry and facilitates generation of IP_3. IP_3 binds to $InsP_3R$ which leads to Ca^{2+} exit from ER, thus depleting the intracellular store. Following Ca^{2+} release from $InsP_3R$ channels, Ca^{2+} either leaves the cytosol through PMCA pumps or is transferred to mitochondria, which orient themselves close to ER in response to elevated intracellular Ca^{2+} levels, where Ca^{2+} eventually enters the inner mitochondrial matrix through mitochondria IMM channel, MCU. Lower ER Ca^{2+} levels (lighter blue) lead to activation of ER Ca^{2+} sensors, STIM proteins. STIM then binds to PM Orai Ca^{2+} channels leading to SOCE. SOCE leads to increases in cytosolic Ca^{2+}, which are then pumped into the ER by SERCA pumps to replete the store. Each step of regulating Ca^{2+} homeostasis plays a role in cancer progression. Cancers affected by each step labeled respectively.

B. Environmental triggers

Several members of the TRPV, TRPM, and TRPA family are widely expressed, facilitate Ca^{2+} entry in a variety of cell types, and respond to a variety of environmental factors (see Table 1-1). For example, TRPV1-4, TRPM8, and TRPA1 are thermosensitive channels activated by temperature changes, each within a specific range (27, 28). In addition, there are several chemical activators of TRPs, which ultimately accounts for the sensory confusion between temperature changes and different sensations.

For example, Capsaicin (the active ingredient in pepper) is a vanilloid (29) that stabilizes TRPV1 in its open conformation (30). In this conformation, ATP binds to the intracellular ankyrin-repeat domain (ARD) of TRPV1 (19, 31), lowering the threshold of temperature for channel activation (32). Resultant increases in cytosolic Ca^{2+} content cause channel inactivation due to competition between Ca^{2+}/Calmodulin (Ca^{2+}/CaM) and ATP for ARD binding (31). Independent of capsaicin, TRPV1-4 sense temperature increases, with TRPV2 activated in response to the most extreme temperature changes (27). Indeed, TRPV2 is only activated above 52°C and although the exact mechanism is not fully understood, it is hypothesized that the channel exhibits structural flexibility, resulting from enthalpy and entropy shifts allowing for conformation change in the channel. In support, TRPV2 enthalpy and entropy capacity are 2 fold larger than TRPV1, whose capacity is 5 fold larger than most other ligand- or voltage-gated channels (33), suggesting thermodynamics play a role in channel activation. Interestingly, the mechanisms that activate TRPV channels in response to temperature and agonists diverge in mechanism but converge onto the same activation gate (34-37) demonstrating the flexibility and versatility of these channels. TRPV3 responds to less extreme changes in temperature (~33°C) (27) and is activated through GPCR-induced breakdown of PIP_2 that facilitates a

voltage-independent activation of the channel in response to colder temperatures (38), albeit temperatures resembling physiologic conditions. TRPV4, meanwhile, responds to a wide range of temperature (28-42°C) and is also activated by cAMP-induced PKA phosphorylation) at S824, which creates a binding site to Arachidonic Acid (AA) that can subsequently activate the channel (39). Hence, all 4 thermosensitive TRPV channels are activated in response to similar stimuli although different mechanisms. While temperature changes are not directly cancer relevant, different types of cancers exhibit different signaling dysregulation, which would have differential effects upon different TRPV channels, precisely exemplifying the context-dependent nature of Ca^{2+} signaling in a tumor environment.

Conversely, TRPM8 and TRPA1, also thermo-sensitive, are activated by temperature decreases and agonists such as menthol and mustard oil/wasabi respectively. TRPM8 is activated at 28°C and its level of activation increases in response to temperatures colder than 15°C. It is hypothesized that it can be activated by depletion of membrane lysophospholipids and polyunsaturated fatty acids (PUFAs), since lysophospholipids lower the threshold of activation (40). This would fit into evolutionary biology that membrane fluidity decreases at cold temperatures, however it is more likely that TRPM8 is directly activated by cold temperatures leading to enthalpy and entropy changes (41), similar to te TRPV2 response to heat. Menthol-induced TRPM8 activation occurs through PIP_2 synthesis as depletion inhibits the sensitivity of the channel (42), precisely the opposite relationship to that between PIP_2 and TRPV1. TRPA1 also senses cold temperatures, although only in more noxious cold conditions (<17°C) (28). More importantly, TRPA1 is a potent sensor of exogenous stimuli as it is activated in response to many agonists, mainly mustard oil and wasabi, but also cinnamaldehyde (cinnamon)

and ginger (28) through binding to cysteine residues in the N-terminus of the channel via covalent interactions and/or disulfide bonds (43-46). TRPA1 also has the unique ability to function as a cannabinoid-sensitive pain receptor in response to inflammation (47, 48). These cannabinoids activate Ca^{2+}/CaM signaling cascades which attenuate the response of TRPA1 to the exogenous agonists (47). There is also some evidence that cannabinoids can also inhibit TRPV1 activity (48), which in addition to TRPA1, can regulate inflammation (47).

Table 1-1: Environmental Triggers of Thermosensitive TRP Channel Activation			
TRP Channel	Activators	Cancers Affected	Mechanism of Activation
TRPV1	≥ 43°C1 Capsaicin2 Mustard Oil Garlic	Prostate (S) Cervical (S) Glioma (S) Breast Cancer (S)	1Enthalpy/Entropy induced channel conformation changes 2Stabilized open conformation leading to ATP binding to ARD domain of channel
TRPV2	≥ 52°C	TNBC (S)	Enthalpy and Entropy induced conformation changes
TRPV3	≥ 33°C	NSCLC	Cell Cycle Arrest
TRPV4	28-42°C	Breast (P/S)	Arachidonic Acid/PKA phosphorylation
TRPM8	≤ 28°C1 ≪ 15°C2 Menthol3	Prostate (P) Gastric (P) Pancreatic (P) Lung (P) Breast (P)	1,2(More likely) Enthalpy/Entropy induced channel conformation changes (Activation intensity is inversely related to temperature) or (Less likely) lysophospholipids/PUFAs leading to lower activation threshold temperature 3PIP2 synthesis
TRPA1	Mustard Oil Wasabi Cinnamon Ginger		

Table 1-1. Environmental Triggers of TRP Channel Activation. Activators of TRP channels shown, which include temperature- and agonist-induced activation. Mechanisms of activation associated with each trigger are included as well as cancers affected. (P) indicates promotes, (S) indicates suppresses, (P/S) indicates both promotes and suppresses individual cancer upon activation.

C. Voltage-gated Ca^{2+} channels

Members of the Voltage-Gated Ca^{2+}-permeable Channel (VGCCs) superfamily are primarily expressed in excitable (neurons and muscle) cells and are activated by membrane depolarization (49). VGCCs can have up to 4 subunits, but all contain the α1 subunit which is the pore-forming portion of the channel, consisting of 4 domains (I-IV) each containing 6 transmembrane segments (S1-S6). The S4 segment of each domain acts as a voltage sensor that rotates outward upon exposure to electrical current and facilitates a conformation change opening the pore, while the S5 and S6 subunits form a membrane-associated pore lining loop containing a series of glutamate residues that determine Ca^{2+} selectivity (50). Both α2δ and β subunits have been demonstrated to increase Ca^{2+} current VGCCs by recruiting and allosterically regulating α1 subunits (51). α2δ subunits are extracellular subunits (49) that are linked by disulfide bonds and mainly responsible for anchoring VGCCs to membranes using Glycophosphatidylinositol (GPI) anchoring sites most likely through hydrophobic sequences (52). β subunits are intracellular (49), facilitate channel trafficking to the PM (52) and can also shift voltage dependence to make activation easier (53). Finally, γ subunits are transmembrane glycoproteins that have been shown to actually limit Ca^{2+} current through stabilizing the inactivated state of VGCCs in skeletal muscle cells. Further, this subunit is only present in skeletal muscle cells and is not expressed heterologously in other cell types (54).

Within the VGCC superfamily, there are 5 different classes consisting of L-, N-, P/Q-, R-, T-type channels. CaV1 channels, or L-type channels, are long-lasting dihydropyridine channels and are mainly responsible for excitation-contraction coupling in smooth muscle cells and consist of CaV1 α1 pore-forming subunits (55). N-, P/Q-, and R-type channels are all members of the CaV2 channel family. N-type channels are named

for the nervous system, where they are mainly expressed, however they can also be found in cell types throughout the body (56). P/Q-type channels are named after Purkinje cells where they were discovered and are mainly located in cardiac (Purkinje) and neuronal (cerebrellar granule) cells (57), where R-type channels are also expressed (55). Finally, CaV3 channels are T-type (transient or short-lasting) and can be activated at lower membrane potentials during membrane depolarization. Similar to L-type channels, they are expressed in most excitable cells (58) and involved in excitation-contraction coupling. In neurons, VGCCs are critical for synaptic transmission (59-61) while in muscle, they drive contraction (49, 62, 63). However, it has become increasingly clear that many non-excitable cell types, including cancer cells (56) also express T-type channels. How they function in these systems and might contribute to cancer biology will be discussed further in subsequent sections.

D. Ca^{2+} pumps

As mentioned previously, the ER represents a major Ca^{2+} storage site in the cell. This is generated and maintained by the Sarco/Endoplasmic Reticulum Ca^{2+} ATPase (SERCA) pump, which catalyzes ATP to drive Ca^{2+} from the cytosol to the ER. SERCA exists in 3 isoforms (SERCA1, SERCA2, SERCA3) that are encoded by 3 different genes (*ATP2A1, ATP2A2, ATP2A3* respectively), which all have highly conserved sequences and share similar functions within a variety of cells. SERCA1 is mainly expressed in fast twitch skeletal muscle, SERCA2a is mainly expressed in cardiac muscle cells, and SERCA2b and SERCA3 are ubiquitously co-expressed in most cells (64). As the primary regulator of ER Ca^{2+} content SERCA is not only critical for the generation of Ca^{2+} signals, but also, as discussed further in subsequent sections, protein processing, mitochondrial metabolism and/or Ca^{2+} overload. Hence, dysregulated expression and/or function of

SERCA function can contribute to the behavior of transformed cells while also offer potential insights into therapeutic opportunities.

Ca^{2+} clearance across the PM is mediated by members of the Plasma Membrane Ca^{2+} ATPase (PMCA) family. PMCA proteins pump Ca^{2+} from the cytosol into the extracellular milieu. PMCA exists in 4 isoforms (PMCA1, PMCA2, PMCA3, PMCA4) encoded by 4 different genes (*ATP2B1, ATP2B2, ATP2B3, ATP2B4* respectively) that together contain 20 different splice variants (65). PMCA1 is ubiquitously expressed in all cell types and *ATP2B1KO* is embryonic lethal (66), PMCA2/3 are expressed mainly in excitable cells such as neurons and striated smooth muscle, but also has been found in mammary gland and uterus (67). PMCA4 is expressed in most cells. *ATP2B4KO* is survivable, but leads to male infertility (68). These pumps are primarily activated by Ca^{2+}/Calmodulin when cytosolic Ca^{2+} concentration increases (67), although several recent studies have demonstrated that PMCA is also modulated by protein-protein interactions (reviewed in (69)). PMCA dysregulation leads to a variety of diseases including deafness, hypertension, cardiovascular disease (70) as well as a variety of cancers, which will be detailed below.

II. Effectors:

A. Calcium and cell migration.

Cell migration is a critical Ca^{2+}-regulated cellular function for embryonic development (71), wound healing (72), angiogenesis (73) and cancer metastasis (74, 75). Cell migration involves 3 distinct steps; responding to environmental cues to determine direction of movement, generating and maintaining cell polarity and activating motility processes for linear movement (76). Cells can become polarized by extracellular stimuli,

which drive movement towards the source of the signal mediated by Ca^{2+} flickers caused by $InsP_3$ production (77) and multiple ion channels, including TRPCs (78), and STIM/Orai(79, 80). Upon polarization, the cell commences moving forward with the initial process of protrusion which utilizes actin polymerization on cellular projections such as lamellopodia and filopodia (81). Subsequently, to terminate protrusion, the front of the cell retracts and attaches to lamella (82), located behind lamellipodia. Lamella recruit myosin to contract and turnover F-actin, leading to formation of further focal adhesions (83). Focal adhesions are stabilized by integrins and associated cytoskeletal proteins to withstand strong forces and facilitate forward motion (82). This occurs primarily in the front of the cell (74), fixing the front during forward motion and facilitating retraction of the rear portion of the cell.

Small GTPases are ~20kDa GTP binding proteins that hydrolyze GTP to GDP and serve critical roles in many cellular processes (reviewed in (84)), including migration. Many GTPases such as RhoA, Rac and Cdc42 have positive bidirectional relationships with Ca^{2+} (85, 86), and thus, serve critical roles driving cell migration in response to polarity-induced Ca^{2+}-flickers. These small GTPases are known to coordinate myosin-induced contractions (87) through activity of Myosin Light Chain Kinases (MLCK) (77, 88) for cell movement, which is important for cells to thrive, especially during development, (further reviewed in (77)). MLCK are Ca^{2+}/CaM-dependent kinases that phosphorylate MLC, leading to myosin cross bridging and cell contraction (reviewed in (89)), and have been demonstrated to facilitate cell movement and migration through regulating membrane tension and protrusion through binding and stabilizing F-actin (90). Hence, changes in Ca^{2+} lead to a signaling cascade culminating in increased cell movement and enhanced cell migration.

B. Calcium Signaling and Epithelial to Mesenchymal Transition

An important step in cancer progression is metastasis, which heavily utilizes an invasive process called Epithelial to Mesenchymal Transition (EMT). Unaffected tissue tends to adopt an ordered structure of epithelial cells that exhibit polarity through apical and basolateral membranes attached by tight junctions, adherens junctions, and desmosomes that form an epithelial layer (91). However, when epithelial cells adopt a mesenchymal cell phenotype, they exhibit a change to a front to back polarity conformation (91), that enhances migration, invasiveness to increase cancer metastasis as discussed further below.

i. Growth Factors

EMT is induced by a variety of growth factors (GF) including Epidermal Growth Factor (EGF), Fibroblast Growth Factor (FGF), and Transforming Growth Factor β (TGFβ) (reviewed in (91)). These GFs can induce EMT by facilitating downstream signaling of EMT-associated pathways. For example, EGF can activate Signal Transducer and Activation of Transcription 3 (STAT3) (92, 93) or Similar to Drosophila Mothers Against Decapentaplegic 2/3 (Smad2/3) (94), both of which are transcription factors that transcribe mesenchymal signature genes. TGFβ uses a similar mechanism in that it can activate Smad2/3 (95). FGF uses a different mechanism of action in that it mainly contributes to loss of cell polarity, promotes cell division, and inhibition of cell-cell contact (96). Hence, GFs play several important roles in promoting EMT by facilitating downstream EMT-associated pathways.

Although these GFs use different mechanisms to promote EMT, it is important to note that in both cases, GFs rely on Ca^{2+} signals to exert their effects. This is perhaps

unsurprising as these GFs bind to RTKs that facilitate Ca^{2+} signaling as discussed above (see section IIA(97-101). Ca^{2+} signals serve a critical role in EMT by driving the expression of mesenchymal signature genes and facilitating ECM degradation, as outlined below.

ii. **Mesenchymal Signature**

EMT induction is associated with several transcription factors and changes in gene expression that comprise a mesenchymal signature. The most common of which are Twist, N-Cadherin, Zeb1/2, and Snai1/2 (Snail and Slug); loss of the epithelial marker, E-Cadherin also occurs (91). This leads to the transcription of genes associated with survival and invasion pathways such as Mitogen Associated Protein Kinase (MAPK), AKT, and Smads among others (reviewed in (102)). Thus, cells can activate an entire program of transcriptional machinery to change the genetic profile of the cell, which inflicts invasive properties that allow for dissemination to other organs.

In addition to these transcription factors, another important marker comprising the mesenchymal signature is intermediate filament, Vimentin (91). Vimentin mediates cytoskeletal organization and focal adhesion through modulating the expression of integrins and reorganizing the orientation of microtubules (103), which can lead to changes in cell polarity and increased motility which facilitate EMT (103, 104). Therefore, in addition to reprogramming the transcriptional machinery of a cell, the EMT process leads to changes in morphology and polarity.

As discussed above (see section IIIA), many of the processes involved in focal adhesion and migration are dependent on Ca^{2+}. Hence, CAMKII has been shown to phosphorylate and activate Vimentin (105) and Vimentin activation and STIM1/TRPC1-dependent Ca^{2+} entry has been show to increase Vimentin activity (106). Further, much

of the transcriptional machinery activated during EMT is associated with Ca^{2+}; an effect that appears to be very context-dependent. For example, TRPM7 activates STAT3, driving Twist, Zeb1/2, and N-cadherin expression in a Ca^{2+}-dependent manner (107). Additionally, it has been demonstrated that Orai3 and STIM1 can mediate Ca^{2+}-dependent TGFβ-induced Snai1 activation, yet blocking Orai1 leads has same effect (108), suggesting Orai3-specific control of EMT.

iii. **ECM Degradation**

Sometimes, cells require degrading the surrounding Extracellular Matrix (ECM) in the tissue microenvironment (TME) to facilitate movement. This is facilitated by the modulation of adhesion molecules by degrading appendages; invadopodia and matrix metalloproteinases (MMPs).

Cells contain migratory appendages called podosomes that consist of actin and tyrosine-phosphorylated proteins that mediate cellular adhesion to the ECM (109). However, in transformed cells, podosome activity is altered due to oncogenic induction of aberrant tyrosine kinase activity, ultimately leading to ECM degradation; podosomes capable of this are commonly referred to as invadopodia (110, 111).

Ca^{2+} serves a critical role in the formation of both podosomes and invadopodia (112, 113). For example, SOCE inhibitors block podosome formation through inhibition of MLCK activity (114). Further, STIM1/Orai1-dependent Ca^{2+} oscillations drive invadopodia formation, as well as Matrix Metalloproteinase (MMP) activity (113). Because constitutive Ca^{2+} entry would be cytotoxic for the cell due to mitochondrial Ca^{2+} overload, cells rely specifically on oscillations to regulate ECM degradation and invasion (113). Interestingly, it has been shown that downstream signaling is regulated by these oscillations and is

reliant on oscillation frequency and amplitude (11, 115). This explains the importance of Ca^{2+} signaling, and specifically SOCE, for invadopodia-induced ECM degradation as SOCE provides the metaphorical fuel for the Ca^{2+} oscillations to induce ECM degradation. Findings of this nature have driven numerous investigations of the potential link between Ca^{2+} signaling and metastasis in many different cancer lineages.

Another factor in ECM degradation are MMPs, which are Ca^{2+}-dependent endopeptidases responsible for remodeling of the ECM (116). Although MMPs are involved in non-pathological processes such as wound repair, development, and immune responses (116), MMPs can also exhibit pathological activity and have been found to directly contribute to invasion and metastasis in cancer by degrading adhesion molecules leading to changes in cell-cell contact and cell-ECM interactions (117). For example, MMPs are known to cleave E-Cadherin (118), the most widely studied epithelial marker, as well as bi-directionally associating with GFs such as TGFβ using Ca^{2+}-dependent MAPK pathway in cancer (119, 120). Hence, Ca^{2+}-dependent control of MMP activity plays an important role in EMT and cancer progression.

C. Control of metabolism.

Mitochondria are best known as the site of energy production, but also serve complex roles in ion signaling and cancer biology. The role of metabolism in cancer has been widely investigated, predating the discovery of oncogenes and tumor suppressors by many years (121-123). This “Warburg effect” can be summarized as a metabolic shift away from oxidative phosphorylation in cancer cells, leading to lactic acid fermentation (124). Although less efficient at energy generation, this favors anabolic growth and catabolism-induced cell survival (123, 125). The underlying mechanisms responsible for

the Warburg effect remain under investigation, however, it is important to recognize that increases in matrix Ca^{2+} content drive NADH, and thus ATP, production (126, 127). This is facilitated by a series of mitochondria-specific channels, exchangers and pumps that control mitochondrial ion content (reviewed in (128)).

As shown in Figure 1-2, to enter the mitochondrial matrix, Ca^{2+} must pass through the outer mitochondrial membrane (OMM), the intermembrane space (IMS) and the inner mitochondrial membrane (IMM). Voltage-Dependent Anion Channels (VDACs) are located on the OMM. They are weakly selective for anions at lower membrane potentials (channel is in “open” state), but favor cations at higher membrane potentials (when the channel is in a “closed” state) (128).

Figure 1-2: Mitochondria-ER regulation of Ca2+ and Metabolism

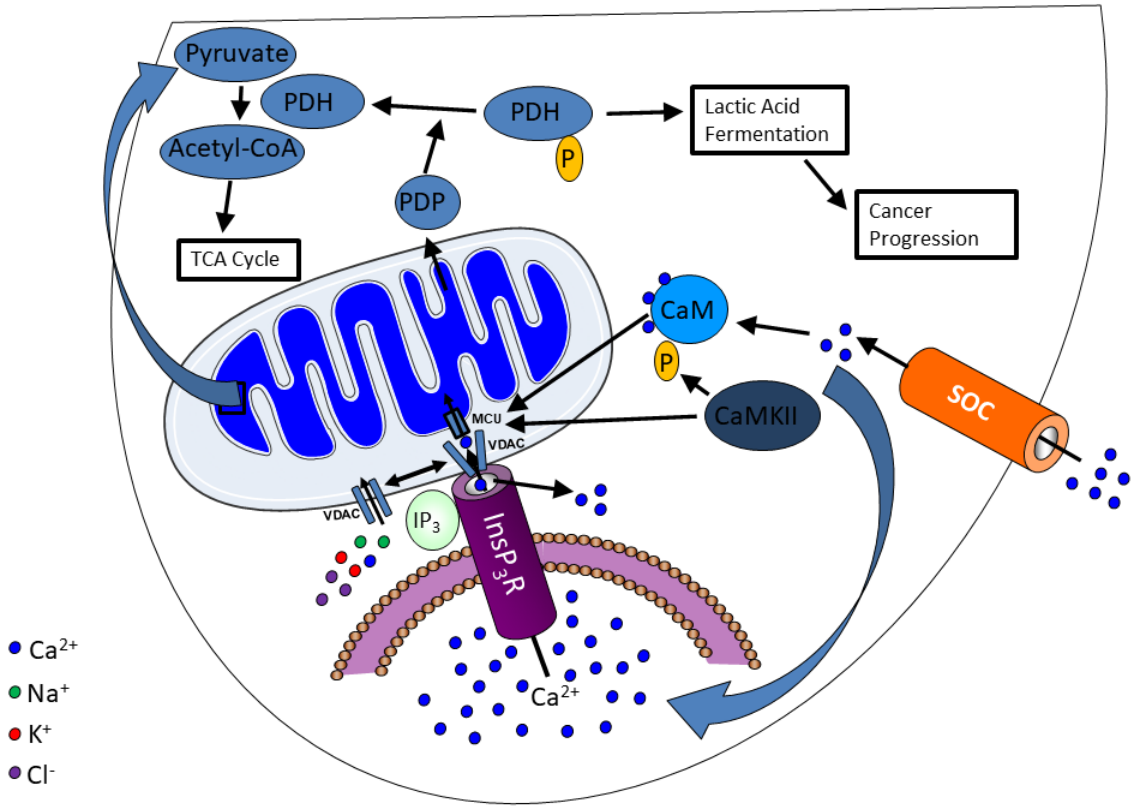

Figure 1-2. Mitochondria-ER Regulation of Ca^{2+} and Metabolism. Upon Ca^{2+} entry through Store-Operated Calcium (SOC) channels, ER Ca^{2+} stores fill and are eventually relieved of Ca^{2+} by PLC-driven IP3 binding to InsP3 receptor (InsP3R). InsP3R directly binds to mitochondrial Voltage Dependent Anion Channel (VDAC), which is more permeable to Ca^{2+} in closed conformation to facilitate Ca^{2+} entry through mitochondrial outer membrane. Subsequently, Ca^{2+} enters into the inner mitochondrial matrix through mitochondrial Ca^{2+} uniporter (MCU) which is positively regulated by Ca^{2+}-dependent Calmodulin (CaM) upon phosphorylation by Calmodulin Kinase II (CaMKII). Higher Ca^{2+} concentration in the inner mitochondrial matrix upregulates Pyruvate Dehydrogenase Phosphatase (PDP) to dephosphorylate Pyruvate Dehydrogenase (PDH) which facilitates pyruvate conversion to Acetyl-CoA and subsequent entry into The Citric Acid (TCA) cycle. Conversely, lower Ca^{2+} concentration inhibits PDP dephosphorylation of PDH leading to Lactic Acid Fermentation and cancer progression.

Although upon closure, VDACs allow entry of other cations, such as Na^+ and K^+, Ca^{2+} is favored (129). VDACs also serve a critical role in linking mitochondria to $InsP_3Rs$ and the ER, critical for mitochondrial Ca^{2+} loading (128, 130). These links permit preferential loading of the mitochondria since they experience Ca^{2+} concentrations at near ER Ca^{2+} levels, critical for the entry of Ca^{2+} into the matrix. Previously, it was thought that the major Ca^{2+} channel on the IMM is the mitochondrial Ca^{2+} uniporter (MCU) was a high capacity, low affinity Ca^{2+} channel (reviewed in (131)) that does not permit Ca^{2+} entry at less than 10 μM (132), a concentration not normally observed in the cytosol (on average). However, it has been recently determined that MCU actually is a high affinity Ca^{2+} channel that is regulated by MCU channel regulators, Mitochondrial Ca^{2+} uptake 1/2 (MICU1/2) (133). This movement across the IMM is driven by its highly negative membrane potential (~-180 mV) produced due to proton pumping during oxidative phosphorylation. Upon entry into the matrix, Ca^{2+} binds directly to pyruvate dehydrogenase phosphatase (PDP) (134), the first step in the generation of acetyl CoA at the beginning of the TCA cycle along with the rate-limiting TCA cycle enzymes α-ketoglutarate dehydrogenase (αKGDH) and isocitrate dehydrogenase (IDH) (135) increasing their activity and driving NADH generation. Notably, decreased pyruvate dehydrogenase phosphatase activity at lower mitochondrial Ca^{2+} content leads to conversion into lactate via lactic acid fermentation(136, 137) . Hence, changes in mitochondrial Ca^{2+} loading may contribute to the Warburg effect and can be greatly altered in transformed cells.

The sensitivity of mitochondria to Ca^{2+} levels has been considered a significant therapeutic opportunity. Hence, mitochondrial Ca^{2+} overload leads to Reactive Oxygen Species (ROS) generation due to overproduction of electrons from the ETC during oxidative phosphorylation (138). In contrast, if too little Ca^{2+} enters the mitochondria,

decreased ATP generation can lead to autophagy (139) due to AMPK activation (139, 140). Although mitochondrial Ca^{2+} loading is primarily dependent upon MCU and VDAC, ultimately, it is dependent upon the overall availability of Ca^{2+} to the cell. As such, mitochondrial function represents a significant potential implication of any change in cytosolic Ca^{2+} signaling in cancer cells.

D. Calcium and transcription factors.

Ca^{2+} regulation throughout the cell has the ability to not only drive cellular processes, but also affect cellular physiology through control of transcription factor activity. Although crosstalk between signaling pathways can lead to pleiotropic effect on gene expression, several transcription factors are directly Ca^{2+}-sensitive as shown in Figure 1-3A and as discussed further below.

1. NFAT

The Nuclear Factor of Activated T-Cells (NFAT) family of Ca^{2+}-dependent transcription factors consists of 4 classic NFAT family members: NFATc1 (NFATc or NFAT2), NFATc2 (NFATp or NFAT1), NFATc3 (NFAT4), and NFATc4 (NFAT3) and the Ca^{2+}-insensitive NFAT5. Originally discovered in T cells, NFAT family members are widely expressed, with well-defined roles in muscle, neurons, heart, osteoclasts and adipocytes (reviewed in (141)).

Structurally, NFAT members share a highly conserved Rel-Homology Domain (RHD) that gives them a similar DNA-binding specificity (142, 143). NFAT homology region (NHR), which regulates NFAT activity, consists of approximately 12 regulatory regions including: an N-terminal Transactivation Domain (TAD) (1) with a Casein Kinase 1 (CK1) docking site (2), a Calcineurin Docking Site (CDS) (3), an additional CK1 docking

site outside of the TAD (4) 2 serine rich regions (SRR1 and SRR2) (6), 4 serine rich motifs (SRM (SP1, SP2, SP3, KTS)) (10), a Nuclear Localization Sequence (NLS) (11), and Nuclear Export Signal (NES) (12) (141) (144) (see Figure 1-3B).

As shown in Figure 1-3A, at rest, NFAT members reside in the cytoplasm (145). In response to increased intracellular Ca^{2+}, PKC is activated and Ca^{2+}/Calmodulin regulated protein phosphatase complex (CaM) associate with calcineurin. Following PKC activation and complex association, PKC activates Ca^{2+}/CaM/Calcineurin complex to dephosphorylate NFAT, leading to translocation to the nucleus and subsequent transcription of target genes (144, 146, 147). Within NFAT, CDS facilitates calcineurin docking interactions (148) for dephosphorylation of NFAT at conserved phosphoserine residues (143). Mechanistically, dephosphorylation of NFAT SRR and SRM lead to a conformational change and subsequent exposure of its NLS (149). Following NFAT NLS exposure, NFAT proteins then translocate to the nucleus and transcribe NFAT target genes (141). In fact, it has also been shown that not only does NFAT dephosphorylation lead to nuclear localization, but it also leads to higher NFAT affinity for specific regions of DNA, further promoting transcription of NFAT target genes (145, 150-152). Following return to basal Ca^{2+} levels, SRR and SRM serve as phosphorylation sites (143, 145) leading to exposure of the NES which facilitates NFAT exit from the nucleus (145, 153). Hence, sustained NFAT-mediated gene transcription requires sustained Ca^{2+} signals. NFAT is linked to a variety of oncogenic pathways in different capacities including but not limited to: JAK/STAT(154), COX2(155), and MAPK(156). Because NFAT activity is dependent on Ca^{2+}, it underscores the importance of Ca^{2+} in the context of cancer. In this regard, targeting NFAT could be an efficacious therapy for a variety of cancers which will be discussed in great detail below.

Fig 1-3: Transcriptional Regulators of Ca^{2+} Homeostasis

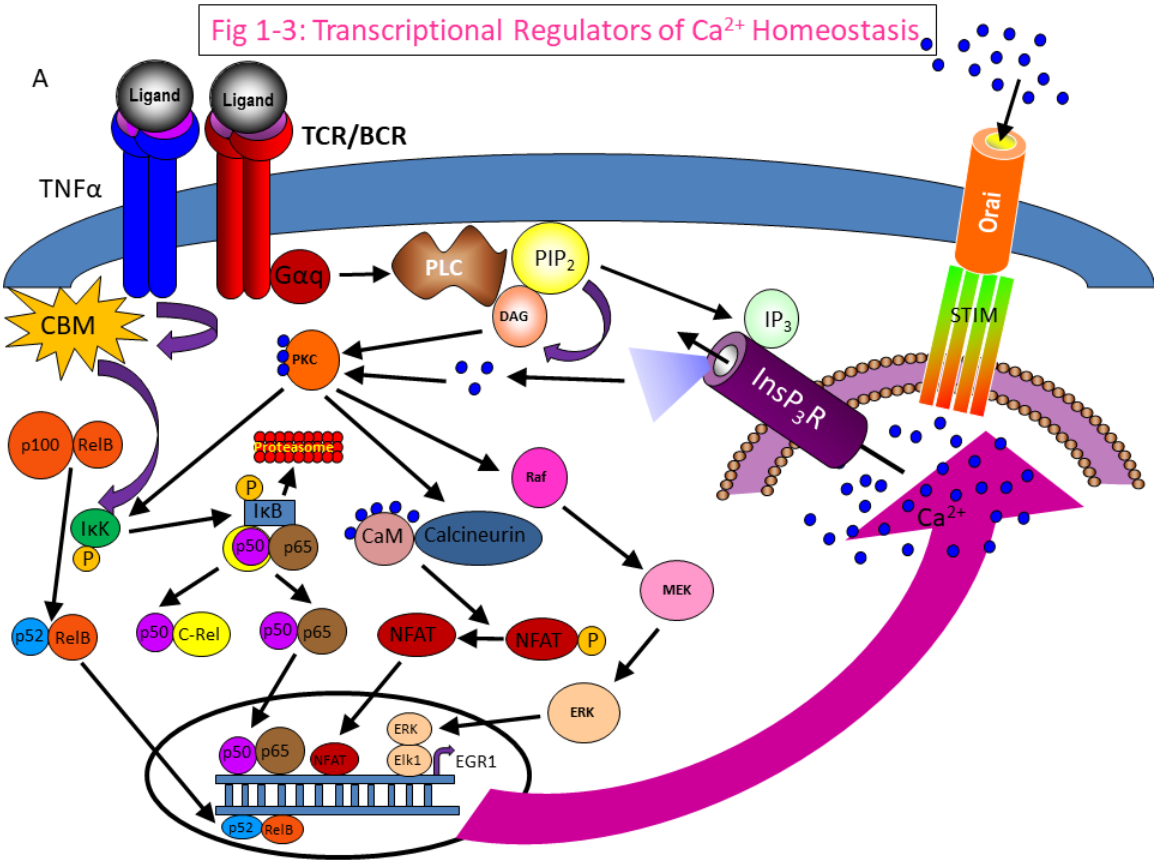

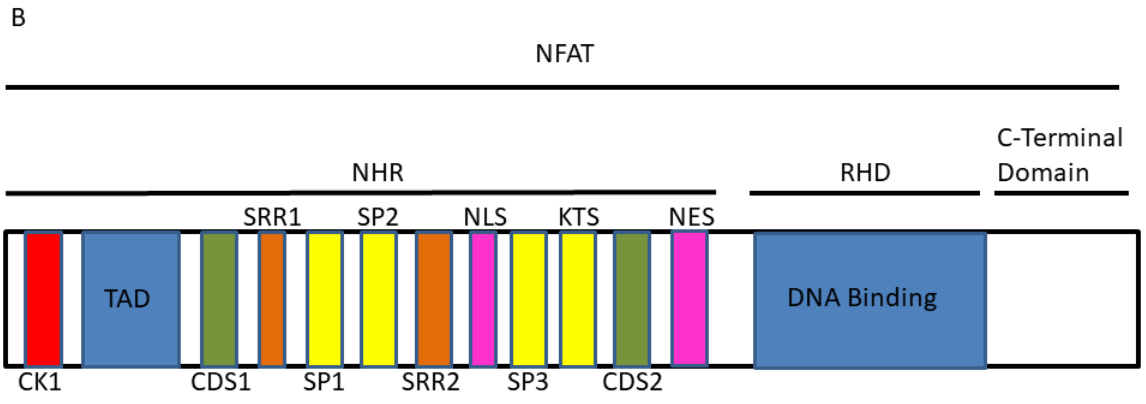

Figure 1-3. Transcriptional Regulators of Ca^{2+} Homeostasis. Upon ligand binding to receptors such as GPCR/RTK, Gαq activates PLC to breakdown PIP_2 into IP_3 and DAG. IP_3 binds to $InsP_3R$ which facilitates Ca^{2+} release from ER store into the cytosol. DAG activates PKC, which is further activated by increases in cytosolic Ca^{2+} levels. PKC. PKC, then, facilitates 3 transcription regulating cascades. First, PKC phosphorylates IκK which facilitates the breakdown of p100 into p52 which is an active transcription factor within NFκB pathway. Subsequently, p52/RelB dimer translocates to nucleus, leading to transcription of NFκB-associated genes. Second, PKC activates calcineurin, which complexes with Ca^{2+}/calmodulin regulated protein phosphatase (CaM) to dephosphorylate NFAT. Dephosphorylated NFAT translocates to nucleus to facilitate NFAT-associated genes, including EGR genes among others. Third, PKC phosphorylates Raf, which activates MAPK pathway. ERK translocates to nucleus and binds to Elk1 substrate, facilitating transcription of EGR1, among other MAPK-associated genes. EGR1 activates ER Ca^{2+} sensor, STIM, which binds to PM Orai Ca^{2+} channel, which promotes SOCE upon ER Ca^{2+} store depletion.

2. NF-κB

NF-κB is a family of transcription factors that give rise to seven proteins from the combination of five gene-coding subunits, RelA/p65, c-Rel, RelB, p50, and p52 (157). This family of inducible transcription factors with pleiotropic functions. Although heavily studied in lymphocytes, NF-κB signaling is present in a wide variety of cells(158). Further, its capacity to regulate cell survival can facilitate resistance to apoptosis in transformed cells.

As shown in Figure 1-3A, although canonical NF-κB activation is Ca^{2+}-independent, Ca^{2+}-dependent PKC activation facilitates CARMA1 phosphorylation to produce the CARMA1-Bcl10-MALT1 (CBM) complex in lymphocytes (159, 160). Further, calcineurin can promote NF-κB activation by promoting IKK phosphorylation of IκB (161-163) (164), ultimately leading to proteasomal degradation. Upon IκB degradation, NFκB complexes translocate to the nucleus where they can drive gene transcription. NF-κB targets include cell cycle progression regulators such as Cyclin D, E, c-myc, and c-myb (as reviewed in {Dolcet, 2005 #6120)). Cyclin D and E induce cell cycle progression during mid-late G1 phase (165), and while Cyclin D suppresses differentiation (166). Concurrently, c-myc promotes many survival processes such as cell growth, while also facilitating differentiation, and death (167) and c-myb regulates growth through a variety of mechanisms depending on tissue type (168, 169).

3. WT1/EGR1

Wilm's Tumor Suppressor 1 (WT1) and Early Growth Response 1 (EGR1) proteins are dueling zinc finger transcription factors that regulate Ca^{2+} homeostasis in a variety of cell types. Over the last 10 years, our group has demonstrated that WT1 expression leads to decreased STIM1 expression and SOCE, while EGR1 expression leads to enhanced

STIM1 and SOCE (170, 171), discussed in great detail in our recent review (172). Briefly, EGR1 is activated downstream of a wide variety of growth and stress signals (173). Although primarily associated with MAPK signaling, Ca^{2+} signals can also drive EGR expression (174, 175), revealing an intriguing feedback loop between Ca^{2+} and EGR1 expression. The EGR1 promoter consists of 5 Serum Response Elements (SREs) and a cAMP Response Element (CRE). Currently, there is considerable evidence that Ca^{2+} regulates the transcription of CRE- and SRE-containing genes (176, 177), likely through Ca^{2+}-dependent (178, 179) ERK activation (180). Dysregulated expression and function of WT1 and EGR1 are observed in a wide variety of cancers (reviewed in (172)), providing a potential causative explanation for why cancer cells often exhibit changes in Ca^{2+} signaling regulation.

WT1 and EGR1 contribute to a variety of cellular processes including but not limited to cell cycle regulation, differentiation, and apoptosis. EGR1 controls cell cycle progression by downregulating CDK4, which maintains quiescence (181), Further, EGR1 promotes the transcription of genes driving differentiation in response to a variety of growth factors the development of breast epithelial cells and immune cells among others (182, 183), whereas WT1 inhibits differentiation by displacing EGR transcription factors from its response elements (184). Under some conditions, EGR1 can induce apoptosis through activating pro-apoptotic factors such as p53 in response to increased intracellular Ca^{2+} in melanoma cells (185) whereas specific WT1 splice variants can facilitate apoptosis through repressing both intrinsic and extrinsic survival factors such as Bcl2 and IGF1 respectively in hepatoma cells (186). As these processes are important for normal cellular physiology, they are also important for cancer progression. As discussed previously (172), EGR1 and WT1 play dual and opposing roles in cancer progression. Thus, targeting EGR1

and WT1 could be an effective, and further improved upon, therapeutic target in a variety of cancers and the current landscape of EGR1 and WT1 role in specific cancers, as well as any therapeutics targeting these transcription factors.

Part 2: Controversy Of Ca^{2+} Role In Cancer

As discussed above, Ca^{2+} plays a dynamic role in many cellular processes. Therefore, it is perhaps not surprising that not only does Ca^{2+}-dependent signaling plays a role in cancer progression, but it is a continued interest of the field to understand the mechanisms behind Ca^{2+} signaling and cancer. While many Ca^{2+}-dependent processes affect cancer progression (187), here, we will delve into the affects SOCE has on many cancer-dependent processes and how SOCE ultimately can promote or inhibit cancer progression across many cancers in certain contexts.

I. Breast Cancer

a. Introduction

According to 2019 cancer statistics from the American Cancer Society, breast cancer has the highest incidence and second highest total mortalities among women nationwide (188). Although breast cancer can be easily treated when detected early, high mortality rates indicate that breast cancer still presents challenges in treatment, especially in advanced stage disease. Clearly, the need for novel treatments exists.

Breast cancer is considered an adenocarcinoma, a cancer that starts in glandular tissue, and is heavily reliant on receptor-mediated signaling to proliferate. Like normal cells, cancer cells receive extracellular signals to facilitate their growth. Within breast cancer, there are 3 major subtypes broken down by receptor status. The 3 major receptors involved in breast cancer are steroid hormone receptors, estrogen receptor (ER), and progesterone receptor (PR), as well as non-steroid hormone receptor Human Epidermal Growth Factor Receptor 2 (HER2). To this end, clinically breast cancer is either: hormone receptor positive or negative (HR±; expressing estrogen receptor (ER) and/or

progesterone receptor (PR)), HER2±, or triple negative (TNBC, negative for all 3 receptors) (189). In addition to hormone and HER2 receptor status, a recently discovered marker for breast cancer classification is Ki67, which is normally a marker for proliferation, leading to additional classification subtypes: Luminal A (ER+, HER2-, PR+/Ki67-), Luminal B (ER+, HER2-, PR- or Ki67+), Luminal B-like (ER+, HER2+, PR+/-, Ki67+/-), HER2+ (ER-, HER2+, PR-, Ki67+/-), and TNBC (ER-, HER2-, PR-, Ki67+/-). Further, there is some evidence of a basal-like subform of TNBC, that overexpresses basal cytokeratins, Epidermal Growth Factor Receptor (EGFR) and caveolin (CAV) 1/2 separate from traditional TNBC (190, 191). Although the luminal subtypes tend to be the most common, TNBC is the most aggressive (192). While treatment strategies are improving for breast cancer, it is important to note the highly mutually exclusive genetics between the subtypes, which can become even more variable between individual cases. This clearly presents a challenge that still exists in the breast cancer field in generating treatments amenable for the majority of breast cancer patients. Here, we delve into the current understanding of the role of Ca^{2+} signals in breast cancer biology and discuss its potential as a therapeutic target.

Given the heavy reliance of breast cancer on receptor-mediated signaling, particularly in early stages, it's reliance on multiple Ca^{2+}-dependent signaling pathways including SOCE is, perhaps, not surprising. For example, it has been demonstrated that Orai1 RNAi attenuates proliferation, migration, invasion, and formation of lung metastases *in vivo* due to impaired focal adhesion turnover caused by impaired SOCE (193). Hence, not only does impaired SOCE limit the size of focal adhesions formed, the ability of focal adhesions to act as traction points for cellular movement was also compromised (193). Most likely, impaired SOCE inhibits polarization, causing retention of ER Ca^{2+}, which inhibits $InsP_3$-

induced store depletion and Ca^{2+} flickers to allow cell movement. These observations implicate SOCE as a fundamental driver of breast cancer metastasis and could justify targeting SOCE to impede disease progression, although the efficacy of this strategy in patients has not been established.

b. SOCE effects on Breast Cancer

Interestingly, different subtypes of breast cancer exhibit distinct expression patterns of STIM/Orai, which serve distinct roles in cancer progression. Hence, it has been demonstrated that elevated STIM1/STIM2 ratio is associated with poor patient prognosis in TNBC (194). This is most likely because STIM1 is the more effective facilitator of SOCE and SOCE is associated with poor prognosis in TNBC. Furthermore, induction of EMT has been shown to elevate the expression of STIM1 along with associated SOCE in MCF7 HR^+ breast cancer cells (195, 196). Thus, STIM1 appears to be important in both HR+ and HR- subtypes of breast cancer. Further, differences in androgen signaling between ER+ and ER- breast cancer lead to a switch in Orai expression from Orai3 to Orai1 (197, 198). Hence, androgens are converted into estrogen using the enzyme aromatase (199), the primary therapeutic target for HR+ breast cancer (192). Androgen deprivation has been shown to inhibit Orai1 production in other tissues such as prostate cancer (200). Hence, differences in androgen-mediated Orai1 expression may contribute to fundamental differences between HR+ and HR- breast cancer, with Orai3 expression being driven as a compensatory mechanism due to loss of Orai1 in early stage disease (198). Notably, Orai1-mediated SOCE in TNBC drives Notch-mediated invasiveness under hypoxic conditions (Liu et al., 2018c). Hence, breast cancer progression is marked by significant changes in how SOCE is generated and resultant invasive behavior.

II. Ovarian Cancer

a. Introduction

Although breast cancer is the most common gynecologic cancer diagnosis among women, ovarian cancer is the most lethal (188, 201, 202). Generally, ovarian cancer is broken up into 3 subtypes. First, epithelial tumors account for up to 90% of ovarian cancers that consist of many different histological subtypes including serous, endometroid, clear cell, and mucinous carcinomas. (reviewed in (203)). Less commonly, ovarian cancer can also exist as germ cell and sex cord stromal tumors (202). Importantly, although it was previously thought that ovarian cancer arises from one entity, it is now accepted that ovarian cancers can form in different reproductive organs including the fallopian tube and peritoneum (202, 204). Formation of tumors in these other gynecologic areas yield similar molecular profiles, which clinically categorizes them as the same disease even if the site of origin is different. Because tumors can originate in multiple areas of the reproductive system, ovarian cancer is very difficult to detect early, and most clinically diagnosed cases are of higher grade. Hence, the most common form of ovarian cancer is High Grade Serous Carcinoma (HGSC) which accounts for roughly 70-80% of all ovarian cancer compared to 5% for its low-grade counterpart. This is significant as ovarian cancer typically presents as an aggressive malignancy that likely has generated invasive properties and because it can originate in many different organs, treatment is very challenging. Thus, novel therapeutic strategies are needed to treat this disease.

Several different Ca^{2+}-related pathways such as EGR1/WT1, TRP channels, and VGCC channels have been shown to cause ovarian cancer progression. Interestingly, much of what is known about ovarian cancer and Ca^{2+} is based on expression and prognosis correlations, yet no real consensus has been reached on mechanistic

contributions of many of these channels, or even transcription factors regulating Ca^{2+} signals, which will be discussed below.

b. SOCE effects on Ovarian Cancer

There have been a number of studies demonstrating dysregulation of SOCE during ovarian cancer progression, although the relationship between SOCE and ovarian cancer progression remains unclear. Hence, STIM1 and Orai1 expression are both upregulated in therapy-resistant ovarian cancer cells compared to therapy-sensitive cells, leading to increased AKT activity that promotes therapy resistance (205). Further, Placental Growth Factor (PlGF), which is produced by gynecologic tumor cells, also upregulates expression of both STIM1 and Orai1, but has been proposed to promote ovarian cancer progression through STIM1- and Orai1-induced HIF1α expression (206). However, SOCE inhibition is protective against ROS-induced apoptosis (207) likely as a result of decreased mitochondrial Ca^{2+}. Hence, SOCE both promotes ovarian cancer progression and sensitizes cells to apoptosis Future investigations may help to delineate the complex relationship between SOCE and ovarian cancer progression and survival.

Interestingly, there have also been a number of studies linking EGR1 and WT1 with ovarian cancer progression; as discussed in section IIID, EGR1 and WT1 regulate STIM1 expression (170-172) . The extent to which changes in STIM1 contributes to these effects is not currently clear, although these possibilities should be considered. For example, EGF-induced EGR1 expression has been demonstrated to upregulate the E-cadherin repressor Slug, leading to EMT which increases the invasive capacity and EMT activity of ovarian cancer *in vitro* (208) (209). Downstream of EGR1, STIM1 expression has also been shown to be upregulated in cisplatin-resistant ovarian cancer leading to subsequent

activation of AKT (205). However, the effect of STIM1 on ovarian cancer progression is somewhat understudied, there is preliminary evidence that STIM1 is associated with disease progression. In this context, EGR1 would increase ovarian cancer invasiveness. Interestingly, the role of EGR1 shifts in late-stage ovarian cancer; analysis of patient databases reveal several-fold decreases in EGR1 expression in advanced carcinomas (210). Further, EGR1 can inhibit cyto-protective autophagy in the absence of autophagy regulator, ATG14, (211) indicating that these effects can be highly context-dependent.

Interestingly, WT1 has been shown to drive EMT in early ovarian tumorigenesis (212, 213). Further, because WT1 can be correlated with poor prognosis, it is usedas a marker to track ovarian cancer progression (214). The extent to which WT1-mediated suppression of STIM1 expression and SOCE affects EMT in ovarian cancer is unknown. However, given the established relationship between Ca^{2+} signals and EMT (see section IIID), it is reasonable to speculate on this possibility.

c. Treatments targeting SOCE in Ovarian Cancer

Therapeutically, Carboxyamidotriazole (CAI) (see table 1-2), has been proposed as a treatment for ovarian cancer (215, 216), has undergone phase II clinical trials and has been suggested as a maintenance drug for relapsed epithelial ovarian cancer (217), but has not been investigated as a first-line therapy. Although CAI has been well-established as a SOCE inhibitor, as an ovarian cancer therapeutic, CAI utilizes a different mechanism of action. Thus, CAI inhibits the expression of the Bcl2 family member myeloid leukemia cell differentiation 1 (Mcl-1) (218), itself a negative regulator of mitochondrial Ca^{2+} loading (219). As such, Mcl1 is highly protective against mitochondrial Ca^{2+} overload and is associated with poor prognosis in ovarian cancer (220). Further, CAI-induced Mcl-1

inhibition is correlated with inhibition of the mTORC1 pathway (215) because mTORC1 controls Mcl-1 translation through 4E-BP1 phosphorylation in ovarian carcinoma (221). This process relies on Ca^{2+} as Ca^{2+}/calmodulin regulates mTORC1 activity since CAMKs activate mTORC1 (222). In conclusion, CAI-inhibition of SOCE occurs through changes in Mcl1 expression which likely inhibits both Ca^{2+}-dependent survival pathways and leads to mitochondrial Ca^{2+} overload as its primary mechanisms of action. This can prove to be promising as a novel potential target in treating ovarian cancer.

III. Prostate Cancer

a. Introduction

Analogous to breast cancer in women, prostate cancer is treatable when detected early, yet prostate cancer has the highest cancer incidence and second highest total mortalities among cancers in men in the US (188). This portrays the challenge of treatments for advanced stages of disease and the need for novel treatments. Prostate cancer is also a form of adenocarcinoma mainly divided into subgroups consisting of Androgen Receptor positive (AR+) and negative (AR-). The differences between the subgroups and their dependence on Ca^{2+} will be discussed in great detail below.

Also similar to breast cancer, prostate cancer is heavily reliant on receptor-mediated signaling. Specifically, normal prostates use nuclear receptor, AR, which are activated in response to androgens (223). Activation of this receptor leads to translocation to the nucleus where it facilitates transcription of androgen related genes, such as Prostate Specific Antigen (PSA), human glandular kallikrein (hK2), kallikrein related peptidase/serine protease 18 (prostase/PRSS18), and transmembrane serine protease 2 (TMPRSS2). These genes encode for serine proteases that regulate the prostate gland

including facilitating proteolytic cascades leading to production of semen (224) and promoting sperm motility and cell movement (224, 225). However, because these proteases are involved in cell movement, it also has been characterized as invasive by degrading the surrounding ECM (224, 225). Among these proteases, there is some evidence that the presence of TMPRSS2 can act as a switch between normal prostate epithelium and prostate cancer. If untranslated, this gene fuses with E26 Transformation Specific (ETS)-transcription factors to form fusion proteins that make up the vast majority of prostate cancer subtypes (226). The most common ETS transcription factor is ERG. Thus, TMPRSS2-ERG (T2E) is the most common genetic background of prostate cancer (227). Furthermore, it has been shown that T2E is associated with Ca^{2+}. Indeed, use of Ca^{2+} channel blockers has actually been shown to reduce risk of developing T2E prostate cancer (228), since T2E is heavily reliant on CaV1.3; CaV1.3-mediated Ca^{2+} entry activates AR (229). Additionally, other ETS-transcription factor subtypes, as well as subforms with mutations of Ras/Raf, and Speckle Type POZ Protein (SPOP), a cullin-based E3 ubiquitin ligase, also make up many individual prostate cancer genetic backgrounds (226). Hence, Ca^{2+} regulation has been shown to play an important role in governing AR activity, which implicates Ca^{2+} as a promising target for prostate cancer.

Currently, for AR+ prostate cancer, there are treatments involving inhibition of androgen production, namely Androgen-Deprivation Therapy (ADT). However, this appears to only be effective in early stages of prostate cancer and delay in treatment can lead to progression into castration resistance stages (230-233). This is significant as it appears that hormonal regulation of prostate cells can prevent progression into later stages of disease. Most likely this is because AR actually suppresses later stages of prostate cancer progression (230, 234-236), as androgen deprivation leads to EMT since

AR inhibits EMT marker, Zeb1 (237). This is further supported by evidence that androgens also contribute to homeostasis as deprivation activates damage-repairing cellular programs. For example, in the absence of androgens, cells upregulate anti-stress genes regulating detoxification, hypoxia response, DNA damage-repair, and p53 activation (238). Hence, targeting androgens appears to be very dependent on timing for effectiveness.

Along with timing, one of the biggest downfalls of androgen deprivation is in addition to AR+ subtype, AR- subtype also interacts with RTKs such as JAK/STAT pathways (reviewed in (239)), which makes targeting specific pathways difficult. For example, whereas Stat5a/b are known to directly bind to AR and facilitate translocation to the nucleus in response to androgens (240), this effect can also occur in the absence of androgens due to genomic reprogramming in response to androgen deprivation (241). Thus, progression to AR- prostate cancer occurs through the upregulation of AR-independent pathways that bypass or parallel AR signaling and lead to progression into CRPC and AR- prostate cancer (239, 242-244). An example of a bypass pathway includes activating the compensatory GPCR, glucocorticoid receptor (GR), in the absence of AR that induces a similar effect on disease progression (239, 243, 245, 246). However, in addition to receptor-mediated signaling, it is also proposed that prostate cancer cells can undergo a Darwinian-type event where cells are selected for surviving in androgen deprived conditions (239) most likely by the onset of Bcl2 expression (242). Because AR- prostate cancer is more advanced, it is more resistant to therapies including radiation, chemotherapy, and cytotoxic exposure attributing to stress responses activated in the absence of androgens (238). This makes treating AR- prostate cancer especially challenging. As a result, AR- prostate cancer therapies are limited at best. One attempt at

treating AR- prostate cancer is Diethylbestrol (DES) (see table 1-2), which is a synthetic ethinyl estrogen used to treat hormone-induced cancers such as CRPC in men and breast cancer in postmenopausal women[42]. In prostate cancer, DES reduces production of testosterone (androgen), which slows prostate cancer growth, however this was discontinued as it showed limited clinical response (247), demonstrating the clear need for novel therapeutics. Because AR+ and AR- subtypes of cancer rely on receptor-mediated signaling, Ca^{2+} homeostasis has been implicated in the progression of prostate cancer with several Ca^{2+}-sensitive pathways dysregulated in prostate cancer, (reviewed in (248)) which will be discussed in detail below.

b. SOCE effects on Prostate Cancer

Prostate cancer appears to rely heavily on Ca^{2+}-dependent signaling that dynamically regulates disease progression based on disease stage and genetic background. To this end, STIM1 and Orai1 expression have been shown to be correlated with AR levels (249) (250, 251). This is likely because STIM1 and Orai1 activate signaling cascades that activate AR. For example, normally, IP_3 is generated from the cleavage of PIP_2 as discussed above. However, PIP_2 also can be phosphorylated by PM-associated PI3 kinase (PI3K) leading to the production of PI triphosphate (PIP_3). PIP_3 leads to activation of many downstream oncogenic pathways such as AKT and mTOR. In this regard, it has been shown that PI3K/AKT/mTOR pathway contributes to prostate cancer progression. In a previous cohort of prostate cancer patients, profound alterations were reported, in each of the three genes within this pathway. Further the entire pathway was deregulated in some capacity in 42% of localized and 100% of metastatic disease cases (252, 253). PI3K/AKT/mTOR pathway is Ca^{2+}-dependent; an effect demonstrated in prostate cancer as STIM1 suppression inhibited migration and invasion of prostate cancer cells *in vitro*

through suppression of PI3K/AKT/mTOR pathway (254). Thus, Ca^{2+}-regulation of pro-invasive pathways such as PI3K/AKT/mTOR appear to play an instrumental role in prostate cancer progression. Further, this pathway also interacts with AR signaling (255), providing PI3K/AKT/mTOR as a potential mediator for how Ca^{2+} activates AR, a process that is known to occur in conjunction with gene fusions, such as T2E (256, 257). This implicates SOCE as extremely important since it may serve as a marker for disease progression.

A driving force for SOCE is receptor-mediated depletion of ER Ca^{2+} store release as a result of PIP_2 cleavage. In contrast to PI3K converting PIP2 into PIP3, Phosphatase And Tensin Homolog (PTEN) is a PM-associated Phosphatidylinositol (PI) phosphatase which reverses this conversion leading to higher production of PIP_2, and eventually IP_3 ,and is widely portrayed as a tumor suppressor in prostate cancer (258). In essence, it opposes PI3K, which is discussed above. However, depletion of PTEN is also exhibited in prostate cancer (Li et al., 2018; Wise et al., 2017). PTEN actually uses a 2-pronged approach to suppressing prostate cancer progression. First, it blocks oncogenic pathways such as PI3K and AKT, but also helps restore normal Ca^{2+} homeostasis by facilitating SOCE through PIP_2 production leading to IP_3-induced ER Ca^{2+} store release. Clinically, there are no current agonists that directly bind to and activate PTEN, however, there are many agonists that activate upstream proteins that upregulate PTEN expression (reviewed in(259)). Hence, PTEN agonists could present a new therapeutic target in treating prostate cancer, partially through regulating Ca^{2+} homeostasis.

In addition to AR directly regulating both STIM and Orai, it appears androgens also regulate upstream transcriptional regulators of STIM and Orai such as WT1/EGR1. Since

EGR1/WT1 play a vital role in regulation of STIM1, and thus SOCE, it is unsurprising they significantly impact prostate cancer progression. In support, examination of WT1 and EGR1 expression in several prostate cancer cell lines revealed mainly elevated WT1 expression coinciding with low EGR1 expression (260). However clinically, in some prostate cancer patient cohorts, EGR1 is overexpressed, and in *EGR1*-deficient mice, prostate tumorigenesis was impaired (261, 262). In this case, EGR1-induced STIM1 expression may be vital for AR activity and disease induction, while serving as an inhibitory feature of disease progression. There is also evidence this effect could be further exacerbated by faulty imbalance between EGR1 and its corepressor, NAB2 (261). Conversely, corroborative studies show that WT1 is important to tumor angiogenesis and cell migration in prostate cancer (263, 264), as well as inhibition of STIM1 and SOCE (172), which promote disease progression. Because WT1 and EGR1 work in a dual and opposing fashion to regulate STIM1 (172), considered together, timing appears to be paramount as EGR1 promotes tumorigenesis and may be reliant on NAB2 expression while WT1 promotes prostate cancer progression. Although the main role of EGR1 is transcriptional regulation of STIM1, interestingly, a group studying EGR1 binding to CpG sites in prostate cancer saw that CpG methylation was inversely correlated with disease severity, and that EGR1 binding was reduced in later stages of disease (265). This presents the possibility that CpG methylation and EGR1 binding could contribute to the mechanism of how EGR1 is inversely associated with disease progression as demethylation of EGR1 CpG-binding sites could be a potential target of prostate cancer therapy to facilitate EGR1 binding to suppress progression.

SOCE as a marker for disease progression also has been substantiated clinically. STIM1 and Orai1 expression are inversely correlated with Gleason Score (266). Because

Gleason Score is a representative marker for prostate cancer progression, this supports the model that in early stages of disease exhibiting AR+ status, STIM1 and Orai1 levels, as well as SOCE, are increased, whereas advanced AR- stages of prostate cancer exhibit lower STIM1, Orai1, and ultimately SOCE. In support, it has been further demonstrated in an androgen-sensitive cell line derived from a lymph node carcinoma of prostate cells, androgen deprivation resulted in downregulation of Orai1, and that Orai1 knockdown conferred resistance to apoptosis. This suggests that acquired resistance to apoptosis arises in part from decreased Ca^{2+} influx (200). Collectively, both in basic and translational research loss of SOCE appears to be a marker for disease progression.

c. Treatments targeting SOCE in Prostate Cancer

Therapeutically, there are several promising SOCE-targeting candidates for treatment of prostate cancer. For early stages of disease, Drebrin, an actin reorganizing protein (see table 1-2), may be a potential prostate cancer target. Drebrin has been shown to facilitate invasion through colocalizing with actin filaments and filopodia increasing Ca^{2+} influx (267). Although this would inhibit disease progression as AR status changes expression of STIM1 and Orai1, this is likely a key step in facilitating early stage progression of prostate cancer. A potential method to thwart Drebrin-induced invasion, is through the use of pyzaroles, such as 3,5-bistrifluoromethyl pyrazole (BTP2), inhibit SOCE. Pyrazoles are pharmacological inhibitors of Orai, and can be used to therapeutically block SOCE in a dose-dependent manner (268, 269). However, not only is Drebrin associated with a variety of cancers including prostate (267) and bladder (270) among others, but knockdown of Drebrin inhibits SOCE to the same extent as inhibition by BTP2, suggesting BTP2 may inhibit Drebrin (271). Although it has not been fully proven that BTP2 is associated with

Drebrin, it would strengthen an already known connection between Ca^{2+} channels and cytoskeletal organization and integrity. Therefore, using pyrazoles could effectively act as a Drebrin antagonist, leading to lower SOCE in presumably early stages of prostate cancer including High Grade Prostate Intraepithelial Neoplasia (HGPIN), which is a precursor for prostate cancer(272), or early AR+ stages. Although the distinction of Drebrin association with prostate cancer has been recently made known, this could be a potentially promising therapeutic target in early stages of prostate cancer, as well as other cancers where SOCE potentiates disease progression. For treatment of later stages of prostate cancer, in a first-in-human phase I clinical trial, mipsagargin, a prostate-specific membrane antigen-targeted SERCA inhibitor, was able to stabilize disease in patients with advanced prostate cancer and other solid tumors(273). By inhibiting SERCA, Ca^{2+} stores are depleted leading to activated SOCE, a known suppressor of prostate cancer progression during AR- stages. Thus, mipsagargin is a promising therapeutic target for late stages of prostate cancer by inducing SOCE.

Reflecting this, SOCE plays dual and opposing roles in prostate cancer that are receptor-status dependent. However, it is intriguing that prostate cancer and breast cancer, which both use hormone-based mechanisms for disease progression demonstrate different effects resulting from changes in SOCE. Although different, these changes are stark and conclusive which underscores the importance of studying SOCE in the context of disease progression. Because SOCE plays different roles in different prostate cancer stages, it is important to develop therapies that both potentiate and attenuate SOCE, as these could make treatment for a wide range of prostate cancer cases more feasible. Although biologics targeting SOCE are beginning to emerge, efforts should continue to be made to investigate other drugs targeting SOCE, such as PTEN agonists,

as well as Drebrin and SERCA inhibitors, as novel therapeutic strategies for prostate cancer.

IV. Glioblastoma

a. Introduction

Glioblastoma Multiforme (GBM) is the most common and aggressive brain malignancy and is characterized as a form of astrocytic tumor (274), arising from astrocytes, which are a subtype of glial cells, the most common cell type in the brain (275). As reviewed in (276), these astrocytes form as a result of Neural Stem Cell (NSC) differentiation that undergoes many intermediate steps including the formation of Multipotent Progenitors (MPPs) and Bipotential Progenitors (BPPs) (276). It is important to note that GBM is highly invasive and can spread throughout the brain. This occurs because not only does GBM exhibit high tumor heterogeneity, which often leads to recurrence (277), but during surgical removal, it is challenging to remove surrounding tissue. Therefore, it is paramount to find druggable targets to treat GBM.

A significant challenge in treating GBM is generating drugs that cross the Blood-Brain Barrier (BBB). The BBB consists of endothelial cells that form adherens and tight junctions (AJ and TJ respectively). On the luminal side of this barrier, endothelial cells possess efflux pumps such as ABC transporters that prevent influx of lipophilic molecules, toxic reagents and many drugs (277, 278). This severely limits the treatment options for GBM, contributing to the bleak therapeutic outcomes of this disease. As reviewed in (277), the current standard of care is maximal surgical resection followed by post-surgical treatment using alkylating agents such as temozolomide (which can cross the BBB (279)) in conjunction with radiation (280). Unfortunately, only ~10% of GBM patients survive 2 years

on this regimen (281). Immunotherapies are amongst the potential future strategies; the checkpoint inhibitors targeting Programmed Death 1 (PD-1), Programmed Death Ligand 1 (PD-L1) and Cytotoxic T-Lymphocyte-associated Antigen 4 (CTLA4) are all being targeted in clinical trials for recurrent GBM (282). However, the most promising targeted therapies consist of classes of GBM treatments targeting anti-angiogenesis, since not only is GBM among the most vascularized tumors (283), but VEGF is a major mediator of vascularization and has been linked to GBM progression (284). This can be therapeutically targeted with monoclonal antibodies, such as bevacizumab, an approach that has shown itself to be particularly effective in patients with recurrent GBM (285, 286). It appears that almost all GBM cases become recurrent, which demonstrates the lack of effectiveness in these targets in achieving prevention of relapse in primary GBM.

b. SOCE effects on Glioblastoma

There is considerable published evidence that GBM is highly dependent on Ca^{2+} signaling in general and SOCE specifically. For example, it has been shown that, compared to human primary astrocytes, malignant GBM cells derived from GBM patient explants exhibited increased SOCE and Ca^{2+}-Release Activated Ca^{2+} (CRAC) current (287). Further, it was shown siRNA-mediated knockdown of STIM1 and Orai1 inhibited invasion *in vitro* based on a matrigel transwell invasion assay (287). These and other prior studies [376,377] illustrate the potential of regulating SOCE as a therapeutic target for GBM(288, 289)(288, 289)(288, 289).

Considering the role of SOCE in GBM invasiveness, one might predict that EGR1 would also promote GBM invasion since it drives STIM1 expression (172). Consistent with this concept, gene expression profiles show that both STIM1 (290) and STIM2 (291) are

upregulated in primary GBM. Interestingly, Cyclin D1 transcription has been shown to be EGR1-dependent (292), which drives cell cycle progression while shRNA-mediated STIM1 knockdown also led to cell cycle arrest at G0/G1 in GBM (293); the implication is that STIM1 is required for EGR1-induced cell cycle progression. This is further supported by previous observations that SOCE is required for CDK2 phosphorylation, driving the transition from G1 to S phase (294). Additionally, EGR1 drives the expression of both EGFR and PDGFαR, both of which are associated with enhanced cell motility and metastasis (288), as reported in multiple GBM cell lines (288). Since both receptors are PLC-linked, it is highly likely that SOCE contributes to these effects, particularly considering the established role of Ca^{2+} in cell motility (see section 3A). Future investigations delineating the relative roles of EGR1, STIM1 and Orai1 in GBM proliferation and invasion may be informative.

Interestingly, EGR1 was originally identified as a tumor suppressor in GBM; NMDA-induced EGR1 expression was decreased in primary GBM and was associated with decreased patient survival (295). Further, WT1 expression is increased in GBM, which supports GBM proliferation (296), and can be a marker for distinguishing between astrocytoma and normal astrocytic cells (297). This unusual dichotomy is likely explained by differences in other factors, such as p53 (298), the presence or absence of which may determine whether EGR1 functions as a tumor promoter or a tumor suppressor in this cancer type. Further, whereas WT1 is a marker for grades II and III GBM, it is not present in recurrent GBM (299). Hence, the timing of their expression may ultimately determine their roles with WT1 promoting initial tumorigenesis and EGR1 driving a metastatic phenotype. If so, then the introduction of WT1 in recurrent GBM or EGR1 to primary GBM would be expected to drive opposing processes. Since EGR1 and WT1 also have mutually

opposing roles in STIM1 transcription, differences in SOCE are likely in GBM from different stages, although the extent to which that is correct has yet to be established.

c. Treatments Targeting SOCE in Glioblastoma

Imidazoles (see table 1-2) are a class of antimycotics used as inhibitors of SOCE channels, both *in vitro* and *in vivo* (300). Preliminary investigations using imidazoles have been performed as proof-of-principle regarding the potential of SOCE as a therapeutic target for GBM. SKF-96365 (1-[2-(4-methoxyphenyl)-2-[3-(4-methoxyphenyl) propoxy]ethyl-1H-imidazole) blocks cell proliferation and SOCE in GBM cells *in vitro* (289, 301). Although *in vivo* studies have demonstrated effectiveness of this drug on metastasis in breast cancer (193), some hurdles exist in GBM treatment. For example, SKF-96365 not only blocks Orai1, but also is a pan-TRPC antagonist as well (301). Because TRPC-mediated Ca^{2+} influx leads to myosin-actin contractions on the cells of the BBB(302), SKF-93635 inhibits this effect (303), thereby strengthening BBB integrity. As such, future investigations using more specific SOCE inhibitors are needed to assess the viability of SOCE as a GBM target *in vivo*. By understanding *in vivo* effects, further development of drugs targeting SOCE can be generated to treat GBM.

Overall, it is notable that, GBM is highly Ca^{2+}-dependent. Not only does Ca^{2+} homeostasis regulate BBB integrity, but also drives GBM progression. The therapeutic landscape is currently very bleak as it is difficult to effectively treat a highly heterogeneous tumor without flexibility in removing surrounding tissue to prevent recurrence. With that said, there are many Ca^{2+}-modulating therapeutic pathways that warrant further investigation and therapeutic strategies to further target to create improved approaches for treating GBM.

V. Myeloid Leukemia

a. Introduction

Leukemia is a group of cancers that arise from white blood cells generated from the bone marrow. Leukemia is stratified by the precursor cells from which it arises, which include lymphocytes and myeloid cells. Lymphocytic Leukemia derived from B-cells (and also sometimes T-cells), are broken down into chronic (CLL) and acute (ALL). In parallel, myeloid-derived Leukemia arising from the bone marrow are also broken up into chronic (CML) and acute (AML) reviewed in (304). The role of Ca^{2+} in the progression of myeloid-derived tumors is much more extensively described, which will be the focus of this section. Normally, leukocytes undergo multiple steps of maturation starting as Hematopoietic Stem Cells (HSCs) and later differentiating into mature immune cells. HSCs are mainly present in the bone marrow where they differentiate into multipotent progenitors (MPPs) and gradually lose their potential for differentiating into different lineages. Specifically, HSCs exist in 2 populations. Long-term HSCs (LT-HSCs) have life-long self-renewal capabilities and contribute to multiple lineages upon necessity, while Short-term HSCs (ST-HSCs) have limited self-renewal capabilities, but can give rise to MPPs (reviewed in (305)). In fact, LT-HSCs can also differentiate into ST-HSCs (306, 307). Subsequently, MPPs differentiate into either Common Lymphoid Progenitors (CLPs) or Common Myeloid Progenitors (CMPs).

CMP production is dependent on expression of 2 genes during MPP differentiation: FMS-like Tyrosine Kinase 3 (Flt3) and Vascular Cell Adhesion Molecule 1 (VCAM-1). During differentiation, MPPs undergo lineage-restricted differentiation, that are broken into 3 subgroups based on expression ($Flt3^{lo}VCAM\text{-}1^{+}$, $Flt3^{hi}VCAM\text{-}1^{+}$, and $Flt3^{hi}VCAM\text{-}1^{-}$) (305, 308, 309). $Flt3^{lo}VCAM\text{-}1^{+}$ subgroup has full multipotent potential, marking it the

"classical MPP" that can subsequently generate CMPs, whereas Flt3^{hi}VCAM-1^{+} cells typically precede differentiation into granulocyte/macrophage lineage-restricted progenitors (GMPs) or lymphocytes and Flt3^{hi}VCAM-1^{-} cells lymphocytic progenitors (309). Therefore, it is likely that canonical CMP generation proceeds through Flt3^{lo} selection, while non-canonical proceeds through Flt3^{hi} selection. Upon differentiation of MPPs into CMPs, CMPs differentiate into myeloid cells. However, aberrations in the differentiation process can lead to myelopathies including myeloid leukemia, which is the focus of this section.

Flt3 expression has been closely linked with AML progression. Hence, Flt3 expression is normally lost normal myeloid cell development, but expressed in most AML and some CML patients (310, 311). Further, roughly 1/3 of AML patients exhibit mutations in Flt3 which include constitutively activating internal tandem repeats (Flt3-ITD; 25% of AML patients) and D835 and I836 point mutations of the kinase domain (Flt3-TKD; 7-10% of AML patients) (310, 311). Although both mutations appear to be important, Flt3-ITD is more prevalent and of more clinical interest. In this regard, there is a stark contrast in patient survival in those with and without Flt3-ITD mutations (7% to 44% respectively) (312). Mechanistically, Flt3 mutations function through RTK signaling by facilitating downstream STAT3 pathway, which stimulates proliferation and survival (reviewed in (313)). Clinically, AML progression has poorer prognosis in response to higher allelic ratio of mutant to wild type Flt3 and larger size of the ITD (311). Furthermore, it has also been found that Flt3 mutations can be acquired during relapse when no original mutation was present but 75% of patients that originally have the mutation maintain the mutation through relapse (311). Hence, Flt3 mutations, especially Flt3-ITD, are important to AML

progression and have been a widespread target for therapies, which will be discussed below.

To treat AML, most patients start with induction therapy to achieve complete remission. Induction therapy usually consists of a “7+3 regimen” of 7 consecutive days of infusion with cytarabine (ara-C; antimetabolic agent) followed by 3 days of anthracycline (DNA-intercalating agent). However, other therapeutic options include FLT3-ITD inhibitors for those exhibiting this mutation (314) and monoclonal antibodies targeting FLT3, FLT3-ITD and other RTKs associated with initiating AML (313). Despite the promise of these therapies in targeting a variety of RTKs, long-term prognoses of patients with AML remains poor as a major challenge is targeting specifically malignant and not unaffected myeloid precursors (313). Thus, most AML treatments exist targeting RTKs, there is a need for novel AML-specific treatments that come with less off-target and clinical side effects.

Although CML arises differently than AML, a common similarity between these subsets of Leukemia is their reliance on RTK signaling. CML arises from splenomegaly and hyperactive bone marrow expanding the abundance of pluripotent hematopoietic progenitor cells and blood leukocytes (315). In CML, this occurs over a long (chronic) period of time followed by an acute crisis of an overabundance of undifferentiated myeloblasts (often referred to as blasts) (304), whereas AML arises from an acute massive increase in blast cells without the chronic phase preceding it. Although both CML and AML arise from blast crises, they have different genetic profiles both reliant on RTKs that initiate disease. For example, CML is well-established to be caused by Breakpoint Cluster Region-Abelson Murine Leukemia 1 fusion (Bcr-Abl) (316), that occurs during the incomplete differentiation of CD34 and CD90 myeloid progenitors (317), similar to AML. Bcr-Abl promotes cancer-promoting processes such as growth and proliferation as well as

downstream signaling of cancer pathways such as Ras, Raf, Jun, Myc and STAT (reviewed in (316)). Together, CML differs from AML in its initiating mechanism, but exerts its effects similarly by targeting RTKs for progression.

Unsurprisingly based on the mechanism of action of CML, currently, one of the most widespread treatments for CML are small RTK inhibitors such as Imatinib. Imatinib is an inhibitor of Bcr-Abl and has been shown as an effective therapeutic against CML. Specifically, in clinical trials examining Imatinib efficacy, it was shown that overall survival (OS) of patients who took Imatinib reached 85%, while 49-77% exhibited complete cytogenic response (CCyR) and 18-58% of patients exhibited a major molecular response (MMR). However, even those that demonstrate MMR initially are at risk for resistance to RTK inhibitors (316). Furthermore, approximately 1/3 of patients who discontinued administration of the drug exhibited molecular relapse (318), suggesting both the dependency on this drug for long-term survival and the transient nature of its effect simultaneously. In addition to Imatinib, there are other RTK inhibitors available such as Dasitinib (350x more potent second generation analog of Imatinib), Nilotinib (30-50x stronger affinity for Bcr-Abl than Imatinib), and Bosutinib (targets both Src kinase and Abl) that all exhibited drawbacks of low to modest clinical tolerability including gastrointestinal and pulmonary clinical side effects (reviewed in (316)). Hence, although these drugs may be promising for CML treatment, newer drugs with fewer or no clinical side effects are needed.

b. SOCE effects on Myeloid Leukemia

Leukemia is among the cancer types that is reliant on lower SOCE for disease progression. Previously, we showed minimal SOCE to be observed in 3 of 5 AML cell lines

examined (170, 319). Yet, the underlying mechanistic link between dysregulation of SOCE and leukemia is poorly defined.

One possible mechanism is through changes in WT1 and EGR1, whose expression and activity are known to be dysregulated in AML. Hence, whereas WT1 expression is normally lost during leukocyte maturation, it is expressed in 73-93% of primary AML samples (170, 320, 321). Further, inactivating WT1 mutations are observed in 10–12% of patients, which is a negative prognostic indicator for AML (321, 322). WT1-inactivating mutations have been linked to the failure of WT1 to direct TET2 to its transcription site, leading to hypermethylation signatures that resemble TET2 mutant-induced hypermethylation (323). Because WT1 expression is lost during leukocyte maturation and AML is associated with lower SOCE, it is quite possible that loss of SOCE is a prognostic marker for leukemia, and could be associated with enhanced WT1 expression and activity. This would be an interesting future direction to examine, as it could reveal a previously unknown mechanism in how SOCE drives AML.

Conversely, EGR1 is expressed during normal myeloid differentiation (324, 325) and may prevent leukemogenesis through inhibiting oncogenes E2F-1 and c-myc (326, 327). Furthermore, it has been demonstrated that HL60 AML cells, which normally have low SOCE, can induce EGR1 expression in response to vitamin D3, which leads to differentiation into monocytes and recovered SOCE (328-330), which suggests that Ca^{2+} plays a vital role in differentiation and could be a powerful tool in preventing disease progression.

Another possible mechanism contributing to SOCE effect on myeloid leukemia is deregulation of STIM and Orai proteins. In support, it has been shown in Bcr-Abl-

dependent CML, that STIM1/Orai1 ratio is deregulated and TRPC1 expression is decreased leading to suppressed SOCE (331). Notably, the main culprit in SOCE suppression here is not the levels of Orai1 and STIM1 expression but actually the stoichiometry between STIM1 and Orai1. In support, it has been shown previously that stoichiometric imbalance between STIM and Orai, actually leads to SOCE suppression (332-334), even if Orai1 is overexpressed (335). This is important since it was found that Orai1, Orai2, STIM1 and STIM2 are actually overexpressed, but disproportionately, at the transcript level, while Orai2 and STIM2 levels are overexpressed at the protein level in HL60 AML cells with knockdown of Orai1 and Orai2 leading to inhibition of migration via focal adhesion (336). Therefore, it is possible HL60 cells begin with a disproportionate amount of STIM and Orai proteins, that lead to suppressed SOCE compared to differentiated myeloid cells which subsequently facilitates cancer-driving pathways such as PKC which can inhibit Orai1 (see melanoma section) as well as deregulate Mitochondrial Redox homeostasis in AML (337), but knocking down Orai proteins leads to inhibition of Ca^{2+}-dependent cancer-related pathways such as focal adhesion regulation (336). Interestingly, time appears to be a factor in their activity, as in early stages of migration, Orai2 knockdown induces a more significant inhibition of migration, while Orai1 knockdown contributes in later stages (336). Further, this is supported by evidence that knockdown of STIM1 in HL60 cells can lead to impaired activation of Ca^{2+}-dependent cancer driving pathways including AKT, Src, and cytoskeletal remodeling Rac2, which subsequently impairs AML progression (338). Considered together, it is likely that deregulation of the ratio of STIM and Orai proteins, which leads to SOCE suppression, could be a mechanism that can be further extrapolated therapeutically for the treatment of ovarian cancer.

VI. Concluding Remarks

Considered together, this presents a wide body of evidence that the relationship between Ca^{2+} and cancer is not so much linear, as it is contextual in nature. For example, many hormone-induced processes such as ER and AR, as well as receptor-mediated processes such as AKT and Src tend to rely on higher levels of SOCE. Conversely, there are also some contexts where gene expression and activity of transcription factors governing STIM1 and Orai1 expression (such as WT1/EGR1) can facilitate lower SOCE levels leading to cancer progression. This brings to light the concept that Ca^{2+} signaling can lead to dual and opposing effects on cancer progression. In the next section, we will discuss melanoma specifically. While melanoma progression was thought to rely on higher levels of SOCE, recently previous work done by our group as well as the work discussed in these investigations demonstrates that just like throughout cancer, in some contexts lower SOCE levels can be indicative of enhanced invasiveness and progression as well.

Part 3: Melanoma

I. Introduction

Skin cancer, including melanoma as well as other forms of skin cancer, while trailing cancers such as breast and prostate cancer in total incidence, are the most common type of malignancy among Caucasians (339). Although, the most common forms of skin cancer are carcinomas including Basal Cell, Squamous Cell, and Merkel Cell, the deadliest and most challenging skin cancer to attenuate is melanoma. Melanoma is the fifth deadliest cancer among men and women (188). Not only is it deadly, its incidence is rising especially in younger patients as evidenced by surpassing breast cancer as the most prevalent cancer among women under 40 (340). Melanoma arises from neural-crest derived melanocytes, which are the pigment-producing cells found in the skin, ears, eyes, meninges, and other mucosal surfaces (341). This disease is normally classified in 2 subtypes, sporadic and familial, with sporadic being considerably more common (342). Thus, the high prevalence and mortality of this disease illustrates the importance of finding novel treatments for this disease.

Melanoma, exhibits a significant sex bias, in which women are diagnosed more frequently at younger ages and men are diagnosed more frequently at older ages (343). There are 2 distinct factors that contribute to this phenomenon. First, younger women have a higher likelihood to use artificial tanning booths, which emit a UVA concentration approximately 13 times higher than peak summer sun exposure. The likelihood of melanoma is raised 16-20% if tanning booths have ever been used; this likelihood is doubled when used before the age of 35 (344, 345). Second, melanoma appears to be heavily regulated by hormones. For example, estrogen binding to ERβ has been shown

to occur in early stages of melanomagenesis and is a marker for melanoma proliferation (345, 346). However ERβ expression is decreased during melanoma progression and its expression is actually inversely correlated with progression into later stages (347). This is likely because ERβ induces phosphorylation of ERK1/2 to promote proliferation (348), but inhibits the PI3K/AKT pathway, thereby inhibiting invasion (347). Therefore, it appears the timing of ERβ expression and function is key to determining the role it plays in melanoma progression. Further, during menopause, ERβ diminishes rapidly, leading to impaired melanomagenesis and progression for post-menopausal women (345). Whereas women tend to have decreased Hormone Receptor (HR) over time and use HR signaling as a protective factor against melanoma progression, the opposite is true in men. Unlike women who have diminished production of hormones over time, men produce androgens throughout their lives (349) and androgens promote melanomagenesis and progression (345). This is likely because not only does testosterone inhibit protective enzymes against oxidative stress like Superoxide Dismutase (SOD) and Catalase (350), but AR directly promotes transcription of miRNA that suppress the inhibition of melanoma-inducing oncogenes, such as microphthalmia-associated transcription factor (MITF) and leads to subsequent invasion (351). Therefore, women, especially post-menopausal women, have a survival advantage over men (345). In conclusion, both behavioral factors such as frequent exposure to artificial tanning, as well as hormonal factors, such as androgen production, lead to a considerable sex bias for age at diagnosis of melanoma.

The most common cause of melanoma is UV radiation (UVR). UVR is considered a “complete carcinogen” (352) and consists of long wavelength UVA (320-400nm), shorter wavelength UVB (290-320), and shortest wavelength UVC (~200-280nm), the last of which is blocked by the ozone layer and does not reach the earth (353). UVR is well known

for its role in inducing melanin production, with melanin acting as a protecting factor against UV-induced damage in skin (354). Therefore, the relative lack of melanin in Caucasians makes them the most susceptible to UV-induced DNA damage and, ultimately, melanoma (355). Although about 95% of the rays absorbed in skin are UVA, UVB is more heavily associated with skin cancer as it directly induces DNA damage (352). The response to UVB starts in keratinocytes; UVB-induced DNA damage leads to αMelanin-Stimulating Hormone (αMSH) production on the keratinocytes which binds to Melanocortin 1 Receptor (MC1R) on the melanocytes, which stimulates melanin production and whose variants lead to either protective eumelanin, creating darker skin and hair color or pheomelanin production leading to pale skin, red hair and increased melanoma risk (356-358). Melanin is then transported in melanosomes to the keratinocytes where it is positioned facing outward from the nucleus toward the sun to act as a shield against further DNA damage (358). Unfortunately, each UV exposure leads to the introduction of C→T and G→T mutations, ultimately leading to DNA damage and/or mutations that tend to promote melanomagenesis and progression. However, while it is clear that UVR is the major driver of melanomagenesis, the molecular pathways linking UVR and driver mutations is somewhat unclear since the most common mutations associated with melanoma do not have a UV signature mutation of C/G→T. For example, $BRAF^{V600E}$, which is found in 50% of melanoma cases (341, 342, 359), does not consist of a C/G→T mutation, and is UV-independent (360). Conversely, NRAS mutations tend to appear in older patients with chronic sun exposure (reviewed in (361). The most common NRAS mutations occur at G12 (G12D, G12S), G13 (G13R), and Q61 (Q61K, Q61R, Q61L, Q61V, Q61H) (362), which are found in 15-20% of melanoma cases (361), do not have an association with MC1R (363) and are also not UV-signature mutations. Hence, despite

the fact that NRAS mutations are not UV signature mutations, UVR may be required for transformation associated with NRAS mutations. The remaining 30-35% of melanoma exhibit a variety of mutations including Neurofimbrin 1 (NF1), KIT, CDKN2A, PTEN and many others (342). Considered collectively, it is surprising that, despite the well-established role of UVR in melanomagenesis and progression, the underlying molecular mechanisms remain very unclear. A more fundamental understanding of the disease is needed to address this shortcoming.

II. SOCE:

1. Src and Increased SOCE

As previously discussed in (364), melanoma is a highly heterogeneous disease with SOCE demonstrating differential, context-dependent roles in melanoma progression like many other cancers as discussed in Part 2. Hence, SOCE has been strongly associated with disease progression in many different tumor types (365). Similar observations have been made in melanoma in some contexts. For example, it has been shown that Orai1 and STIM2 expression and activation, which lead to higher intracellular Ca^{2+} levels, can induce a shift between proliferative and migratory activity (366), suggesting that timing of SOCE can play an important role in melanoma disease progression. This effect is demonstrated by the fact that B16BL6 mouse melanoma cells have enhanced invasiveness resulting from higher SOCE because higher intracellular Ca^{2+} levels lead to higher levels of constitutively active PKB/AKT and increased cell survival (367). Moreover, in this case, PKB is activated by mitochondrial Ca^{2+} flux that shunts Ca^{2+} away from Store-Operated Channels. In turn, this enables a feedback mechanism with mitochondrial Na^{+}/Ca^{2+} exchanger (NCLX). NCLX further facilitates trans-mitochondrial Ca^{2+} flux contributing to intracellular Ca^{2+} shuttling (367) and is known to

induce SOCE through regulating Orai1 redox at C195 (368, 369). Further, the effect of this signaling cascade was supported by SOCE coupling with lipid rafts to activate lipid raft-residing calmodulin and subsequent activation of protein tyrosine kinase, Src, as well as AKT (370). Because it has been shown that tyrosine phosphorylation by Src is essential for biological function of AKT (371), it is likely that lipid raft-activation of Src phosphorylates and activates AKT in a Ca^{2+}-dependent manner and leads to melanoma progression through Ca^{2+}-activated Calmodulin binding to Src kinase which administers an inhibitory phosphorylation of PP2A, preventing dephosphorylation and inhibition of AKT (370). Interestingly though, the relationship between SOCE and Src activation goes beyond just AKT activation. For example, Ca^{2+} oscillations activate Src to recruit cortactin and the adaptor protein, SH3 containing protein 2a (TKS5), to promote invadopodia-induced degradation of the ECM through actin remodeling (113), suggesting that Src activation could have dual effects on melanoma progression, both of which are Ca^{2+}-dependent. The concept that SOCE drives melanoma progression is further supported by the observation that SOCE blockade through either genetic or pharmacological strategies decreases invasion both *in vitro* and *in vivo* (372). Thus, it appears that SOCE can induce melanoma progression when melanoma is highly dependent on Src signaling.

Currently, there are 2 strategies for targeting melanoma in the context of suppressing melanomas reliant on enhanced SOCE. First, Pyrazoles are a class of drugs that are heterocyclic nitrogen-containing molecules that have been shown to inhibit SOCE. A commonly used pyrazole, 3,5-Bis(trifluoromethyl)pyrazole (BTP2/Pyr2) has been shown to block both Orai1-mediated SOCE and TRPC-mediated Ca^{2+} entry (373-375) and inhibit melanoma in some contexts (376). Although these drugs have not undergone clinical trials in melanoma patients, the potential drawback of these drugs is globally inhibiting SOCE,

could have off-target effects on melanoma that have not yet been examined. Second, BRAF inhibitors, such as Vemurafenib and Trametinib, are currently a widespread therapeutic for melanomas, but a major drawback is that resistance is acquired in approximately 50% patients after 6 months (377). This resistance occurs mainly because of reactivation of the MAPK pathway. In this regard, Src activation has been shown to be an important tyrosine kinase that can reactivate the MAPK pathway, which contrives Src activation important in these melanoma types (378). In this regard, the most commonly Src-activated melanomas are those exhibiting Src pY416, for which inhibitors have been generated (379), and have undergone clinical trials (380). However, clinical trials have been moderately effective at best only providing clinical benefit to less than a quarter of patients (380). Novel Src inhibitors continue to be examined (381), and could perhaps be more effective than previous generations of Src inhibitors. However, a new strategy for treating melanoma has been the development of inhibitors that have dual roles as pan-RAF inhibitors (including targeting of BRAF) and Src inhibitors (CCT196969 and CCT241161) (378). Moreover, these inhibitors appear to be effective in both cells harboring BRAF and NRAS mutations (378), which broadens the candidacy of these therapeutics. Clinical trials assessing the efficacy of these drugs were planned for 2015 (378), but there is no update on results from these studies. Yet, this offers a novel and exciting strategy to combat melanomas in specific contexts, and may present fewer off-target effects than global SOCE inhibition via Pyrazoles. Thus, administering a dual inhibitor for BRAF and Src could provide a method to permanently turn off the MAPK pathway and prevent resistance in BRAF mutant melanomas that are highly dependent on Src signaling.

Considered together, some subsets of melanoma rely heavily on enhanced intracellular Ca^{2+} levels and SOCE. SOCE can act not only as a dynamic switch of cellular activity, but also functions as an important mediator for cell signaling that enhances cell survival and drug resistance. As melanoma is heterogeneous, it is important to understand which subtypes of melanoma exhibit reliance on enhanced SOCE. Characterizing a profile of melanoma subtypes that rely on enhanced SOCE for progression could increase the efficacy of targeting SOCE as a novel therapeutic and could improve personalizing medicine for patients based on the genetic background of their melanomas.

2. Wnt5a and Decreased SOCE

As noted above, melanoma is highly heterogeneous; in some contexts, the role of SOCE in melanoma is fundamentally changed. Wnt5a is an oncogene strongly associated with aggressive melanoma (382-384). In a recent study from our group, we observed that highly invasive Wnt5a-expressing human melanoma cells exhibited marked SOCE suppression (385). Further, it was demonstrated that knockdown of Wnt5a in invasive cell lines raised SOCE and inhibited invasiveness, while overexpressing Wnt5a in non-invasive cells had the inverse effect (385). This effect was mediated by PKC, which suppresses SOCE via phosphorylation of Orai1 S27 and S30 (385, 386), which provides a potential mechanism for how Wnt5a induces SOCE suppression. Since PKC appears to be the mediator between Wnt5a and SOCE suppression, it is logical to associate PKC with invasive melanomas that rely on suppressed SOCE. This logical assumption is supported by that fact that PKC is associated with melanoma progression in a context-specific manner, that is discussed extensively in (387). Although PKC facilitates melanoma progression in a context-specific manner, it is important to note this occurs across many different types of melanoma including BRAF and NRAS mutant subsets.

Interestingly, PKC has been shown to negatively regulate AKT (388), which as described previously facilitates progression in melanomas reliant on enhanced SOCE. This puts considerable intrigue into the relationship between AKT and PKC, which could be significant in understanding how Ca^{2+} regulation affects melanoma. Because melanoma is highly heterogeneous with SOCE playing opposing context-dependent roles depending on the subtype, AKT and PKC could provide a biological switch that each melanoma utilizes differently depending on the genetic mutations of the melanoma. Although the relationship between AKT/PKC and common genetic or UV-induced mutations have not been examined, it has been previously suggested that targeting PKC could be effective for NRAS mutant melanomas (389), which provides insight into where to commence these investigations. Therefore, elucidating and understanding the role of AKT and PKC in melanoma progression and their relationships with common genetic mutations could shed light on molecular mechanisms underlying the context-specific roles of SOCE in melanoma progression. Understanding these mechanisms would not only be instrumental in clarifying some of the heterogeneity in melanomas, but also improve targeting of specific Ca^{2+}-dependent pathways in specific melanoma contexts as a novel therapeutic strategy across different melanomas.

The heterogeneity of melanoma makes generating treatments extremely challenging, which is illustrated by the fact that currently there are minimal therapeutic strategies targeting Ca^{2+} that exist for melanoma. It has been discussed earlier that melanomas reliant on AKT and enhanced SOCE could benefit from treatment with BRAF/Src dual inhibitors, but treatments for melanomas reliant on PKC and suppressed SOCE must also be addressed. Although treatments such as previously aforementioned PTEN-upregulating molecules, as well as Drebrin, would all theoretically increase SOCE

and inhibit melanoma progression in melanomas that are Wnt5a-positive and rely on suppressed SOCE (385), the most promising treatments are Wnt5a biologics. Although most Wnt-targeting molecules target the canonical pathway (Wnt3a), other biologics targeting the non-canonical pathway (Wnt5a) are currently being investigated. For example, Box5 is a hexapeptide containing a t-butyloxide carbonyl developed by the laboratory of Tommy Andersson that mimics a fragment of Wnt5a (390). This peptide antagonizes the effect of Wnt5a by binding to the frizzled 5 GPCR (FZD5), which directly inhibits Wnt5a activation of PKC. This molecule has been developed as a Wnt5a antagonist in metastatic melanoma (390), and has been shown to inhibit both migration and invasion of melanoma cells *in vitro*. Although this molecule is a derivative of Foxy5, an N-formyl group-containing small molecule agonist of Wnt5a that has undergone clinical trials for cancers reliant on enhanced SOCE, such as breast cancer (391), the effects of Box5 have not yet been examined *in vivo* and this molecule has not undergone clinical trials. Other Wnt5a biologics have been developed, which mainly act as Porcupine inhibitors. Porcupine is a membrane-bound O-acetyltransferase that facilitates acylation of Wnt molecules, which is required for Wnt secretion (392). A specific example of this within industry is LGK974 (Novartis), which is currently undergoing clinical trials for melanoma (391). Together, there is promise in targeting Wnt5a as a novel class of therapeutics that could be effective in melanomas reliant on suppressed SOCE.

In conclusion, because melanomas are highly heterogeneous, conversely to melanomas that utilize AKT and enhanced SOCE, some melanomas utilize Wnt5a/PKC and suppressed SOCE for progression. This necessitates discovering and generating novel drugs that enhance SOCE to combat melanoma in some contexts. The most effective way to target these melanoma subtypes is to explore drugs that inhibit the non-

canonical Wnt5a pathway, especially Wnt5a itself. Currently drugs targeting this pathway are still being explored. Although understanding of the *in vivo* effects of Wnt5a antagonists like Box5 leave more to be desired, there is promising progression of novel therapies inhibiting Wnt5a secretion (Porcupine inhibitors) and activity (Box5) ongoing, which offers exciting new opportunities to treating Wnt5a-expressing melanomas reliant on lower SOCE for progression.

3. RAS, RAF and Altered SOCE

RAS and RAF family of proteins are small GTPases that facilitate transduction of signals from plasma membrane growth factors to downstream pathways regulating proliferation, migration and survival (393). Mutations within RAS and RAF can lead to constitutive activation and cancer progression including in melanoma, where 15-20% of all melanomas exhibit NRAS mutations (361) and BRAF accounts for up to 50-60% of melanomas (394). Although well-known for being an oncogenes involved in the MAPK pathway (395, 396), recent attention has been given to RAS and RAF interaction with Ca^{2+} signals. For example, when compared to one another, it was shown that while melanoma exhibiting $NRAS^{Q61R}$ mutations led to increased sensitivity of extracellular Ca^{2+} withdraw and lower SOCE, $BRAF^{V600E}$ mutations led to enhanced cytosolic Ca^{2+} increase and SOCE (397). In fact, there appears to be mounting evidence that NRAS and BRAF mutations actually exert different effects on SOCE in cancer. For example, it has been shown that $KRAS^{G13D}$ mutation leads to suppressed SOCE, ER Ca^{2+} release, and mitochondrial Ca^{2+} uptake leading to enhanced survival in colorectal cancer. Further, MEK inhibition, which functions downstream of RAS and RAF, enhanced STIM1 expression and rescued this effect (393). Finally, it has been shown that BRAF resistant cells also exhibit upregulated Wnt5a expression which is likely associated to lower SOCE (364, 385, 398). Thus, there

appears to be a relationship in which RAS is associated with lower SOCE and RAF is associated with higher SOCE. A possibility for this difference is that RAF has been shown to be activated via Src to facilitate changes in Ca^{2+} homeostasis (399), which may provide an alternative context that is already associated with increased SOCE (see Part II-1) for RAF activation independent of RAS. In addition, RAS being upstream of RAF is involved in activating many other pathways. For example, it has been shown that PI3K signaling, which is a downstream effector of NRAS (400), was inhibited by STIM1 suppression (254). Therefore, it is plausible that NRAS mutations contribute to a variety of downstream pathways including PI3K signaling, whereas BRAF mutations drive changes in MAPK pathway leading to dual and opposing effects on SOCE. Even though we have some insight into RAS and RAF effects on SOCE, the molecular mechanisms driving these changes still remains not fully clear and should be investigated further. Considered together, as melanoma is very heterogeneous, as are the driver mutations regulating progression through cellular functions such as SOCE, which offer novel avenues of research in creating potential therapeutics combating melanoma.

III. TRP Channels:

Melastatin, the protein defining the TRPM channel family, is produced on the N-terminal side of the TRP protein (401), was originally discovered in melanocytes, and was shown to be downregulated in melanoma cells compared to melanocytes (402). Hence, melastatin has been characterized as a tumor suppressor in melanoma (403) and the potential involvement of the TRPM channel family in melanoma has been carefully investigated. For example, TRPM1, the founding member of the TRPM channel family (404) is heavily expressed in normal human epidermal melanocytes, however, its expression is lost as cells progress through the radial and vertical growth phases; TRPM1

expression is ablated in metastatic melanoma (402). As a result of these findings, TRPM1 expression is a therapeutic marker for disease-free survival (404). Mechanistically, it is proposed that melastatin may facilitate differentiation of neural crest stem cells into melanocytes (402). However, it is also feasible that expression of TRPM1-mediated Ca^{2+} entry counteracts Wnt5a-mediated SOCE suppression, thereby attenuating the progression of Wnt5a-expressing, aggressive melanomas. Consistent with this concept, TRPM1 expression and intracellular Ca^{2+} levels are both lowered in rapidly dividing melanocytes, compared to slower growing and differentiated melanocytes. This is likely because induction of p53 by ultraviolet B (UVB) leads to inhibited TRPM1 expression and Ca^{2+} influx (405). Therefore, a potential alternative mechanism by which UV, and specifically UVB, induces melanomagenesis is through suppression of TRPM1 expression and Ca^{2+} influx, whereas TRPM1 inhibits this process by slowing melanocyte growth and promoting differentiation. Although Wnt5a status was unknown in these investigations, it is likely that rapidly developing melanocytes exhibited high Wnt5a as they transform and become malignant melanoma cells. Overall, activation of TRPM1, and its subsequent promotion of Ca^{2+} influx, leads to tumor suppressive roles such as promotion of differentiation and suppression of growth and proliferation in melanoma cells.

Currently, little is known about what specifically activates TRPM1 (406), especially in melanoma, although it is likely activated by GPCRs (407). One potential mechanism is TRPM1 is kept closed by metabotropic glutamate receptor 6 (mGlur6), which is a GPCR predominantly located on retinal cells (408). In support, a specific subset of melanoma patients exhibit melanoma-associated retinopathy (MAR) and TRPM1 is the likely link between melanoma and MAR (409). Additionally, it has been previously shown that mGlur6 antagonists transiently open TRPM1 channels in mouse retinal cells (410),

therefore it is likely mGlur6 is the predominant regulator of TRPM1 in melanoma. Once it is clearly determined how TRPM1 is activated, TRPM1 agonists, such as potentially mGlur6 antagonists, could be a promising candidate for novel therapeutic treatments for melanoma as a way to slow progression and potentially induce differentiation of melanocytes.

Besides TRPM1, other TRPM channels such as TRPM7 and TRPM8, as well as TRPV1, have been demonstrated to play a role in melanoma progression through various mechanisms. First, TRPM7 can act as a tumor suppressor in melanoma by preventing the accumulation of cytotoxic intermediates of melanin synthesis in melanophores (fish equivalent of melanocytes) (411) leading to the detoxification of melanocytes (412). In addition, TRPM7 has the capacity, through Ca^{2+} influx, to activate Ca^{2+}-dependent protease, m-calpain, (411), which inhibits focal adhesion (413), and in turn likely leads to anoikis. In this regard, TRPM7 agonists have been identified (414, 415), but have not undergone clinical trials. Thus, TRPM7 remains a promising therapeutic target in the treatment of melanoma. Second, TRPM8 has also been demonstrated to act as a tumor suppressor in melanoma. This is demonstrated by the fact that menthol has been shown to inhibit melanoma cell viability in a dose-dependent manner through activation of TRPM8, leading to increased Ca^{2+} influx (416). This increased Ca^{2+} influx has been shown to cause Ca^{2+}-dependent cell death in melanoma cells (417), an effect that intriguingly also occurred in capsaicin-induced TRPV1 activation. Although capsaicin-induced TRPV1 activation leads to a similar raise in intracellular Ca^{2+}, the downstream effects are slightly different. Whereas TRPM8 activation can suppress cell viability and has been proposed to be an effect of Ca^{2+}-dependent inhibition of cell cycle progression (416), TRPV1-induced Ca^{2+} entry leads to activation of calcineurin, which suppresses expression of p53

transcriptional repressor, ATF3, subsequently activating p53, and inducing programmed cell death (418). Therefore, different TRP channels activate different Ca^{2+}-dependent pathways, even if they all induce similar increases in intracellular Ca^{2+} entry. In this regard, biologics targeting TRPM1, TRPM7, TRPM8, and TRPV1 are currently being investigated (419), and could provide novel therapeutics preventing melanoma progression, through activation of different Ca^{2+}-dependent pathways that attenuate melanoma. However, collectively, it appears that TRP channels play many roles, mainly as tumor suppressors in preventing melanoma progression, and should continue to be further investigated as potential melanoma therapeutics.

IV. Melanoma Treatments

Recently, melanoma treatments have been revolutionized by the emergence of immunotherapies. Currently, there are 2 major approaches to treating metastatic melanoma which include targeted therapies and immunotherapies (420). Immunotherapies are an exciting new class of therapeutics that were designed based on the rising melanoma incidence observed in immunosuppressed patients (421). Immune checkpoint inhibitors targeting Cytotoxic T-Lymphocyte Antigen 4 (CTLA4) (ipilimumab) and Programmed Cell Death-1 (PD1) (Pembrolizumab) have shown significant promise and are currently being tested in clinical trials in conjunction with targeted therapies. Targeted therapies include inhibitors of the Mitogen-Activated Protein Kinase (MAPK) pathway such as Vemurafenib, which specifically targets the oncogenic $BRAF^{V600E}$ mutant and the MEK inhibitor Trametinib (422, 423). Unfortunately, this strategy has demonstrated only short-term success thus far due to drug resistance and relapse through reactivation of MAPK or PI3K/AKT pathways, which can lead to decreased immune function or epigenetic changes (reviewed in (424)). Interestingly, Vemurafenib has been

shown to increase intracellular cytosolic Ca^{2+} levels coincident with initiation of an ER stress response (425), implying that ER Ca^{2+} release may contribute to its effectiveness. It is possible that this transient effect occurs because raising intracellular Ca^{2+} inhibits progression transiently followed by relapse in response to eventual Ca^{2+}-dependent PI3K/AKT activation in conjunction with immune suppression, important factors leading to melanoma progression. Considered in combination with the observations above, these observations highlight the potential significance of investigating Ca^{2+} signaling in the design of future therapeutic strategies for the treatment of melanoma.

Table 1-2: Ca^{2+} Therapeutics For Cancer

Non-SOCE/SOCE	Class of Drug Target	Drug	Specific target of drug	Mechanism of Action
Non-SOCE	Voltage gated	Amlodipine	L/N-Type	Binds directly to channel and blocks external surface
		Diltiazem	L/T-type	Decreases basal $[Ca^{2+}]_i$
	TRP	SOR-C13	TRPV6	Inhibits TRPV6 activity
		Capsazepine	TRPM8	Inhibits TRPM8 activity
	P2X	BBG	P2X7R antagonist	Competitive inhibition
		oATP	P2X7R agonist	
		AZD9056		
		eATP		Bind to N-terminal domain
		Alu-RNA		P2X7R agonist- bind to C-terminal domain
	Ca^{2+}-related Transcription Factors	Cyclosporin A	NFAT	Blocks nuclear translocation of NFAT
	Pumps	Thapsigargin/Mipsagargin	SERCA	Blocks ATPase activity
		Cyclopiazonic Acid		
		2,5-di-tert-butylhydroquinone (BHQ)		
		CXL-017		Enhanced lysosomal Ca^{2+} release, blocks SERCA ATPase activity
		Ipramine Blue		
		Sodium Orthovanadate	PMCA	Inhibits PMCA activity
SOCE	SOCE activity	CAI	SOCE	Targets anti-apoptotic, Mcl1
		Drebrin		Promotes actin reorganization and increased SOCE
		RP4010		Synergistic with RTK inhibitor, preventing SOCE activation
	Orai channel	Diethylbestrol	Orai	DES may bind to steroid binding pockets in Orai channels or may modify Orai channel properties
		BTP2/Pyr2, Pyr3	Pyrazole	Block STIM1, Orai1, TRPC3, can interact with extracellular surface of Orai channels
		SKF-96365	Imidazole	

Table 1-2. Ca^{2+} Therapeutics for Cancer. Therapies that either target Non-SOCE- or SOCE-based mechanisms of Ca^{2+} regulation. Within Non-SOCE, classes of drugs include drugs targeting VGCC, TRP, and P2X channels. Within SOCE, classes of drugs include those targeting multiple modulators of SOCE (SOCE) or Orai or STIM1 individually. Known mechanisms of action for each drug are listed as described.

Part 4: Cholesterol

I. Cholesterol in Cancer

1. Introduction

Evidence for a role of cholesterol (CHL) in cancer cells was first discovered in the early 1900s (426, 427). Indeed, CHL levels tend to be higher in cancer (428). Hence, it has been shown that increased serum CHL levels have been widely associated with increased risk of a variety of cancers including colon, rectal, renal, prostate, testicular and breast cancer among others (426, 429). Additionally, previous research showed melanoma cell CHL uptake contributed to melanoma progression *in vivo* (430). Furthermore, it has been shown that CHL facilitates oncogenic activities such as GPCR and RTK signaling, and lipid raft production (429) perhaps providing mechanistic insight into CHL contribution to cancer progression. Finally, it has also widely been accepted that metabolic disruptions such as changes in CHL levels are now considered a “cancer hallmark” (431). Thus, CHL production, processing, and metabolism is a potentially paramount avenue for cancer research.

As the role of CHL in cancer has gained attention in recent years, CHL levels have also been examined as potential causes of melanoma. In fact, it has been demonstrated that melanoma cells are more sensitive to changes in intracellular CHL transport, potentially through CHL regulating cell-surface expression of integrins that are facilitate migration and metastasis (reviewed in (428)). Hence, the introduction and wide-spread use of statins for the control of clinical CHL levels has facilitated research of the association between statins and cancer progression. Hence, evidence suggests that statins inhibit melanomagenesis (432) and slow progression (433). Also, statin-

independent therapeutics targeting CHL biosynthesis pathways have shown suppressed metastasis (434). Thus, a clear therapeutic target has emerged to combat melanoma.

CHL association with melanoma metastasis has even been shown on a population science level. It is well established that minority groups such as South Asians (Indian subcontinent), Filipinos, Hispanics, and African-Americans have increased susceptibility to dyslipidemia and other cardiovascular diseases associated with aberrant CHL regulation compared to Caucasians (435, 436). Additionally, although Caucasians have a 27-fold higher likelihood of melanomagenesis, the 5 year survival rate is 17.8% lower in African Americans (437), and also significantly lower in Hispanics with both African-Americans and Hispanics usually presenting more advanced tumor progression at diagnosis (438). Further, it is known that cancer cells rely on increased CHL levels that can occur through either enhanced CHL biosynthesis via the Mevalonate Pathway or enhanced uptake of CHL via Low Density Lipoprotein Receptor (LDLR). Together, this provides evidence that CHL facilitates disease progression to some capacity. Thus, as CHL has wide ranging effects across multiple populations, there is a clear need to investigate the role of CHL in cancer as a future potential therapeutic.

2. CHL and SOCE

CHL has previously been established as a negative SOCE regulator. For instance, it was reported that CHL depletion enhanced SOCE in both human embryonic kidney (HEK) 293 and rat basophilic leukemia (RBL) 2H3 cells since CHL can directly bind to Orai1 in an N-terminal region termed “CHL binding” (CB) region between amino acids 74-83 leading to steric hindrance (439, 440). Interestingly, the effect of CHL on STIM-Orai interaction is debatable. For example, the Romanin group showed while CHL had no effect on STIM-Orai interaction, it bound directly to Orai1 in a region critical for

the STIM-mediated transition to the open state (440). However, the Vaca group showed that CHL bound to the SOAR region of STIM1, where depletion of CHL induces SOAR detachment from the plasma membrane to associate with Orai1 (441). Hence, CHL appears to play a role in the regulation of SOCE but the exact mechanism of how CHL regulating SOCE leads to cancer progression remains unknown.

II. CHL Production via the Mevalonate Pathway

1. Introduction to the Mevalonate Pathway

CHL is mainly produced within cells via the Mevalonate Pathway which converts Acetyl-CoA into sterol isoprenoids, as well as non-sterol isoprenoids such as heme-A, dolichol, ubiquinone, and isopentenyl tRNA (442). In brief, the Mevalonate Pathway has many intermediate steps, the first of which is combining 3 molecules of Acetyl-CoA to form 3-hydroxy-3-methylglutaryl CoA (HMG-CoA) via enzyme HMG-CoA Synthase (HMGCS). HMG-CoA is then reduced to Mevalonate through rate-limiting enzyme HMG-CoA Reductase (HMGCR), which is the mechanism of action of a well-known class of clinical drugs combating high cholesterol called statins (443). Mevalonate is then phosphorylated by Mevalonate Kinase (MVK) to form Mevalonate 5-Phosphate (M5P). M5P is then phosphorylated a second time by Phosphomevalonate Kinase (PMVK) to form Mevalonate Pyrophosphate (MPP). MPP is subsequently decarboxylated by Mevalonate Decarboxylase (MVD) to form Isopentenyl-5-Pyrophosphate (IPP). Equal portions of IPP produced remain or are siphoned off to be isomerized via IPP Isomerase (IDI1) into Dimethylallyl Pyrophosphate (DMAPP) which is combined with IPP to form Geranyl-Pyrophosphate (GPP) via Geranyl Pyrophosphate Synthase (GPPS). Following production of GPP, Farnesyl Diphosphate Synthase (FDPS) converts GPP into Farnesyl

Pyrophosphate (FPP). FPP is the main precursor for all downstream branches and end products of the Mevalonate Pathway.

The Mevalonate Pathway creates many endpoints. For example, Farnesyl Diphosphate Farnesyl Transferase/Squalene Synthase (FDFT1/SS) attaches a C-15 isoprene FPP group to commence a series of intermediate steps to form CHL including the production and oxidation of squalene and lanosterol as well as the reduction of 7-dehydroxysterol into CHL (444). Furthermore, FPP can be converted to GGPP through enzyme, Geranylgeranyl pyrophosphate synthase (GGPS) which is then utilized for protein prenylation of membrane proteins via Geranylgeranyl Transferase (GGT) (431) which is discussed in greater detail below.

In addition to CHL and GGPP, other endpoints of the Mevalonate Pathway include Ubiquinone (CoQ10) and Dolichol. CoQ10 is an antioxidant that is essential for the electron transport chain (ETC). Isoprenoids such as FPP and GGPP transport CoQ10 to the mitochondria. Once in the mitochondria, the quinone group of CoQ10 transfers electrons from either complex I or complex II to complex III of the ETC, which facilitates energy production (431, 445). Dolichol is also an antioxidant that acts as a carrier of lipids and oligosaccharides in the production of complex sugars such as Uridyl-Diphosphate-Glucose (UDP-Glc) and Guanosine-5-Diphosphoglucose-mannose (GDP-Man), which facilitate N-linked glycosylation (446). Thus, the Mevalonate Pathway is multifaceted in that many endpoints are produced, contributing to a variety of cellular processes.

2. Regulation of the Mevalonate Pathway

The Mevalonate Pathway is regulated by a series of transcription factors that facilitate the production of the rate-limiting enzyme HMGCR. Transcriptional regulation of

HMGCR occurs through 2 members of a family of transcription factors called Sterol Regulatory Binding Element Proteins 1 and 2 (SREBP1 and SREBP2; reviewed in (447)). SREBP1 generally regulates lipid and fatty acid synthesis, whereas SREBP2 generally regulates sterol production. SREBP proteins have a basic helix-loop-helix-leucine zipper (bHLH-LZ) structure and are bound to the ER at their C-terminal domain through binding to SREBP-cleavage activating protein (SCAP) which interacts with Insulin-induced Gene 1 proteins (INSIGs) under high sterol conditions. Under low sterol conditions, INSIG is ubiquitylated and degraded which allows SCAP to escort SREBP2 from the ER to the Golgi via COPII vesicle coat protein, followed by cleavage via site-1 protease (S1P) and site-2 protease (S2P) which generates a transcriptionally active N-terminal SRE domain which can be translocated to the nucleus via Importin-B to allow transcription of Mevalonate Pathway genes such as HMGCR (447-449).

3. Mevalonate Pathway and Cancer

As CHL levels have been demonstrated to be altered across many cancer types, the Mevalonate Pathway has become a target of cancer therapeutics. For instance, it has been shown that low CHL levels are associated with increased antiviral type 1 interferon (IFN) response, suggesting CHL plays a role in evading immunosurveillance (450-452). Yet, CHL is not the only target among the Mevalonate Pathway.

For example, although mostly studied in metabolic cancers such as Hepatocellular Carcinoma (HCC), it is known that Mevalonate Pathway master transcription factor SREBP2 is regulated by PI3K/AKT, mTORC1, AMPK, p53, RB, and MYC (reviewed in (450)). Further, it has been shown across a variety of cancers that mutations of p53 (TP53R273H and TP53R280K) enable functional interaction with SREBP2 to increase production of Mevalonate Pathway genes (453). Within melanoma,

it has been shown that circulating tumor cells (CTCs) have increased levels of SREBP2 which confer resistance to cell death and promote dissemination (454).

In addition to upstream regulation of the Mevalonate Pathway, CHL also have downstream effectors. Further, it is known that CHL production can lead to covalent attachment of CHL to Hedgehog (Hh) ligands for Hh activation, which has been shown to be very prevalent in melanoma metastasis (455-457), or can be converted into steroid hormones such as Estrogen Receptor (ER) or Androgen Receptor (AR) leading to oncogenic signaling (450). Thus, Mevalonate Pathway not only is regulated by oncogenic signaling but also regulates downstream effectors of oncogenic signaling as well. Collectively, as the Mevalonate Pathway seems to be heavily intertwined with a variety of oncogenic pathways, it presents an exciting and impactful avenue for future therapeutic research.

III. CHL Uptake via LDLR

To this point we have mainly discussed CHL biosynthesis as a means of enhanced CHL levels, however CHL can also be taken in from outside of cells. Indeed, CHL esters and triglycerides are lipid molecules needed for cell function including membrane fluidity and trafficking paramount for a cell to thrive (458). However, CHL and triglycerides are water insoluble, therefore they have to associate with a water-soluble transporter that can travel through the bloodstream (459). In this case, the water-soluble transporters are lipoproteins such as Low Density Lipoprotein (LDL) and Very Low Density Lipoprotein (VLDL). LDL is the most common ligand for Low Density Lipoprotein Receptor (LDLR) which are a family of lipoproteins receptors primarily responsible for binding and internalizing apolipoprotein E and B (apoE- and apoB)-containing

lipoproteins (460). As lipoproteins function as transporters, apolipoproteins are proteins found within lipoproteins that allow for binding to receptors (461). Thus, LDL containing a single copy of apoB-100 is responsible for carrying about 65-70% of all CHL in humans (462). In brief, CHL is internalized by apolipoproteins undergoing endocytic clustering of coated pits followed by transport into early and late endosomes followed by lysosomal processing and recycling of lipids through the cell to the membrane (460).

CHL internalization and homeostasis is an important process for organism viability. For example, it has been previously demonstrated that mice that have LDLR knockout genetic background (LDLR-/-) and fed a high fat diet exhibit enhanced hyperlipidemia, hypercholesterolemia, and atherosclerosis (463, 464). This is because if CHL cannot be internalized by the cell, the CHL esters remain in the plasma where they form atherosclerotic lesions and cause endogenous CHL synthesis of cells that are not receiving CHL from the extracellular environment (465). Atherosclerotic lesions can lead to cancer progression through promoting oxidative stress, inflammation, dysregulated proliferation, and angiogenesis (466). Thus, LDLR-/- mice provide a good *in vivo* model for examining CHL in the context of melanoma progression.

Part 5: Glycosylation

I. Glycosylation and SOCE

i. Introduction to Glycosylation

Glycosylation is a post-translational modification of proteins where sugars (glycans) are covalently added to proteins and lipids to form glycoproteins (467, 468) leading to differences in protein expression, degradation, trafficking (469, 470) and protein stability (471). Glycoproteins consist of Uridyl-acetylglucosamine (UDP-GlcNAc) and sometimes other sugars that are formed via the Hexosamine Biosynthesis Pathway (HBP) and derivative glycosylation pathways (472). While many alternative glycosylation pathways exist such as the formation of proteoglycans, glycosphingolipids, and glycosaminoglycans (467), as well as less commonly utilized in cancer and less elucidated C-linked glycosylation (473), the 2 main types of glycosylation in a cell are N-linked and O-linked glycosylation will be discussed in-depth below.

N-linked glycosylation occurs in the ER (472) when UDP-GlcNAc is added to an amino group (N) at the glycosylation consensus motif Asn-X-Ser/Thr (where X is any amino acid except Proline) (467). The *N*-linked glycosylation mechanism begins with two *N*-acetylglucosamines (GlcNAc) binding to dolichol pyrophosphate on the cytosolic side of the ER (474). Dolichol is a long unsaturated chain of isoprene units and acts as a carrier in *N*-linked glycosylation (474). The lipid linked glycan is then inverted to the luminal side of the ER and nine mannoses and three glucoses are added to form a more mature lipid linked glycan (474, 475). Then oligosaccharyltransferase (OST) transfers the structure to the amide of asparagine residue within the consensus sequence -N-X-T/S (474) with the catalytic region of OST (Subunit Of The Oligosaccharyltransferase

Complex 3A/3B (STT3A/STT3B) also known as oligosaccharyltransferase catalytic subunit/tumor suppressor candidate 3 (OSTC/TUSC3) respectively (476) completing the transfer (477).

Conversely, O-linked glycosylation occurs primarily in the Golgi apparatus where different sugars including UDP-GlcNAc and N-acetylgalactosamine (UDP-GalNAc) are added to a hydroxyl group (O) of a S/T amino acid (467, 472). In parallel, O-GlcNAcylation is special type of O-glycosylation where UDP-GlcNAc is transferred via O-GlcNac Transferase (OGT) to proteins primarily in the cytosol and less commonly in the nucleus or mitochondria of eukaryotic cells (467, 468, 472). O-GlcNAcylation is the most common form of O-linked glycosylation in mammals (478) and most commonly dysregulated in cancer progression (472).

The level of *O*-GlcNAcylation depends on glucose metabolism by the hexosamine biosynthesis pathway (HBP), which forms the substrate for *O*-GlcNAcylation (479, 480). Extracellular glucose can be taken up by the cell through glucose transporter (GLUT) proteins (481). After being phosphorylated and/or isomerized, the majority of this glucose is utilized in glycolysis, glycogen synthesis, or the pentose phosphate shunt, but about 2-5% fluxes through the HBP in non-cancerous cells (482, 483). Glutamine-fructose-6-phosphate aminotransferase 1 (GFAT1) is the first and the rate-limiting enzyme of the HBP, which converts fructose-6-phosphate (F6P) and glutamine into glucosamine-6-phosphate (GlcN-6P) (484). After subsequent acetylation and isomerization, newly formed *N*-acetylglucosamine-1-phosphate (GlcNAc-1P) goes through uridylation to yield UDP-GlcNAc, which is the substrate for *O*-GlcNAcylation (481). *O*-GlcNAc addition to proteins is regulated by 2 opposing enzymes; *O*-GlcNAc transferase (OGT) attaches *O*-GlcNAc to proteins, while *O*-GlcNAcase (OGA) removes

O-GlcNAc from protein to its unmodified state (485, 486). It should be noted, OGT and OGA function in equilibrium, however, shifting the equilibrium dysregulates O-GlcNAcylation, leading to pathology (487). Subsequently, we will discuss the effects of *O*-GlcNAcylation on STIM and Orai function.

ii. STIM1 N-linked Glycosylation

STIM1 and STIM2 can both be *N*-linked glycosylated within the sterile alpha motif (SAM) domain at glycosylation sites Asn131 and Asn171 (488). Analysis of the primary amino acid sequence of human STIM1 determined three consensus sites for *N*-linked glycosylation at N131, N171, and N658, however only N131 and N171 could only be modified *in vivo* (470). Determination of these two sites was further verified through titration of STIM1 treated with Endoglycosidase H (EndoH) and truncated STIM1 that is terminated at the N658 site (470). EndoH is an enzyme that cleaves glycan groups attached by *N*-linked glycosylation and is utilized to monitor *N*-linked glycosylation. When both variations of STIM1 were added to immunoblots, they migrated as a mixture of three isoforms: non-, mono-, and diglycosylated STIM1 species (470). These results demonstrated STIM1 is *N*-linked glycosylated *in vivo* at both N131 and N171 (470). In comparison to STIM1, STIM2 only has one site for *N*-linked glycosylation at the Asn135 site, which is analogous to the Asn131 site in STIM1 (470, 471). STIM1 and STIM2 contain a single SAM (sterile α-motif) and an unpaired EF-hand in the extracellular region but diverge structurally in the C-terminal half of the cytoplasmic domain (488). Although the interactions of STIM1 glycosylation are known, the topic of STIM2 glycosylation is still not well understood.

STIM and Orai are primarily known for their role in the formation of the CRAC channel, however, they have also been shown to form arachidonate-regulated Ca^{2+}-

selective (ARC) channels (489, 490). ARC channels function independently of ER Ca^{2+} depletion and are activated by arachidonic acid production at the PM (491, 492). While this activity has been well demonstrated, the underlying mechanisms driving these distinct roles for STIM and Orai are somewhat unclear. One possibility is that PM-STIM1 contributes to ARC function; a fraction representing ~10% of STIM1 in the cell (493-496). This concept is based on several lines of evidence. First, tunicamycin, a non-selective blocker of *N*-linked glycosylation, blocks ARC activity (489). Further, although antibodies targeting the STIM1 N-terminus block CRAC channel function (494), in a subsequent study inhibition of ARC channels was shown to occur with greater efficacy (489, 490). Finally, the introduction of N131Q/N171Q (QQ) mutants led to a marked reduction in ARC activity (490). However, while *N*-linked glycosylation at N131 and N171 of STIM1 has been conceptually linked with the delivery and insertion of STIM1 into the PM (470, 497), it has seen been established that the STIM1-QQ mutant does not exhibit any defect in PM localization (498). As such, whether or not STIM1 glycosylation contributes to ARC activity due to control of PM localization or due to other as-yet-to-be established mechanisms remains unclear.

Irrespective of its role in ARC activity, STIM1 glycosylation has also been shown to contribute to CRAC channel activation (490, 499). This was demonstrated through the smaller Ca^{2+} influx and smaller current density through CRAC channels compared to the STIM WT in smooth muscle cells (490, 499). This was established using both the STIM1-QQ mutant and a STIM1 N131D/N171Q (DQ) mutant, both of which eliminate N-linked glycosylation of STIM1 (498, 500). Interestingly, while expression of STIM1-QQ led to decreased CRAC channel function, STIM1-DQ proved to be a gain of function mutation, driving increased current density and Ca^{2+} entry through store-operated

channels (490, 498). This was shown to be the result of increased translocation to the ER/PM junction resulting in a decrease in current latency through CRAC channels due at least in part to a partial destabilization of the EF-SAM domain (471, 498). It was also observed that co-expression of STIM1-DQ with Orai1 led to a three-fold increase in the STIM1:Orai1 ratio relative to STIM1-WT: Orai1 (498). In contrast, co-expression of STIM1-QQ with Orai1 decreased the STIM1:Orai1 ratio (498). These observations reveal that N131 and N171 serve critical roles in control of STIM1 activation, likely due to the cross proximity of these residues to the EF and SAM domains. The fact that different mutations of these residues led to mutually opposing outcomes reveals how functionally significant glycosylation of these residues would have to be, although how glycosylation would affect function is somewhat more difficult to assess given the profound impact of residue changes at these sites.

iii. Orai1 N-linked Glycosylation

Orai1 contains an *N*-linked glycosylation site at asparagine 223 (N223) that regulates CRAC channel function (501), while Orai2 and Orai3 do not contain any known *N*-linked glycosylation sites (502, 503). Determining the functional role of *N*-linked glycosylation of Orai1 has been somewhat challenging due to celltype-specificity. Hence, in HEK293 cells, no differences in Orai1 localization or function were observed between Orai1-N223A and Orai1-WT (498), yet, in both Jurkat T cells and SCID fibroblasts, expression of Orai1-N223A led to enhanced SOCE either, suggesting that glycosylation attenuates Orai1 function in these cell types (502, 504). While the reasons for these differences are not fully established, it is likely a reflection of the fact that glycosylation patterns exhibit considerable cell type specificity due to differences in when the terminal sialic acid is added and which sialic acid-binding partners are expressed (503, 505).

Further, alterations to the glycosylation of Orai1 has been observed in aging, cancer, and immune disease (504, 505). For instance, the enzyme β-Galactoside α-2,6-sialyltransferase 1 (ST6GAL1) has been implication in cancer invasiveness and metastatic spread when elevated and has been shown to glycosylate Orai1, leading to reduced SOCE due to attachment of α-2,6-linked sialic acids (504). In addition, sialic acid-binding immunoglobulin-type lectins (Siglecs) are glycan-binding proteins (504) with roles in mast cell and eosinophil-associated disease (504, 505). Further, desulfation of Orai1 leads to an increase in Orai1-mediated Ca^{2+} entry and downregulation of Siglec-8 (504, 505). Considered collectively, these data reveal Orai1 glycosylation as a fundamental contributor to celltype-specific differences in Orai1 function.

iv. STIM1 O-linked Glycosylation

STIM1 function can be significantly altered by *O*-GlcNAc modification, which has been shown to regulate SOCE (479). As previously discussed, ER Ca^{2+} depletion leads to the translocation of STIM1 to ER/PM junctions (506, 507), where it physically associates with Orai1, ultimately leading to its activation and Ca^{2+} entry (506). Interesingly, STIM1 *O*-GlcNAcylation impairs its translocation to the ER/PM junction, which prevents STIM1-Orai1 association, thereby impairing SOCE (479, 508). This to STIM1 translocation was shown by immunostaining of primary hepatocytes from genetically obese and lean wild-type (WT) mice treated with the irreversible SERCA pump inhibitor, thapsigargin (Tg), to induce ER Ca^{2+} depletion (508). In WT hepatocytes from the lean mice, STIM1 is distributed throughout the ER at rest; Tg treatment led to marked STIM1 translocation to ER/PM junctions (508). In contrast to hepatocytes from lean mice, in hepatocytes from obese mice treated with Tg, exhibited increased STIM1 signal intensity, but no translocation of STIM1 from the cytosol to the periphery of the

cell (508). Notably, obese mice are known to have generally higher global *O*-GlcNAcylation levels (509), which has been specifically demonstrated for STIM1 (508). Elevated *O*-GlcNAc levels can result from a higher flux through the HBP which have been demonstrated by an increase of HBP metabolites, induced by glucosamine (510, 511) or caused by hyperglycemia (512) and obesity (508), or through alterations to HBP enzymes, like in the inhibition of OGA or overexpression of OGT (508). This is important because that indicates that obesity might lead to impaired STIM1 translocation and lower SOCE, which, may contribute to cardiovascular disease, diabetes (see Diabetes section) and, potentially, other pathological conditions.

Similar observations were made in neonatal cardiomyocytes treated with Tg (479). STIM1 oligomerization and translocation to the ER-PM junction to form puncta structures are key features in STIM1-mediated SOCE. These features were seen in neonatal cardiomyocytes transfected with enhanced yellow fluorescent protein (eYFP)-STIM1 and treated with EGTA and Tg to replicate Ca^{2+} depletion. However when *O*-GlcNAcylation levels were increased with thiamet-G (TMG; highly-selective OGA inhibitor (513)) or glucosamine, there was a decrease in both the number of puncta positive cells and the average number of STIM1 puncta per cell (479). Increased *O*-GlcNAcylation demonstrated through metabolic stress in obesity or through the use of glucosamine or TMG has been shown to inhibit STIM1 oligomerization, translocation, and puncta formation, which are sequential steps in SOCE activation (479).

Since serine/threonine can be both phosphorylated and glycosylated (514), investigations into post-translational modifications of STIM1 can be somewhat complex. Initial interest in *O*-GlcNAcylation modification of STIM1 arose from the fact that STIM1 contains cytosolic regions rich in proline (P), glutamic acid (E), serine (S), and threonine

(T), which has a high tendency to by modified by *O*-GlcNAcylation (479, 515). Proteins that contain PEST sequences are often targeted for rapid degradation (516, 517). However, O-GlcNAcylation of PEST sequences may slow or prevents proteins, like STIM1, from degradation (469). STIM1 has a PEST sequence in the cytosolic C-terminal region (479, 516) and where *O*-GlcNAcylation occurs at both Ser621 and Thr626 (518). Since Ser621 is also phosphorylated (519), this creates a scenario where the processes of phosphorylation and *O*-GlcNAcylation compete for the same residues, with functional consequences.

Computational prediction identified STIM1's *O*-GlcNAcylation sites at Ser621 and Thr626 and these results were confirmed in HEK293 cells by co-immunoprecipitation assay. Further, since no *O*-GlcNAcylation occurred in an S621A/T626A STIM1 mutant, these may be the sole *O*-GlcNAcylation sites in STIM1 (518). Further, the fact that TMG treatment increased *O*-GlcNAcylation in $STIM1_{WT}$ and $STIM1_{T626A}$ but, not $STIM1_{S621A}$ or $STIM1_{S621/T626A}$ indicates that T626 is constitutively *O*-GlcNAcylated, while S621 *O*-GlcNAcylation is inducible (518). Since S621 phosphorylation promotes STIM1 activation (see phosphorylation section), it is not surprising that *O*-GlcNAcylation at this site would lead to the opposite outcome. That seems to be the case, since TMG treatments resulting in S621 *O*-GlcNAcylation ultimately resulted in SOCE suppression. However, the relationship between Thr626 *O*-GlcNAcylation, Ser621 phosphorylation and SOCE is more complex.

To determine the relationship between STIM1 *O*-GlcNAcylation at T626 and phosphorylation of STIM1 at S621, STIM1-null HEK293 cells were transfected with $STIM1_{T626A}$ exhibiting at least one of the phosphomimetic mutations S575E, S608E and/or S621E (518). STIM1-KO cells expressing $STIM1_{S621E/T626A}$ exhibited increased SOCE

while no differences in SOCE were observed in cells expressing $STIM1_{T626A}$, $STIM1_{S575E/T626A}$ or $STIM1_{S508E/T626A}$ (518). Therefore, this suggests that decreased STIM1 *O*-GlcNAcylation at T626 can lower SOCE activity by decreasing STIM1 phosphorylation at S621 (518). Precisely how T626 *O*-GlcNAcylation controls S621 phosphorylation is not entirely clear, although it seems reasonable to speculate that it may increase access for modification of S621 through conformational changes.

v. Orai1 O-linked Glycosylation

The topic of Orai *O*-linked glycosylation has not been specific explored. However, the established effects of STIM1 *O*-GlcNAcylation, the required STIM1-Orai1 association for SOCE and the cytosolic domains of Orai1, may point to the possibility of Orai1 being regulated by *O*-linked glycosylation (479).

II. Glycosylation and Cancer

i. Oncogenic Signaling

There is extensive evidence that glycosylation is linked to cancer that dates back over 70 years ago (520-522). This is a bidirectional process where HBP is upregulated in response to oncogenic signaling such as Ras (523), mTORC2 (524, 525), and TGFb (526), but it is also well-known that many proteins involved in EMT such as Snai1, YAP/TAZ, NFκB, and c-myc rely on O-GlcNAcylation for activation (472). Further, many of these signaling molecules interact bidirectionally with OGT. For example, studies have shown crosstalk between AMPK, mTOR, and O-GlcNAcylation. AMPK is known to phosphorylate OGT at Thr244, thus activating it, while creating a negative feedback loop where O-GlcNAcylation of AMPK inactivates it (527). Additionally. when cancer cells were treated with mTOR inhibitor Rapamycin, this actually led to reduced O-

GlcNAcylation and even reduced OGT levels (472, 528, 529). Thus, it is quite possible that OGT and oncogenic signals interact bidirectionally to promote cancer progression.

ii. EMT

In addition to the effects of glycosylation on signaling, glycans also can affect cell-cell adhesion and promote EMT. Similar to oncogenic signaling, this appears to be bidirectional. For example, it has been shown that EMT results in enhanced levels of UDP-GlcNAc and OGT in cancer cells (530). In addition, OGT levels have been shown to specifically correlate with invasiveness (526). To this end, it also has been shown that OGT levels directly correlate with IL6-induced N-Cadherin upregulation leading to EMT (531). Conversely, there is an inverse correlation with expression of E-Cadherin with the addition of UDP-GlcNAc to E-Cadherin in an O-GlcNAcylation process impairing cell adhesion and promoting tumor cell invasion (522, 532). Further, it has been shown that many integrins, receptor tyrosine kinases, as well as Wnt, Notch and Hh proteins are dependent on N-linked glycosylation that regulates EMT (533), while many EMT-associated proteins like TGFb, NFkB, and FOXO1 are regulated trough O-GlcNAcylation (102). Therefore, it appears that bidirectional interaction between OGT/O-GlcNAcylation and oncogenic signaling is driving cancer progression which provides a foundation for studying SOCE as a potential mediator of this process.

III. Targeting Glycosylation

Currently, there is evidence that targeting HBP can facilitate anti-tumor activity. For example, Azaserine (Aza) and 6-diazo-5-oxo-L-norleucine (DON) can inhibit HBP via inhibition of GFAT1 (534) and inhibit tumor progression *in vitro* (535) and *in vivo* (536). However, these drugs generally have off-target effects and exhibit high toxicity (472). Within the current study, we utilized a small molecule OGT inhibitor (OSMI1) developed

from a high-throughput screen that does not affect cell surface glycans and has less off-target effects (537). Since some toxicity is still observed, future new generations of compounds targeting OGT could be a future avenue of therapeutic research with potential to attenuate cellular glycosylation and cancer progression.

CHAPTER 2

STATEMENT OF GOALS

Melanoma is a cancer of the cells of the melanocyte lineage, which are predominantly responsible for the melanin pigment production that defines skin and eye tone (Slominski et al, 2004). Melanoma incidence has progressively risen over the last 30 years (Schadendorf et al, 2018), and is now the fifth most common cancer among men and women in the US (Alteri, 2019). Although melanoma is easily treated by surgical resection when detected early, if undetected, melanoma progresses from a radial to vertical growth phase to become an aggressive malignancy that easily metastasizes from the skin to the lymph nodes and other distal sites (Schadendorf et al., 2018). Currently, there are two major approaches to treating metastatic melanoma: targeted therapies and immunotherapies (Neves de Oliveira et al, 2018). Targeted therapies include inhibitors of targets in the Mitogen-Activated Protein Kinase (MAPK) pathway, including oncogenic $BRAF^{V600E}$ and MEK1/2 (trametinib) inhibitors. These drugs transiently increase progression-free survival, although this is typically followed by drug resistance and relapse (Neves de Oliveira et al., 2018). Additionally, though promising, MAPK pathway inhibitors inhibit immune cell function, leading to increased clinical toxicity (Boni et al, 2010). Immunotherapies were first explored as first-line melanoma treatments due to the observation that incidence of melanoma increased in immunosuppressed patients (Greene et al, 1981); targets of immune checkpoint inhibitors (ICIs) including Cytotoxic T-Lymphocyte Antigen 4 (CTLA4) (ipilimumab) and Programmed Cell Death-1 (PD1) (pembrolizumab). ICI therapies in conjunction with targeted therapies are currently in use. Continued efforts to identify new strategies are needed to control this deadly disease.

Ultraviolet (UV) radiation exposure is a major risk factor in melanoma, and the rising incidence of melanoma has been linked to increased sun exposure and artificial tanning (Matthews, 2017; Schadendorf et al., 2018). UV triggers melanin production in melanocytes, which protects against UV-induced damage in skin (Brenner & Hearing, 2008). However, UV exposure affects multiple cellular processes ultimately promoting cancer initiation and progression; as such, UV is considered a “complete carcinogen”, (D'Orazio et al, 2013). The most immediate consequence of UV exposure is induction of pyrimidine dimers that can cause DNA damage and/or mutations. While the evidence that UV drives melanomagenesis is undeniable, the molecular pathways linking UV and driver mutations are unclear since the most common mutations associated with melanoma, such as BRAF and NRAS mutations, do not possess the UV signature mutations. Further, while UV has long been associated with melanomagenesis, UV also has been reported to drive melanoma progression (Arisi et al, 2018; Bald et al, 2014), marked by entry into the vertical growth phase (Guerry et al, 1993). The mechanism by which UV supports progression is not well understood and is thus the focus of the current study, which identifies a critical role for UV-dependent suppression of store-operated Ca^{2+} entry (SOCE) in regulating melanoma migration and invasion.

SOCE is mediated by the members of the Orai and STIM families. Orai channels are Ca^{2+}- selective ion channels located at the plasma membrane (PM) (Feske et al, 2006; Vig et al, 2006b; Zhang et al, 2006); STIM is a type 1A transmembrane protein primarily found in the endoplasmic reticulum (ER) membrane (Liou et al, 2005; Roos et al, 2005). STIM responds to ER Ca^{2+} depletion by translocating within the ER towards the PM, and physically associates with PM-localized Orai channels to facilitate Ca^{2+} entry (ie SOCE (Putney, 1986); reviewed in (Soboloff et al, 2012)). SOCE has been

linked to melanoma progression previously, although the nature of this relationship is somewhat unclear. Hence, a prior study from our group, revealed an inverse correlation between SOCE and invasiveness (Hooper et al, 2015), suggestive of an inverse relationship between SOCE and melanoma progression. Further, a randomized, unbiased ribozyme screen for metastasis related genes identified STIM1 as a repressor of melanoma metastasis (Suyama et al, 2004). In contrast, invasive melanoma has been shown to rely on enhanced SOCE and AKT activity for growth and survival (Fedida-Metula et al, 2012; 5 Feldman et al, 2010). Further, invasive melanoma exhibiting activated MAPKs were shown to exhibit higher STIM1 and Orai1 expression (Stanisz et al, 2014; Sun et al, 2014; Umemura et al, 2014). Given these seemingly contradictory findings, further effort is needed to understand the relationship between SOCE and melanoma progression, an important goal of the current investigation. Further, since UV exposure is the major driver of melanoma progression and the relationship between UV and SOCE has not previously been determined, this investigation focuses on UV-dependent control of both SOCE and melanoma progression, using both in vitro and in vivo approaches.

Currently, it is widely believed that STIM1- and Orai1-generated Ca^{2+} signals facilitate cancer progression (364). Numerous studies have shown that STIM1 and Orai1 expression are correlated with melanoma progression (365, 366, 372, 538). Likely, this is a result of STIM1- and Orai1-dependent processes promoting invasiveness such as control of migration (79, 80) and invadopodia formation (539-541), or reliance on lipid raft modulation by membrane kinases Src/AKT (367, 370, 371). However, it is likely that STIM1- and Orai1-mediated melanoma progression is context specific (187). For example, previous work showed that Wnt5a phosphorylates and inactivates Orai1

leading to diminished SOCE and enhanced invasion *in vitro* (385). Likely this is due to the fact that Ca^{2+} can be protective against certain cellular processes leading to melanoma progression such as pyruvate dehydrogenase phosphatase (PDP) promoting dephosphorylation of PDH leading to TCA cycle and oxidative phosphorylation (134)(See Fig 1-2). Due to the heterogeneity of melanoma, it is perhaps unsurprising that it is not a clear linear relationship between SOCE and melanoma progression.

UV is well-known to induce melanoma progression (425, 542). Yet, very few prior investigations previously examined whether UV has any effect on Ca^{2+} signaling, and more specifically SOCE. Yet, previous studies suggest SOCE is an underappreciated, and relatively unknown potential therapeutic target in melanoma. In this regard, understanding the mechanisms behind how UV modulates SOCE and how SOCE regulates melanoma progression could yield a whole new avenue of research and potentially a new class of therapeutic drugs combating melanoma progression. Thus, the identification of regulatory mechanisms modulating suppression of SOCE mediated by UV would yield a better understanding of the basic biological mechanisms facilitating melanoma progression.

CHAPTER 3

MATERIALS AND METHODS

Methods

Cell Culture- SKMEL5, UACC1273, SKMEL2, FS13, WM983 B-Raf-inhibitor resistant (WM983BR), SKMEL28, WM983, UACC257, B16N, B2905A cells were grown in DMEM with 4.5g/L glucose supplemented with 10% FBS and 1% Gentamycin (Full DMEM media; ThermoFisher Scientific, Waltham, MA) at 37°C and 5% CO2. Cells were grown in Falcon T75 flasks until ~70% confluency. Cells in conditions <70% confluency were removed of media, washed with PBS and then administered fresh Full DMEM media and incubated until confluency. Upon confluency, cells were removed of media, washed with PBS and treated with 0.25% Trypsin for 10 minutes at 37°C and 5% CO2. Cells were then split 1:10 and allowed to incubate in 37°C and 5% CO2 and while cells were checked daily, they typically grew for 3 days before reaching ~70% confluency.

UV Exposure- Cells were plated on glass coverslips for 24 hrs before changing to PBS. Lids were replaced with a thin layer of taut plastic wrap before irradiating with two FS20 bulbs (with the same spectral output as FS40 bulbs used in reference) which emit a broadband UV spectrum containing 35% UVA and 65% UVB (with peak emission at 313nm in the UVB range (543)). Cells received a total UV dose of 175J/M^2 over 90 seconds at a rate of 1.94W/m^2. Approximately 80% of the melanoma cells survive this exposure. Cells were cultured under growth optimal conditions (B16N cells were split 1:20 while every other cell lines line was split 1:10 approximately every 3 days) for the indicated time period before subsequent experimentation.

Generating Stable Lentiviral Transduction of GFP- (Adapted from Applied Biological Materials, Inc.) B16N cells were plated in a 24 well plate at a density of 1E4 cells/well in 500ul Full DMEM, 24 hours prior to viral infection in Full DMEM media. Cells grown to 50% confluency and spinoculated with 2.19E7virus/ml and incubated for 1-2 days. Cells were then grown on larger tissue culture dishes and allowed to grow to 10E6 cells following ≥2 passages. Cells then sorted in the middle of the distribution curve eliminating very high and low expressing GFP.

Generating stable Orai1-WT-CFP and Orai1-E106A-CFP cell lines- B16N-GFP and WM983 cells were grown to 50% confluency followed by transfection with 14ug of pIRES-NEO Orai1-WT-CFP, B16N-GFP cells were grown to 50% confluency followed by transfection with 14ug of pIRES-NEO Orai1-E106A-CFP vector via electroporation using Gene Pulser Xcell (Biorad). After electroporation, cells were incubated in Opti-MEM Reduced Serum Media (described above) for 2 hours before adding 10% FBS and 1% antibiotics and incubating overnight. After overnight incubation cells were supplied Full DMEM media and cultured for 1 week. After 1 week, cells were treated with 500ng/ml of G418 antibiotic for selection and selected for 2 weeks. Following selection, cells were sorted by FACS for top 5% expression of CFP (and GFP in B16N cells) and placed as single cell clones in a 96 well plate. Individual clones took about 2 months to grow to either 70% confluency of the entire plate or a noticeable colony. Clones were then expanded and examined for GFP and CFP fluorescence intensity and SOCE on Leica DMI 6000B fluorescence microscope controlled by Slidebook software.

Transient transfection of mCherry-PFO-D4H - WM983 and UACC257 human melanoma cells were grown to 50% confluency on 10cm3 plates and transfected with PFO D4H-mcherry plasmid via electroporation using Gene Pulser Xcell (Biorad, Hercules, CA).

After electroporation, cells were plated on glass coverslips under growth optimal conditions before capturing images by confocal microscopy (Leica SP8 Laser Scanning Microscope; Buffalo Grove, IL). Fluorescence intensity was measured using Leica LASX software.

Plasmid	Protocol Type	Voltage	Pulse Length	Number of Pulses
Orai1-WT	Square Wave	220	25ms	1
Orai1-DN	Square Wave	220	25ms	1
PFO-D4H	Square Wave	220	25ms	1x2

siRNA transfection- $5x10^5$ cells were plated in 6 well plates overnight prior to treatment. Cells were transfected with 25 pmol of scRNA kit (Invitrogen, Waltham, MA) or siOGT (Sense: 5'- GCAGUUCGCUUGUAUCGUAtt-3'; Antisense: 5'- UACGAUACAAGCGAACUGct-3'; Invitrogen, Waltham, MA) using a Lipofectamine-based RNAimax kit (Invitrogen, Waltham, MA) according to kit protocol (DOI: 10.1016/j.cell.2010.05.017).

SOCE Measurement- Cells grown on glass coverslips were incubated in a cation-safe buffer (107mM NaCl, 7.2mM KCl, 1.2mM $MgCl_2$, 11.5mM Glucose, 20mM HEPES-NaOH, 1mM $CaCl_2$, pH 7.2) and loaded with Fura2-acetoxymethylester (Fura2-AM; 2μM) for 30 min at 24°C as previously described (385, 544). Cells were washed and allowed to de-esterify for a minimum of 30 min at 24°C. Following de-esterification, cells were treated with 2 μM Thapsigargin (SERCA inhibitor) for 10 minutes prior to imaging. Ca^{2+} measurements were taken using a Leica DMI 6000B fluorescence microscope controlled by Slidebook software (Intelligent Imaging Innovations, Denver, CO). Fluorescence emission at 505nm was monitored in response to excitation at alternating 340nm and 380nm wavelengths at a frequency of 0.67 Hz; intracellular Ca^{2+} measurements are shown

at 340/380nm ratios obtained from groups (2-45 for patient samples, 35-45 for established cell lines) of single cells.

RT-qPCR- Cells were grown to 70% confluency and collected as cell pellets prior to RNA extraction using a kit (Ambion, Austin, TX). Following RNA extraction, 500ng RNA was converted to cDNA using ezDNAse and Superscript IV Reverse Transcriptase Assay Kit (Invitrogen, Waltham, MA) and diluted 1:10 for working concentration of 50ng per reaction. 500nM housekeeping 18S ribosomal RNA (18S) and genes of interest were used for each reaction mixed with Powerhouse SYBR green (Applied Biosystems, Bedford, MA) and analyzed using QuantStudio8 software (Applied Biosystems, Bedford, MA).

Proliferation Assays- 500 cells/well were plated on a 96 well plate for the indicated time point and treated with 1:10 Water Soluble Tetrazolium (WST-1) dye that forms water-soluble formazan for 1 hour at 37°C, 5% CO2. The conversion of WST-1 to Formazan leads to oxidation of mitochondrial NADH to NAD+ which changes color and can be measured through absorption via GloMax plate reader at 450nm.

Migration Assay - Cells were plated on glass coverslips (Ibidi, Fitchburg, WI) overnight to form a complete monolayer before “wounding” with a p20 pipette tip. Coverslips were placed in an incubation chamber (37°C; 5% CO_2) and monitored by confocal microscopy (Leica SP8 Laser Scanning Microscope). Z-stack brightfield images were obtained every 20 minutes for 20 hours; the % of the would that was refilled over time was calculated using ImageJ.

Transwell Migration Assays- Matrigel transwell chambers were purchased (Corning, Bedford, MA) and stored at -20C until use. Chambers were thawed at 24C and hydrated with Opti-MEM Reduced Serum Media with Glutamax, HEPES, 2.4g/L Sodium

Bicarbonate (Full Opti-MEM media) for 2 hours at 37C in 4% CO2. After hydration, 2500 cells were plated on top of the chambers in same Opti-MEM media. Full DMEM media as a chemoattractant was placed on the bottom of the chamber and incubated at 37C and 4% CO2 for approximately 20 hours. After incubation, cells were placed on ice and media was removed. After media removal, top of the chamber was swept with a wet Q-tip to move all non-invasive cells to the edges. Top and bottom of chambers were then soaked in 500ul of ice-cold PBS and then 500ul of ice-cold 100% methanol and stored at -20C for 10 minutes. After storage, methanol was removed and cells were stained with 0.5% Crystal Violet for 2 minutes and then de-stained with water 1-3x depending on the intensity of the crystal violet stain and then allowed to dry overnight. Images were taken by EVOS cell imager and quantified on ImageJ.

Viability Assays- 500,000 cells were plated in 24 well plates overnight in the absence or presence of 2 μM IA65. Cells were then trypsinized with 0.25% Trypsin-EDTA for 10 minutes at 37°C. Following, cells were treated with 0.4% Trypan Blue and placed in Countess II FL slidereader (Invitrogen, Waltham, MA) and comparing the number of stained vs. unstained cells.

***In vivo* metastasis assays-** Experiments were performed in C57Bl/6 mice (Jax) housed in standard cages (≤5/cage) at LKSOM in accordance with Temple University guidelines (Animal welfare # A3594-01). B16N cells were counted using a hemocytometer and 1x106 cells in 200 μl sterile PBS were injected subcutaneously on the right flank of syngeneic C57BL6 mice. Mice were monitored for 14 days and then sacrificed followed by full body dissection and histopathological analysis. Tissues were fixed in 10% Neutral-Buffered Formalin (pH 6.8-7.2) followed by H&E staining and Aperio Imagescope software (Leica Biosystems; Buffalo Grove, IL) scan for peritoneal wall invasion.

RNA sequencing analysis- Raw RNA-Seq data was processed using the subread algorithm established in (545). Preprocessed data files from the samples were subject to RNA sequencing data analysis using *Rsubread* package (546). Genome indices were built using the *buildindex* function in *Rsubread* package. RNA transcripts from each sample were mapped to the mouse genome reference consortium build 38 (GRCm38) genome. Alignment of the sample reads to the reference genome was performed using the *align* function within the *Rsubread* package. *featureCounts* function within the *Rsubread* package was used to summarize the data to integer-based, gene-level read counts. Read counts generated from the pipeline were annotated using mm10 annotation. Differential expression analysis of the read counts was performed using the DESeq2 package (547). Differentially expressed genes generated from the DESeq2 analysis were subjected to pathway analysis using Ingenuity Pathway Analysis tool (Ingenuity® Inc, Redwood city, CA) with default settings.

Cholesterol measurement- WM983 and UACC257 human melanoma cells were grown to 50% confluency before transfecting with PFO D4H-mcherry via electroporation using Gene Pulser Xcell (Biorad, Hercules, CA). Cells were then plated on glass coverslips under growth optimal conditions before capturing images by confocal microscopy (Leica SP8 Laser Scanning Microscope; Buffalo Grove, IL). Fluorescence intensity was measured using Leica LASX software.

Isolation of Cells from Patient Surgical Explants - Freshly isolated Patient Surgical Explants - Patient surgical explants were received from Dr. Jeffrey Farma at Fox Chase Cancer Center with all personal identification information being protected by HIPAA privacy. All patients had given informed consent to have their tissue used for research in accordance to protocols from Fox Chase Cancer Center. Freshly isolated patient explants

were incubated in DMEM containing Liberase TL (Roche Applied Science; 37°C, 30 min). Following incubation, tissue was cut using a sharp razor and dissociated through 50 μM Medicon screens (Becton Dickinson Biosciences, San Jose, CA; 2 min). Tissue samples were resuspended in DFD media (DMEM, 20% FBS; 500ug/ml DNAse I, Sigma, St. Louis, MO) and passed through an 18-gauge syringe to break up clumps of cells before filtration (70 μm, Corning, Glendale, AZ, centrifugation and resuspension in DMEM (2% FBS; 1% Gentamycin) for 3 days before use.

Metabolism Assays:

Glucose Uptake Assay – Glucose Uptake-Glo Assay (Promega) uses 2-deoxyglucose (2-DG) which is a fluorescent glucose analog that can be absorbed into cells similarly to glucose. Once in cells, 2-DG is converted to 2-Deoxyglucose-6-Phosphate (2DG6P) by cellular hexokinases. 2DG6P can then be oxidized into Glucose-6-Phosphate Dehyodrogranse (6PDG) via Glucose-6-Phosphate Dehydrogenase (G6PDH). In parallel, G6PDH also simultaneously reduces NADP+ to NADPH, which in turn is used by a kit reductase given to cells to convert proluciferin to luciferin which is used by kit luciferase enzymes to create luminescence. B16N, WM983 and UACC257 cells either overexpressing Orai1 or UV exposed (permitted to recover for 5 weeks) were cultured under growth optimal conditions parallel to unmanipulated control cells. Cells were seeded at density of 15,000 cells/well in 96 well plates. Glucose uptake was measured using the Promega Glucose Uptake-Glo Assay (Madison, WI); luminescence was recorded using 0.3-1 second integration using a Tecan INFINITE M1000 PRO monochromator-based microplate reader.

1. Diluted 100mM 2-deoxyglucose (2-DG) to 1mM 2-DG in PBS

2. Added 50ul of 1mM 2-DG, shaken briefly and incubated at room temperature for 10 minutes.
3. Added 25ul of Stop Buffer, shake briefly
4. Added 25ul of Neutralization Buffer, shake briefly
5. Added 100ul of 2-DG6P detection reagent (100ul Luciferase reagent, 1ul NADP+, 2.5ul G6PDH, 0.5ul Reductase, 0.0625ul Reductase Substrate), shake briefly
6. Incubate at room temperature for 0.5-5 hours
7. Record luminescence using 0.3-1 second integration on a luminometer

Seahorse Assays – Oxygen Consumption Rate (OCR) and Extracellular Acidification rate (ECAR) were measured using an Agilent Seahorse XF96 (Wilmington, DE). B16N, WM983 and UACC257 cells either overexpressing Orai1 or UV exposed (permitted to recover for 5 weeks) were cultured under growth optimal conditions parallel to unmanipulated control cells. 15,000 cells/well were seeded in Seahorse 96 well cell culture plates for all experiments. Basal OCR was measured in media supplemented with 1mM pyruvate, 2mM glutamine, and 10mM glucose followed by the sequential addition of Oligomycin (1.5μM), FCCP (1μM) and Rotenone/Antimycin-A (1μM) to perform the mitochondrial stress test. Basal ECAR was measured in media supplemented with 2mM glutamine followed by the sequential addition of glucose (10mM), oligomycin (1μM) and 2-Deoxy-d-glucose (2-DG: 50mM) to perform the glycolysis stress test. Results were quantified using Wave software (Agilent Technologies, Santa Clara, CA).

OCR-

1. Turn on Agilent Seahorse XFe/XF Analyzer and allowed to warm up overnight
2. Plate 15,000 cells/well in 96 well plate

3. Hydrate a sensor cartridge in Seahorse XF Calibrant at 37C in a non-CO2 incubator overnight.
4. Supplement Seahorse XF with 1mM pyruvate, 2mM glutamine, and 10mM glucose
5. Bring XF medium with pH 7.4 and XF supplements into a cell culture hood and transfer to sterile bottle
6. Warm XF medium with supplements to 37C in waterbath
7. While XF media is warming in water bath, resuspend compounds (Oligomycin, FCCP, Rotenone/Antimycin A(AA)) in XF medium
8. Use compound stock solutions (10X) to make working solutions (1.5μM Oligomycin, 0.5μM FCCP, 0.5μM Rot/AA)
9. Add 1/10 volume of each compound to port for future administration to cells
10. Remove cells from 37C incubator and add warm XF media to cells and place in 37C non-CO2 incubator for 1 hour prior to assay
11. Place port over plate with cells and run Seahorse Agilent XF Analyzer which will add indicated compounds at indicated time points
12. Quantify results in Wave software

ECAR-

1. Turn on Agilent Seahorse XFe/XF Analyzer and allowed to warm up overnight
2. Plate 15,000 cells/well in 96 well plate
3. Hydrate a sensor cartridge in Seahorse XF Calibrant at 37C in a non-CO2 incubator overnight.
4. Prepare stock solutions of 100mM Glucose, 100μM Oligomycin, 500mM 2-DG in XF glycolysis medium

5. Add proper volumes to achieve 10mM Glucose, 1μM Oligomycin, and 50mM 2-DG to the port in XF glycolysis medium
6. Remove cells from 37C incubator, remove DMEM media and add warmed XF glycolysis medium
7. Incubate in 37C, non-CO2 incubator for 1 hour prior to assay
8. Place port over plate with cells and run Seahorse Agilent XF Analyzer which will add indicated compounds at indicated time points
9. Quantify results in Wave software

FRET- HEK293 cells were transfected with pIRES-NEO-STIM1-YFP or pIRES-NEO-ORAI-CFP plasmids and then isolated as individual clones as described (see Generating stable Orai1-WT-CFP and Orai1-E106A-CFP cell lines). Following, cells were grown on glass coverslips overnight in Full DMEM media in the presence or absence of GGPP (3μM), GGTI (15μM), or both. After overnight incubation cells were photobleached (90% gain, 10% laser power, 405nm excitation) before and 15 minutes after the addition of 2μM Thapsigargin. FRET efficiency was measured by Leica LASX software.

Materials

All cell lines were acquired from American Type Culture Collection (ATCC; Manassas, VA). All patient melanoma surgical explants were acquired under IRB protocols from Fox Chase Cancer Center Biosample Repository. Media was purchased from Corning and Gibco (Waltham, MA). TAK475 and DNAse I were purchased from Sigma-Aldrich (St. Louis, MO). Compactin and BTP2 were purchased from Tocris Bio-Techne Corporation (Minneapolis, MN). OSMI1 was purchased from Millipore Sigma (Burlington, MA). Matrigel Transwell Chambers were purchased from Corning (Waltham, MA). Liberase TL was purchased from Roche Applied Science (Indianapolis, IN). 50μM Medicons and the medimachine were purchased from Becton Dickinson Biosciences (San Jose, CA). 8 well u-slides migration plates were purchased from Ibidi (Fitchburg, WI). Fura2-AM was purchased from Thermo-Scientific (Waltham, MA). Glucose Uptake Kit was purchased from Promega (Madison, WI), Lactate Production Kit was purchased from Sigma-Aldrich (St. Louis, MO). High fat mouse chow was purchased from Harlan labs (Frederick, MD). Orai1-WT-CFP and Orai1-E106A-CFP were generated as previously described (12); the mCherry-PFO-D4 gene was synthesized by Integrated DNA Technologies (Coralville, IA) and combined via PCR into an mCherry-C1 backbone (Addgene). PFO-D4H was constructed via site-directed mutagenesis.

Primer Sequences:

18S:

Forward: CTT AGA GGG ACA AGT GGC G

Reverse: ACG CTG AGC CAG TCA GTG TA

hOrai1:

Forward: AGG TGA TGA GCC TCA ACG AGC A

Reverse: AGT CGT GGT CAG CGT CCA GCT

hOrai2:

Forward: CCT GTC GTG GCG GAA GCT CTA

Reverse: ACT GGT ACT GCG TCT CCA GCT G

hOrai3:

Forward: TTA GCA AGG GTT GGG TAA GG

Reverse: TTT CCA GGG CTA AGG ACT GG

hSTIM1:

Forward: CAC TCT TTG GCA CCT TCC ACG T

Reverse: CTG TCA CCT CGC TCA GTG CTT G

hSTIM2:

Forward: CAG TCT TTG GGA CTC TGC ACG T

Reverse: GCC AGC GAA AAA GTC GTT CTC G

mOrai1:

Forward: GTT ACT CCG AGG TGA TGA GCC T

Reverse: AGC TGG ACT TCC ACC ATC GCT A

mOrai2:

Forward: GAC ACA GAC GCT AGC CAC GA

Reverse: ATG GGC ACA TTG AGC TCT GC

mOrai3:

Forward: TTA CCA CAT CAC AAC AGC CT

Reverse: TGG TCC ATG AGC ACT ATC AC

mSTIM1:

Forward: TGG ATG AGG AGA TTG TGT CGC C

Reverse: GAC TCC GAA TCG GAA TGG GTC A

mSTIM2:

Forward: GCC AGT ATG CAG AGC AGG AAC T

Reverse: GCT GAA GCC ATT TCT GTA GTG CG

hOGT:

Forward: CAG GAA GGC TAT TGC TGA GAG G

Reverse: CGG AAC TCA CAT ATC CTA CAC GC

Statistics

Unpaired T-test- Unpaired T-test statistical analysis compares the averages/means of two independent or unrelated groups to determine if there is a significance between the groups. The Unpaired T-Test can either compare between two unrelated groups that have normal and equal distributions or can be amended using Welch's correction which does not assume equal distribution between the groups.

Equal Distribution:

$$T = \frac{X_1 - X_2}{s^2(\left(\frac{1}{n}\right) + \left(\frac{1}{n}\right))}$$

where X are the group means, s is the standard deviation, and n is the number of samples

Welch's Correction:

$$T = \frac{m_A - m_B}{\sqrt{\frac{s_A^2}{n_A} + \frac{s_B^2}{n_B}}}$$

where m are the group means, s is the standard deviation, and n is the number of samples. The difference between the two tests is that classic Unpaired T-test pools the standard deviations together of the samples, whereas the Welch's correction separates each standard deviation for comparison.

Paired T-test- Paired T-test statistical analysis compares the difference of means between pairs. The T-test compares the means between pairs assuming normal distribution of both groups and uses the following equation:

$$T = \frac{\sqrt{n} * (\bar{x} - D)}{S}$$

where n is the number of samples, $\bar{x}$ is the sample mean difference between the observations, D is the expected mean difference (different from the null hypothesis), and S is standard deviation. Significance was measured by α=0.05. Therefore, to determine whether the result was significant the T statistic was compared to the corresponding value of the t table of significance, with a larger T statistic resulting in significance.

One-Way ANOVA- One-Way ANOVA statistical analysis compares the mean of one variable across more than two groups assuming normal distribution and equal variance among the dependent variable. The ANOVA produces the f statistic, the ratio of the variance among the means to the variance within the samples, which basically is demonstrating the ratio of variance across the groups compared to within the groups. This ratio directly correlates with significance and the equation for the F ratio is as follows:

$$f = \frac{[\frac{s^2}{\sigma^2}]}{[\frac{s^2}{\sigma^2}]}$$

where the numerator is population 1 and denominator is population 2. S represents standard deviation of the sample drawn from the population while σ is standard deviation of the population. The F ratio is then compared to the F statistic (degrees of freedom; number of samples subtracting 1), and if the F ratio is greater than the F statistic, the differences are statistically significant.

Chi-Squared Test- Chi-Squared statistic analysis is used to determine whether there is a statistically significant difference between the expected and observed frequencies in a contingency table to determine if sample data matches a population. Thus, calculating a Chi-square (X^2) statistic. The X^2 statistic is calculated using the following formula:

$$X^2 = \sum (O - E)^2 / E$$

$$\boldsymbol{E = \left(\frac{RT}{n}\right)\left(\frac{CT}{n}\right) * n}$$

where O is observed number of changes in a population and E is expected number of changes in a population. Expected value is calculated by taking the Row Total and Column totals divided by the amount of samples tested (n) and multiplying them by the number of samples tested (n). To determine if the X^2 statistic is significant you calculate the alpha statistic (α=0.05) and the degrees of freedom (the number of groups subtracting 1) to generate a critical value. If the X^2 statistic is greater than the critical value, the statistic is significant.

Kruskal-Wallis Non-Parametric Test- Non-Parametric statistical analyses compares groups of data when data is not normally distributed. Kruskal-Wallis test is used in place of a One-Way ANOVA with non-normal distribution datasets and is performed by ranking the data points and then comparing the median ranks instead of the raw data points to calculate the H statistic. The H statistic is calculated using the following formula:

$$H = \left[\frac{12}{n(n+1)} \sum_{j=1}^{c} \frac{T^2}{nj}\right] - 3(n+1)$$

Where n is the sum of the sample sizes for all samples, c is the number of samples, T is the sum of ranks in the j^{th} percentile, nj is the size of the j^{th} sample. To determine significance, you find the critical X^2 value and if the H statistic is greater than the critical X^2 value, then the differences in medians are significant.

Two-Way ANOVA- A Two-Way ANOVA compares the means of 2 variables across multiple groups assuming normal distribution and equal variance among the dependent variable. Two-Way ANOVA is calculated using sum of squares (SS) statistic, mean of squares (MS) statistic and degrees of freedom within and across groups.

$$SS(within) = \sum_{i=1}^{1} 1 \sum_{j=1}^{2} 1 \sum_{k=1}^{3} (Yijk - Yij)\text{^}2$$

$$df(within) = n - 1$$

$$MS(within) = SS(within)/df(within)$$

Here, Yijk are the elements within a single group and Yij are the number of combinations possible. N is the number of samples tested. Then, these same calculations occur across groups for how many variables there are across groups.

Group 1 (“A” number of groups)

$$SS(across) = r * a * \sum_{i=1}^{2} (Yi - Y)\text{^}2$$

$$df(across) = a - 1$$

$$MS(across) = SS(across)/df(across)$$

Group 2 (“B” number of groups)

$$SS(across) = r * b * \sum_{i=1}^{3} (Yi - Y)\text{^}2$$

$$df(across) = a - 1$$

$$MS(across) = SS(across)/df(across)$$

Finally, we calculate the interaction within and across groups

$$SS(interaction) = \sum_{i=1}^{2} 1 \sum_{j=1}^{3} (Yij - Yi - Yj - Y)\text{^}2$$

$$df(interaction) = (a * b) - 1$$

$$MS(interaction) = SS(interaction)/df(interaction)$$

After calculating the within, across, and interaction between group deviation we calculate the F-value:

MS(group A)/MS(within)= F(group A)

MS(group B)/MS(within)=F(group B)

MS(interaction)/MS(within)=F(interaction)

Finally, we take the F values and compare to the F critical values in an F table and if the F value is higher, we have a statistically significant difference.

CHAPTER 4

RESULTS

UV Suppresses SOCE And Enhances Invasion In Melanoma

We assessed the effect of UV on SOCE in melanoma in a panel of established non-metastatic human melanoma cell lines containing a range of different common driver mutations common to melanoma (SKMEL5, UACC1273, SKMEL2, FS13, SKMEL28, UACC257)(548)) and ((WM983, WM983BR)(549)) (Table 4-1). Cells were exposed to UV (175J/M^2), then allowed to recover for 24 hours. To induce SOCE, cells were treated with the Sarco/Endoplasmic Reticulum Calcium ATPase (SERCA) pump inhibitor thapsigargin (Tg; 2μM) for 10 minutes to deplete the ER of Ca^{2+} prior to the addition of 1mM Ca^{2+}. Addition of exogenous Ca^{2+} induced SOCE in all cell lines, although variable SOCE amplitudes were observed amongst the different cell lines (Fig 4-1A). Prior exposure to UV suppressed SOCE in all cell lines tested 24 hours after a single UV exposure (Fig 4-1A-B); no relationship to driver mutations in the different cell lines could be detected. To determine if this was a transient or stable effect, Basal Calcium (Fig 4-2A-C), Tg-Induced Ca^{2+} release (Fig 4-2A-B,D), and SOCE (Fig 4-1C, 4-2A-B) were tracked on a weekly basis for 5 weeks in WM983 and UACC257 cells after a single exposure to UV. In result, WM983 cells exhibited substantial SOCE suppression at 2-3 weeks after UV exposure, after which, there was a short recovery period followed by a second, steeper suppression of SOCE between 4 and 5 weeks. Despite these differences in SOCE, there were no significant changes in Basal or Tg-Induced Ca^{2+} release in response to UV exposure (Fig 4-2A,C-D). Conversely, UACC257 cells did not exhibit any significant changes in Basal

(Fig 4-2B-C), Tg-Induced Ca^{2+} release (Fig 4-2B,D) or SOCE (Fig 4-1D, 4-2B) in response to UV exposure.

To determine if differences in the stability of UV-induced SOCE suppression in WM983 and UACC257 cells correlated with invasiveness, transwell invasion assays were performed on non-irradiated cells or cells exposed to UV and allowed to recover for either 2 or 5 weeks (hereafter termed UV2 or UV5, respectively; Fig 4-1D). Notably, whereas several-fold increases in the number of invasive UV2 and UV5 WM983 cells were observed, at the 2 and 5 week timepoints, WM983, but not UACC257, cells exhibited increased invasiveness, correlating with the SOCE phenotypes of these models.

A significant question to consider is whether UV exposure and SOCE suppression cause changes in proliferative ability since melanoma is well-known to undergo a phenotypic switch from radial to vertical growth phase (342) and a widespread hypothesis of cancer cell behavior is that cancer cells follow a “go or grow” hypothesis where cells either proliferate or invade; an effect that is widely considered mutually exclusive (550). To determine if increased invasiveness might reflect UV-dependent effects on cell viability and/or proliferation, we performed WST-1 proliferation assays (Fig 4-3A-B), with no UV-dependent differences found in WM983 or UACC257 cells, suggesting that UV-exposed melanoma cells are not only still viable after UV exposure, but are able to invade without changes to their proliferative capacity. Hence, these data demonstrate a direct correlation between SOCE suppression and invasive behavior in UV-induced melanoma progression, along with an intriguing delay between UV exposure and reprogramming of invasive responses.

To determine if UV-induced SOCE suppression and invasiveness would also occur *in vivo*, we extended our study to B16N melanoma cells, with the ultimate goal of assessing metastasis in immunocompetent C57Bl/6 mice. Paralleling results in human melanoma cells, UV exposure led to SOCE suppression after a 5-week incubation (Fig 4-1E-F), with a similar increase in invasion through Matrigel in a transwell invasion assay *in vitro* (Fig 4-1G). In complementary work, untreated, UV2 or UV5 B16N cells were injected s.c. in syngeneic C57BL/6 mice and allowed to grow for 2 weeks before being euthanized and assessing metastasis by pathology. Consistent with prior studies (551, 552), in 26 out of 28 mice injected with untreated B16N cells, no evidence of metastasis was found using full body histopathology and aperio scan analysis (Table 4-2). In contrast, over half of the mice (8/15) injected with UV2 B16N cells had detectable metastases, as did 79% (19/24) of mice injected with UV5 B16N cells (Table 4-2). Interestingly, for all B16N models, infiltration was observed throughout the peritoneum, but not in the lungs (Fig 4-1H; Table 4-2). While it is more typical for melanoma to metastasize to the lungs, these data nevertheless demonstrate a potent UV-dependent shift towards invasive behavior.

Table 4-1: Mutation Status of Human Melanoma Cell lines

	BRAF	NRAS	TP53	EGFR	CDKN2A	TERT	Other
SKMEL5	Het V600E				X	C242T/ C243T	
UACC1273							
SKMEL2		Q61R	Het G245S			C250T	
FS13							
WM983BR	V600E		P278F		X	X	Homozygous Loss- CCND1, CCND2, FGF4, HRAS, MMP8
SKMEL28	V600E		L145R	P753S		A161C	PTEN T167A Het CDK4 R24C
WM983	Het V600E		P278F		X		Homozygous Loss- CCND2, MMP8
							High Copy Gain- MITF
UACC257	Het V600E					C250T	

X- Mutation exists but is not specified

Figure 4-1

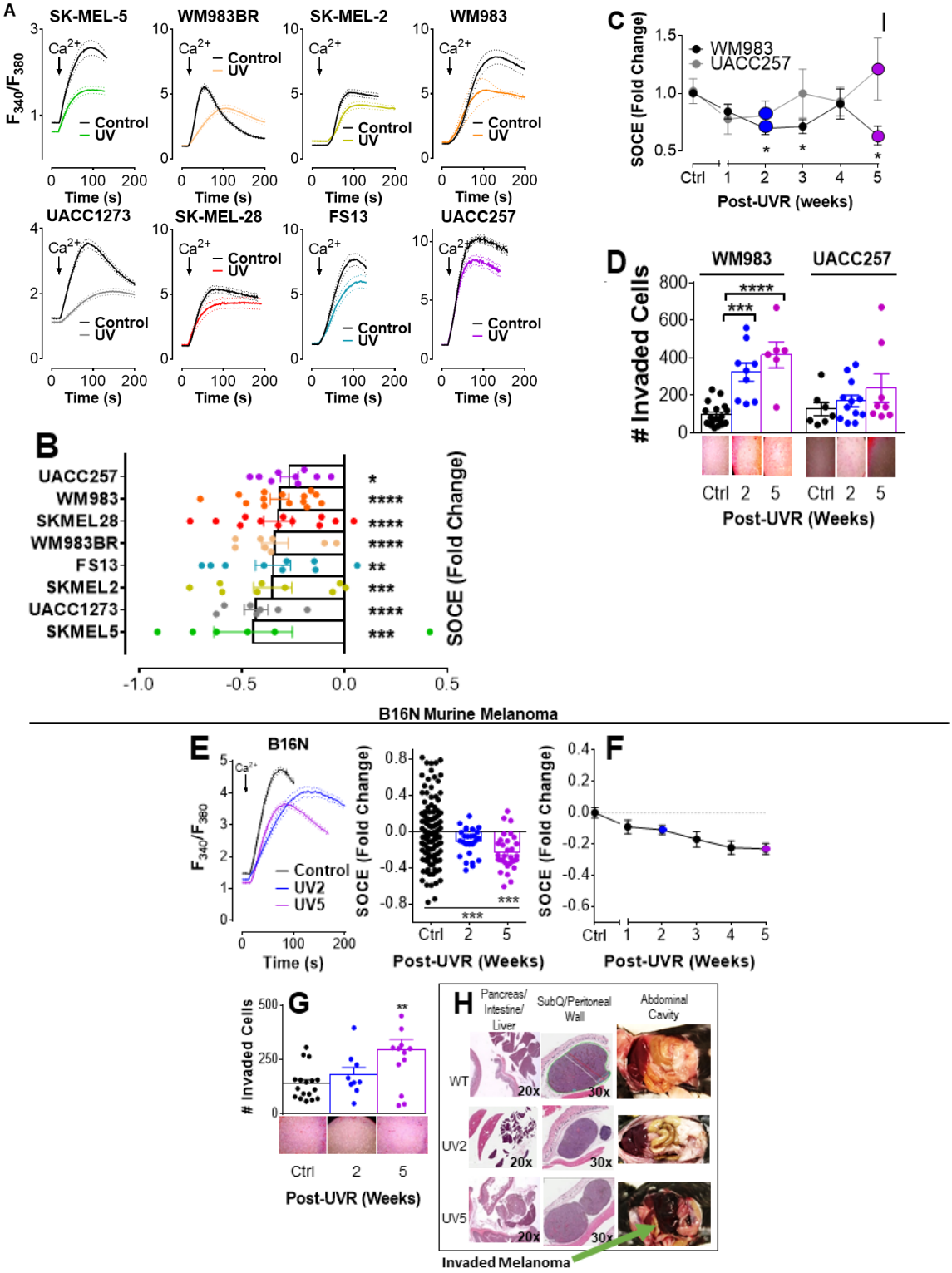
A
SK-MEL-5
WM983BR
SK-MEL-2
WM983
UACC1273
SK-MEL-28
FS13
UACC257
Ca2+
Control
UV
F340/F380
Time (s)
C
WM983
UACC257
SOCE (Fold Change)
Post-UVR (weeks)
D
WM983
UACC257
Invaded Cells
Ctrl 2 5
Post-UVR (Weeks)
B
UACC257
WM983
SKMEL28
WM983BR
FS13
SKMEL2
UACC1273
SKMEL5
SOCE (Fold Change)
B16N Murine Melanoma
E
B16N
Control
UV2
UV5
SOCE (Fold Change)
Post-UVR (Weeks)
F
SOCE (Fold Change)
Post-UVR (Weeks)
G
Invaded Cells
Ctrl 2 5
Post-UVR (Weeks)
H
Pancreas/ Intestine/ Liver
SubQ/Peritoneal Wall
Abdominal Cavity
WT
UV2
UV5
20x
30x
Invaded Melanoma

Figure 4-1: UV exposure suppresses SOCE and enhances invasion. (A-D) Human melanoma cells were plated on glass coverslips overnight before exposure to 175J/m^2 UV. **(A)** Representative traces showing the effect of UV on SOCE in 8 human melanoma cell lines. Cells were incubated overnight before loading with Fura2; cells were treated with 2μM Tg for 15 minutes in the absence of extracellular Ca^{2+} (not shown) before the addition of 1mM Ca^{2+}. Dashed lines indicate SEM. **(B)** UV-dependent differences in SOCE were determined by comparing the maximal change in Fura2 ratio between UV-treated and untreated cells after the addition of extracellular Ca^2. There was no statistically significant change in rate of entry (not shown). Each cell line is represented as a different color as depicted; each replicate included 10 to 60 individual cells. Data was analyzed by two-way ANOVA with multiple comparisons (UV effect, $p < 0.0001$; effect of cell line, $p > 0.05$; interaction, $p > 0.05$). **(C-D)** UACC257 and WM983 cells were treated as described for panel A, except the incubation periods were extended as depicted (N≥3). Data was analyzed by 2-way ANOVA with multiple comparisons (UV effect, $p < 0.01$; Effect of cell line, $p < 0.05$; interaction, $p > 0.05$). **(E)** UV-treated cells were placed in Matrigel transwell inserts in OptiMEM reduced serum media; DMEM with 10% FBS was used as a chemoattractant. Crystal violet-stained invaded cells were measured 20 hrs after initiation of assay (N≥4). Sample images for each condition are shown above the corresponding bar. Data was analyzed by two-way ANOVA with multiple comparisons (UV effect, $p < 0.0001$; Effect of cell line, $p > 0.05$; interaction, $p < 0.01$). **(F-G)** B16N murine melanoma cells were plated on glass coverslips overnight before exposure to 175J/m^2 UV and then incubated under growth optimal conditions for 0, 2 or 5 weeks. **(F)** SOCE was measured in B16N murine melanoma cells as in **(A)**. **(G)** SOCE results from (**F**) were quantified as in (**B**) (N≥15). Data were analyzed by one way ANOVA with multiple comparisons (p <

0.05). **(I-J)** B16N cell gene expression was measured as in **(C-D)** **(I)** B16N invasiveness was determined as in (**E**) (N≥9). Data was analyzed by one way ANOVA with multiple comparisons (p = 0.0001). **(J)** B16N cells were exposed to UV and incubated for the indicated time before subcutaneous injection into the right flank of syngeneic C57Bl6 mice. Shown, representative pictures of abdominal organs, peritoneal wall, and crude abdomen after 2 weeks of tumor cell *in vivo* growth (N≥9). Each dot on each bar is a biological replicate. *p<0.05, **p<0.01, ***p<0.001, ****p<0.0001.

Figure 4-2

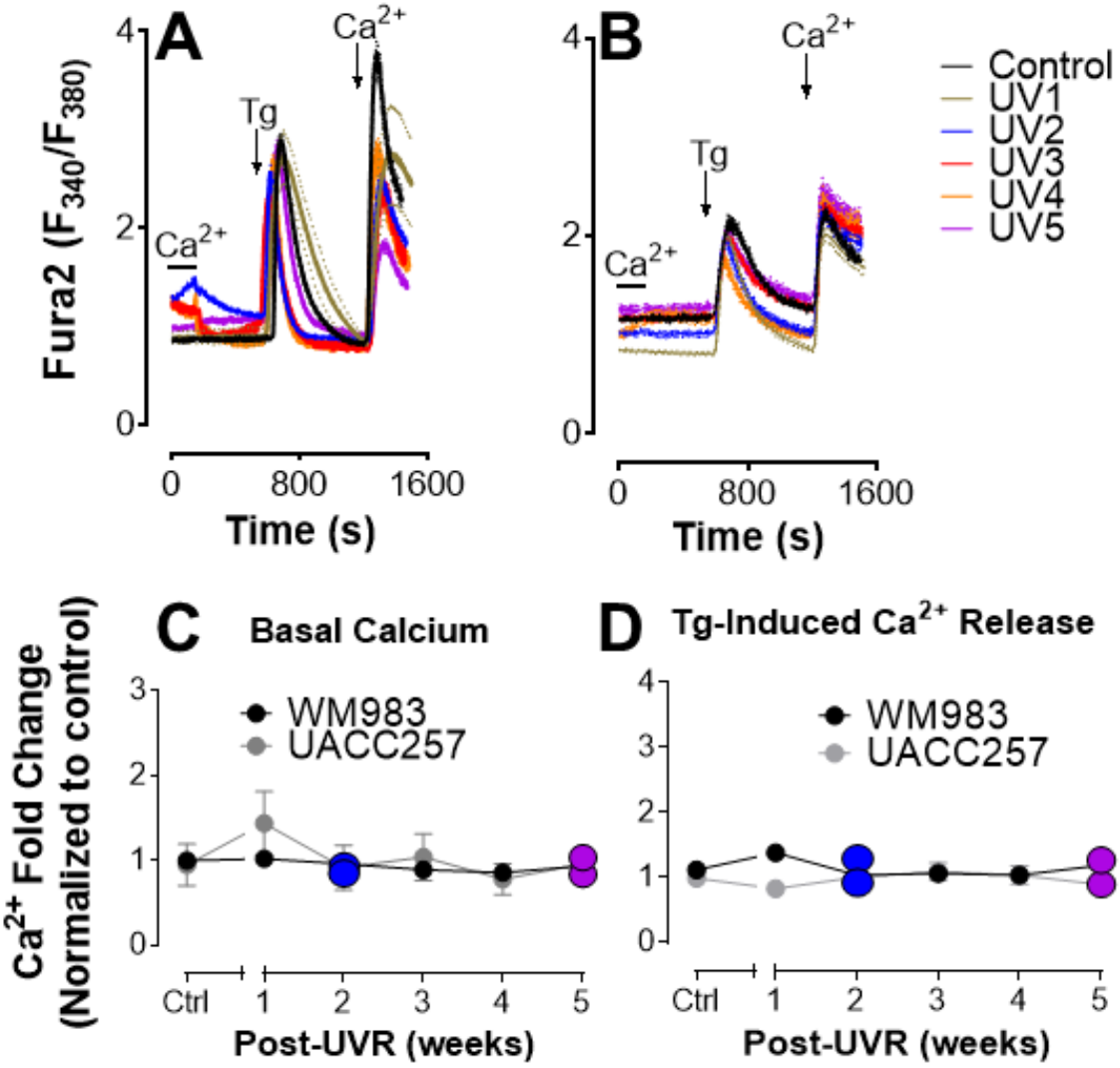
A
B
C
D
Fura2 (F_{340}/F_{380})
Ca^{2+}
Tg
Time (s)
Control
UV1
UV2
UV3
UV4
UV5
Ca^{2+} Fold Change (Normalized to control)
Basal Calcium
Tg-Induced Ca^{2+} Release
WM983
UACC257
Ctrl
Post-UVR (weeks)

Figure 4-2. Extended Calcium data from UVR-treated Human Melanoma Cells from Figure 4-1. WM983 and UACC257 human melanoma cells were plated overnight before exposure to 175 J/m^2 UVR. Cells were cultured under growth optimal conditions for the indicated time period before plating on glass coverslips and loading with Fura2. (A,B) Representative examples of Ca^{2+} measurements; recording began in the presence of Ca^{2+} (1mM). Ca^{2+} was removed at least 1 minute prior to the addition of Tg (2μM) followed by the re-addition of Ca^{2+} (1mM). (C) Basal Ca^{2+} is the average Fura2 ratio or Rhod2 fluorescence during the first minute. (D) Tg-induced Ca^{2+} release was quantified by calculating "area under curve" as a measure of total concentration to determine total Ca^{2+} release after the addition of Tg, but prior to the re-addition of Ca^{2+}. Data (n≥3) was analyzed by one way ANOVA.

Figure 4-3

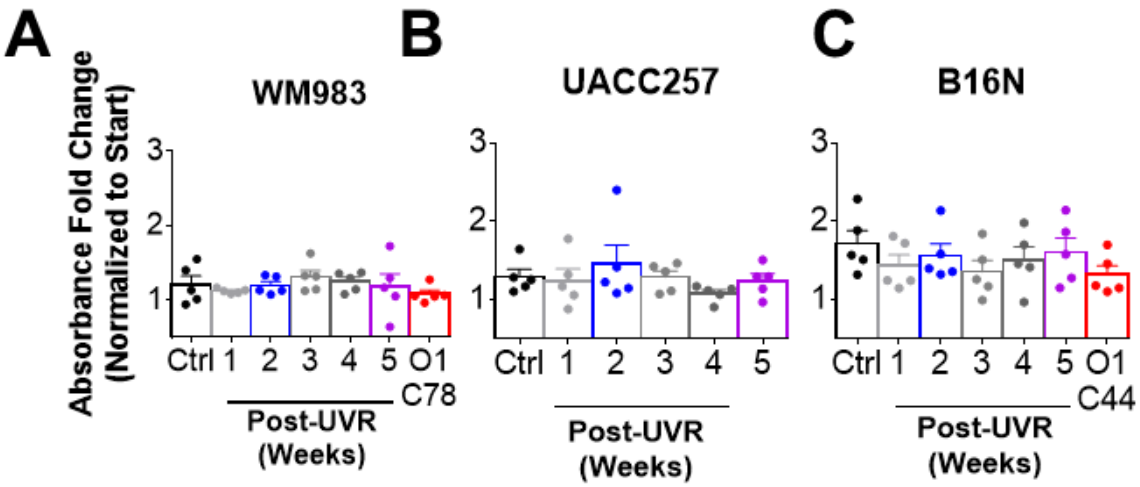
A
B
C
WM983
UACC257
B16N
Absorbance Fold Change (Normalized to Start)
3
2
1
Ctrl 1 2 3 4 5 O1
C78
Post-UVR (Weeks)
Ctrl 1 2 3 4 5
Post-UVR (Weeks)
Ctrl 1 2 3 4 5 O1
C44
Post-UVR (Weeks)

Figure 4-3. **Effect of UV and SOCE Suppression on Proliferation.** WM983 (A), UACC257 (B) and B16N (C) cells were exposed to 175J/m^2 UVR followed by 1 to 5 week incubations in growth optimal media, respectively. O1C78 (WM983) and O1C44 (B16N) are melanoma cells stably expressing Orai1-WT-CFP. To measure proliferation, equal numbers of cells were plated in 96 well plates and incubated for 3 days before being treated with 10% WST-1 for 1 hour prior to absorbance reading. Each dot on each bar is a biological replicate. Data was analyzed by one way ANOVA. *** $P < 0.001$

Table 4-2: Metastasis in mice after introduction of subcutaneous B16N tumors

Mouse Condition	Total Mouse Number	Invasion through Peritoneal Wall****	Abdominal Metastases Formed from Subcutaneous Tumors**	Sites of Mets Found
Control	28	2/28 (7.14%)	0/28 (0%)	Peritoneum (2 mice)
UV2	15	8/15 (53.3%)	2/15 (13.3%)	Peritoneum (2 mice) Liver (2 mice) Pancreas (2 mice) Kidney (1 mouse)
UV5	24	19/24 (79.1%)	9/24 (37.5%)	Peritoneum (9 mice) LN (8 mice) Pancreas (4 mice) Intestine (3 mice) Liver (8 mice) Mesentery (1 mouse) Spleen (1 mouse)
O1C44	14	13/14 (92.9%)	3/14 (21.4%)	Peritoneum (3 mice) LN (3 mice) Kidney (3 mice) Intestine (2 mice) Spleen (1 mouse) Liver
O1DN	10	3/10 (30%)	1/10 (10%)	Peritoneum (3 mice) Mesentery (1 mouse)

Significant differences in invasiveness through the peritoneal wall and into the abdomen was determined by the chi squared test. ** $P<0.01$; **** $P<0.0001$

Melanoma Progression Mediated By SOCE Suppression Exhibits A "Goldilocks Effect".

UV has a wide range of short- and long-term effects on cell function (Coelho et al, 2009), only one of which is SOCE suppression. To more directly establish a relationship between suppressed SOCE and invasiveness, we suppressed SOCE in B16N cells using 3,5- Bis(trifluoromethyl)pyrazole (BTP2), a well-established inhibitor of both Orai1-mediated SOCE and TRPC-mediated Ca^{2+} entry (He et al, 2005; Ishikawa et al, 2003; Schleifer et al, 2012; Zitt et al, 2004). Titration of BTP2 at a concentration range of 20 to 100nM suppressed SOCE at levels comparable to UV (Fig 4-4A-B) and additionally stimulated several-fold increases in invasiveness through transwell invasion assays (Fig 4-4C). The effect on invasiveness was lost at higher BTP2 concentrations (e.g. 200nM) suggesting an intriguing "Goldilocks effect." Similar observations were made in WM983 cells (Fig 4-5A-B). To further probe this concept, non-invasive UV2 B16N melanoma cells were treated with BTP2 (20nM), a concentration that had no effect on invasiveness in parental B16N cells (Fig 4-4D). Remarkably, increased invasiveness was observed, suggesting that SOCE was insufficiently suppressed in both cases to drive an increase in invasiveness through Matrigel. We then assessed the contribution of SOCE to the enhanced invasiveness of B16N UV5 cells by measuring invasiveness in the presence of BTP2 (200nM; Fig 4-4E). This completely blocked invasiveness, indicating that a minimum amount of SOCE is needed to support invasive behavior, consistent with the proposed "Goldilocks Effect." We note that these are very low concentrations of BTP2, well below toxic levels (Ishikawa et al., 2003; Zitt et al., 2004).

As another approach, we asked if genetic manipulation of SOCE would lead to a similar outcome. Overexpression of Orai1 has been reported to suppress SOCE through

stoichiometric imbalance with STIM1 (Hoover & Lewis, 2011; Soboloff et al, 2006). Therefore, we generated a series of B16N cell lines stably expressing Orai1 and screened them to determine the level of SOCE suppression. Two Orai1-overexpressing clones that exhibited SOCE suppression at levels similar to UV5 B16N cells were identified and designated O1C3 and O1C44 (Fig 4-4F-G). In both cases, these cells demonstrated enhanced invasion through Matrigel in a transwell invasion assay, to levels similar to those seen with UV5 B16N cells (Fig 4-4H). Similar observations were made in an Orai1-overexpressing clone of WM983 cells (Fig 4-5C-D).

Finally, we assessed the impact of a dominant negative Orai1 mutant (Orai1-E106ACFP; Orai1-DN; (Prakriya et al, 2006; Vig et al, 2006a; Yeromin et al, 2006)) previously shown to block invasion (Sun et al., 2014; Umemura et al., 2014). B16N cells stably expressing Orai1- DN (O1DN) exhibited both ablated SOCE (Fig 4-4I) and diminished invasion in a transwell invasion assay (Fig 4-4J). These observations reveal a non-linear relationship between SOCE and invasiveness in melanoma, in which partial suppression enhances invasion, but SOCE blockade abrogates it. An important property of invasion is migration, which is regulated in part by transient changes in Ca^{2+} levels that facilitate filipodia formation, lamellipodia attachment, and activation of myosin light chain kinases (MLCKs) that control movement (reviewed in (Gross et al, 2020b)). To assess the effect of SOCE on migratory potential, O1C44 and UV5 B16N cells were seeded as monolayers, grown overnight, scratched to create a wound, then imaged every 20 minutes for 20 hours. Both O1C44 and UV5 B16N cells exhibited greater migratory behavior compared to control cells (Fig 4-4K; 4-6). Interestingly, SOCE suppression in the absence of UV had a more profound effect on migration, with Orai1-overexpressing cells nearly completely filling the wound 10 hours after initial scratch.

Considered together, these data demonstrate SOCE suppression as a driving force behind migration and a mediator of UV-dependent enhancement of melanoma invasion. To determine if SOCE suppression is sufficient to drive invasiveness in syngeneic mice, Orai1-overexpressing B16N cells were injected s.c. and metastasis was assessed by pathology. Similar to mice injected with UV-irradiated cells, extensive metastasis was observed throughout the peritoneal cavity in 13 out of 14 mice (Table 4-2; Fig 4-4L). Although less common for melanoma, there is evidence showing that several metastatic cancers have been known to penetrate the peritoneal cavity through the peritoneal wall, a process commonly referred to as intraperitoneal carcinomatosis (IC) (Desai Jay P., 2020; Lee et al, 2014; McBride & Calhoun, 2019; Mikuła-Pietrasik et al, 2018). Additionally, when O1DN cells were injected s.c., 3 out of 10 mice exhibited contact with the peritoneal wall (Table 4-2; Fig 4-4L, M). Further, high resolution images of the peritoneal wall reveal no untreated B16N cells, but significant penetration of UVirradiated or Orai1-expressing B16N cells (Fig 4-4M,N). The 3 mice containing O1DN tumors showed less than 0.1 mm^2 of total invasion, even less than the 2 control mice, exhibiting peritoneal wall invasion (Fig 4-4N). Considered collectively, these data reveal that modest SOCE suppression promotes metastasis from an s.c. melanoma, while SOCE ablation has minimal or no effect.

Figure 4-4

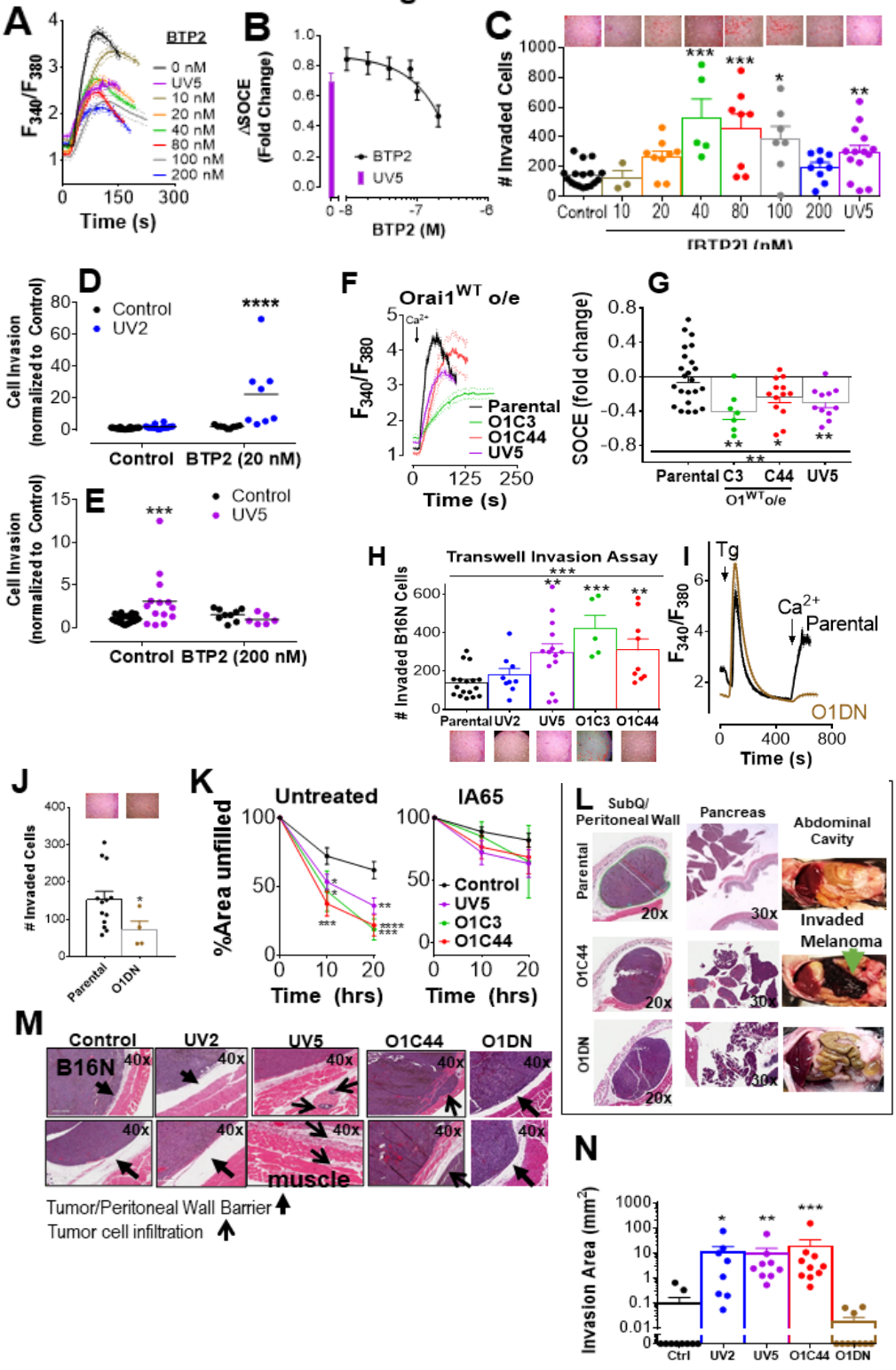
A
BTP2
0 nM
UV5
10 nM
20 nM
40 nM
80 nM
100 nM
200 nM
F340/F380
Time (s)
B
ΔSOCE (Fold Change)
BTP2
UV5
BTP2 (M)
C
Invaded Cells
Control
10
20
40
80
100
200
UV5
[BTP2] (nM)
D
Cell Invasion (normalized to Control)
Control
UV2
Control
BTP2 (20 nM)
E
Cell Invasion (normalized to Control)
Control
UV5
Control
BTP2 (200 nM)
F
Orai1WT o/e
Ca2+
F340/F380
Parental
O1C3
O1C44
UV5
Time (s)
G
SOCE (fold change)
Parental
C3
C44
UV5
O1WTo/e
H
Transwell Invasion Assay
Invaded B16N Cells
Parental
UV2
UV5
O1C3
O1C44
I
Tg
Ca2+
Parental
O1DN
F340/F380
Time (s)
J
Invaded Cells
Parental
O1DN
K
Untreated
IA65
%Area unfilled
Control
UV5
O1C3
O1C44
Time (hrs)
Time (hrs)
L
SubQ/ Peritoneal Wall
Pancreas
Abdominal Cavity
Parental
O1C44
O1DN
Invaded Melanoma
20x
30x
M
Control
UV2
UV5
O1C44
O1DN
B16N
40x
muscle
Tumor/Peritoneal Wall Barrier
Tumor cell infiltration
N
Invasion Area (mm2)
Ctrl
UV2
UV5
O1C44
O1DN

Figure 4-4. Partial SOCE suppression increases invasiveness. (A) Representative traces of SOCE in Fura-2 loaded B16N cells treated with the indicated concentrations of BTP2 for 15 minutes, in the presence of Tg. A representative trace of UV5 B16N is also shown for reference. (B) SOCE from (A) was quantified; dose dependence was measured by non-linear regression (n= 6). UV5 SOCE is shown as a purple bar for comparison (C) BTP2-treated B16N cells were plated on Matrigel transwell inserts in OptiMEM reduced serum media; DMEM with 10% FBS was used as a chemoattractant. Crystal violet-stained invaded cells were measured 20 hrs after initiation of assay (N≥3). Sample images for each condition are shown above the corresponding bar. Data were analyzed by one-way ANOVA with multiple comparisons ($p < 0.01$). (D) UV2 or (E) UV5 B16N cellstreated with indicated concentrations of BTP2 followed by plating on matrigel transwell inserts as described (C). (F) Representative traces of SOCE in 2 Orai1-CFPexpressing cell lines exhibiting SOCE suppression similar to BTP2 (40nM). (G) Relative SOCE suppression observed in Orai1-expressing or UV5 B16N cells (N≥5). Data were analyzed by one-way ANOVA with multiple comparisons ($p < 0.01$). (H) Transwell migration assays of Parental, UV2, UV5, O1C3 and O1C44 B16N cells as described in (C) (N≥6). Data were analyzed by one-way ANOVA with multiple comparisons ($p < 0.001$). (I) Representative traces of SOCE in B16N cells stably expressing the dominant negative form of Orai1-CFP (E106A; O1-DN). (J) Transwell migration assays of B16N parental versus O1-DN-expressing cells as described in (C) (N≥4). Data was analyzed by unpaired T test ($p < 0.05$). (K) Quantitation of B16N cell monolayers 20 hours after being scratched (representative images in Figure S3). UV2, UV5 and O1C44 cells were incubated overnight in the presence (+) or absence (-) of 2 μM IA65. The cell-free area was quantified by ImageJ (N≥3). Data was analyzed by 2-way ANOVA. In the absence of IA65, SOCE suppression

effect was p< 0.0001; interaction was p>0.05. In the presence of IA65, SOCE suppression effect was p>0.05; effect of time was p < 0.0001; interaction was p< 0.001. (L-N) B16N parental, O1C44, and O1DN cells were subcutaneously injected in the right flank of syngeneic C57Bl6 mice revealing the presence of O1C44 (but not B16N-WT) cells in abdominal organs and within the peritoneal wall (L). (M) H&E stains of the peritoneal wall revealing the presence of melanoma cells in the peritoneal wall (↟=Tumor/Peritoneal wall barrier,↑=Tumor cell infiltration). (N) Quantitative measurement of degree of invasion within and through the peritoneal wall. Data was analyzed using the Kruskal-Wallis Rank Sum test (P < 0.001). Each dot on each bar is a biological replicate *p<0.05, **p<0.01, ***p<0.001, ****p<0.0001.

Figure 4-5

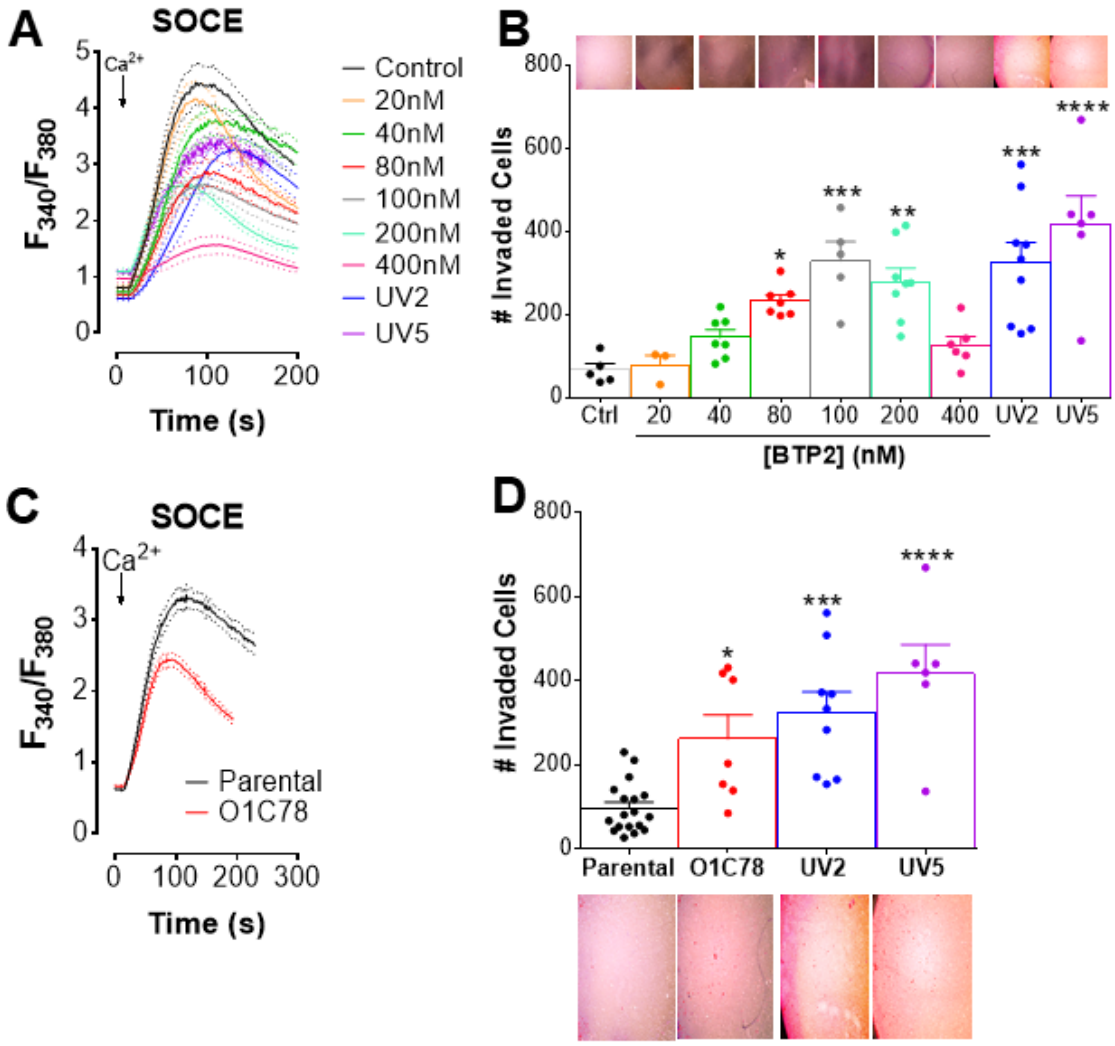
A
SOCE
Ca2+
F340/F380
Time (s)
Control
20nM
40nM
80nM
100nM
200nM
400nM
UV2
UV5
B
Invaded Cells
Ctrl
20
40
80
100
200
400
UV2
UV5
[BTP2] (nM)
C
SOCE
Ca2+
F340/F380
Time (s)
Parental
O1C78
D
Invaded Cells
Parental
O1C78
UV2
UV5

Figure 4-5. SOCE Suppression in Human Melanoma Cells Exhibits a "Goldilocks Effect". (A) Representative traces of SOCE in Fura-2 loaded WM983 cells treated with the indicated concentrations of BTP2 for 15 minutes in the presence of Tg. Data are representative of 5 experiments. UV2 and UV5 WM983 cells are also shown for comparison. (B) BTP2-treated WM983 cells were plated on Matrigel transwell inserts in OptiMEM reduced serum media; DMEM with 10% FBS was used as a chemoattractant. Invaded cells were measured after 20 hrs after staining with crystal violet (N≥3). UV2 and UV5 WM983 cells are also shown for comparison. (C) Representative traces of SOCE in parental and an Orai1-CFP-expressing WM983 cells named O1C78 exhibiting SOCE suppression similar to BTP2 (80nM). (D) Invasion assays performed as in panel B comparing the number of invaded cells in O1C78 cells to either untreated parental WM983 cells or WM983 cells exposed to UV irradiation and allowed to recover for 2 weeks (N≥4). Data was analyzed by one way ANOVA. Each dot on each bar is a biological replicate * $P < 0.05$; ** $P < 0.01$; *** $P < 0.001$; **** $P < 0.0001$

Figure 4-6

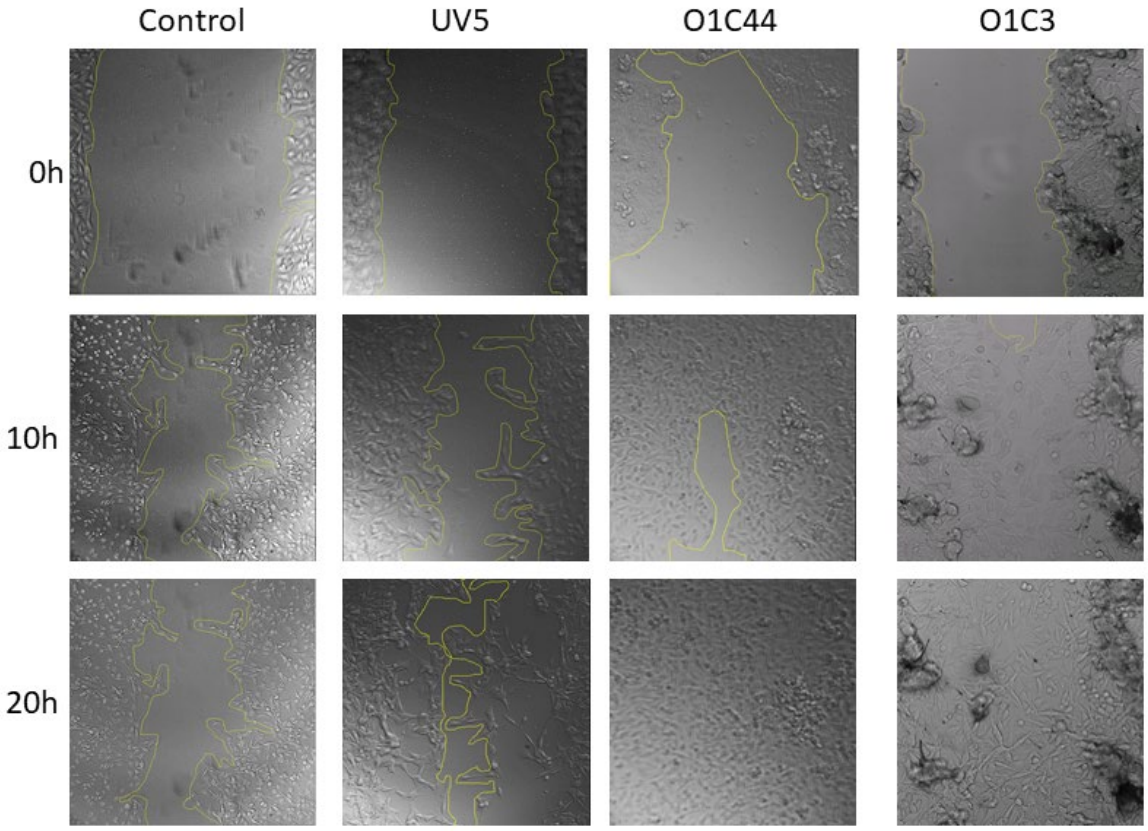

Figure 4-6. Pictures in support of Figure 4-4K. Untreated, UV5 or Orai1 overexpressing clones O1C44 and O1C3 B16N cells were plated in a monolayer overnight followed by scratching with a p10 pipette to create a cell-free zone. Migration into this zone was monitored by time lapse bright field microscopy for 20 hrs at 37°C and 5% CO_2. Representative images and times 0, 10 and 20 hrs are depicted, with cell-free areas demarcated by the yellow lines.

SOCE Recovery Inhibits Invasion

To further establish the concept that SOCE suppression contributes to UV-induced invasiveness, we used 4-((5-Phenyl-4-(trifluoromethyl)thiazol-2- yl)amino)benzoic acid (IA65), a potentiator of Orai1 and SOCE (Azimi et al, 2020; Zhang et al, 2020). IA65 had no effect on cell viability (Fig 4-7) or on SOCE in untreated WM983 cells, but strikingly reversed UV-induced SOCE suppression (Fig 4-8A-B). Notably, WM983 cells treated with IA65 failed to invade through Matrigel in a transwell assay even after exposure to UV (Fig 4-8C) and did not have UV-induced enhanced cell migration (Fig 4-8D-F). Similar observations of the effect of IA65 on SOCE, migration, and invasion were made in B16N cells (Fig 4-9). Collectively, these observations indicate that SOCE suppression is a required component of UV-induced increases in invasiveness in melanoma cells.

Figure 4-7

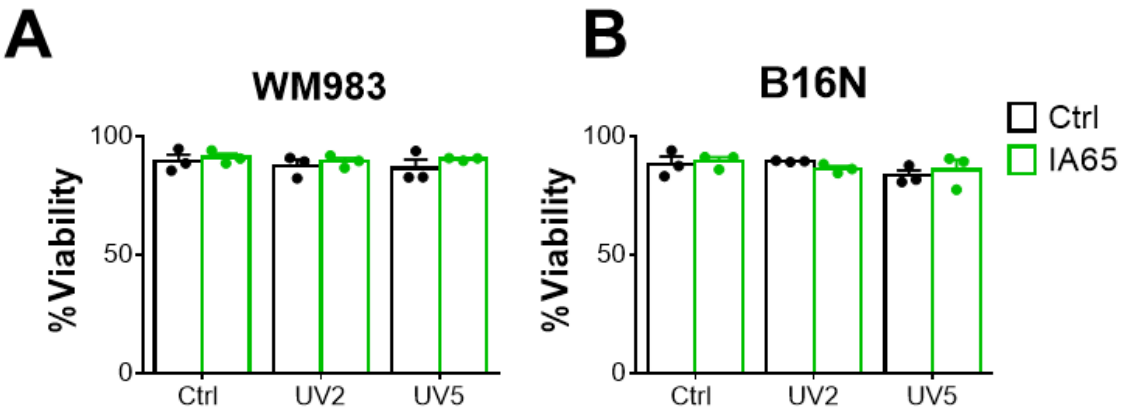
A
WM983
% Viability
100
50
0
Ctrl
UV2
UV5
B
B16N
% Viability
100
50
0
Ctrl
UV2
UV5
Ctrl
IA65

Figure 4-7. Assessing toxicity of IA65 on melanoma cells. WM983 **(A)** and B16N **(B)** cells were exposed to 175J/m^2 UVR followed by 2 (UV2) or 5 (UV5) weeks incubation in growth optimal media, respectively. To measure viability, equal numbers of cells were plated in 24 well plates and incubated overnight before being treated with 0.4% Trypan Blue and comparing the number of stained vs. unstained cells. Each dot on each bar is a biological replicate. Data was analyzed by one way ANOVA. *** $P < 0.001$

Figure 4-8

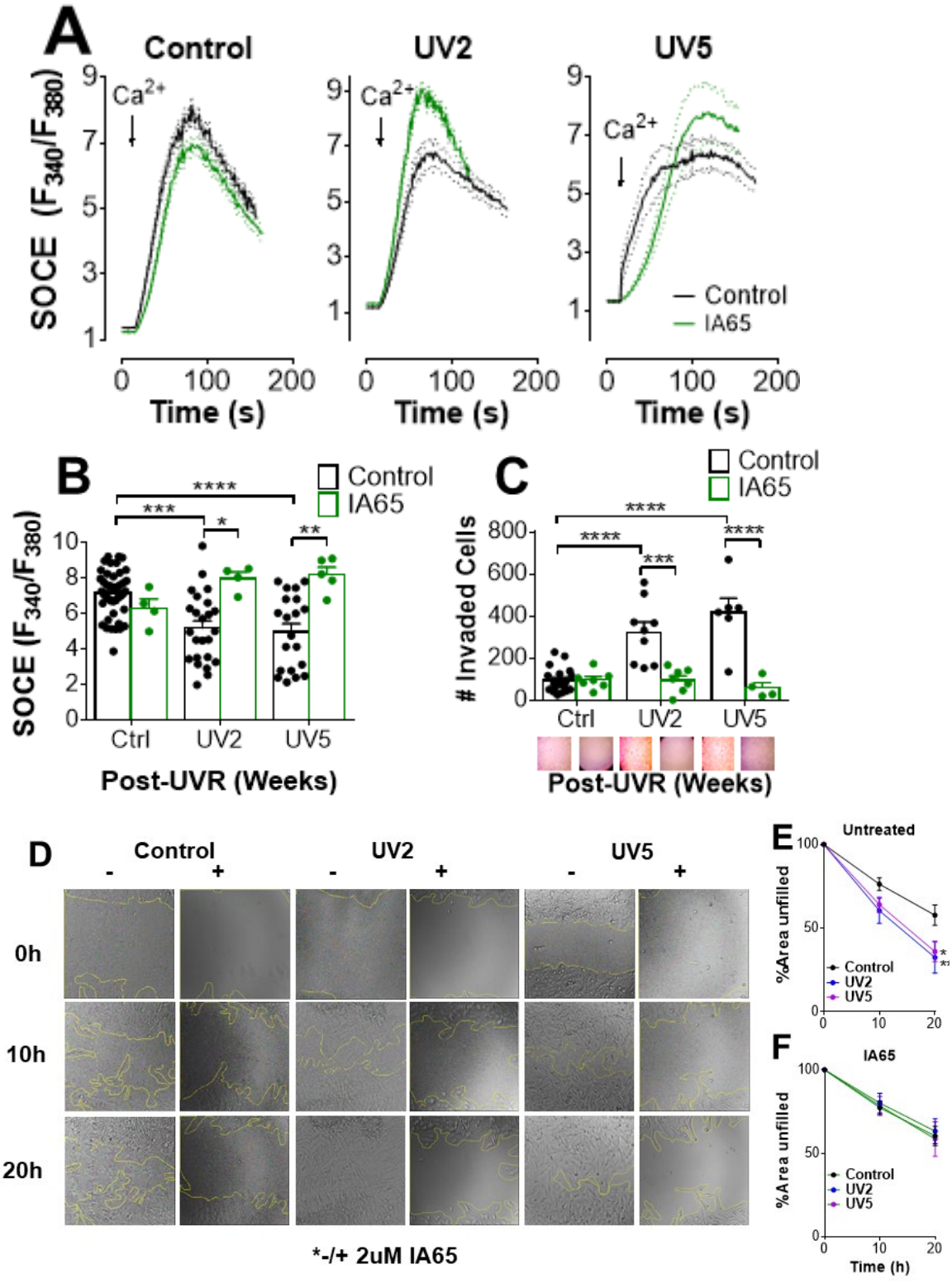
A
Control
UV2
UV5
SOCE (F340/F380)
Ca2+
Time (s)
Control
IA65
B
SOCE (F340/F380)
Control
IA65
Ctrl
UV2
UV5
Post-UVR (Weeks)
C
Invaded Cells
Control
IA65
Ctrl
UV2
UV5
Post-UVR (Weeks)
D
Control
UV2
UV5
0h
10h
20h
*-/+ 2uM IA65
E
Untreated
%Area unfilled
Control
UV2
UV5
F
IA65
%Area unfilled
Control
UV2
UV5
Time (h)

Figure 4-8: Enhancing SOCE suppresses UV-induced invasiveness. WM983 cells were plated on glass coverslips overnight before exposure to 175J/m2 UV and then incubated under growth optimal conditions for 0 (control), 2 (UV2) or 5 (UV5) weeks. (A) Representative traces of SOCE in Fura2-loaded cells treated with 2 μM IA65 or vehicle (Control) in the presence of Tg in nominally Ca^{2+}-free media for 15 minutes prior to the addition of Ca^{2+} (1mM) (B) Quantitation of SOCE from panel A (N≥4); data was analyzed by 2-way ANOVA (effect of UV, $p > 0.05$; IA65, $p < 0.001$; interaction was $p < 0.01$). (C) Control, UV2 and UV5 cells were treated with IA65 (0 or 2 μM) for 15 minutes before being placed in Matrigel transwell inserts in OptiMEM reduced serum media; DMEM with 10% FBS was used as a chemoattractant. Crystal violet-stained invaded cells were measured 20 hrs after initiation of assay (N≥4). Sample images for each condition are shown above the corresponding bar. Data was analyzed by 2-way ANOVA (effect of UV, $p < 0.01$; IA65, $p < 0.0001$; interaction was $p < 0.01$). (D-F) Confluent layers of WM983 cells treated as indicated were 'scratched' followed by a 20 hour incubation at 37°C with 5% CO2. (D) Representative images of cells after being scratched after being incubated for 0, 10 or 20 hours in the absence (-) or presence (+) of 2μM IA65. (E-F) The cell-free area was quantified by ImageJ (N≥8). Data was analyzed by 2-way ANOVA. In the absence of IA65, SOCE suppression effect was p< 0.0001; interaction was p0.05; effect of time was $p < 0.0001$; interaction was p>0.05. Each dot on each bar is a biological replicate. In the presence of IA65, SOCE suppression effect was p>0.05; effect of time was $p < 0.0001$; interaction was p>0.05. *p<0.05, **p<0.01, ***p<0.001, ****p<0.0001

Figure 4-9

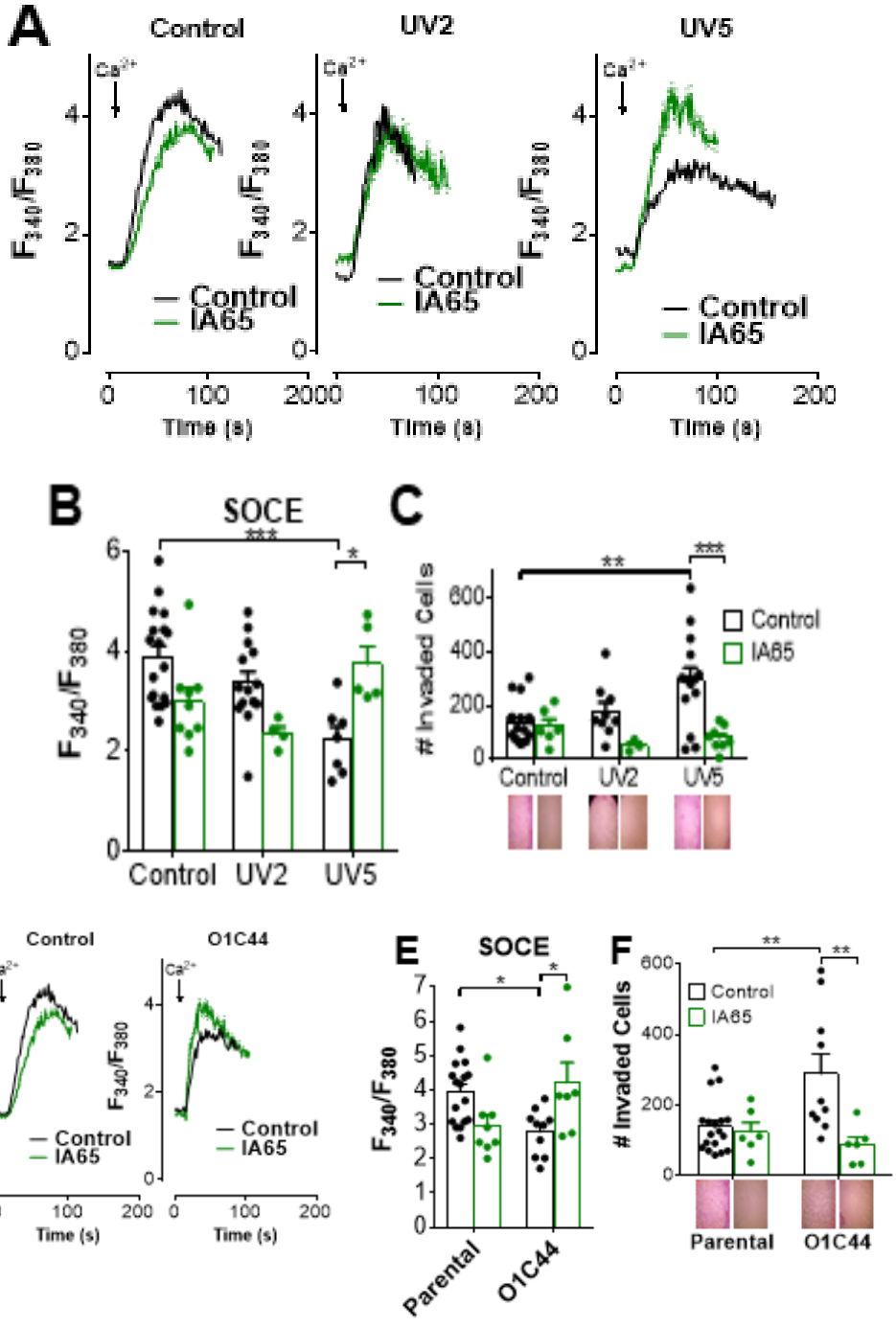
A
Control
UV2
UV5
Ca2+
F340/F380
Control
IA65
Time (s)
B
SOCE
***
*
F340/F380
Control
UV2
UV5
C
**
***
Invaded Cells
Control
IA65
Control
UV2
UV5
D
Control
O1C44
Ca2+
F340/F380
Control
IA65
Time (s)
E
SOCE
*
*
F340/F380
Parental
O1C44
F
**
**
Invaded Cells
Control
IA65
Parental
O1C44

Figure 4-9. IA65 reverses SOCE suppression and inhibits invasiveness in B16N melanoma cells. (A-C) B16N cells were plated on glass coverslips overnight before exposure to 175J/m^2 UVR and then incubated under growth optimal conditions for 0 (control), 2 (UV2) or 5 (UV5) weeks. (A) Representative traces of SOCE in Fura2-loaded cells treated with IA65 (0 or 2 μM) in the presence of Tg in nominally Ca^{2+}-free media for 15 minutes prior to the addition of Ca^{2+} (1mM) (B) Quantitation of SOCE from panel A (N≥4). (C) Control, UV2 and UV5 cells were treated with IA65 (0 or 2 μM) for 15 minutes before placing in Matrigel transwell inserts; the number of cells migrating through Matrigel was quantified as described in figure 4-1F (N≥3). (D) Representative traces of SOCE in Fura2-loaded cells treated with IA65 (0 or 2 μM) in the presence of Tg in nominally Ca^{2+}-free media for 15 minutes prior to the addition of Ca^{2+} (1mM) (E) Quantitation of SOCE from panel D (N≥4). (F) Parental and O1C44 cells were treated with IA65 (0 or 2 μM) for 15 minutes before placing in Matrigel transwell inserts; the number of cells migrating through Matrigel was quantified as described in figure 4-1F (N≥6). Each dot on each bar is a biological replicate

Identification Of The Mechanism Of UV-Induced SOCE Suppression

To determine the mechanism of UV-induced SOCE suppression, we first measured the level of expression of the 5 members of the STIM and Orai families by RT-qPCR (Fig 4-10). No significant UV-induced changes in the expression of Orai genes were observed in WM983 or B16N cells (Fig 4-10A, C), although significant UV-induced increases in Orai1 expression did occur in UACC257 ($p=0.0441$; Fig 4-10B). Since no significant UV-induced changes in SOCE were observed in UACC257 cells, the biological significance of this observation is unclear. Both O1C78 WM983 and O1C44 B16N cells exhibited a modest, but statistically significant increase in Orai1 expression (Fig 4-10A,C). No significant, changes in the expression of either STIM1 or STIM2 were observed in WM983, UACC257 or B16N cells (Fig 4-10D-F). Since no decreases in STIM or Orai expression were observed in UV5 cells, these data do not provide an explanation for UVinduced SOCE suppression. Therefore, we performed RNAseq, taking advantage of the observed differences in SOCE suppression in WM983 and UACC257 cells 2 weeks after UV exposure, comparing each cell model to non-irradiated cells (see Figs 1C; 4-11A-C). Principal component analysis (PCA) revealed both minimal replicate variability and the existence of 4 discrete groups, with UV having distinct effects in WM983 and UACC257 cells (Fig 4-11D). Comparison of the genes changed in these cell types reveals marked expression differences in the effect of UV on UACC257 and WM983 cells (Fig 4-11E). To identify those genes whose expression was altered by UV that could contribute to SOCE suppression, we then performed a Venn analysis comparing the genes whose expression was significantly altered ($p<0.01$) by UV exposure in WM983, but not UACC257 cells (Fig 4-11F), performing Ingenuity Pathway Analysis (IPA) on this group of 421 genes. Interestingly, the pathway whose expression was most altered was the superpathway of

cholesterol (CHL) biosynthesis (also known as the mevalonate pathway; Table 4-3) with 8 out of 28 genes upregulated (Table 4-3). CHL has been previously identified as an endogenous inhibitor of SOCE due to a direct interaction with Orai1 (Derler et al, 2016). Further, the mevalonate pathway has been to shown to contribute to melanoma progression in vivo (Pencheva et al, 2014). Finally, we performed Cancer Genome Atlas (TCGA) analysis to determine if the mevalonate pathway was similarly altered in clinical tumor samples (Fig 4-11G). Notably, melanoma was the second most likely tumor-type to exhibit mevalonate pathway dysregulation (3.4%); the most likely tumor type to exhibit mevalonate pathway dysregulation was anal cancer; however, since this was based on only 1 tumor (out of only 21 total), this is likely irrelevant. Therefore, we assessed the possibility that enhanced CHL biosynthetic pathways contributes to SOCE suppression and UV-induced melanoma invasiveness and metastasis.

To determine if UV treatment increased CHL content, we designed CHL sensors based on Perfringolysin O (PFO) toxin), a toxin with CHL-binding activity (Maekawa, 2017). Briefly, the CHL-binding portion of the PFO toxin was mutated to increase affinity with a D434S point mutation within the D4 domain (D4H), tagged with mCherry and transfected into WM983 and UACC257 cells (Fig 4-11H-I). UV markedly increased mCherry expression in WM983 in a time-dependent manner but did not do so in UACC257 cells (Fig 4-11H-I), consistent with the effect of UV on SOCE on these 2 cell types (Fig 4-1C). Analogous experiments were done in an Orai1 overexpressing clone of WM983 cells (O1C78) and showed no significant change in mCherry fluorescence, indicative of no change in cholesterol levels, revealing that cholesterol upregulation is upstream of SOCE suppression and is likely not bidirectional (Fig 4-11J-K). To assess if UV-induced CHL production contributes to UV-induced SOCE suppression, cells were treated with either

the HMG-CoA reductase inhibitor compactin (a statin drug) or the squalene synthase (SS) inhibitor TAK475, which targets a downstream step in the CHL biosynthesis pathway. While neither agent significantly affected SOCE in untreated WM983 cells, SOCE in UV5 WM983 cells was markedly enhanced after a 24 hr treatment with either agent (Fig 4-12A-B). Further, when these same CHL inhibitor drugs were given to non-SOCE suppressed UACC257 UV5 cells, no change occurred in SOCE (Fig 4-13). Additionally, both drugs abrogated UV-induced increases in WM983 melanoma invasiveness through Matrigel on a transwell assay, while having no effect on invasiveness in untreated cells (Fig 4-12).

Finally, to assess the contribution of CHL on melanoma metastasis in vivo, we analyzed the metastasis of parental and UV5 B16N cells grown for 5 weeks post-irradiation before implantation s.c. in Ldlr-/- mice (Fig 4-12D-E). Ldlr-/- mice exhibit relatively modest 50 to 300% increases in CHL levels when fed regular chow and a greater than 800% increase in CHL when fed high fat diet in comparison to WT C57Bl/6 mice (Franciosi et al, 2009; Hartvigsen et al, 2007). Interestingly, very modest invasion of untreated B16N cells into the peritoneal wall was observed in mice fed regular chow that was dramatically increased by high fat chow (Fig 4-12D-E). UV5 B16N cells exhibited substantial invasiveness in Ldlr-/- mice fed either regular chow or high fat diet. These data demonstrate that elevated CHL levels are sufficient to mimic UV-induced melanoma metastasis and support a model in which UV drives melanoma metastasis due to SOCE suppression mediated by increased CHL biosynthesis.

Figure 4-10

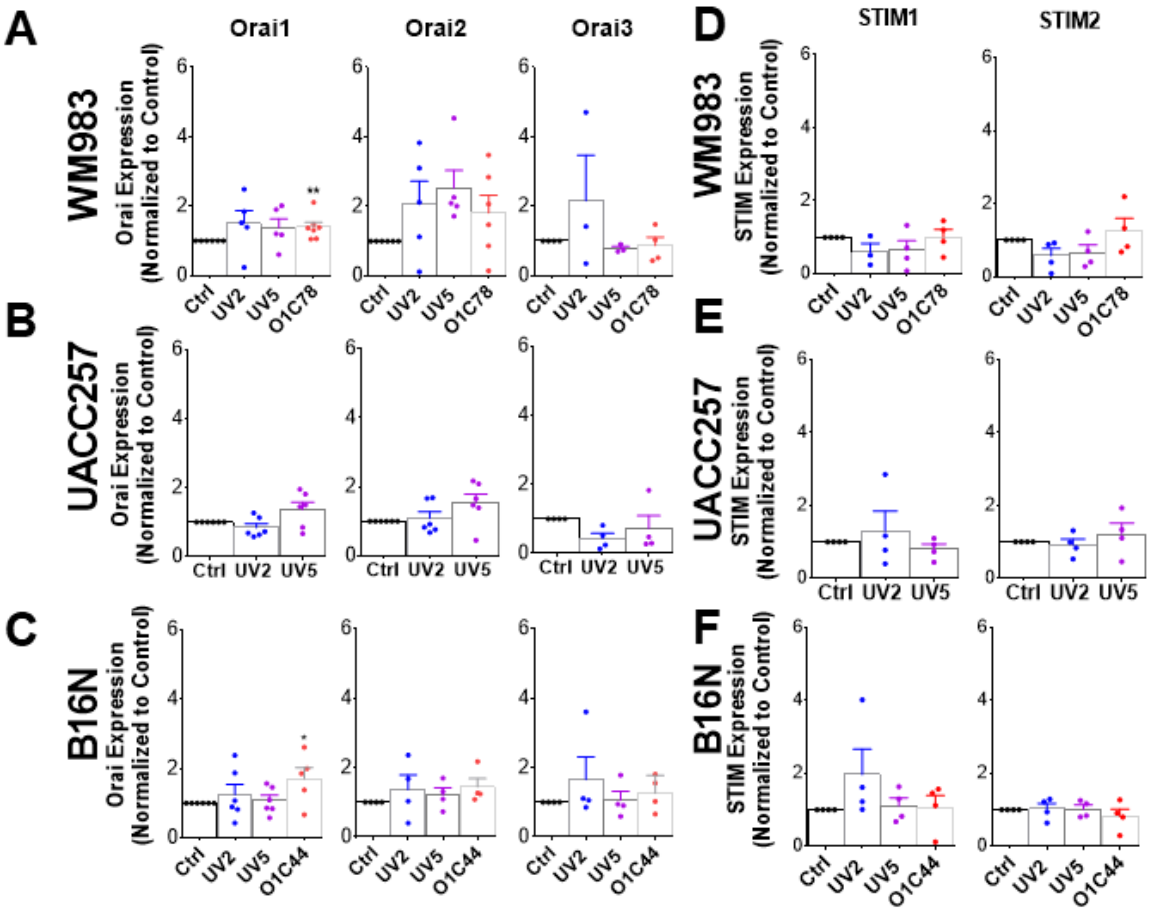
A
Orai1
Orai2
Orai3
WM983
Orai Expression (Normalized to Control)
Ctrl UV2 UV5 O1C78
B
UACC257
Ctrl UV2 UV5
C
B16N
Ctrl UV2 UV5 O1C44
D
STIM1
STIM2
STIM Expression (Normalized to Control)
E
F

Figure 4-10. Orai and STIM family gene expression patterns in response to SOCE suppression. Orai1 (A-C) and STIM (D-F) expression were measured by RT-qPCR from WM983 (A,D) UACC257 (B,E) human and B16N (C,F) murine melanoma cell lines. UV2 and UV5 cells are melanoma cells that were exposed to 175J/m^2 UVR followed by 2 or 5 week incubations in growth optimal media, respectively. O1C78 (WM983) and O1C44 (B16N) are melanoma cells stably expressing Orai1-WT-CFP. 18S rRNA was used as a housekeeping gene; data (N≥3) are presented as normalized to control. Each dot on each bar is a biological replicate. UV data was analyzed by one way ANOVA; Orai1 overexpressing clones were compared to control by T test.

Figure 4-11

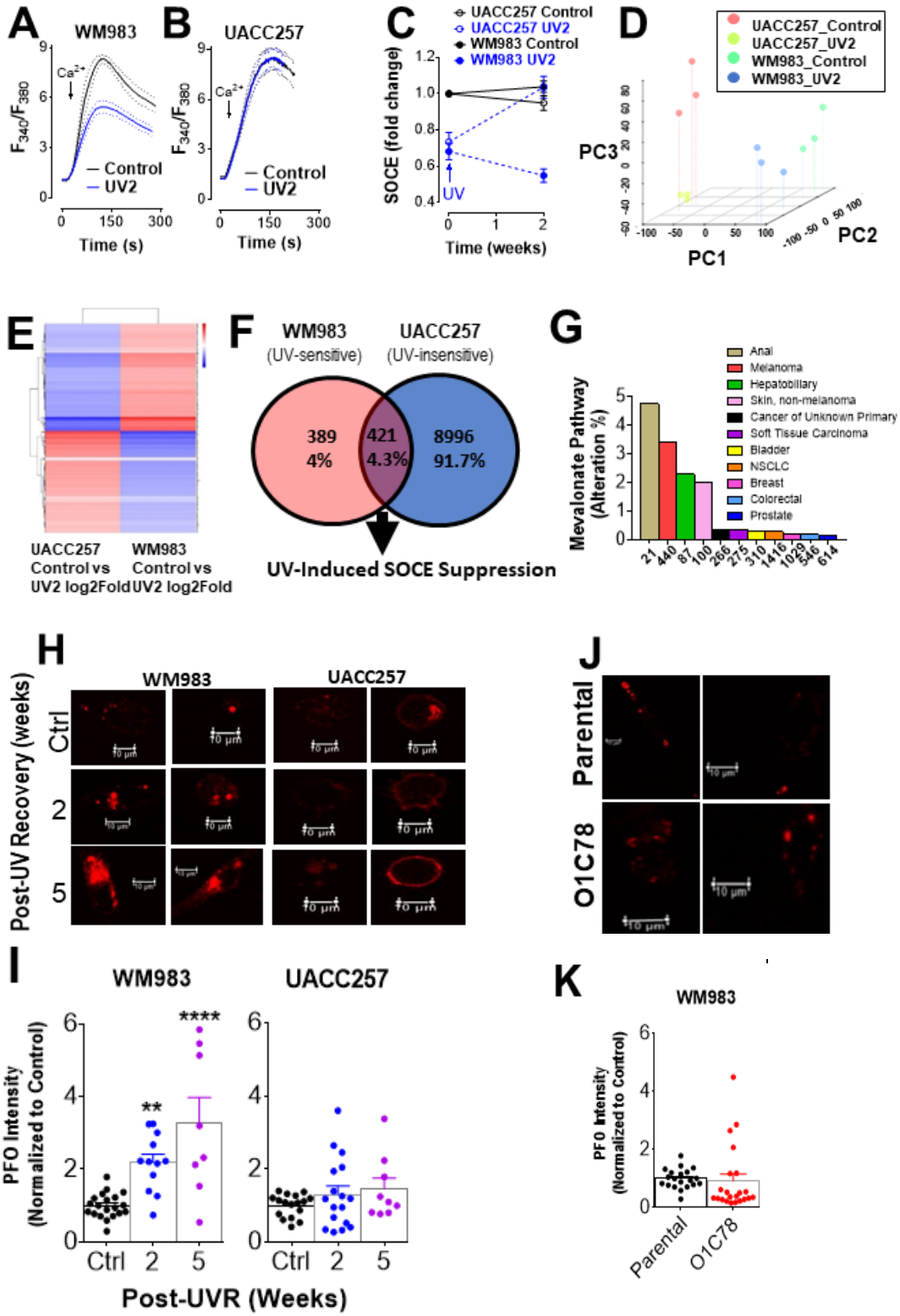
A
WM983
B
UACC257
F340/F380
Ca2+
Control
UV2
Time (s)
C
UACC257 Control
UACC257 UV2
WM983 Control
WM983 UV2
SOCE (fold change)
UV
Time (weeks)
D
UACC257_Control
UACC257_UV2
WM983_Control
WM983_UV2
PC1
PC2
PC3
E
UACC257 Control vs UV2 log2Fold
WM983 Control vs UV2 log2Fold
F
WM983 (UV-sensitive)
UACC257 (UV-insensitive)
389 4%
421 4.3%
8996 91.7%
UV-Induced SOCE Suppression
G
Mevalonate Pathway (Alteration %)
Anal
Melanoma
Hepatobiliary
Skin, non-melanoma
Cancer of Unknown Primary
Soft Tissue Carcinoma
Bladder
NSCLC
Breast
Colorectal
Prostate
21
440
87
100
266
275
310
1416
1029
546
614
H
WM983
UACC257
Post-UV Recovery (weeks)
Ctrl
2
5
J
Parental
O1C78
I
WM983
UACC257
PFO Intensity (Normalized to Control)
**
****
Ctrl
2
5
Post-UVR (Weeks)
K
WM983
PFO Intensity (Normalized to Control)
Parental
O1C78

Figure 4-11. Mevalonate pathway upregulation correlates with UV-induced SOCE suppression. (A-C) WM983 and UACC257 cells were plated on glass coverslips overnight before exposure to 175J/m2 UV and then incubated under growth optimal conditions for 0 (control) or 2 (UV) weeks followed by plating on glass coverslips, Fura2 loading and administration of Tg in nominally Ca^{2+}-free media for 15 minutes prior to the addition of Ca^{2+} (1mM), as in Fig 1A-C. (D-F) RNA was extracted from WM983 or UACC257 cells 2 weeks after UV exposure (0 or 175 J/m^2) followed by cDNA production and analysis (3 biological replicates per condition). (D) Principal component (PC) analysis showing the variability between the replicates. (E) Heatmap comparing genes significantly differing in WM983 and UACC257 cells two weeks after UV exposure ($p< 0.001$, $q<0.01$). (F) Venn diagram showing the genes significantly changed due to UV in WM983 but not significantly changed in UACC257 cells. (G) The percentage of tumors in which the mevalonate pathway by tumor type; data was obtained from TCGA. The numbers indicate the total number of samples available for each tumor type; the. (H-K) WM983 and UACC257 human melanoma cells were transfected with Perfringolysin O (PFO)-mCherry D4H cholesterol sensor and plated on glass coverslips. (H-J) Cells were exposed to UV (0 or 175 J/m^2) and incubated for 0, 2 or 5 weeks as indicated. (H) Representative cell images. (I) Fluorescence intensity from cells analyzed in (H) was measured and quantified using LASX analysis software (N≥8). Each dot on each bar is a biological replicate. Data was analyzed using 1-way ANOVA with multiple comparisons (WM983, $p < 0.001$; UACC257 $p > 0.05$). *p<0.05, **p<0.01, ***p<0.001, ****p<0.0001. (J-K) O1C78 WM983 cells expressing the PFO-mCherry D4H cholesterol sensor were examined as in panels H and I (N≥8).

Table 4-3: IPA Analysis of RNAseq of WM983 and UACC257 from Figure 7-4 showing top ranked upregulated pathways

Ingenuity Canonical Pathways	-log p-value	Ratio	Molecules
Superpathway of Cholesterol Biosynthesis	7.76	0.286	MVD, FDPS, IDI1, LSS, HMGCR, HMGCS1, GGPS1
Superpathway of Geranylgeranyldiphosphate Biosynthesis I (via Mevalonate)	6.56	0.353	MVD, FDPS, IDI1, HMGCR, HMGCS1, GGPS1
Ethanol Degradation IV	5.46	0.24	TYRP1, ALDH1L2, ALDH1A3, ACSS2, CAT, ALDH3B1
Trans, trans-farnesyl Diphosphate Biosynthesis	4.3	0.6	FDPS, IDI1, GGPS1
Mevalonate Pathway I	4.25	0.308	MVD, IDI1, HMGCR, HMGCS1
Oxidative Ethanol Degradation III	3.38	0.19	ALDH1L2, ALDH1A3, ACSS2, ALDH3B1
Oleate Biosynthesis II (Animals)	2.89	0.231	FADS2, ALDH6A1, FADS1
Geranylgeranyldiphosphate Biosynthesis	2.76	0.5	FDPS, GGPS1
Ethanol Degradation II	2.43	0.108	ALDH1L2, ALDH1A3, ACSS2, ALDH3B1
Histamine Degradation	2.39	0.158	ALDH1L2, ALDH1A3, ALDH3B1
Antigen Presentation Pathway	2.39	0.105	HLA-A, HLA-F, TAP2, HLA-DPA1
Fatty Acid α-oxidation	2.21	0.136	ALDH1L2, ALDH1A3, ALDH3B1
Putrescine Degradation III	2.15	0.13	ALDH1L2, ALDH1A3, ALDH3B1
Molecular Mechanisms of Cancer	1.69	0.033	ALDH1L2, ALDH1A3, ALDH3B1, RAC2, LRP5, GSK3A, RALBP1, CCND1, PAK1, CCNE, CDK11B, SMO, PRKAR1B, APH1B, ARHGEF9, BCL2L11

Figure 4-12

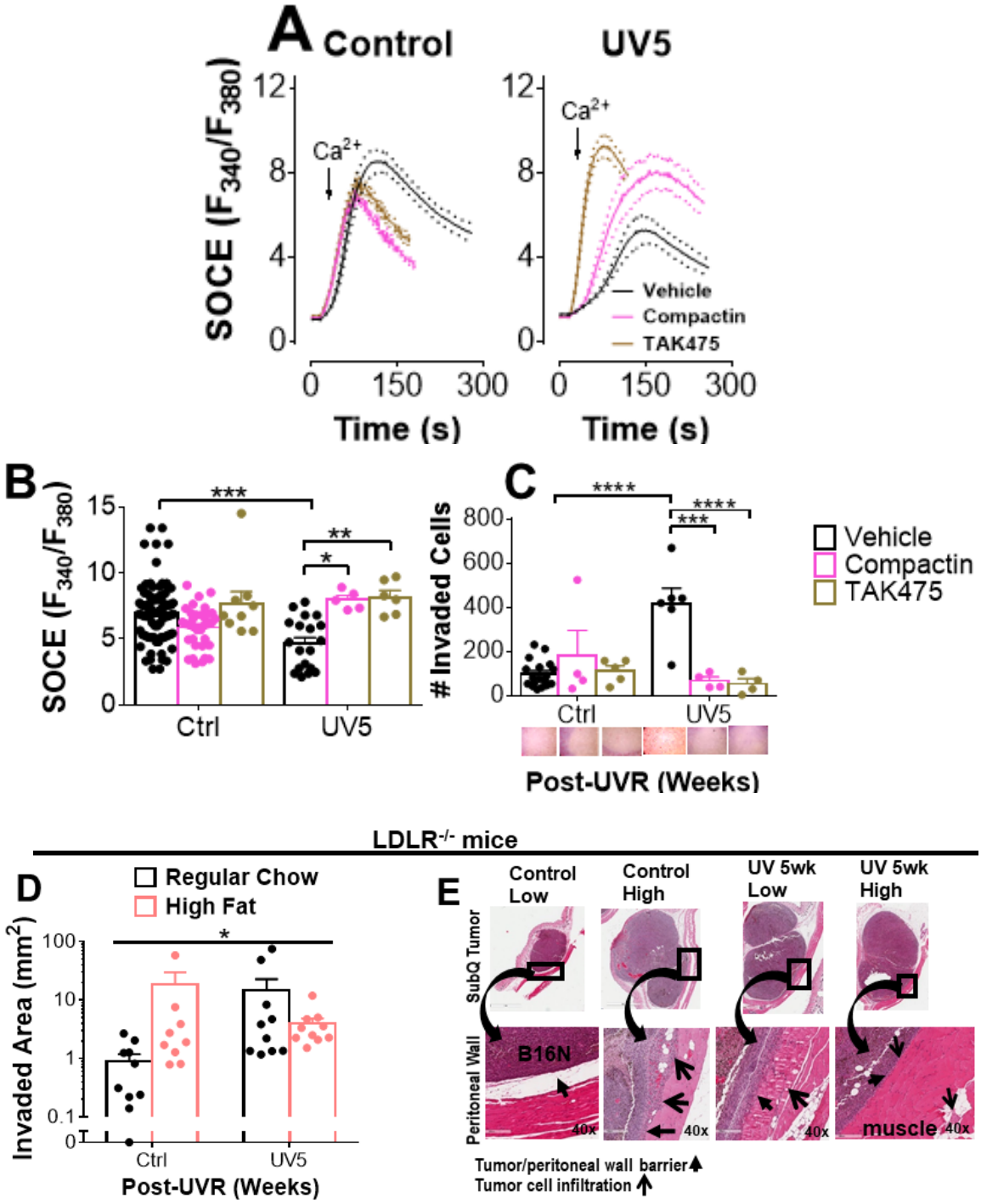
A
Control
UV5
SOCE (F340/F380)
Ca2+
Vehicle
Compactin
TAK475
Time (s)
B
SOCE (F340/F380)
Ctrl
UV5
C
Invaded Cells
Post-UVR (Weeks)
Vehicle
Compactin
TAK475
LDLR-/- mice
D
Regular Chow
High Fat
Invaded Area (mm2)
Post-UVR (Weeks)
E
Control Low
Control High
UV 5wk Low
UV 5wk High
SubQ Tumor
Peritoneal Wall
B16N
muscle
40x
Tumor/peritoneal wall barrier
Tumor cell infiltration

Figure 4-12. Cholesterol production is a key mediator of UV-induced metastasis. WM983 cells were plated overnight before exposure to 175 J/m^2 UV and then incubated under growth optimal conditions for 0 (control), 2 (UV2) or 5 (UV5) weeks. (A) Following UV exposure and incubation, WM983 human melanoma cells were plated on glass coverslips and treated with or without the cholesterol synthesis inhibitors TAK475 (10μM) or compactin (2μM) overnight followed by Fura2 loading and administration of Tg in nominally Ca^{2+}-free media for 15 minutes prior to the addition of Ca^{2+} (1mM). (B) SOCE from panel A was quantified and compared by two-way ANOVA (N≥5; cholesterol inhibition was $p = 0.0014$; incubation time, $p > 0.05$; interaction was $p < 0.0001$). (C) UV5 or control WM983 cells were placed in Matrigel transwell inserts in OptiMEM reduced serum media with or without TAK475 or compactin; DMEM with 10% FBS was used as a chemoattractant. Crystal violet-stained invaded cells were measured 20 hrs after initiation of assay (N≥4). Sample images for each condition are shown above the corresponding bar. Data was analyzed by 2-way ANOVA (cholesterol inhibition was $p = 0.0004$; incubation time, $p > 0.05$; interaction was $p = 0.0002$). (D) B16N murine melanoma cells were treated with or without UV and incubated for 5 weeks. Ldlr-/- C57Bl6 mice were fed with regular chow or high fat diet for 2 weeks prior to administration of syngeneic B16N cells (N=10). Each dot on each bar is a biological replicate. The area of cell invasion into and through peritoneal wall measured using Aperio Imagescope software and analyzed by 2- way ANOVA (high fat diet, $p > 0.05$; UV exposure, $p > 0.05$; interaction was $p < 0.05$). (E) Representative images of invasion into the peritoneal wall. *p<0.05, **p<0.01, ***p<0.001, ****p<0.0001

Figure 4-13

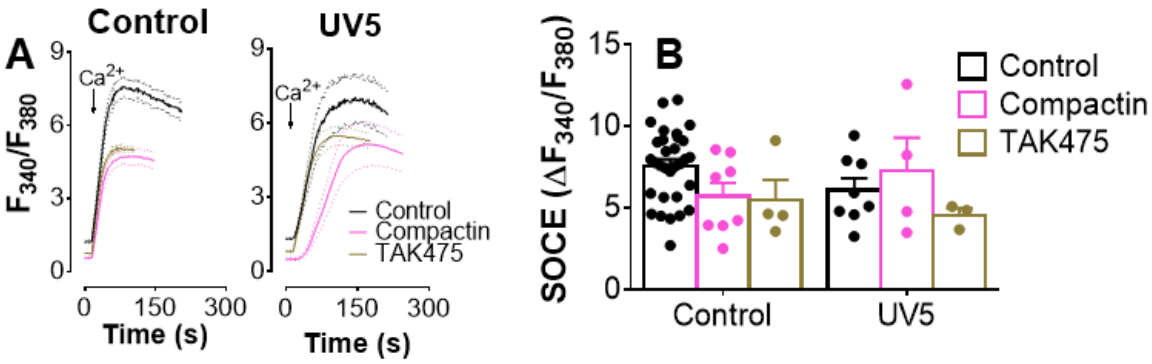
A
Control
UV5
F_{340}/F_{380}
Ca^{2+}
Control
Compactin
TAK475
Time (s)
B
SOCE ($\Delta F_{340}/F_{380}$)
Control
Compactin
TAK475
Control
UV5

Figure 4-13. No effect of cholesterol synthesis inhibitors on SOCE in UACC257 cells. UACC257 cells were plated on glass coverslips overnight before exposure to 175 J/m^2 UV and then incubated under growth optimal conditions for 0 (control), 2 (UV2) or 5 (UV5) weeks. (A) Following UV exposure and incubation, WM983 human melanoma cells were plated on glass coverslips and treated with or without the CHL synthesis inhibitors TAK475 or Compactin overnight followed by Fura2 loading and administration of Tg in nominally Ca^{2+}-free media for 15 minutes prior to the addition of Ca^{2+} (1mM). (B) SOCE from panel A was quantified and compared by two way ANOVA ($N \geq 5$; CHL inhibition was $p = 0.0014$; incubation time, $p > 0.05$; interaction was $p < 0.0001$). Each dot on each bar is a biological replicate.

SOCE Suppression Drives A Metabolic Shift Towards Anabolic Pathways

In an effort to determine how SOCE suppression might contribute to invasive behavior in melanoma, we performed RNAseq analysis of untreated, UV2, UV5 and O1C44 B16N cells (Fig 4-14A-B). PCA revealed minimal replicate variability and significant differences from control for each experimental condition (Fig 4-15) and marked differences in expression patterns between each of the 3 groups (Fig 4-14A; 4-15). To identify genes associated with both SOCE suppression and invasiveness, we then performed a Venn analysis comparing the genes whose expression was significantly altered ($p<0.01$, $q<0.01$) in UV5, O1C44 and/or UV2. The exclusion of UV2 in one group was performed because these cells did not exhibit SOCE suppression (Fig 4-1E-F), were not invasive through a transwell assay (Fig 4-1G) but did exhibit metastatic properties in a small subset of mice (Fig 4-4M,N; Table 4-2). There were 187 genes changed that were common to all 3 groups, including multiple genes associated with epithelial-mesenchymal transition (EMT), melanocyte dedifferentiation, metabolism and cell survival (Table 4-4, Table 4-5, Table 4-6). If the non-SOCE suppressed UV2 cells are excluded, there were 472 genes changed. Interestingly, with the exception of dedifferentiation, the number of pathways changed in each category increased when UV2 was excluded, particularly as related to control of glucose uptake and metabolism (Table 4-4, Table 4-6). Dysregulation of both Ca^{2+} signals and metabolism in the context of cancer has been extensively reported (Reviewed in (Dejos et al, 2020; Prevarskaya et al, 2018)); since all gene changes were observed in O1C44 cells in which SOCE is suppressed, we assessed metabolic function.

Analysis of glucose uptake revealed significant many-fold increases in the highly invasive UV5 and O1C44 B16N cells, UV5 and O1C78 WM983 cells, although not in

UV5 UACC257 cells (Fig 4-14C). Further, analysis of oxygen consumption rate (OCR) and extracellular acidification rate (ECAR) revealed only modest UV or Orai1-dependent changes in OCR in B16N, WM983, and UACC257 cells (Fig 4-14D) and either decreased or unchanged ECAR (Fig 4-14E). Measurements of Basal Respiration and Basal Glycolysis show either decreased or unchanged aerobic respiration of glycolytic activity across both human and murine cells (Fig 4-14F). Importantly, these changes in ECAR and OCR did not correlate well with the invasiveness phenotypes of these cells, implying the highly elevated levels of imported glucose were being used for alternative purposes than glycolysis.

Although most glucose is normally processed through glycolysis, glucose can also be shunted down an alternative biosynthetic route, the hexosamine biosynthetic pathway (HBP). In normal cells, this represents roughly 2-5% of glucose consumption, however, cancer cells have been shown upregulate use of the HBP (Akella et al, 2019; Marshall et al, 1991). Elevated HBP 14 increases uridine diphosphate-N-acetylglucosamine (UDP-GlcNAc) production, which ultimately drives post-transcriptional O-GlcNAcylation mediated by the enzyme O-linked Nacetylglucosamine (GlcNAc) transferase (OGT), promoting EMT, proliferation, cell survival, and transcription (Akella et al., 2019). Interestingly, RT-qPCR analysis of OGT gene expression revealed either unchanged or decreased levels of OGT in response to UV exposure or SOCE suppression (Fig 4-14G) which implies that changes in HBP activity are likely caused by increased substrate and OGT activity. To determine whether elevated OGT activity contributes to the increased invasiveness of cells with depressed SOCE, cells were either transfected with an siRNA targeting OGT (siOGT; Fig 4-14G) or incubated with specific and selective pharmacological inhibitor of OGT, OSMI1 (Barkovskaya et al,

2019) (Fig 4-14H). OGT knockdown decreased OGT expression between 50-70% across all conditions relative to scrambled RNA control (Fig 6G). Further, both OGT knockdown and OGT inhibition using OSMI1 blocked invasiveness for both WM983 and B16N cells (Fig 4-14H). These observations reveal a critical role for OGT activity in the observed increase in invasiveness due to SOCE suppression in melanoma cells.

Figure 4-14

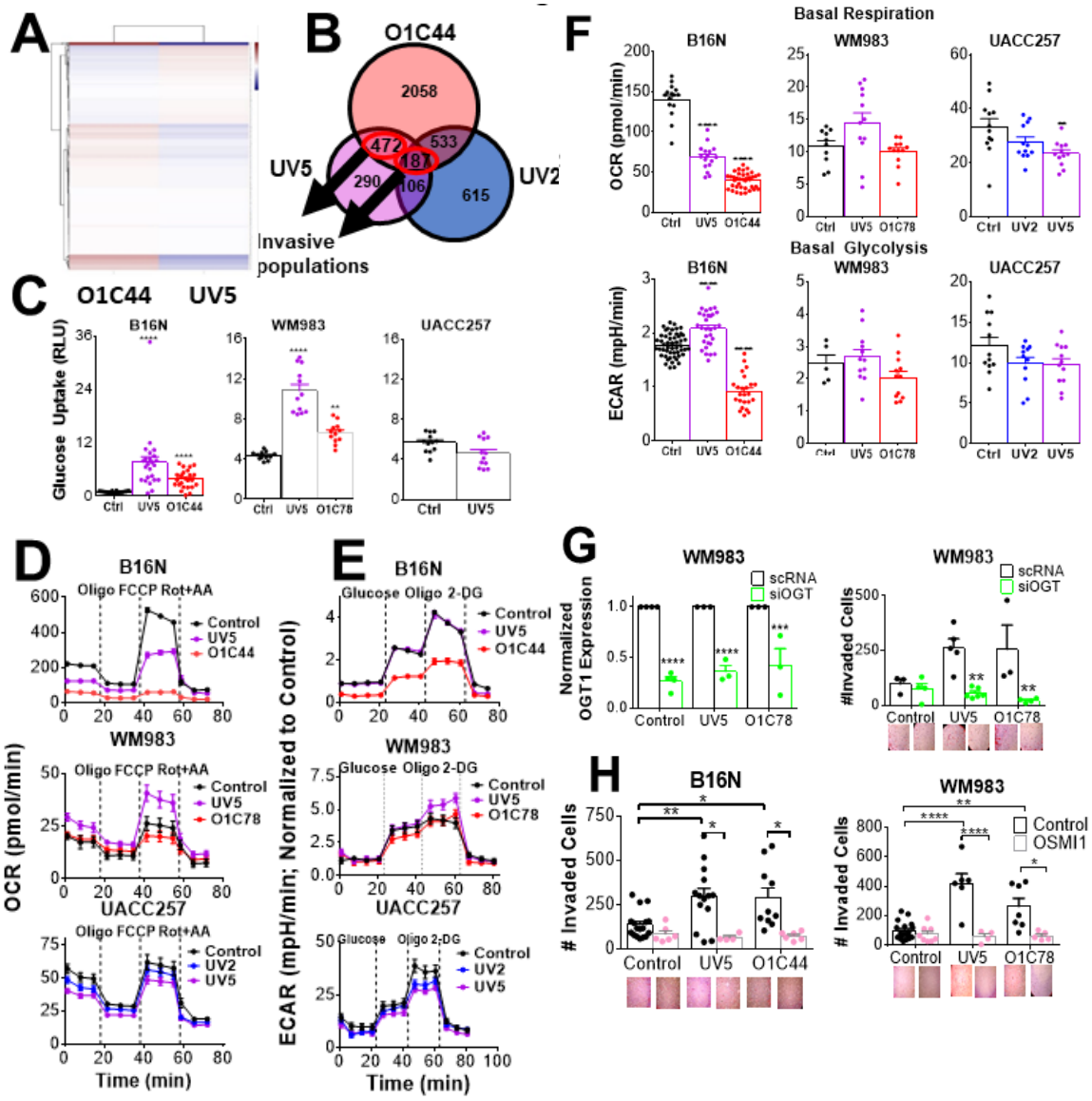
A
B
O1C44
2058
472
533
187
UV5
290
106
615
UV2
Invasive populations
C
O1C44
UV5
B16N
WM983
UACC257
Glucose Uptake (RLU)
Ctrl
UV5
O1C44
O1C78
F
Basal Respiration
B16N
WM983
UACC257
OCR (pmol/min)
Basal Glycolysis
ECAR (mpH/min)
D
B16N
Oligo FCCP Rot+AA
Control
UV5
O1C44
WM983
O1C78
UACC257
UV2
OCR (pmol/min)
Time (min)
E
B16N
Glucose Oligo 2-DG
WM983
UACC257
ECAR (mpH/min; Normalized to Control)
Time (min)
G
WM983
scRNA
siOGT
Normalized OGT1 Expression
#Invaded Cells
H
B16N
Invaded Cells
WM983
OSMI1

Figure 4-14. RNAseq reveals SOCE suppression drives invasion. (A-B) RNA was extracted from UV2, UV5, O1C44 or control B16N murine melanoma cells followed by RNAseq analysis (3 biological replicates per condition). (A) Heatmap containing gene expression differences. (B) Venn diagram comparing genes significant changed in B16N cells 2 weeks (UV2) or 5 weeks (UV5) after exposure to those changed by Orai1 overexpression (O1C44) (p0.05). (D-E) Oxygen consumption rate (OCR; D) extracellular acidification rate (ECAR; E), were measured in Control, UV5 and O1C44 B16N melanoma cells (n≥15), Control, UV5 and O1C78 WM983 melanoma cells (n≥10) and Control, UV2 and UV5 UACC257 melanoma cells (n≥12) using an Agilent Seahorse XF96. (F) Basal respiration and basal glycolysis data were determined based on data in panels D and E, respectively, prior to the addition of oligomycin and glucose, respectively. Data was analyzed by one way ANOVA ($p<0.0001$). (G) $5x10^5$ WM983 cells were transfected with 25 pmol siOGT (Invitrogen) or a scrambled control RNA (Ambion). Cells were split into 2 groups and incubated under growth optimal conditions for 2 days. LEFT: Cells were lysed and qPCR for OGT1 was performed using 18S ribosomal gene as a control. data was analyzed by two-way ANOVA (siRNA effect was $p<0.0001$; no change in OGT1 expression between control, UV5, and O1C78), RIGHT: Cells were plated in Matrigel transwell inserts in OptiMEM reduced serum media. Crystal violetstained invaded cells were measured 20 hrs after initiation of assay (N≥3). Invasion data was analyzed by 2-way ANOVA (siOGT effect was $p=0.0002$; interaction of treatment and siOGT was $p=0.0449$) (H) B16N or WM983 cells were placed in Matrigel transwell inserts in OptiMEM reduced-serum media, with or without OSMI1 (40 μM); DMEM with 10% FBS was used as a chemoattractant. Crystal violet-stained invaded cells were measured 20 hrs after initiation of assay (N≥4). Sample images for each

condition are shown above the corresponding bar. Each dot on each bar is a biological replicate. Data was analyzed by 2-way ANOVA (OSMI1 effect was $p<0.0001$ in B16N and WM983 cells). *$p<0.05$, **$p<0.01$, ***$p<0.001$, ****$p<0.0001$.

Figure 4-15

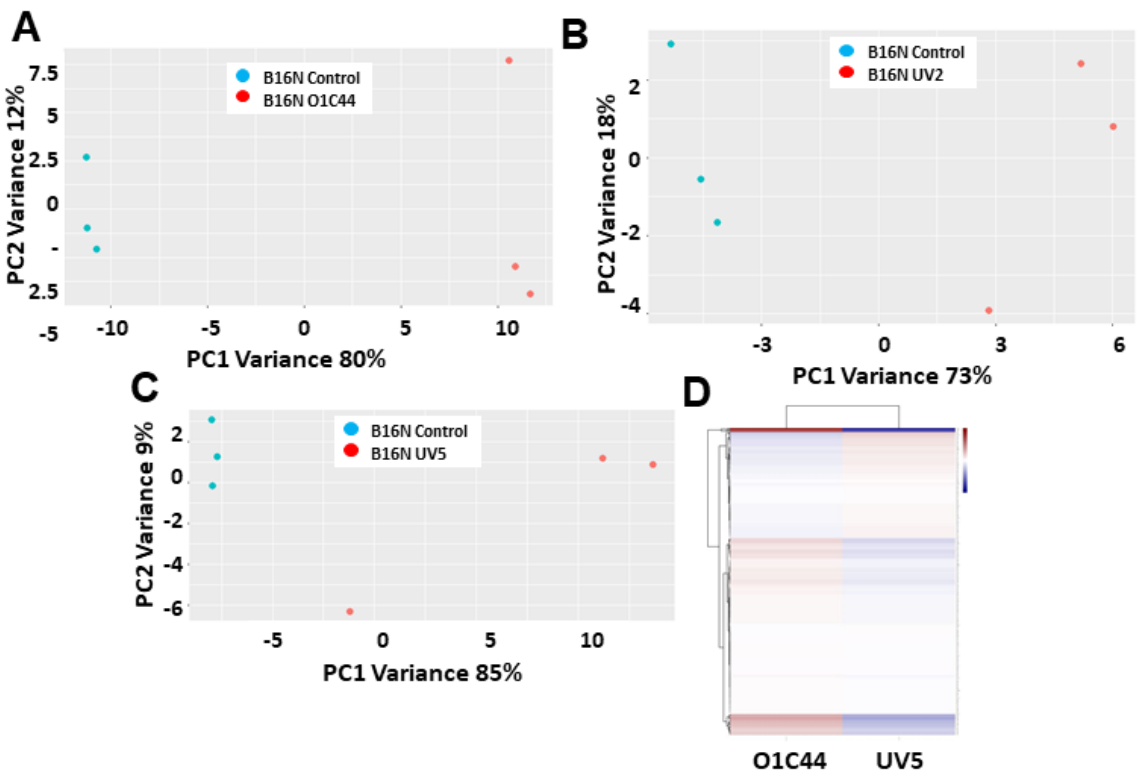
A
B16N Control
B16N O1C44
PC2 Variance 12%
PC1 Variance 80%
B
B16N Control
B16N UV2
PC2 Variance 18%
PC1 Variance 73%
C
B16N Control
B16N UV5
PC2 Variance 9%
PC1 Variance 85%
D
O1C44
UV5

Figure 4-15. RNAseq analysis in support of Figure 4-14A. (A-C) PCA analysis of (A) Orai1 over-expressing and (B-C) UV exposed B16N cells relative to control. (D) Heatmap comparing the genes altered in O1C44 and UV5 cells relative to B16N WT cells.

Table 4-4: IPA Analysis showing key pathways altered from RNAseq

Target groups	Category	Pathway	-log(p-value)	#genes affected*
O1C44, UV5 and UV2	Cancer Biology	Molecular Mechanisms of Cancer	2.52	9/453
		Wnt-Beta Catenin Signaling	2.99	6/174
		ERBB Signaling	3.42	5/94
	Invasion	Epithelial-Mesenchymal Transition	3.52	7/195
		Epithelial Adherens Junction Signaling	4.05	7/160
		Gap Junction Signaling	3.31	7/211
		Integrin Signaling	2.54	6/214
	Dedifferentiation	Melanocyte Development and Pigmentation Signaling	4.39	6/96
	Metabolism	Acetyl-CoA Biosynthesis from Citrate	2.94	2/8
	Cell survival	Ferroptosis	4.11	7/156
O1C44, UV5 not UV2	Cancer Biology	Molecular Mechanisms of Cancer	1.77	14/400
	Metabolism	Aryl Hydrocarbon Signaling	5.6	13/143
		Xenobiotic Metabolism of Aryl Hydrocarbon Signaling	4.58	9/85
		Pentose Phosphate Pathway (Non-oxidative)	2.32	2/6
		Glucose Metabolism Disorder	3.78	69/472**
		Impaired Glucose Tolerance	2.85	10/472**
	Cell Survival	ERK/MAPK Signaling	2.36	10/202
		Sirtuin Signaling	2.1	12/291
		Myc-Mediated Apoptosis Signaling	1.87	4/50
	Invasion/Cell-Cell Contact	Gap Junction Signaling	1.95	9/198
		FAK Signaling	1.9	6/104
		Integrin Signaling	1.76	9/213

*Number of genes changed out of the number of genes in the pathway
**Number of genes in the category out of the number entered into IPA

Table 4-5: Selected Genes Altered in Epithelial-Mesenchymal Transition Pathway

Gene	Log2Fold Change	p-value
CDH2	1.155354	4.19E-23
FGFR1	1.794002	7.39E-11
FZD2	0.689054	3.83E-07
FZD7	0.376354	0.000169
KRAS	0.947452	9.31E-21
SOS1	1.158508	1.53E-17
TCF7L1	1.247981	1.36E-11

Table 4-6: Genes associated with melanocyte dedifferentiation significantly altered in UV2, UV5 and O1C44 B16N cells from Figure 4-14A

Gene	Fold Change	p-value
AXL	2.745258616	6.06E-77
FGFR1	1.794001682	7.39E-11
ADAMTS1	1.779215309	3.61E-66
S100B	1.68057003	3.94E-25
SLC16a1	1.158508258	1.53E-17
CDH2	1.155354466	4.19E-23
MC1R	1.061204029	6.92E-27
ERBB3	0.998760776	6.39E-09
TIMP2	0.969856716	2.27E-28
KRAS	0.947452115	9.31E-21
SOX4	0.829085205	1.11E-16
DCT	0.610499384	3.70E-11
SLC45a2	-1.636666872	5.25E-52
SLC24a5	-1.532121739	5.92E-44
PMEL	-0.918125782	5.41E-21

Table 4-7: Selected Genes Altered in Glucose Metabolism Disorder Pathway

Gene	Expression Log Ratio	Function
PAM	0.751	Regulates Glucose-Responsive Insulin Secretion(553)
ANXA2	0.599	Involved in Insulin-Induced GLUT4 Translocation(554)
MEN1	0.515	Mutations lead to hyperglycemia(555)
GRB2	0.338	Downregulation leads to insulin sensitivity(556)
LRP1	-1.233	Regulates Glucose Metabolism(557) and Homeostasis(558)
ANK2	-0.895	Loss of AnkB in Adipose Tissue leads to enhanced glucose uptake(559)
HAX1	-0.749	Loss of HAX1 activates Pyruvate Dehydrogenase to facilitate glucose metabolism(560)

Patient Surgical Explants Have Low SOCE And A Similar Pharmacological Profile To Melanoma Cell Lines

To determine the extent to which the observations reported here can be extended to human melanoma, we used a series of freshly isolated primary patient surgical explants (Fig 4-16). The majority of patient samples exhibited a “low SOCE” profile (Fig 4-16A), similar to the SOCE suppressed samples reported elsewhere in this study. Given this profile, it is not entirely surprising that UV-irradiation failed to further suppress SOCE across all 27 samples (Fig 4-16B) although the top 15% of SOCE responders (4 highest out of 27 tested) tended to respond more to UV exposure (Fig 4-16A). We were able to obtain both primary and metastatic lymph nodes (LN) tumor samples from two of the 27 patients (P4 and P8; Fig 4-16C); the LN tumors in both patients exhibited substantially lower SOCE than the primary tumor (Fig 4-16C) consistent with the concept that SOCE suppression is a component of metastasis. Finally, since all samples were genetically profiled for somatic mutations (Table 4-8), we attempted to determine if SOCE levels had any link to mutation status. Consistent with prior studies (Esteves et al, 2020), BRAF mutations were associated with significantly elevated SOCE (Fig 4-16D); although, inconsistent with this previous study, statistically significant changes in SOCE due to NRAS mutations were not observed ($p=0.09$; Fig 4-16D), although, we attribute this discrepancy primarily to sample size. No other relationships between SOCE and mutations were observed within the statistical power of our sample size. To assess the effect of inhibition of CHL biosynthesis and SOCE augmentation on human melanomas, several of the patient samples were treated with the mevalonate pathway inhibitors compactin and TAK475 and the Orai potentiator IA65 (Fig 4-16E). Both TAK475 and compactin significantly enhanced SOCE, indicating SOCE was being suppressed by CHL

biosynthesis in the clinical samples. No significant effect of IA65 was observed, although a smaller pool was tested due to limited sample availability. Finally, treatment with mevalonate pathway inhibitors compactin and TAK475, the Orai1 potentiator IA65 or the OGT inhibitor OSMI1 all led to diminished invasion in vitro (Fig 4-16F). Overall, these observations reveal the clinical relevance of CHL-mediated SOCE suppression and subsequent O-GlcNAcylation in melanoma.

Figure 4-16

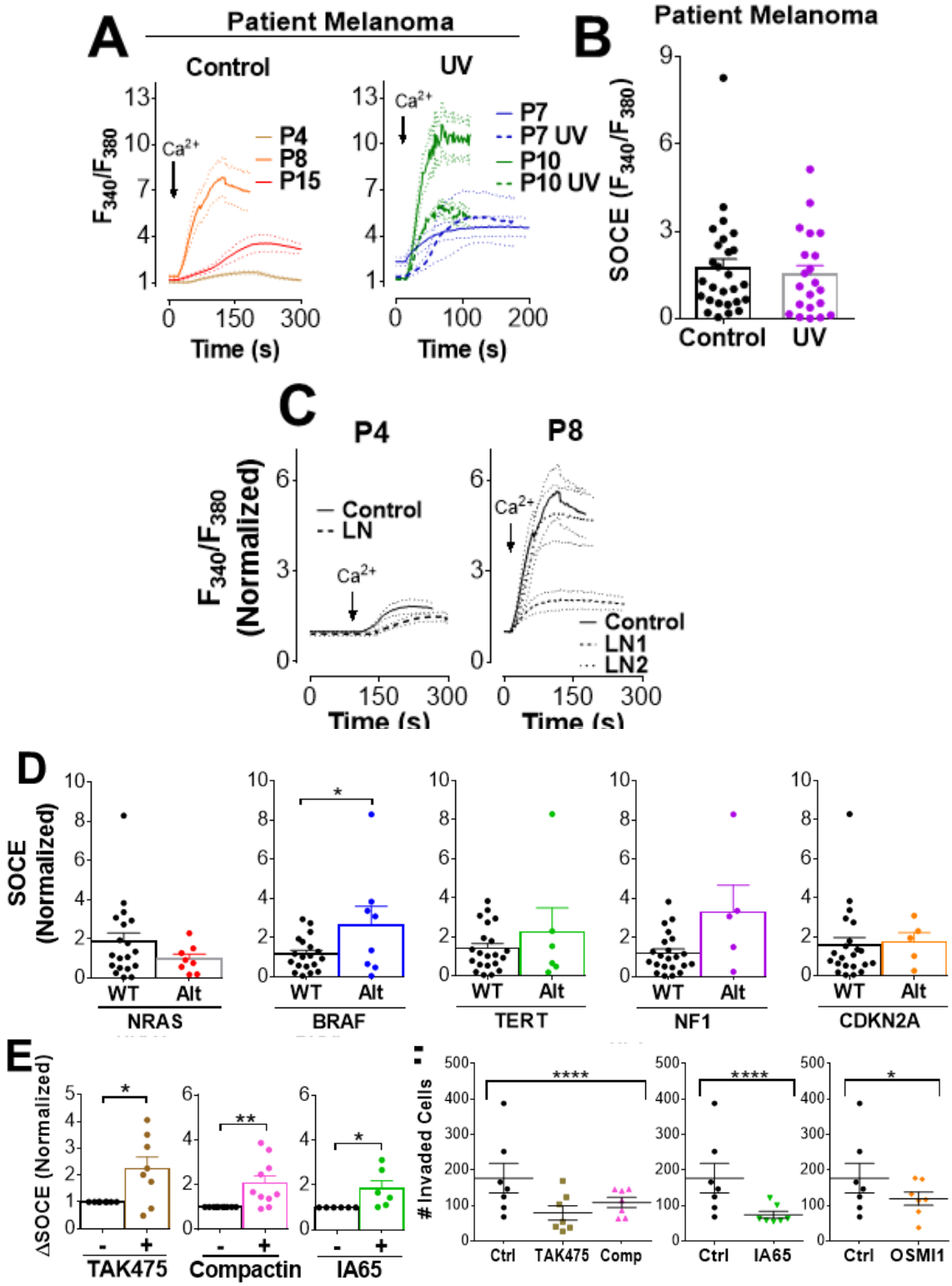
A
Patient Melanoma
Control
UV
F_{340}/F_{380}
Ca^{2+}
P4
P8
P15
P7
P7 UV
P10
P10 UV
Time (s)
B
Patient Melanoma
SOCE (F_{340}/F_{380})
Control
UV
C
P4
P8
F_{340}/F_{380} (Normalized)
Control
LN
LN1
LN2
Time (s)
D
SOCE (Normalized)
WT
Alt
NRAS
BRAF
TERT
NF1
CDKN2A
E
ΔSOCE (Normalized)
TAK475
Compactin
IA65
Invaded Cells
Ctrl
TAK475
Comp
IA65
OSMI1

Figure 4-16. Analysis of patient surgical explants reveals clinical relevance of low SOCE and cholesterol. Patient surgical explants were received from the biosample repository of FCCC. Cells were isolated from tumors using 50 μM Medicons and the Medimachine system and grown for 3 days before experimentation to eliminate non-melanoma cells. (A-B) Plated control or UV irradiated (175J/m^2) cells were then incubated overnight on glass coverslips prior to Fura2 loading and administration of Tg in Ca^{2+}-free media for 15 minutes. (A) Representative examples of SOCE responses in patient samples following the addition of Ca^{2+} (1mM). (B) Each dot represents SOCE in a different patient sample. The effect of UV on SOCE was determined by one way ANOVA ($p > 0.05$). (C) Comparison of SOCE in cells collected from both primary tumors and metastatic lymph nodes from the same patient (from patients analyzed in panels A, B). (D) SOCE in samples exhibiting NRAS (8 of 27 samples), BRAF (8 of 27 samples), TERT promoter (6 of 27 samples), NF1 (5 of 27 samples), and CDKN2A (5 of 27 samples) alterations were compared to SOCE in samples that expressed WT or the unaltered gene. (E) Single cells from patient samples were treated with or without the indicated drug in the presence of Tg in nominally Ca^{2+}-free media for 15 minutes prior to the addition of Ca^{2+} (1mM). The number on each bar represents the number of patient specimens tested. Data were compared against their matched control analyzed by the unpaired T test (Tak475, $p = 0.015$; compactin, $p = 0.0049$; IA65, $p = 0.0390$). (F) Patient cells were placed in Matrigel transwell inserts in OptiMEM reduced serum media with or without TAK475 (10μM), compactin (2μM), IA65 (2μM) or OSMI1 (40μM); DMEM with 10% FBS was used as a chemoattractant. Crystal violet-stained invaded cells were measured 20 hrs after initiation of assay. Each dot represents 1 patient sample. Each dot on each bar is a biological replicate. Data analyzed by 2-way ANOVA (cholesterol inhibition was $p < 0.0001$; patient

samples were $p < 0.001$; interaction was $p < 0.01$). For IA65, (inhibition was $p < 0.0001$; patient samples were $p < 0.01$; interaction was $p < 0.0001$). For OSMI1, (inhibition was $p < 0.05$; patient samples were $p > 0.05$; interaction was $p < 0.05$). *p<0.05, **p<0.01, ***p<0.001, ****p<0.0001

Table 4-8: List of genes altered in freshly isolated patient samples.

Gene	# of Alterations	Type of Alteration (Total # affected; (PT#))
NRAS	8	Q61R (4; (3, 4, 6, 11)) Q61L (2; (5, 27)) Q61H (1; (13)) Unknown mutation (1; (15))
BRAF	6	D594N (1; (8)) G469K (1; (10)) V600K (1; (16)) V600E (3; (22, 26, 31))
TERT	6	Expression (6; (10, 11, 12, 13, 15, 16)
CDKN2A	5	R80* (2; (1, 31)) Expression (2; (11, 15) Loss (1; (20)) P114L (1; (30))
NF1	5	Q1158 (1; (8)) Q853 (1; (8)) R2450 (1; (10)) Q1336 (1; (10)) Expression (4; (11, 12, 20, 31))
FGFR2	1	VUS (1; (8))
FGF3/4/19	1	Amplification (1; (12))
ATM	2	N6* (1; (12)) Unknown mutation (1; (28))
CBL	1	E366K (1; (12)) Alternative Splice site (1; (12))
CCND1	1	Amplification (1; (12))
CHEK2	1	S248F (1; (13))
STK11	3	Q302S (1; (14)) Expression (2; (16, 20))
TP53	1	Expression (1; (16))
LRP1B	1	Expression (1; (27))
HRAS	1	Expression (1; (10))
KRAS	1	S65N (1; (30))
ROS1	1	VUS (1; (8))
EGFR	1	L862V (1; (5))
PTEN	2	Expression (2; (3, 10))
ARAF	1	S214F (1; (13))
TET2	1	Unknown mutation (1; (28))
EPHA3	1	Expression (1; (11))
RBM10	1	Expression (1; (11))
EMSY	1	Amplification (1; (12))
JAK3	1	Amplification (1; (10))
No specific mutations reported		2, 7, 9, 14, 21, 23, 25, 29, 33

CHAPTER 5

DISCUSSION

In the current study, we have demonstrated that a single exposure to UV suppresses SOCE, which promotes melanoma migration, invasion, and metastasis. This effect is both rapid, occurring within 24 hours after UV exposure, and durable for at least 5 weeks after exposure. This effect is reversable, in that an Orai1 potentiator blocked both migration and invasion. We further established UV-induced SOCE suppression was mediated by induction of CHL, which is not only an established inhibitor of endogenous Orai1 channel activity (Derler et al., 2016), but also a modulator of UV-induced ROS production (561). Finally, we established that UV-induced SOCE suppression drives a phenotypic shift towards invasive behavior due to a combination of transcriptional and post-transcriptional changes.

This study demonstrates that suppression of Ca^{2+} signals through UV exposure or inhibition of Orai1-STIM signaling drives invasion and metastasis; however, numerous prior investigations have observed that increased Ca^{2+} signals drive invasive behavior (Bong & Monteith, 2018; Gross et al, 2020a; Umemura et al., 2014). While the conclusions of these investigations would seem to be contradictory, it is likely a reflection of different contexts. Importantly, using both pharmacological and genetic approaches, we established that the anti-invasive properties of Ca^{2+} are limited to a very narrow range; if SOCE is abrogated rather than attenuated, invasion did not occur. The major pathway identified in other works as responsible for pro-invasive Ca^{2+} functions is invadopodia formation (Leslie, 2014; Pourfarhangi et al, 2018; Sun et al, 2015). In the current study, we show that SOCE suppression drives changes in the expression of a large number of

genes associated with EMT, cell survival, contact inhibition and metabolism. We further establish that post-translational O-GlcNAcylation drives invasive behavior in multiple cell lines and surgically collected patient explants. Given that Ca^{2+}-dependent signaling is highly dependent upon concentration, context and intracellular location, these data are consistent with a model in which Ca^{2+} signals can be either pro- or anti-invasive depending on cell type, degree of change and the signaling environment.

RNA-seq analysis of UV- and SOCE suppression sensitive genes revealed Aryl Hydrocarbon Signaling, Glucose Metabolism Disorder and Impaired Glucose Metabolism as 3 of the top hits (Table 4-4). It is interesting to note that these pathways are associated with altered insulin sensitivity leading to increased glucose uptake (Natividad et al, 2018; Wang et al, 2011), which ultimately does occur in these cells. Further, within glucose metabolism disorder pathways, many genes were altered including those associated with glucose uptake, insulin sensitivity, glucose homeostasis, GLUT4 translocation and regulation of pyruvate dehydrogenase (Table 4-4). We were also intrigued by the observation that 7 genes associated with EMT were upregulated, since the activity of some EMT genes (eg. Snai1, c-myc, YAP, and NF-κB) is driven by O-GlcNAcylation (Akella et al., 2019). Further, a shift to HBP could drive other pro-EMT posttranslational modifications such as TGFβ glycosylation (Akella et al., 2019), although this was not demonstrated in this study. Considered collectively, these observations demonstrate that SOCE suppression drives a shift to EMT through coordinated changes in both transcriptional and post-translational events.

In considering the lack of effect of UV exposure on SOCE in patient melanoma samples, it is important to recognize that the series of human cell lines exhibiting UV-induced SOCE suppression in Figure 4-1A were all non-invasive. This is because we

established that invasive melanoma cells exhibit lower SOCE in a prior study (Hooper et al., 2015); the goal of this investigation was to examine the relationship between SOCE suppression and invasiveness within the same cell lines. Since a selection process like this was not possible with freshly isolated surgical explants, the likely explanation for the lack of effect of UV on SOCE is that the majority of the patients that donated melanoma samples for this study were afflicted with an invasive form of this disease.

The connection between UV and CHL production established here is also of clinical relevance. The introduction and wide-spread use of statins for the control of clinical CHL levels has provided an opportunity to assess the relationship between CHL and cancer progression. Statins have been shown to significantly decrease melanomagenesis (Lee et al, 2016) and slow progression (Pich et al, 2013), although, they cannot decrease the number or clinical profile of pre-existing dysplastic nevi (Linden et al, 2014). Further, it was found that melanoma metastasis could be suppressed in mice using therapeutics including LXRb (a CHL sensor/transcription factor) agonists GW3965 or T0901317 (Pencheva et al., 2014; Zhao & Dahlman-Wright, 2010)), and statins (Favero et al, 2010; Tsubaki et al, 2015) which target CHL biosynthetic pathways. In the current investigation, we show that UV exposure leads to upregulation of the mevalonate pathway and increases cellular CHL levels. While it is known that CHL can sterically hinder Orai1 as discussed above, it should also be noted that CHL can also independently promote ROS production and mitochondrial dysfunction (561) as well as directly facilitating UV-induced generation of ROS (562). Thus, it appears that CHL has a multifaceted effect on inhibition of SOCE, while also enhancing invasiveness in melanoma cells. Since blocking the mevalonate pathway blocked invasion in vitro and metastasis and high CHL in vivo was sufficient to promote metastasis independent of UV, our findings support the concept that

CHL serves a critical role as a mediator of UV-induced melanoma metastasis and reveals a new mechanism through which CHL promotes metastasis; SOCE inhibition. Hence, blockade of the mevalonate pathway completely reversed UV-induced SOCE inhibition and invasiveness in vitro. Since SOCE inhibition was sufficient to drive invasiveness both in vitro and in vivo, these data reveal SOCE suppression as a new mechanism for CHL-induced metastasis. While we have not investigated how CHL inhibits SOCE in this study, CHL has previously been shown to bind directly to Orai1 where it interferes with the STIM-mediated transition to the open state (Derler et al., 2016; Hooper et al, 2016). Interestingly, the effect of CHL on SOCE appears to be unidirectional with CHL serving as an endogenous upstream inhibitor SOCE. Our data are highly consistent with these findings and provides a new pathophysiological context for this observation.

It was notable that the majority of samples tested exhibited a “low SOCE” phenotype, showing no change in SOCE in response to UV exposure. In our prior study (Hooper et al., 2015), we observed that invasive melanoma exhibits a “low SOCE” phenotype, while noninvasive cells have substantially more SOCE. In the current study, only non-invasive melanoma cell lines exhibiting “higher SOCE” were exposed to UV and tested, as the focus of the work was to determine if SOCE had a mediatory role in UV-induced melanoma progression. However, this principle was not applied to obtaining patient surgical explants; here, we examined all samples that were made available to us. Further, since the clinic retains tissue samples for pathological analysis and genetic profiling, patients with relatively small lesions had insufficient material to be shared with us; as such we only received samples from relatively advanced patient samples, likely creating a selection bias towards more advanced melanoma.

CHAPTER 6

UVA AND UVB EXERT DIFFERENTIAL EFFECTS ON SOCE SUPPRESION AND INVASION

I. Introduction

As described in Chapter 1: Part 3, UV is a complete carcinogen consisting of longer wavelength UVA and shorter wavelength UVB which have dual and differing effects on melanoma progression. While UVA is much more abundant in normal UV exposure from the sun (95%; (563)) and penetrates deeper into the sublayers of the skin than UVB (564), UVB is more genotoxic (565, 566). This is important to note since UVA and UVB appear to facilitate different mechanisms for inducing melanoma progression.

UVA appears to mainly facilitate oxidative stress through impaired DNA damage response leading to the production of 8-oxo-7,8-dihydroguanine. In turn, this leads to an oxidated guanine and production of a singlet oxygen radical and oxidative stress (567). Oxidative stress, normally in the form of ROS, yields the production of Dark cyclobutene pyrimidine dimer (CPDs) (565) in both melanocytes and keratinocytes containing primarily pheomelanin (568). Conversely, UVB appears to cause direct DNA damage through formation of CPDs, and their subsequent covalent bonds between the adjacent pyrimidine carbons (C6 of 5' base, C4 of 3' base), called 6-4 photoproducts (6-4PPs) (569, 570). These CPDs and 6-4 photoproducts lead to DNA damage response ATR activation (571), and if the DNA damage remains unrepaired it can cause gene mutations leading to melanomagenesis and progression (572).

As UVA and UVB both induce DNA damage in some capacity, it is perhaps unsurprising that melanoma has a very high mutational load with genetic changes

occurring from both UVA and UVB leading to thymine dimer formation (C→T resulting from UVB, G→T resulting from UVA) (reviewed in (342)) and epigenetic modulation from increased methylation. Since UVA and UVB have shown ability to cause CPDs, it is thought that UV leads to its own unique signature of mutations that are set apart from the more common melanoma mutations such as BRAF, NRAS, CDKN2A, etc. (342, 573). While it is now known that UV can synergize these mutations to promote melanomagenesis and progression, it is not a direct cause of these mutations (reviewed in (573)). For example, it has been shown that UVB contributes little to epigenetic changes of cells since irradiation did not change levels of DNA methylation in keratinocytes (574). As a result, UVB tends to lead to more direct DNA damage activating downstream pathways such as mutant p53 and c-myc leading to cell survival pathways and cancer progression (575). In parallel, UVA exposure has been shown to have both a transient and long-term DNA methylation response, indicative of epigenetic changes (576). This leads to longer term changes in cell growth such as epigenetic regulation of p16(INK4a) enrichment of histone H3K9me3 (577). Much of the work done on genetic and epigenetic mutation profiles of UVA and UVB have been done using genomic sequencing, yet further investigating which genes are mutated or are methylated still remain a promising therapeutic. Thus, while there are similarities in how UVA and UVB facilitate melanoma progression, their specific mechanistic functions vary leading to intrigue of investigating whether there are ways to individually target UVA and UVB for novel therapeutics. Therefore, a goal of this chapter of work is to examine the role of UVA and UVB in SOCE suppression and melanoma invasiveness.

II. Results

UVA And UVB Exert Differing Effect On SOCE And Invasion. To determine the independent effects (if any) of UVA vs. UVB on both SOCE and invasion, WM983 cells and B16N cells were treated with UVA (N to N J/m^2) or 175 J/m^2 UVA+B as previously described (see Chapter 4; Fig 4.1). Notably, even significantly higher doses of UVA alone had no significant impact on SOCE 24 hours after exposure (Fig 6-1A-B) in WM983 cells. This correlated with no change in invasiveness relative to control in WM983 cells exposed to only UVA, even though UVA+B led to enhanced invasion at 2 weeks after UV exposure (Fig 6-1D). However, 4 to 5 weeks after exposure to UVA, a sharp decreases in SOCE were observed (Fig 6-1C). Interestingly, 5 weeks after UVA exposure, no change in invasion occurred relative to control, while enhanced invasion occurred after UVA+B exposure (Fig 6-1D).

Figure 6-1

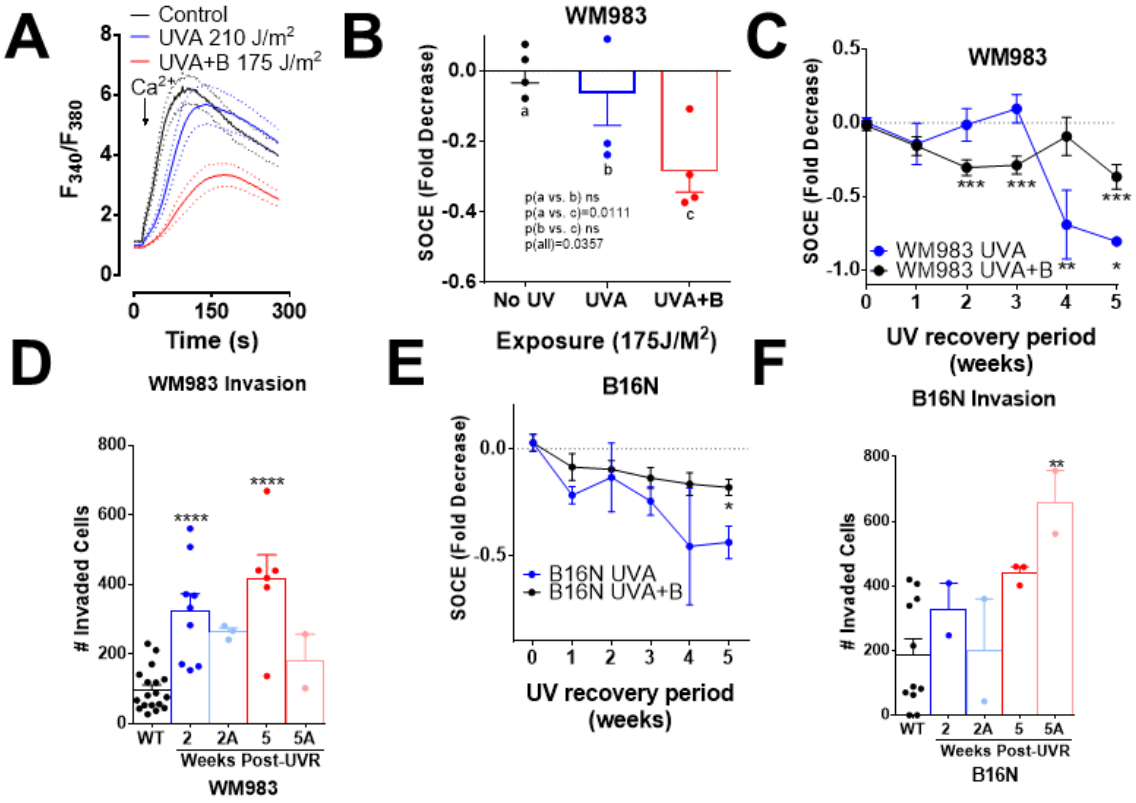
A
Control
UVA 210 J/m2
UVA+B 175 J/m2
Ca2+
F340/F380
Time (s)
B
WM983
SOCE (Fold Decrease)
p(a vs. b) ns
p(a vs. c)=0.0111
p(b vs. c) ns
p(all)=0.0357
No UV
UVA
UVA+B
Exposure (175J/M2)
C
WM983
SOCE (Fold Decrease)
WM983 UVA
WM983 UVA+B
UV recovery period (weeks)
D
WM983 Invasion
Invaded Cells
WT
2
2A
5
5A
Weeks Post-UVR
WM983
E
B16N
SOCE (Fold Decrease)
B16N UVA
B16N UVA+B
UV recovery period (weeks)
F
B16N Invasion
Invaded Cells
WT
2
2A
5
5A
Weeks Post-UVR
B16N

Figure 6-1. UVA and UVB exert differing effects on SOCE and invasion. (A-B) WM983 cells were plated on glass coverslips overnight prior to UV exposure. Cells exposed to UVA only were provided a thin layer of mylar film to filter out UVB during UV exposure. (A) Representative traces of SOCE in Fura2 loaded B16N cells treated with the indicated UV exposure conditions, in the presence of Tg for 15 minutes. (B) Cells were plated on glass coverslips overnight in the presence or absence of UVA and/or UVB (N≥3) (Effect of UVA+B compared to No UV p=0.0111, Effect of UVA or UVA+B compared to No UV p=0.0357). (C) WM983 cells were treated as described for panel A, except the incubation periods were extended as depicted (N≥2). Data was analyzed by 2-way ANOVA with multiple comparisons (interaction p = 0.0214; Effect of Time, p = 0.0005; Effect of UV, p > 0.05). (D) UVA and UVA+B-treated cells were placed in Matrigel transwell inserts in OptiMEM reduced serum media; DMEM with 10% FBS was used as a chemoattractant. Crystal violet-stained invaded cells were measured 20 hrs after initiation of assay (N≥2). Sample images for each condition are shown above the corresponding bar. Data was analyzed by one-way ANOVA with multiple comparisons (ANOVA effect, p < 0.0001). (E) B16N cells were plated on glass coverslips as described in panels A-C with amount of time incubated post-UV indicated (N≥2). Data was analyzed by two-way ANOVA with multiple comparisons (Effect of Time, p=0.0009; Effect of UV, p>0.05, interaction p>0.05). (F) UVA and UVA+B-treated cells were placed in Matrigel transwell inserts as described in panel D (N≥2). Each dot on each bar is a biological replicate. Data was analyzed by one-way ANOVA with multiple comparisons (ANOVA effect, p=0.0094).

III. Discussion

In this current study, we have suggested that UVA and UVB have differing effects on SOCE. In this regard, UVB to be the driving force behind transient UV-induced SOCE suppression. In support, UVA exposure at intensities greater than UVA+B exposure had no change in SOCE for not only 24 hours (Fig 6-1A) but also for as long as 3 weeks after exposure (Fig 6-1C). While a sharp decrease in SOCE occurs from weeks 4-5, it is interesting that 5 weeks after UVA exposure, there was no increase in invasion (Fig 6-1C-D). As discussed in Chapter 4, SOCE suppression the results demonstrate a "Goldilocks Effect" on invasion. Therefore, it can be speculated that 5 weeks after UVA exposure SOCE has been suppressed past the point of the "Goldilocks Effect" optimal level for invasion. Thus, 5 weeks after UVA exposure may actually inhibit Ca^{2+}-dependent invasive properties such as invadopodia formation.

B16N cells revealed a similar effect where UVA is shown to drive long-term SOCE suppression similar to WM983 cells (Fig 6-1E). However contrary to WM983 cells, 5 weeks after UVA exposure also led to increased invasiveness (Fig 6-1F). One possibility for this is that since B16N cells are already pigmented, whereas WM983 cells are amelanotic, it is possible they would be more sensitive to UVA which causes less DNA-damage inducing responses such as pigmentation and would be more prone to epigenetic modifications. Considered together, we have demonstrated differing effects of UVA and UVB on SOCE suppression with further evidence supporting a "Goldilocks Effect" of optimal SOCE suppression leading to enhanced invasion.

CHAPTER 7

GERANYLGERANYL TRANSFERASE INHIBITORS AS A NOVEL STIM2 INHIBITOR

I. Introduction

We have previously focused on how UV induces Mevalonate Pathway upregulation and enhanced cholesterol biosynthesis, which in turn leads to SOCE suppression-induced changes in glycosylation and subsequent invasion. However, the Mevalonate Pathway has many intermediate steps that lead to the production of many different molecules. Besides CHL, one molecule produced as a function of the Mevalonate Pathway is Geranylgeranyl Pyrophosphate (GGPP), known for its role in protein prenylation. In short, FPP can also be utilized via Geranylgeranylpyrophosphate Synthase (GGPS1) to form Geranylgeranylpyrophosphate (GGPP). GGPP is then transferred as a C-20 isoprenyl group using Geranylgeranyltransferase 1 (GGT; PGGT1B) to a protein containing a CaaX motif at the C-terminus for protein prenylation (431, 442, 444, 578). Farnesyl Pyrophosphate (FPP), GGPP, and even upstream molecule Isopentyl Pyrophosphate (IPP), have all garnered clinical attention as cancer therapeutics. This is likely since the majority of prenylated proteins are small GTPases involved in cancer progression like Ras, RhoA, and Arf among others (444). Hence, it is perhaps unsurprising that FPP and GGPP have been shown to be paramount in promoting tumor cell viability as inhibition of Mevalonate Pathway leads to reduced isoprenylation of many small GTPases leading to cell death. Conversely this effect can be rescued with addition of FPP and GGPP (reviewed in (450). Together this demonstrates a clear link between prenylation and cancer progression.

Generally, the mechanisms behind FPP and GGPP facilitating tumor progression are widely under investigated, but there is some recent evidence that FPP and GGPP can induce oncogenic signaling pathways such as Hh, PI3K, AKT, mTORC1, Wnt/β-catenin pathways (reviewed in (579)). Further it is known that prenylation of RhoA leads to dephosphorylation of YAP/TAZ which facilitates nuclear translocation. YAP/TAZ is a tumor promoter within melanoma as BRAF, NRAS, and KRAS mutant melanomas with high YAP/TAZ expression confer low sensitivity to RAF/MEK inhibitors (580). However, more investigation is needed for how FPP and GGP individually exert prenylation since this process appears to be dependent on a "class effect" where FPP and GGPP are interchangeable for prenylation (581). With regards to this class effect, targeting the inhibition of prenyltransferase enzymes (Farnesyl Transferase Inhibitor (FTI) and Geranylgeranyltransferase Inhibitor (GGTI)) has had little therapeutic success due to isoprenylation compensation and toxicity issues respectively (450). Previous research has provided optimism that inhibition of the Mevalonate Pathway can have therapeutics effects. In support, a previous melanoma using FTI with an M1 virus to induce oncolysis and inhibit melanoma progression *in vitro, in vivo,* and *ex vivo* (582), but no clinical trials have been done targeting prenylation in melanoma. Since the mechanisms behind prenylation and how inhibition diminishes cancer progression are widely understudied and not fully understood, this presents future avenues of research for therapeutics targeting Mevalonate Pathway in cancer.

While there is currently no previous literature regarding GGPP regulating SOCE or interacting with STIM1 or Orai1, our previous work showed a UV-induced upregulation of the Mevalonate Pathway (see Chapter 4) driving investigations into GGPP and GGT

effects on SOCE. Previous literature within the last year found that GGPP can counteract statin-induced changes in cholesterol levels in human and rat pulmonary smooth muscle cells via RhoA/ROCK2 cascade activating Calcium Sensing Receptor (CaSR) membrane trafficking (583). This suggests that products of the Mevalonate Pathway may positively regulate the activity of each other, driving cancer progression and these processes could rely on Ca^{2+} signaling. By examining this, we can hopefully provide new insights into metabolic regulation of SOCE that could lead to novel and potentially impactful future avenues of therapeutic research targeting metabolism and Ca^{2+} signaling. Therefore, the goal of this investigation was to determine whether GGPP, GGT, as well as other molecules along the Mevalonate Pathway, regulate SOCE.

II. Results

Characterization Of Mevalonate Pathway Endpoints. Since Mevalonate Pathway endpoints CHL production lead to SOCE suppression, we investigated other endpoints of the Mevalonate Pathway to determine if other endpoints have effects on SOCE. Therefore, we plated cells on glass coverslips overnight in the presence or absence of indicated substances (Farnesyl Pyrophosphate (FPP; Fig 7-1A), Ubiquinone (CoQ10; Fig 7-1B) and Dolichol; Fig 7-1C, GGPP and/or GGTI-298 (GGTI); Fig 7-1D-E). Astonishingly, while FPP, CoQ10 and Dolichol failed to achieve any significant changes in SOCE, addition of GGTI yielded highly significant inhibition of SOCE; an effect that was synergized by the addition of GGPP. Thus, ruling out the possibility that SOCE is affected by CoQ10-induced changes in energy production, or Dolichol-induced changes in N-linked glycosylation. Further, this suggests that the conversion of FPP to GGPP is pivotal in the SOCE suppression since FPP accumulation failed to suppress SOCE, while GGPP synergized the effect of inhibition of GGT transfer of GGPP to membrane proteins. This suggests the effects GGTI on SOCE results from accumulation of GGPP in the cytosol that is unable to be transferred to the membrane.

Figure 7-1

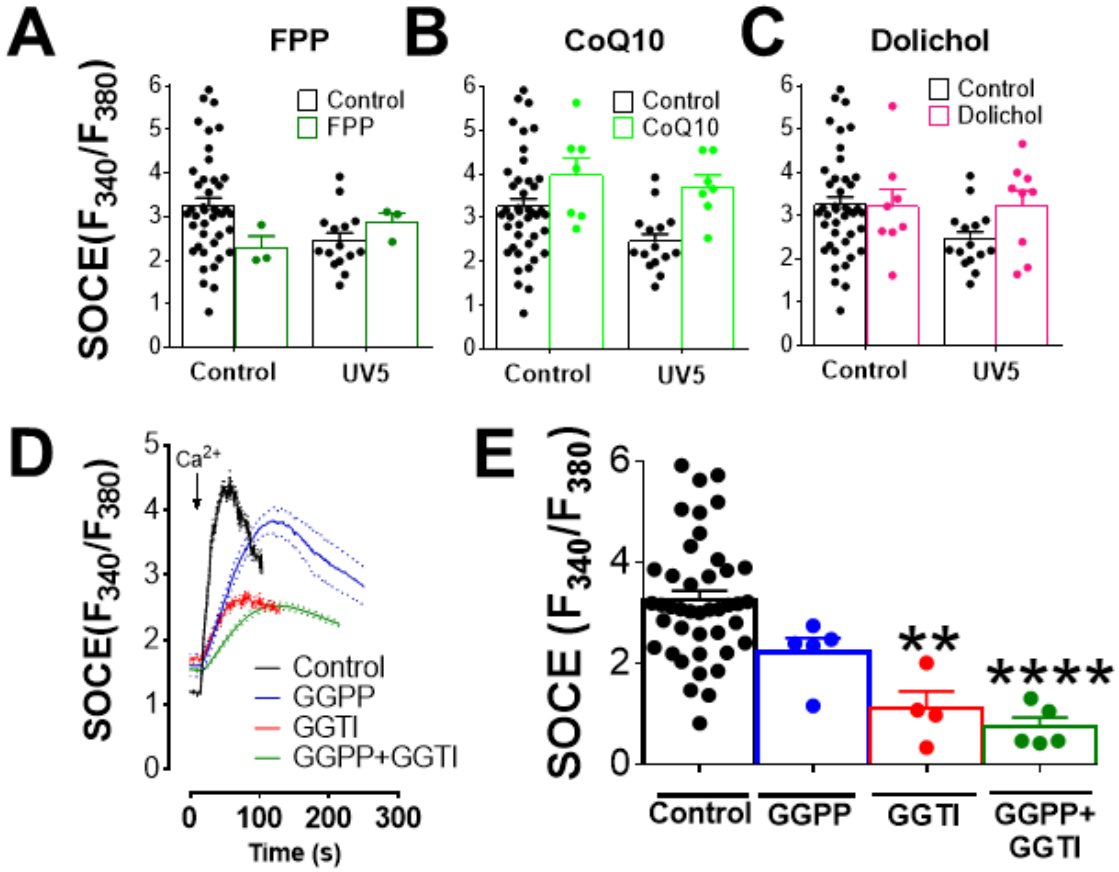
A
FPP
B
CoQ10
C
Dolichol
SOCE(F340/F380)
Control
FPP
CoQ10
Dolichol
UV5
D
Ca2+
Control
GGPP
GGTI
GGPP+GGTI
Time (s)
E
SOCE (F340/F380)
**
****
Control
GGPP
GGTI
GGPP+ GGTI

Figure 7-1 Characterization Of Mevalonate Pathway Endpoints. (A-E) B16N murine melanoma were exposed incubated after the absence (Control) or presence of 175J/m^2 UV for 5 weeks (UV5) (see Fig 4-1). (A-C) Following incubation, cells were plated on glass coverslips and incubated with the indicated substance overnight (A- Farnesyl Pyrophosphate (FPP; 10μM), B- Ubiquinone (CoQ10; 50μM), C- Dolichol (10μM)). Following overnight incubation, cells were loaded with Fura2 and treated with Tg for 15 minutes in the absence of extracellular Ca^{2+} (not shown) before the addition of 1mM Ca^{2+} (see Fig 4-1). Error bars represent SEM, data was analyzed by two way ANOVA with multiple comparisons *p<0.05, **p<0.01, ***p<0.001, ****p<0.0001. (Effect of FPP, CoQ10, Dolichol, p>0.05). (D-E) Cells were plated on glass coverslips and incubated with the indicated substance overnight (D- Geranylgeranyl pyrophosphate (GGPP; 3μM), E- Geranylgeranyltransferase Inhibitor (GGTI; 15μM). Following overnight incubation, cells were loaded with Fura2 and treated with Tg for 15 minutes in the absence of extracellular Ca^{2+} (not shown) before the addition of 1mM Ca^{2+} (see Fig 4-1). Each dot on each bar is a biological replicate. Error bars represent SEM, data was analyzed by one-way ANOVA with multiple comparisons (ANOVA, p<0.0001; Effect of GGTI, p<0.001; Effect of GGPP+GGTI, p<0.0001) *p<0.05, **p<0.01, ***p<0.001, ****p<0.0001.

Depletion Of Lipids Drives GGPP Accumulation In Cytosol And SOCE Suppression. Since we have demonstrated that inhibition of GGPP transfer to the membrane is paramount to SOCE suppression, we assessed the effect of lipid depletion on SOCE in both human (WM983) and mouse (B16N) melanoma cell lines to determine whether the effect of lipid depletion on the membrane regulates SOCE. Hence, cells were treated either in the presence or absence of GGTI overnight and Lipid Depleted Serum (LDS) for 4 hours prior to loading with Fura2 and addition of Tg (see Fig 4-1). Addition of GGTI led to full suppression of SOCE with no observable impact on cell viability, while addition of LDS only led to no significant change in SOCE, while also not visibly affecting viability. Interestingly, addition of LDS to GGTI-treated cells, led to partial rescue of SOCE, suggesting that lipid composition on the membrane plays a role in GGTI-induced SOCE suppression (Fig 7-2A-B). Since GGPP is transferred to the membrane to activate membrane proteins, this further suggests a likelihood of GGPP accumulation in the cytosol is inhibiting SOCE, which can be combated by clearing membrane of lipids to rescue SOCE activity.

Figure 7-2

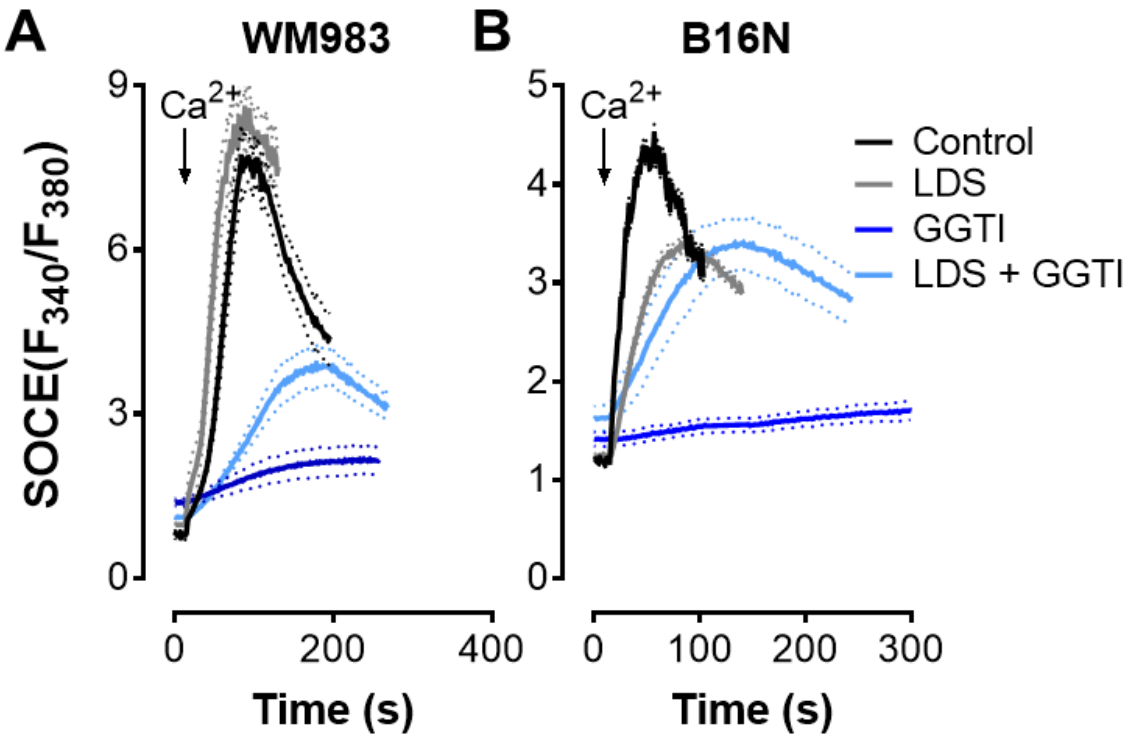
A
WM983
B
B16N
Ca2+
Ca2+
SOCE(F340/F380)
9
6
3
0
5
4
3
2
1
0
0
200
400
0
100
200
300
Time (s)
Time (s)
Control
LDS
GGTI
LDS + GGTI

Figure 7-2. Depletion Of Lipids Drives GGPP Accumulation In Cytosol And SOCE Suppression. WM983 (A) and B16N (B) cells were treated either in the presence or absence of GGTI (15μM, overnight) and Lipid Depleted Serum (LDS; 40mg/ml) for 4 hours. Following incubation, cells were loaded with Fura2 and treated with Tg for 15 minutes in the absence of extracellular Ca^{2+} (not shown) before the addition of 1mM Ca^{2+} (see Fig 4-1). Error bars represent SEM.

Variable Inhibition Of SOCE By A GeranylgernaylTransferase Inhibitor (GGTI-298). We investigated whether GGT inhibition led to reduction in SOCE across multiple types of human cell lines including Jurkat (T-cells), CEM (lymphoblasts), MG63 (osteosarcoma), MDA-MB-231 (triple negative breast cancer), and UACC257 (melanoma). Much to our astonishment, not only did GGTI-298 exert a significant effect on SOCE in melanoma cells, but we found that GGTI led to significant SOCE reduction in a dose dependent manner across all cell lines tested (Fig 7-3A-E). Interestingly, the effect of GGTI on SOCE was not uniform throughout the cell lines. In Jurkat T-cells, GGTI exerted an IC50 of 9.5μM, while CEM lymphoblasts had an IC50 of 25μM demonstrating a 2.6-fold difference in GGTI sensitivity across parallel immune cell lines (Fig 7-3F). Furthermore, IC50 concentrations varied across a variety of cancer cell lines ranging 5.2μM in UAC257 cells to 36μM in MDA-MB-231 cells (Fig 7-3G). Thus, we demonstrate that GGTI is a global SOCE inhibitor with varying degrees of cell-specific sensitivity across both immune and cancer cells.

Figure 7-3

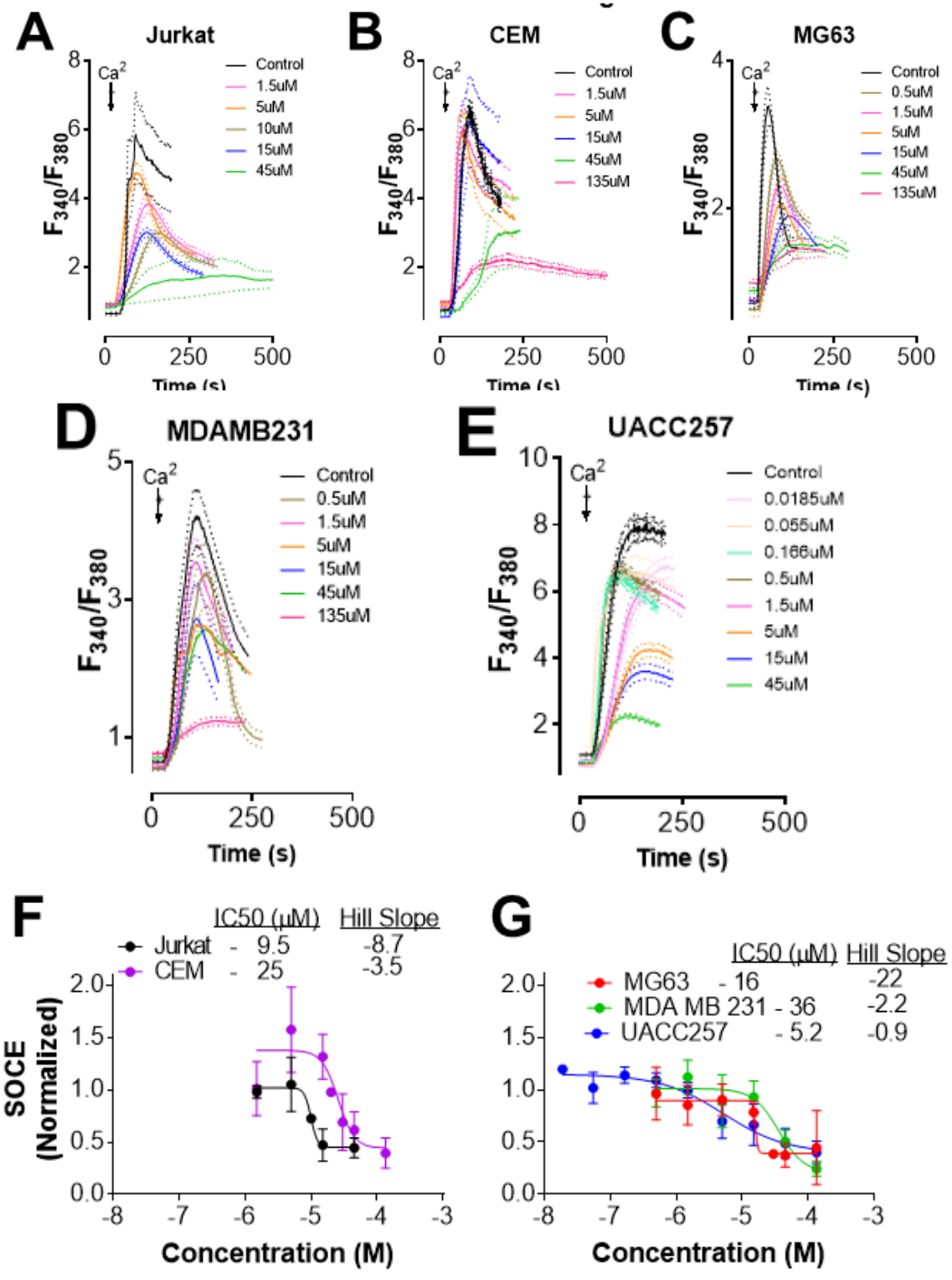
A
Jurkat
Ca2
Control
1.5uM
5uM
10uM
15uM
45uM
F340/F380
Time (s)
B
CEM
Control
1.5uM
5uM
15uM
45uM
135uM
C
MG63
Control
0.5uM
1.5uM
5uM
15uM
45uM
135uM
D
MDAMB231
Control
0.5uM
1.5uM
5uM
15uM
45uM
135uM
E
UACC257
Control
0.0185uM
0.055uM
0.166uM
0.5uM
1.5uM
5uM
15uM
45uM
F
IC50 (μM) Hill Slope
Jurkat - 9.5 -8.7
CEM - 25 -3.5
SOCE (Normalized)
Concentration (M)
G
IC50 (μM) Hill Slope
MG63 - 16 -22
MDA MB 231 - 36 -2.2
UACC257 - 5.2 -0.9
Concentration (M)

Figure 7-3. Variable Inhibition Of SOCE By A GeranylgernaylTransferase Inhibitor (GGTI-298). (A-E) Jurkat (A), CEM (B), MG63 (C), MDA-MB-231 (D), UACC257 (E) cells were plated on glass coverslips overnight, loaded with Fura2, and treated with indicated concentrations of GGTI concurrently with 2μM Tg for 15 min (not shown) in the absence of extracellular Ca^{2+} (not shown), followed by addition of 1mM Ca^{2+} (see Fig 4-1). (F) Jurkat and CEM cells were attached to coverslips using 3ug/ul Poly-D-Lysine for 2 hours prior to treating cells with Fura2 and Tg as described (see Fig 4-1), indicated GGTI concentrations were administered concurrently with Tg for 15 min in the absence of extracellular Ca^{2+} (not shown) followed by the addition of 1mM Ca^{2+}, with IC50 and Hill Slopes analyzed using a non-linear regression as described (see Fig 4-4). (G) MG63, MDA-MB-231 and UACC257 cells were plated on glass coverslips overnight prior to Fura2 loading and concurrent Tg and GGTI addition (see Fig 4-1, 7-1). IC50 and Hill Slopes analyzed using a non-linear regression as described (see Fig 4-4). Error bars represent +/- SEM, IC50 and Hill slopes examined through non-linear regression as described (see Fig 4-5) showing titration of GGTI on 5 different cell lines.

STIM2 Overexpression Increases GGTI Sensitivity. Since we have demonstrated that GGTI is a novel SOCE inhibitor, we aimed to investigate whether there were differences in GGTI sensitivity between cells exhibiting differences in STIM1 and STIM2 expression. Therefore, we transfected HEK293 cells with Orai2-WT-CFP and either STIM1-WT-YFP or STIM2-WT-YFP to create both STIM1/Orai2 (S1O2; Fig 7-4A,C) and STIM2/Orai2 (S2O2; Fig 7-4B-C) overexpressing individual clones as described (see Fig 4-4). Orai2-overexpressed cells were readily available, whereas Orai1- and Orai3- overexpressed cell production is still in progress. Surprisingly, after titration with various GGTI concentrations, we found that STIM2 overexpressed cells had between a 276-828x higher sensitivity to GGTI than STIM1 overexpressed cells with STIM2 overexpressed cells exhibiting IC50 levels in the nM range (Fig 7-4C). This suggests that GGTI's effect is more sensitive to STIM2 expression leading to speculation that STIM2 may have a previously unknown role in facilitating geranylgeranylation of lipids while also regulating the effect of GGPP accumulation on SOCE. Further, this also yields the possibility that cancer cells that exhibit higher levels of STIM2 expression relative to STIM1 may be more sensitive to GGTI as a cancer therapeutic.

Figure 7-4

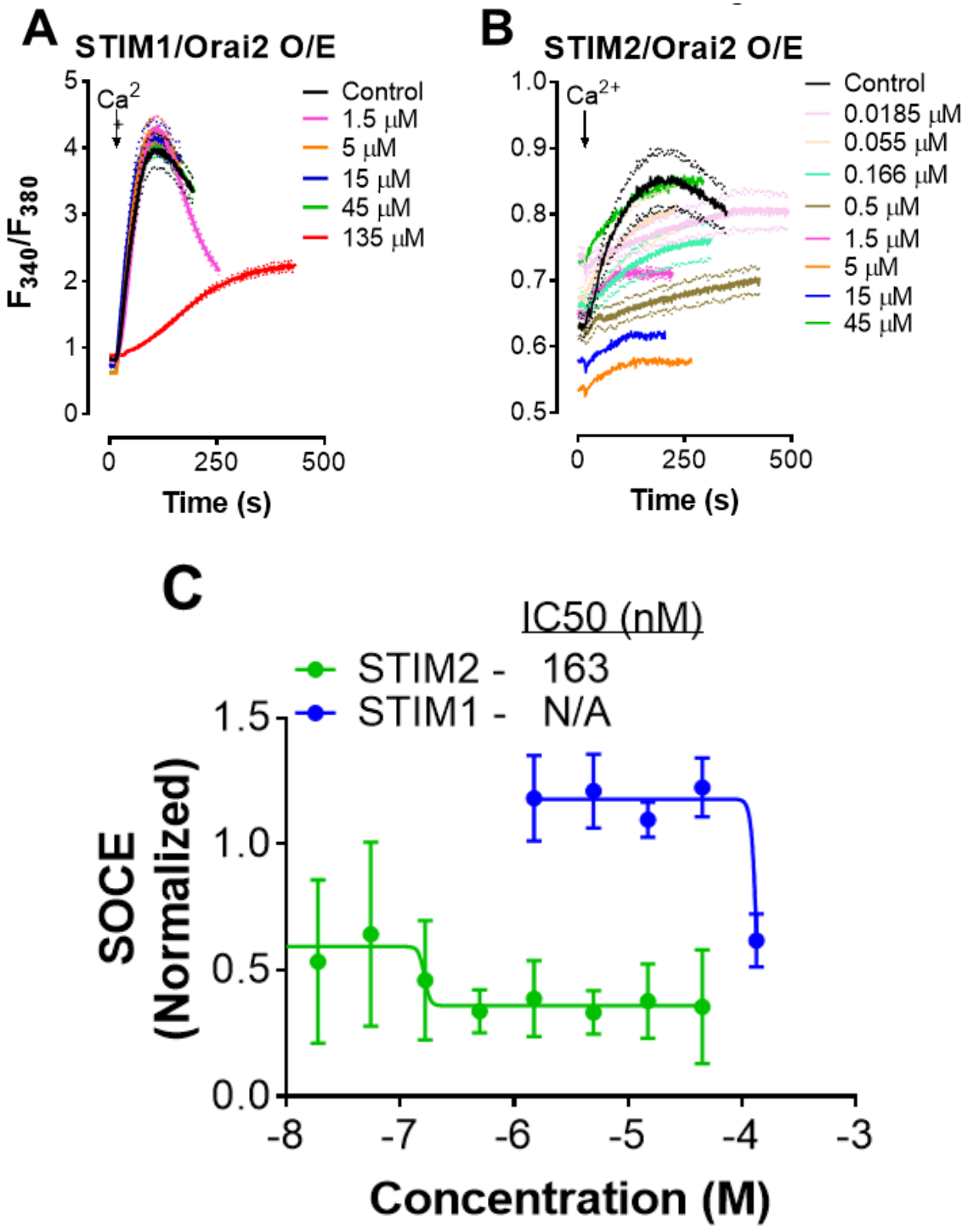
A
STIM1/Orai2 O/E
Ca2+
Control
1.5 μM
5 μM
15 μM
45 μM
135 μM
F340/F380
Time (s)
B
STIM2/Orai2 O/E
Ca2+
Control
0.0185 μM
0.055 μM
0.166 μM
0.5 μM
1.5 μM
5 μM
15 μM
45 μM
Time (s)
C
IC50 (nM)
STIM2 - 163
STIM1 - N/A
SOCE (Normalized)
Concentration (M)

Figure 7-4. STIM2 Overexpression Increases GGTI Sensitivity. HEK293 cells were transfected with Orai2-WT-CFP and either STIM1-WT-CFP (S1O2; A,C) or STIM2-WT-CFP (S2O2; B-C) and selected as described (see Fig 4-4). HEK293 S1O2 and S2O2 cells were plated on glass coverslips overnight prior to Fura2 loading and concurrent Tg and indicated concentration of GGTI addition (see Fig 4-1, Fig 7-1). (A-B) Representative traces showing the effect of GGTI on SOCE on HEK293 S1O2 (A) and HEK293 S2O2 (B) cells following concurrent Tg and indicated concentration of GGTI addition. Dashed lines indicate SEM. (C) MG63, MDA-MB-231 and UACC257 cells were plated on glass coverslips overnight prior to Fura2 loading and concurrent Tg and indicated concentration of GGTI addition (see Fig 4-1, 7-1). IC50 and Hill Slopes analyzed using a non-linear regression as described (see Fig 4-4). Error bars represent +/- SEM, IC50 and Hill slopes examined through non-linear regression as described (see Fig 4-5).

GGPP Accumulation Inhibits STIM/Orai Interactions. As our investigations have shown differences in GGTI sensitivity between cells overexpressing STIM1 and STIM2, we investigated whether GGPP accumulation either through GGPP addition, inhibition of GGT or both inhibited STIM1 and Orai1 interactions. To do so, we plated HEK293 cells transfected with STIM1-YFP and Orai1-CFP (S1O1) on glass coverslips with either GGPP, GGTI or both (Fig 7-5A-D). Following, cell videos were captured before and after the addition of 2μM Tg. It was found that untreated cells appeared to have more STIM1 localization to the membrane following Tg addition than those treated with GGPP, GGTI, or both. Further, HEK293 S1O1 cells were photobleached with high laser intensity before and after the addition of 2μM Tg and measured for FRET intensity via confocal microscopy (Fig 7-5E). Interestingly While GGPP appears to be mildly sufficient to suppress STIM1 and Orai1 interaction, GGTI and GGPP synergistically appear to suppress STIM1 and Orai1 interaction via FRET. Thus, it appears that the inhibition of STIM1 and Orai1 interactions is the result of GGPP accumulation that is driven primarily by the inhibition of endogenous GGPP transfer to the membrane that can be synergized with exogenous addition of GGPP to further accumulate in the cytosol. This sets the foundation for mechanistic insights demonstrating that GGPP accumulation in the cytosol regulates STIM and Orai interactions.

Figure 7-5

A-D

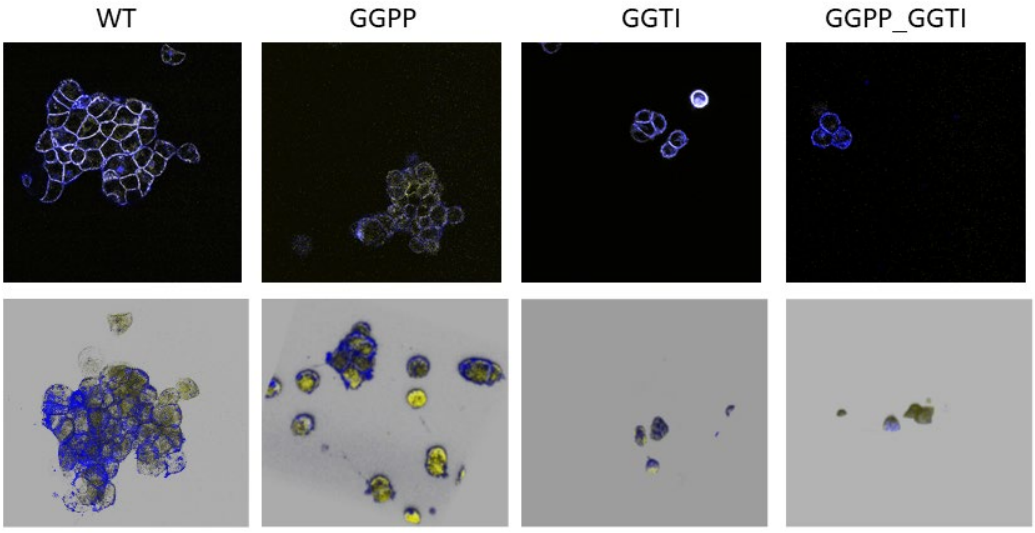

E

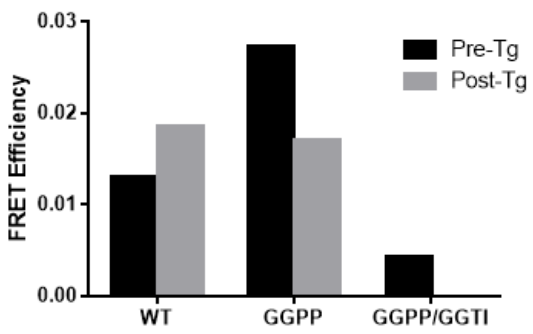

F

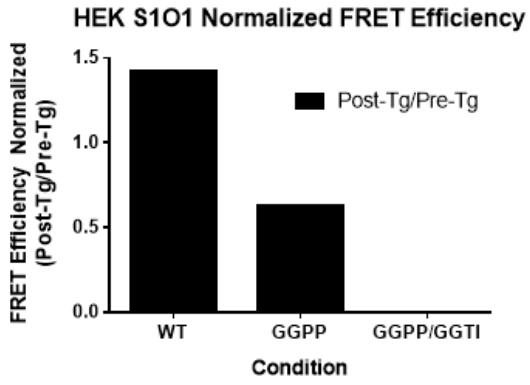

Figure 7-5. GGPP Accumulation Inhibits STIM/Orai1 Interactions. (A-D) Representative images of HEK293 cells previously transfected with STIM1-YFP and Orai1-CFP (HEKS1O1) plated on glass coverslips and treated with either GGPP (3μM, overnight), GGTI (15μM, overnight), or both were measured for fluorescence intensity in 2D (TOP) and 3D (Bottom) before and after the addition of 2μM Tg. (E) HEKS1O1 cells were measured for FRET with photobleaching laser intensity (UV laser, 90% gain, 10%, excitation 405nm) via confocal microscopy before and after being treated with 2μM Tg. Bars represent normalized FRET efficiency of post-Tg acquisition normalized to pre-Tg acquisition, no bars represents lack of measurable FRET occurring.

III. Discussion

In this current investigation, we have shown evidence that GGTI is a novel SOCE inhibitor across a variety of cell types (Fig 7-3), which appears to have some dependence on cell-type specific reliance on STIM2 (Fig 7-2). Interestingly, besides CHL (as discussed in Chapter 4) and inhibition of GGT (as discussed in Chapter 7), no other mevalonate pathway endpoints appear to have any significant effect on SOCE (Fig 7-1). While much of the mechanism remains unknown and requires further investigation, it appears there may be evidence that the effect of GGTI-induced SOCE suppression is lipid dependent (Fig 7-2) with the potential to also inhibit STIM1/Orai1 interactions (Fig 7-5). Collectively, there is foundation for studies on GGTI as a novel STIM2 inhibitor.

While much of the previous research both before and during these studies have investigated the role of CHL as the major endpoint in the mevalonate pathway that facilitates SOCE suppression, we present another endpoint in the mevalonate pathway (GGT inhibition) that plays a vital role in SOCE suppression. Most known inhibitors of SOCE target STIM1 and Orai1, however GGTI seems to target STIM2-dependent cells. This could have significant consequences as STIM2 has roles in disease such as colon cancer, melanoma, esophageal squamous cell carcinoma, triple negative breast cancer, glioblastoma, and acute myeloid leukemia (187, 365). Likely, GGTI inhibits the prenylation of membrane proteins that facilitate STIM2-dependent processes. While it is unknown how lipidation of the membrane targets STIM2 specifically, it sets the foundation for mechanistic studies to understand this process that is currently elusive. Thus, future investigations into the mechanism and understanding of GGTI-induced SOCE suppression could provide a strong foundation for future therapeutic targets for a variety of cancers.

CHAPTER 8

CONCLUSIONS AND FUTURE DIRECTIONS

I. Conclusions

Within the current investigations, we have defined a previously unknown relationship between UV, CHL biosynthesis/mevalonate pathway, Ca^{2+} signaling and invasive behavior. While CHL biosynthetic pathways have been proposed to drive melanoma progression previously, the molecular context for why CHL biosynthesis might be dysregulated in melanoma had not previously been defined. Additionally, the mechanisms why certain mevalonate pathway endpoints and how complete UV exposure regulates SOCE were further explored. As a result, we have demonstrated that UV leads to upregulation of the Mevalonate Pathway and CHL biosynthesis. In turn, CHL biosynthesis facilitates both SOCE suppression and melanoma invasiveness. In addition to CHL, other products of the Mevalonate Pathway have a previously unknown effect on SOCE where accumulation of GGPP in the cytosol either from upregulation of GGPP production or inhibition of transfer of GGPP to membrane proteins leads to SOCE suppression. Further, the effect of GGTI on SOCE occurs in a STIM2-dependent manner, revealing a novel STIM2 inhibitor.

Subsequently, SOCE suppression leads to changes in glucose utilization. As opposed to non-transformed cells preferentially metabolizing glucose for oxidative phosphorylation, cancer cells preferentially metabolizing glucose for lactic acid fermentation via the “Warburg Effect”, melanoma cells exhibiting SOCE suppression prefer an alternative of shunting glycolysis intermediate, F6P, toward anabolic pathways such as HBP leading to enhanced invasiveness. This corroborates previous research

showing upregulation of CHL and HBP lead to cancer progression while introducing a previously unknown mediator of these processes in the form of Ca^{2+} signaling.

While it is clear from these investigations that UV and SOCE suppression lead to enhanced melanoma invasiveness, the relationship presented here is not linear. We have illustrated a "Goldilocks Effect" where a specific window of SOCE suppression is optimal for invasiveness that appears to be between 20-40% suppression. When cells have minimal SOCE suppression, Ca^{2+} levels are elevated enough to not induce metabolic changes, while when SOCE suppression is too severe such as in an Orai1-DN phenotype, it likely inhibits Ca^{2+}-dependent invasive properties like invadopodia formation. Further, it appears that SOCE suppression-induced invasiveness is reversible, as pharmacological enhancement of SOCE removed invasive properties in both UV-exposed and Orai1-overexpressed cells.

Interestingly, it appears that the effects of UV on SOCE differ in UVA and UVA+B exposed cells. While UVA is driving long-term SOCE suppression starting at 4 weeks post-exposure, UVB appears to drive the transient effect of SOCE suppression at 2-3 weeks post-UVA+B exposure. Further, UVA and UVA+B exposure have both shown the ability to induce enhanced invasiveness in cells, but the effect occurs when the condition is sufficient to drive SOCE suppression to the “Goldilocks Effect” optimal window for invasion.

Considered collectively, the relationship between Ca^{2+} signals and tumor progression is less linear than previously believed with Ca^{2+} signals serving anti-invasive role in melanoma progression. It is interesting to note that, unlike most tissues, melanocytes grow within the low extracellular Ca^{2+} concentration of the basal layer of

skin. If so, the suppression of Ca^{2+} entry may be an adaptation used by melanoma cells to tolerate the high extracellular Ca^{2+} content of nonnative tissues. However, whether the anti-invasive properties of Ca^{2+} signals are a property unique to melanoma and/or other skin tumors is not known and may be the topic of future investigations.

II. Future Directions

These investigations have set the foundations for many future directions contributing to cancer therapeutics. First and foremost, while it is clear that HBP upregulation leads to enhanced invasion via OGT and O-GlcNAcylation, questions remain about which proteins are O-GlcNAcylated that drive invasion. While it is known that many oncogenic signals rely on O-GlcNAcylation as previously described (Chapter 1: Part II-i), elucidating which proteins are O-GlcNAcylated as a result of SOCE suppression could drive future therapeutic research to inhibit melanoma progression.

Also, while it is currently known why UVA and UVB lead to melanomagenesis and progression (see Chapter 6: Part I), further investigations are required to understand mechanistic insights into how UVA and UVB lead to SOCE suppression. While it is likely that UVB leads to DNA damage, it is unclear whether UVB leads to synergistic effects with well-established gene mutations or if there are specific gene mutations that occur because of UVB-induced DNA damage. Future investigations could provide therapeutic potential against certain gene mutations. In parallel, while it is likely UVA leads to ROS production and epigenetic changes, it is unclear which if either is the main cause of stable SOCE suppression. With regards to the former, it is unclear if UVA-induced ROS production inhibits SOCE through having effects on STIM and Orai interaction or activity. In regard to the latter, it is unclear whether UVA-induced epigenetic mutation occur and

if they do which genes are modulated. Both of these possibilities warrant further investigation and provide promising therapeutic potential.

Finally, it is clear that GGPP accumulation inhibits SOCE, but the conceptual basis of why GGPP accumulation leads to SOCE suppression and the understanding the complete mechanism of how GGPP inhibits SOCE warrant further investigations. Demonstrating GGPP as a novel STIM2 inhibitor introduces a new class of SOCE-modulating inhibitors that could have novel therapeutic effects, not just on melanoma but also on diseases reliant on STIM2 activity.

III. **Final Remarks**

Collectively, this works provides the foundation for many exciting avenues of research. Introducing Ca^{2+} signaling as a novel class of melanoma therapeutics adds a new and innovative way to target melanoma that has been previously under-investigated. Not only have we presented a context to target melanoma through SOCE levels, but we have presented mechanistic insights that will also drive future research. Further, we have provided context for how other processes such as CHL and anabolic pathways drive progression, which can help advance other fields of research to drive future novel melanoma therapeutics. Thus, these investigations are an exciting, innovative, and novel addition to the landscapes of Ca^{2+} signaling, melanoma, and cancer.

CHAPTER 9
REFERENCES CITED

1. Bong AHL, Monteith GR. Calcium signaling and the therapeutic targeting of cancer cells. Biochimica et Biophysica Acta (BBA) - Molecular Cell Research. 2018;1865(11, Part B):1786-94.

2. Das K. Albuminuria and Eclampsia-Calcium Carbide in the Treatment of Uterine Cancer-Intra-Uterine Infection of Syphilis-Treatment of Retro-Diviation of the Uterus-Management of Pelvic Presentations-Suturing Abdominal Wounds without Buried Sutures to Prevent Ventral Hernia-Presentation of the Foetal Head-Puerperal Convulsions in Twin Sisters-Ovarian Pregnancy-New Method of Inducing Abortion. The Indian medical gazette. 1896;31(12):460-2.

3. Cramer W. On the Biochemical Mechanism of Growth. The Effect of Sodium and Calcium Ions on the Growth of a Transplantable Mouse Carcinoma. The Biochemical journal. 1918;12(3):210-20.

4. Parekh AB, Putney JW, Jr. Store-operated calcium channels. Physiol Rev. 2005;85(2):757-810.

5. Parekh AB. Store-operated channels: mechanisms and function. The Journal of Physiology. 2008;586(13):3033-.

6. Putney JW, Jr. A model for receptor-regulated calcium entry. Cell Calcium. 1986;7(1):1-12.

7. Takemura H, Putney JW, Jr. Capacitative calcium entry in parotid acinar cells. Biochem J. 1989;258(2):409-12.

8. Soboloff J, Rothberg BS, Madesh M, Gill DL. STIM proteins: dynamic calcium signal transducers. Nat Rev Mol Cell Biol. 2012;13(9):549-65.

9. Brandman O, Liou J, Park WS, Meyer T. STIM2 is a feedback regulator that stabilizes basal cytosolic and endoplasmic reticulum Ca^{2+} levels. Cell. 2007;131(7):1327-39.

10. Stathopulos PB, Ikura M. Chapter Three - Structure and Function of Endoplasmic Reticulum STIM Calcium Sensors. In: Prakriya M, editor. Current Topics in Membranes. 71: Academic Press; 2013. p. 59-93.

11. Bird GS, Hwang SY, Smyth JT, Fukushima M, Boyles RR, Putney JW, Jr. STIM1 is a calcium sensor specialized for digital signaling. Curr Biol. 2009;19(20):1724-9.

12. Zhou Y, Mancarella S, Wang Y, Yue C, Ritchie M, Gill DL, et al. The short N-terminal domains of STIM1 and STIM2 control the activation kinetics of Orai1 channels. J Biol Chem. 2009;284(29):19164-8.

13. Wang X, Wang Y, Zhou Y, Hendron E, Mancarella S, Andrake MD, et al. Distinct Orai-coupling domains in STIM1 and STIM2 define the Orai-activating site. Nat Commun. 2014;5:3183.

14. DeHaven WI, Smyth JT, Boyles RR, Putney JW, Jr. Calcium inhibition and calcium potentiation of Orai1, Orai2, and Orai3 calcium release-activated calcium channels. J Biol Chem. 2007;282(24):17548-56.

15. Lis A, Peinelt C, Beck A, Parvez S, Monteilh-Zoller M, Fleig A, et al. CRACM1, CRACM2, and CRACM3 are store-operated Ca^{2+} channels with distinct functional properties. Curr Biol. 2007;17(9):794-800.

16. Nieto Gutierrez A, McDonald PH. GPCRs: Emerging anti-cancer drug targets. Cellular Signalling. 2018;41:65-74.

17. Regad T. Targeting RTK Signaling Pathways in Cancer. Cancers. 2015;7(3):1758-84.

18. Jardin I, Rosado JA. STIM and calcium channel complexes in cancer. Biochim Biophys Acta. 2016;1863(6 Pt B):1418-26.

19. Zheng J. Molecular mechanism of TRP channels. Comprehensive Physiology. 2013;3(1):221-42.

20. Vazquez G, Wedel BJ, Aziz O, Trebak M, Putney JW, Jr. The mammalian TRPC cation channels. Biochim Biophys Acta. 2004;1742(1-3):21-36.

21. Cheng KT, Liu X, Ong HL, Swaim W, Ambudkar IS. Local Ca(2)+ entry via Orai1 regulates plasma membrane recruitment of TRPC1 and controls cytosolic Ca(2)+ signals required for specific cell functions. PLoS Biol. 2011;9(3):e1001025.

22. Dietrich A, Kalwa H, Rost BR, Gudermann T. The diacylgylcerol-sensitive TRPC3/6/7 subfamily of cation channels: functional characterization and physiological relevance. Pflugers Arch. 2005;451(1):72-80.

23. Venkatachalam K, Zheng F, Gill DL. Regulation of canonical transient receptor potential (TRPC) channel function by diacylglycerol and protein kinase C. J Biol Chem. 2003;278(31):29031-40.

24. Trebak M, Lemonnier L, DeHaven WI, Wedel BJ, Bird GS, Putney JW, Jr. Complex functions of phosphatidylinositol 4,5-bisphosphate in regulation of TRPC5 cation channels. Pflugers Arch. 2009;457(4):757-69.

25. Myeong J, Ko J, Kwak M, Kim J, Woo J, Ha K, et al. Dual action of the Gαq-PLCβ-PI(4,5)P2 pathway on TRPC1/4 and TRPC1/5 heterotetramers. Scientific Reports. 2018;8(1):12117.

26. Mast TG, Brann JH, Fadool DA. The TRPC2 channel forms protein-protein interactions with Homer and RTP in the rat vomeronasal organ. BMC neuroscience. 2010;11:61-.

27. Wetsel WC. Sensing hot and cold with TRP channels. International Journal of Hyperthermia. 2011;27(4):388-98.

28. McKemy DD. How cold is it? TRPM8 and TRPA1 in the molecular logic of cold sensation. Molecular Pain. 2005;1(1):16.

29. Szallasi A, Blumberg PM. Vanilloid (Capsaicin) Receptors and Mechanisms. Pharmacological Reviews. 1999;51(2):159.

30. Yang F, Zheng J. Understand spiciness: mechanism of TRPV1 channel activation by capsaicin. Protein & cell. 2017;8(3):169-77.

31. Phelps CB, Wang RR, Choo SS, Gaudet R. Differential regulation of TRPV1, TRPV3, and TRPV4 sensitivity through a conserved binding site on the ankyrin repeat domain. The Journal of biological chemistry. 2010;285(1):731-40.

32. Tominaga M, Caterina MJ. Thermosensation and pain. Journal of Neurobiology. 2004;61(1):3-12.

33. Liu B, Qin F. Use Dependence of Heat Sensitivity of Vanilloid Receptor TRPV2. Biophysical journal. 2016;110(7):1523-37.

34. Cui Y, Yang F, Cao X, Yarov-Yarovoy V, Wang K, Zheng J. Selective disruption of high sensitivity heat activation but not capsaicin activation of TRPV1 channels by pore turret mutations. The Journal of general physiology. 2012;139(4):273-83.

35. Matta JA, Ahern GP. Voltage is a partial activator of rat thermosensitive TRP channels. The Journal of Physiology. 2007;585(2):469-82.

36. Grandl J, Kim SE, Uzzell V, Bursulaya B, Petrus M, Bandell M, et al. Temperature-induced opening of TRPV1 ion channel is stabilized by the pore domain. Nat Neurosci. 2010;13(6):708-14.

37. Yang F, Cui Y, Wang K, Zheng J. Thermosensitive TRP channel pore turret is part of the temperature activation pathway. Proceedings of the National Academy of Sciences of the United States of America. 2010;107(15):7083-8.

38. Doerner JF, Hatt H, Ramsey IS. Voltage- and temperature-dependent activation of TRPV3 channels is potentiated by receptor-mediated PI(4,5)P2 hydrolysis. The Journal of general physiology. 2011;137(3):271-88.

39. Cao S, Anishkin A, Zinkevich NS, Nishijima Y, Korishettar A, Wang Z, et al. Transient receptor potential vanilloid 4 (TRPV4) activation by arachidonic acid requires protein kinase A-mediated phosphorylation. Journal of Biological Chemistry. 2018.

40. Andersson DA, Nash M, Bevan S. Modulation of the cold-activated channel TRPM8 by lysophospholipids and polyunsaturated fatty acids. The Journal of neuroscience : the official journal of the Society for Neuroscience. 2007;27(12):3347-55.

41. Zakharian E, Cao C, Rohacs T. Gating of transient receptor potential melastatin 8 (TRPM8) channels activated by cold and chemical agonists in planar lipid bilayers. The Journal of neuroscience : the official journal of the Society for Neuroscience. 2010;30(37):12526-34.

42. Liu B, Qin F. Functional Control of Cold- and Menthol-Sensitive TRPM8 Ion Channels by Phosphatidylinositol 4,5-Bisphosphate. The Journal of Neuroscience. 2005;25(7):1674.

43. Hinman A, Chuang H-h, Bautista DM, Julius D. TRP channel activation by reversible covalent modification. Proceedings of the National Academy of Sciences. 2006;103(51):19564.

44. Macpherson LJ, Dubin AE, Evans MJ, Marr F, Schultz PG, Cravatt BF, et al. Noxious compounds activate TRPA1 ion channels through covalent modification of cysteines. Nature. 2007;445:541.

45. Takahashi N, Mizuno Y, Kozai D, Yamamoto S, Kiyonaka S, Shibata T, et al. Molecular characterization of TRPA1 channel activation by cysteine-reactive inflammatory mediators. Channels. 2008;2(4):287-98.

46. Samanta A, Kiselar J, Pumroy RA, Han S, Moiseenkova-Bell VY. Structural insights into the molecular mechanism of mouse TRPA1 activation and inhibition. The Journal of General Physiology. 2018;150(5):751.

47. Akopian AN, Ruparel NB, Patwardhan A, Hargreaves KM. Cannabinoids Desensitize Capsaicin and Mustard Oil Responses in Sensory Neurons via TRPA1 Activation. The Journal of Neuroscience. 2008;28(5):1064.

48. Ruparel NB, Patwardhan AM, Akopian AN, Hargreaves KM. Desensitization of Transient Receptor Potential Ankyrin 1 (TRPA1) by the TRP Vanilloid 1-Selective Cannabinoid Arachidonoyl-2 Chloroethanolamine. Molecular Pharmacology. 2011;80(1):117.

49. Catterall WA. Voltage-gated calcium channels. Cold Spring Harbor perspectives in biology. 2011;3(8):a003947-a.

50. Heinemann SH, Terlau H, Stühmer W, Imoto K, Numa S. Calcium channel characteristics conferred on the sodium channel by single mutations. Nature. 1992;356:441.

51. Walker D, De Waard M. Subunit interaction sites in voltage-dependent Ca2+ channels: role in channel function. Trends in Neurosciences. 1998;21(4):148-54.

52. Dolphin AC. The α2δ subunits of voltage-gated calcium channels. Biochimica et Biophysica Acta (BBA) - Biomembranes. 2013;1828(7):1541-9.

53. Dolphin AC. G Protein Modulation of Voltage-Gated Calcium Channels. Pharmacological Reviews. 2003;55(4):607.

54. Campiglio M, Flucher BE. The role of auxiliary subunits for the functional diversity of voltage-gated calcium channels. Journal of cellular physiology. 2015;230(9):2019-31.

55. Zamponi GW, Striessnig J, Koschak A, Dolphin AC. The Physiology, Pathology, and Pharmacology of Voltage-Gated Calcium Channels and Their Future Therapeutic Potential. Pharmacological reviews. 2015;67(4):821-70.

56. Phan NN, Wang C-Y, Chen C-F, Sun Z, Lai M-D, Lin Y-C. Voltage-gated calcium channels: Novel targets for cancer therapy. Oncology letters. 2017;14(2):2059-74.

57. Catterall WA. Structure and function of neuronal Ca2+ channels and their role in neurotransmitter release. Cell Calcium. 1998;24(5):307-23.

58. Dziegielewska B, Casarez EV, Yang WZ, Gray LS, Dziegielewski J, Slack-Davis JK. T-Type Ca2+ Channel Inhibition Sensitizes Ovarian Cancer to Carboplatin. Molecular cancer therapeutics. 2016;15(3):460-70.

59. Tsien RW, Lipscombe D, Madison DV, Bley KR, Fox AP. Multiple types of neuronal calcium channels and their selective modulation. Trends in Neurosciences. 1988;11(10):431-8.

60. Dunlap K, Luebke JI, Turner TJ. Exocytotic Ca2+ channels in mammalian central neurons. Trends in Neurosciences. 1995;18(2):89-98.

61. Catterall WA, Few AP. Calcium Channel Regulation and Presynaptic Plasticity. Neuron. 2008;59(6):882-901.

62. Catterall WA. Excitation-contraction coupling in vertebrate skeletal muscle: A tale of two calcium channels. Cell. 1991;64(5):871-4.

63. Tanabe T, Mikami A, Niidome T, Numa S, Adams BA, Beam KG. Structure and Function of Voltage-Dependent Calcium Channels from Musclea. Annals of the New York Academy of Sciences. 1993;707(1):81-6.

64. Periasamy M, Kalyanasundaram A. SERCA pump isoforms: Their role in calcium transport and disease. Muscle & Nerve. 2007;35(4):430-42.

65. Strehler EE, Thayer SA. Evidence for a role of plasma membrane calcium pumps in neurodegenerative disease: Recent developments. Neuroscience Letters. 2018;663:39-47.

66. F Talarico E, Kennedy B, Marfurt C, U Loeffler K, Mangini N. Expression and immunolocalization of plasma membrane calcium ATPase isoforms in human corneal epithelium2005. 169-78 p.

67. Brini M, Carafoli E. The plasma membrane Ca^{2+} ATPase and the plasma membrane sodium calcium exchanger cooperate in the regulation of cell calcium. Cold Spring Harbor perspectives in biology. 2011;3(2):a004168.

68. Okunade GW, Miller ML, Pyne GJ, Sutliff RL, O'Connor KT, Neumann JC, et al. Targeted Ablation of Plasma Membrane Ca2+-ATPase (PMCA) 1 and 4 Indicates a Major Housekeeping Function for PMCA1 and a Critical Role in Hyperactivated Sperm Motility and Male Fertility for PMCA4. Journal of Biological Chemistry. 2004;279(32):33742-50.

69. Strehler EE, Caride AJ, Filoteo AG, Xiong Y, Penniston JT, Enyedi A. Plasma membrane Ca2+ ATPases as dynamic regulators of cellular calcium handling. Annals of the New York Academy of Sciences. 2007;1099:226-36.

70. Stafford N, Wilson C, Oceandy D, Neyses L, Cartwright EJ. The Plasma Membrane Calcium ATPases and Their Role as Major New Players in Human Disease. Physiological Reviews. 2017;97(3):1089-125.

71. Ridley AJ, Schwartz MA, Burridge K, Firtel RA, Ginsberg MH, Borisy G, et al. Cell Migration: Integrating Signals from Front to Back. Science. 2003;302(5651):1704.

72. Barrientos S, Stojadinovic O, Golinko MS, Brem H, Tomic-Canic M. PERSPECTIVE ARTICLE: Growth factors and cytokines in wound healing. Wound Repair and Regeneration. 2008;16(5):585-601.

73. Lamalice L, Le Boeuf F, Huot J. Endothelial Cell Migration During Angiogenesis. Circulation Research. 2007;100(6):782-94.

74. Vicente-Manzanares M, Horwitz AR. Cell Migration: An Overview. In: Wells CM, Parsons M, editors. Cell Migration: Developmental Methods and Protocols. Totowa, NJ: Humana Press; 2011. p. 1-24.

75. Paul CD, Mistriotis P, Konstantopoulos K. Cancer cell motility: lessons from migration in confined spaces. Nature reviews Cancer. 2017;17(2):131-40.

76. Wei C, Wang X, Zheng M, Cheng H. Calcium gradients underlying cell migration. Curr Opin Cell Biol. 2012;24(2):254-61.

77. Tsai F-C, Kuo G-H, Chang S-W, Tsai P-J. Ca2+ Signaling in Cytoskeletal Reorganization, Cell Migration, and Cancer Metastasis. BioMed Research International. 2015;2015:13.

78. Li F, Abuarab N, Sivaprasadarao A. Reciprocal regulation of actin cytoskeleton remodelling and cell migration by Ca²⁺ and Zn²⁺: role of TRPM2 channels. Journal of Cell Science. 2016;129(10):2016.

79. Chen YF, Chiu WT, Chen YT, Lin PY, Huang HJ, Chou CY, et al. Calcium store sensor stromal-interaction molecule 1-dependent signaling plays an important role in cervical cancer growth, migration, and angiogenesis. Proc Natl Acad Sci U S A. 2011;108(37):15225-30.

80. Tsai FC, Seki A, Yang HW, Hayer A, Carrasco S, Malmersjo S, et al. A polarized Ca^{2+}, diacylglycerol and STIM1 signalling system regulates directed cell migration. Nat Cell Biol. 2014;16(2):133-44.

81. Small JV, Stradal T, Vignal E, Rottner K. The lamellipodium: where motility begins. Trends in Cell Biology. 2002;12(3):112-20.

82. Webb DJ, Parsons JT, Horwitz AF. Adhesion assembly, disassembly and turnover in migrating cells – over and over and over again. Nature Cell Biology. 2002;4:E97.

83. Burnette DT, Manley S, Sengupta P, Sougrat R, Davidson MW, Kachar B, et al. A role for actin arcs in the leading-edge advance of migrating cells. Nature Cell Biology. 2011;13:371.

84. Song S, Cong W, Zhou S, Shi Y, Dai W, Zhang H, et al. Small GTPases: Structure, biological function and its interaction with nanoparticles. Asian Journal of Pharmaceutical Sciences. 2019;14(1):30-9.

85. Aspenström P. Integration of signalling pathways regulated by small GTPases and calcium. Biochimica et Biophysica Acta (BBA) - Molecular Cell Research. 2004;1742(1):51-8.

86. Ridley AJ. Rho GTPase signalling in cell migration. Current Opinion in Cell Biology. 2015;36:103-12.

87. Tsai F-C, Meyer T. Ca2+ Pulses Control Local Cycles of Lamellipodia Retraction and Adhesion along the Front of Migrating Cells. Current Biology. 2012;22(9):837-42.

88. Kasturi R, Vasulka C, Johnson JD. Ca2+, caldesmon, and myosin light chain kinase exchange with calmodulin. Journal of Biological Chemistry. 1993;268(11):7958-64.

89. Chavez A, Smith M, Mehta D. Chapter six - New Insights into the Regulation of Vascular Permeability. In: Jeon KW, editor. International Review of Cell and Molecular Biology. 290: Academic Press; 2011. p. 205-48.

90. Chen C, Tao T, Wen C, He W-Q, Qiao Y-N, Gao Y-Q, et al. Myosin light chain kinase (MLCK) regulates cell migration in a myosin regulatory light chain phosphorylation-independent mechanism. The Journal of biological chemistry. 2014;289(41):28478-88.

91. Dongre A, Weinberg RA. New insights into the mechanisms of epithelial–mesenchymal transition and implications for cancer. Nature Reviews Molecular Cell Biology. 2019;20(2):69-84.

92. Wendt MK, Balanis N, Carlin CR, Schiemann WP. STAT3 and epithelial-mesenchymal transitions in carcinomas. JAKSTAT. 2014;3(1):e28975-e.

93. Zhong Z, Wen Z, Darnell JE. Stat3: a STAT family member activated by tyrosine phosphorylation in response to epidermal growth factor and interleukin-6. Science. 1994;264(5155):95.

94. Kim J, Kong J, Chang H, Kim H, Kim A. EGF induces epithelial-mesenchymal transition through phospho-Smad2/3-Snail signaling pathway in breast cancer cells. Oncotarget. 2016;7(51):85021-32.

95. Xu J, Lamouille S, Derynck R. TGF-beta-induced epithelial to mesenchymal transition. Cell Res. 2009;19(2):156-72.

96. Sun J, Stathopoulos A. FGF controls epithelial-mesenchymal transitions during gastrulation by regulating cell division and apicobasal polarity. Development (Cambridge, England). 2018;145(19):dev161927.

97. Bryant JA, Finn RS, Slamon DJ, Cloughesy TF, Charles AC. EGF activates intracellular and intercellular calcium signaling by distinct pathways in tumor cells. Cancer Biology & Therapy. 2004;3(12):1243-9.

98. Zhang S, Miao Y, Zheng X, Gong Y, Zhang J, Zou F, et al. STIM1 and STIM2 differently regulate endogenous Ca2+ entry and promote TGF-β-induced EMT in breast cancer cells. Biochemical and Biophysical Research Communications. 2017;488(1):74-80.

99. Perez-Garcia J, Muñoz-Couselo E, Soberino J, Racca F, Cortes J. Targeting FGFR pathway in breast cancer. The Breast. 2018;37:126-33.

100. Qi L, Song W, Li L, Cao L, Yu Y, Song C, et al. FGF4 induces epithelial-mesenchymal transition by inducing store-operated calcium entry in lung adenocarcinoma. Oncotarget. 2016;7(45):74015-30.

101. Ornitz DM, Itoh N. The Fibroblast Growth Factor signaling pathway. Wiley Interdiscip Rev Dev Biol. 2015;4(3):215-66.

102. Kalluri R, Weinberg RA. The basics of epithelial-mesenchymal transition. The Journal of clinical investigation. 2009;119(6):1420-8.

103. Liu C-Y, Lin H-H, Tang M-J, Wang Y-K. Vimentin contributes to epithelial-mesenchymal transition cancer cell mechanics by mediating cytoskeletal organization and focal adhesion maturation. Oncotarget. 2015;6(18):15966-83.

104. Mendez MG, Kojima S-I, Goldman RD. Vimentin induces changes in cell shape, motility, and adhesion during the epithelial to mesenchymal transition. FASEB journal : official publication of the Federation of American Societies for Experimental Biology. 2010;24(6):1838-51.

105. Goto H, Kosako H, Tanabe K, Yanagida M, Sakurai M, Amano M, et al. Phosphorylation of Vimentin by Rho-associated Kinase at a Unique Amino-terminal Site That Is Specifically Phosphorylated during Cytokinesis. Journal of Biological Chemistry. 1998;273(19):11728-36.

106. Stewart TA, Azimi I, Marcial D, Peters AA, Chalmers SB, Yapa KTDS, et al. Differential engagement of ORAI1 and TRPC1 in the induction of vimentin expression by different stimuli. Laboratory Investigation. 2019.

107. Davis FM, Azimi I, Faville RA, Peters AA, Jalink K, Putney Jr JW, et al. Induction of epithelial–mesenchymal transition (EMT) in breast cancer cells is calcium signal dependent. Oncogene. 2013;33:2307.

108. Bhattacharya A, Kumar J, Hermanson K, Sun Y, Qureshi H, Perley D, et al. The calcium channel proteins ORAI3 and STIM1 mediate TGF-β induced Snai1 expression. Oncotarget. 2018;9(50):29468-83.

109. Tarone G, Cirillo D, Giancotti FG, Comoglio PM, Marchisio PC. Rous sarcoma virus-transformed fibroblasts adhere primarily at discrete protrusions of the ventral membrane called podosomes. Experimental Cell Research. 1985;159(1):141-57.

110. Chen W-T. Proteolytic activity of specialized surface protrusions formed at rosette contact sites of transformed cells1989. 167-85 p.

111. Murphy DA, Courtneidge SA. The 'ins' and 'outs' of podosomes and invadopodia: characteristics, formation and function. Nature reviews Molecular cell biology. 2011;12(7):413-26.

112. Siddiqui TA, Lively S, Vincent C, Schlichter LC. Regulation of podosome formation, microglial migration and invasion by Ca2+-signaling molecules expressed in podosomes. Journal of Neuroinflammation. 2012;9(1):250.

113. Sun J, Lu F, He H, Shen J, Messina J, Mathew R, et al. STIM1- and Orai1-mediated Ca(2+) oscillation orchestrates invadopodium formation and melanoma invasion. J Cell Biol. 2014;207(4):535-48.

114. Chen Y-W, Chen Y-F, Chiu W-T, Chen H-C, Shen M-R. STIM1-dependent Ca(2+) signaling regulates podosome formation to facilitate cancer cell invasion. Scientific reports. 2017;7(1):11523-.

115. Dupont G, Combettes L, Bird GS, Putney JW. Calcium oscillations. Cold Spring Harb Perspect Biol. 2011;3(3).

116. Cathcart J, Pulkoski-Gross A, Cao J. Targeting Matrix Metalloproteinases in Cancer: Bringing New Life to Old Ideas. Genes Dis. 2015;2(`1):26-34.

117. Gialeli C, Theocharis AD, Karamanos NK. Roles of matrix metalloproteinases in cancer progression and their pharmacological targeting. The FEBS Journal. 2011;278(1):16-27.

118. Noe V, Fingleton B, Jacobs K, Crawford HC, Vermeulen S, Steelant W, et al. Release of an invasion promoter E-cadherin fragment by matrilysin and stromelysin-1. Journal of Cell Science. 2001;114(1):111.

119. Illman SA, Lehti K, Keski-Oja J, Lohi J. Epilysin (MMP-28) induces TGF-β mediated epithelial to mesenchymal transition in lung carcinoma cells. Journal of Cell Science. 2006;119(18):3856.

120. Gomes LR, Terra LF, Wailemann RA, Labriola L, Sogayar MC. TGF-β1 modulates the homeostasis between MMPs and MMP inhibitors through p38 MAPK and ERK1/2 in highly invasive breast cancer cells. BMC cancer. 2012;12:26-.

121. Warburg O. The Metabolism of Carcinoma Cells. The Journal of Cancer Research. 1925;9(1):148.

122. Huebner RJ, Todaro GJ. Oncogenes of RNA tumor viruses as determinants of cancer. Proceedings of the National Academy of Sciences of the United States of America. 1969;64(3):1087-94.

123. DeBerardinis RJ, Chandel NS. Fundamentals of cancer metabolism. Science Advances. 2016;2(5):e1600200.

124. Liberti MV, Locasale JW. The Warburg Effect: How Does it Benefit Cancer Cells? Trends in biochemical sciences. 2016;41(3):211-8.

125. Boroughs LK, DeBerardinis RJ. Metabolic pathways promoting cancer cell survival and growth. Nature cell biology. 2015;17(4):351-9.

126. McCormack JG, Halestrap AP, Denton RM. Role of calcium ions in regulation of mammalian intramitochondrial metabolism. Physiol Rev. 1990;70(2):391-425.

127. Griffiths EJ, Rutter GA. Mitochondrial calcium as a key regulator of mitochondrial ATP production in mammalian cells. Biochimica et Biophysica Acta (BBA) - Bioenergetics. 2009;1787(11):1324-33.

128. Rizzuto R, Marchi S, Bonora M, Aguiari P, Bononi A, De Stefani D, et al. Ca(2+) transfer from the ER to mitochondria: when, how and why. Biochimica et biophysica acta. 2009;1787(11):1342-51.

129. Tan W, Colombini M. VDAC closure increases calcium ion flux. Biochimica et biophysica acta. 2007;1768(10):2510-5.

130. Rapizzi E, Pinton P, Szabadkai G, Wieckowski MR, Vandecasteele G, Baird G, et al. Recombinant expression of the voltage-dependent anion channel enhances the transfer of Ca2+ microdomains to mitochondria. The Journal of cell biology. 2002;159(4):613-24.

131. Kamer KJ, Mootha VK. The molecular era of the mitochondrial calcium uniporter. Nature Reviews Molecular Cell Biology. 2015;16:545.

132. Kirichok Y, Krapivinsky G, Clapham DE. The mitochondrial calcium uniporter is a highly selective ion channel. Nature. 2004;427:360.

133. Vais H, Payne R, Paudel U, Li C, Foskett JK. Coupled transmembrane mechanisms control MCU-mediated mitochondrial Ca2+ uptake. Proceedings of the National Academy of Sciences. 2020;117(35):21731-9.

134. Denton RM. Regulation of mitochondrial dehydrogenases by calcium ions. Biochimica et Biophysica Acta (BBA) - Bioenergetics. 2009;1787(11):1309-16.

135. Gellerich FN, Gizatullina Z, Trumbeckaite S, Nguyen HP, Pallas T, Arandarcikaite O, et al. The regulation of OXPHOS by extramitochondrial calcium. Biochimica et Biophysica Acta (BBA) - Bioenergetics. 2010;1797(6):1018-27.

136. Saunier E, Benelli C, Bortoli S. The pyruvate dehydrogenase complex in cancer: An old metabolic gatekeeper regulated by new pathways and pharmacological agents. International Journal of Cancer. 2016;138(4):809-17.

137. Shan C, Kang H-B, Elf S, Xie J, Gu T-L, Aguiar M, et al. Tyr-94 phosphorylation inhibits pyruvate dehydrogenase phosphatase 1 and promotes tumor growth. The Journal of biological chemistry. 2014;289(31):21413-22.

138. Adam-Vizi V, Starkov AA. Calcium and mitochondrial reactive oxygen species generation: how to read the facts. Journal of Alzheimer's disease : JAD. 2010;20 Suppl 2(Suppl 2):S413-S26.

139. Rossi A, Pizzo P, Filadi R. Calcium, mitochondria and cell metabolism: A functional triangle in bioenergetics. Biochimica et Biophysica Acta (BBA) - Molecular Cell Research. 2018.

140. Bootman MD, Chehab T, Bultynck G, Parys JB, Rietdorf K. The regulation of autophagy by calcium signals: Do we have a consensus? Cell Calcium. 2018;70:32-46.

141. Pan MG, Xiong Y, Chen F. NFAT gene family in inflammation and cancer. Current molecular medicine. 2013;13(4):543-54.

142. Jain J, Burgeon E, Badalian TM, Hogan PG, Rao A. A Similar DNA-binding Motif in NFAT Family Proteins and the Rel Homology Region. Journal of Biological Chemistry. 1995;270(8):4138-45.

143. Qin J-J, Nag S, Wang W, Zhou J, Zhang W-D, Wang H, et al. NFAT as cancer target: mission possible? Biochimica et biophysica acta. 2014;1846(2):297-311.

144. Muller MR, Rao A. NFAT, immunity and cancer: a transcription factor comes of age. Nat Rev Immunol. 2010;10(9):645-56.

145. Okamura H, Aramburu J, García-Rodríguez C, Viola JPB, Raghavan A, Tahiliani M, et al. Concerted Dephosphorylation of the Transcription Factor NFAT1 Induces a Conformational Switch that Regulates Transcriptional Activity. Molecular Cell. 2000;6(3):539-50.

146. Villaseñor T, Madrid-Paulino E, Maldonado-Bravo R, Urbán-Aragón A, Pérez-Martínez L, Pedraza-Alva G. Activation of the Wnt Pathway by Mycobacterium tuberculosis: A Wnt–Wnt Situation2017.

147. Pfeifhofer C, Kofler K, Gruber T, Tabrizi NG, Lutz C, Maly K, et al. Protein kinase C theta affects Ca2+ mobilization and NFAT cell activation in primary mouse T cells. The Journal of experimental medicine. 2003;197(11):1525-35.

148. Garcia-Cozar FJ, Okamura H, Aramburu JF, Shaw KTY, Pelletier L, Showalter R, et al. Two-site Interaction of Nuclear Factor of Activated T Cells with Activated Calcineurin. Journal of Biological Chemistry. 1998;273(37):23877-83.

149. Li H, Rao A, Hogan PG. Interaction of calcineurin with substrates and targeting proteins. Trends Cell Biol. 2011;21(2):91-103.

150. Shaw KT, Ho AM, Raghavan A, Kim J, Jain J, Park J, et al. Immunosuppressive drugs prevent a rapid dephosphorylation of transcription factor NFAT1 in stimulated immune cells. Proceedings of the National Academy of Sciences. 1995;92(24):11205.

151. Porter CM, Clipstone NA. Sustained NFAT Signaling Promotes a Th1-Like Pattern of Gene Expression in Primary Murine CD4⁺ T Cells. The Journal of Immunology. 2002;168(10):4936.

152. Neal JW, Clipstone NA. Glycogen Synthase Kinase-3 Inhibits the DNA Binding Activity of NFATc. Journal of Biological Chemistry. 2001;276(5):3666-73.

153. Beals CR, Clipstone NA, Ho SN, Crabtree GR. Nuclear localization of NF-ATc by a calcineurin-dependent, cyclosporin-sensitive intramolecular interaction. Genes & Development. 1997;11(7):824-34.

154. Lagunas L, Clipstone NA. Deregulated NFATc1 activity transforms murine fibroblasts via an autocrine growth factor-mediated Stat3-dependent pathway. Journal of Cellular Biochemistry. 2009;108(1):237-48.

155. Greenhough A, Smartt HJM, Moore AE, Roberts HR, Williams AC, Paraskeva C, et al. The COX-2/PGE 2 pathway: key roles in the hallmarks of cancer and adaptation to the tumour microenvironment. Carcinogenesis. 2009;30(3):377-86.

156. Flockhart RJ, Armstrong JL, Reynolds NJ, Lovat PE. NFAT signalling is a novel target of oncogenic BRAF in metastatic melanoma. British journal of cancer. 2009;101(8):1448-55.

157. Xia Y, Shen S, Verma IM. NF-κB, an active player in human cancers. Cancer immunology research. 2014;2(9):823-30.

158. Zhang Q, Lenardo MJ, Baltimore D. 30 Years of NF-κB: A Blossoming of Relevance to Human Pathobiology. Cell. 2017;168(1-2):37-57.

159. Altman A, Villalba M. Protein kinase C-θ (PKCθ): it's all about location, location, location. Immunological Reviews. 2003;192(1):53-63.

160. Villalba M, Coudronniere N, Deckert M, Teixeiro E, Mas P, Altman A. A Novel Functional Interaction between Vav and PKCθ Is Required for TCR-Induced T Cell Activation. Immunity. 2000;12(2):151-60.

161. Frantz B, Nordby EC, Bren G, Steffan N, Paya CV, Kincaid RL, et al. Calcineurin acts in synergy with PMA to inactivate 1κB/MAD3 an inhibitor of NF-κB. EMBO Journal. 1994;13(4):861-70.

162. Steffan NM, Bren GD, Frantz B, Tocci MJ, O'Neill EA, Paya CV. Regulation of IκBα phosphorylation by PKC- and Ca2+-dependent signal transduction pathways. Journal of Immunology. 1995;155(10):4685-91.

163. Trushin SA, Pennington KN, Algeciras-Schimnich A, Paya CV. Protein Kinase C and Calcineurin Synergize to Activate IκB Kinase and NF-κB in T Lymphocytes. Journal of Biological Chemistry. 1999;274(33):22923-31.

164. Berry CT, May MJ, Freedman BD. STIM- and Orai-mediated calcium entry controls NF-κB activity and function in lymphocytes. Cell Calcium. 2018;74:131-43.

165. Joyce D, Albanese C, Steer J, Fu M, Bouzahzah B, Pestell RG. NF-κB and cell-cycle regulation: the cyclin connection. Cytokine & Growth Factor Reviews. 2001;12(1):73-90.

166. Guttridge DC, Albanese C, Reuther JY, Pestell RG, Baldwin AS, Jr. NF-kappaB controls cell growth and differentiation through transcriptional regulation of cyclin D1. Molecular and cellular biology. 1999;19(8):5785-99.

167. Romashkova JA, Makarov SS. NF-κB is a target of AKT in anti-apoptotic PDGF signalling. Nature. 1999;401:86.

168. Kim M-S, Kim S-Y, Arunachalam S, Hwang P-H, Yi H-K, Nam S-Y, et al. c-myb stimulates cell growth by regulation of insulin-like growth factor (IGF) and IGF-binding protein-3 in K562 leukemia cells. Biochemical and Biophysical Research Communications. 2009;385(1):38-43.

169. Wang W, Wu S, Shi Y, Miao Y, Luo X, Ji M, et al. c-MYB regulates cell growth and DNA damage repair through modulating MiR-143. FEBS Letters. 2015;589(5):555-64.

170. Ritchie MF, Zhou Y, Soboloff J. WT1/EGR1-mediated control of STIM1 expression and function in cancer cells. Front Biosci (Landmark Ed). 2011;16:2402-15.

171. Samakai E, Hooper R, Martin KA, Shmurak M, Zhang Y, Kappes DJ, et al. Novel STIM1-dependent control of Ca^{2+} clearance regulates NFAT activity during T-cell activation. FASEB J. 2016;30(11):3878-86.

172. Go CK, Gross S, Hooper R, Soboloff J. EGR-mediated control of STIM expression and function. Cell Calcium. 2019;77:58-67.

173. Thiel G, Mayer SI, Müller I, Stefano L, Rössler OG. Egr-1—A Ca2+-regulated transcription factor. Cell Calcium. 2010;47(5):397-403.

174. Flavell SW, Kim T-K, Gray JM, Harmin DA, Hemberg M, Hong EJ, et al. Genome-wide analysis of MEF2 transcriptional program reveals synaptic target genes and neuronal activity-dependent polyadenylation site selection. Neuron. 2008;60(6):1022-38.

175. van Loo KMJ, Rummel CK, Pitsch J, Alexander Müller J, Bikbaev AF, Martinez Chavez E, et al. Calcium channel subunit α2δ4 is regulated by early growth response 1 and facilitates epileptogenesis. The Journal of Neuroscience. 2019:1731-18.

176. Hardingham GE, Chawla S, Johnson CM, Bading H. Distinct functions of nuclear and cytoplasmic calcium in the control of gene expression. Nature. 1997;385:260.

177. Hardingham GE, Arnold FJL, Bading H. Nuclear calcium signaling controls CREB-mediated gene expression triggered by synaptic activity. Nature Neuroscience. 2001;4:261.

178. Chuderland D, Seger R. Calcium regulates ERK signaling by modulating its protein-protein interactions. Communicative & integrative biology. 2008;1(1):4-5.

179. White CD, Sacks DB. Regulation of MAP Kinase Signaling by Calcium. In: Seger R, editor. MAP Kinase Signaling Protocols: Second Edition. Totowa, NJ: Humana Press; 2010. p. 151-65.

180. Müller I, Lipp P, Thiel G. Ca2+ signaling and gene transcription in glucose-stimulated insulinoma cells. Cell Calcium. 2012;52(2):137-51.

181. Min IM, Pietramaggiori G, Kim FS, Passegué E, Stevenson KE, Wagers AJ. The Transcription Factor EGR1 Controls Both the Proliferation and Localization of Hematopoietic Stem Cells. Cell Stem Cell. 2008;2(4):380-91.

182. Tarcic G, Avraham R, Pines G, Amit I, Shay T, Lu Y, et al. EGR1 and the ERK-ERF axis drive mammary cell migration in response to EGF. FASEB journal : official publication of the Federation of American Societies for Experimental Biology. 2012;26(4):1582-92.

183. Dinkel A, Warnatz K, Ledermann B, Rolink A, Zipfel PF, Bürki K, et al. The transcription factor early growth response 1 (Egr-1) advances differentiation of pre-B and immature B cells. The Journal of experimental medicine. 1998;188(12):2215-24.

184. Scharnhorst V, van der Eb AJ, Jochemsen AG. WT1 proteins: functions in growth and differentiation. Gene. 2001;273(2):141-61.

185. Nair P, Muthukkumar S, Sells SF, Han S-S, Sukhatme VP, Rangnekar VM. Early Growth Response-1-dependent Apoptosis Is Mediated by p53. Journal of Biological Chemistry. 1997;272(32):20131-8.

186. Menke AL. Wilms' tumor 1-KTS isoforms induce p53-independent apoptosis that can be partially rescued by expression of the epidermal growth factor receptor or the insulin receptor. Cancer research. 1997;57(7):1353-63.

187. Gross S, Mallu P, Joshi H, Schultz B, Go C, Soboloff J. Ca(2+) as a therapeutic target in cancer. Adv Cancer Res. 2020;148:233-317.

188. Alteri RMea. Cancer Facts & Figures 2019 Atlanta, GA: American Cancer Society 2019 [Available from: https://www.cancer.org/content/dam/cancer-

org/research/cancer-facts-and-statistics/annual-cancer-facts-and-figures/2019/cancer-facts-and-figures-2019.pdf.

189. Waks AG, Winer EP. Breast Cancer Treatment: A ReviewBreast Cancer Treatment in 2019Breast Cancer Treatment in 2019. JAMA. 2019;321(3):288-300.

190. Horton JK, Jagsi R, Woodward WA, Ho A. Breast Cancer Biology: Clinical Implications for Breast Radiation Therapy. International Journal of Radiation Oncology*Biology*Physics. 2018;100(1):23-37.

191. Inic Z, Zegarac M, Inic M, Markovic I, Kozomara Z, Djurisic I, et al. Difference between Luminal A and Luminal B Subtypes According to Ki-67, Tumor Size, and Progesterone Receptor Negativity Providing Prognostic Information. Clinical Medicine Insights Oncology. 2014;8:107-11.

192. Tong CWS, Wu M, Cho WCS, To KKW. Recent Advances in the Treatment of Breast Cancer. Frontiers in oncology. 2018;8:227-.

193. Yang S, Zhang JJ, Huang XY. Orai1 and STIM1 are critical for breast tumor cell migration and metastasis. Cancer Cell. 2009;15(2):124-34.

194. McAndrew D, Grice DM, Peters AA, Davis FM, Stewart T, Rice M, et al. ORAI1-mediated calcium influx in lactation and in breast cancer. Mol Cancer Ther. 2011;10(3):448-60.

195. Hu J, Qin K, Zhang Y, Gong J, Li N, Lv D, et al. Downregulation of transcription factor Oct4 induces an epithelial-to-mesenchymal transition via enhancement of Ca2+ influx in breast cancer cells. Biochemical and Biophysical Research Communications. 2011;411(4):786-91.

196. Mo P, Yang S. The Store-Operated Calcium Channels in Cancer Metastasis: from Cell Migration, Invasion to Metastatic Colonization. Frontiers in bioscience (Landmark edition). 2018;23:1241-56.

197. Motiani RK, Abdullaev IF, Trebak M. A novel native store-operated calcium channel encoded by Orai3: selective requirement of Orai3 versus Orai1 in estrogen receptor-positive versus estrogen receptor-negative breast cancer cells. J Biol Chem. 2010;285(25):19173-83.

198. Motiani RK, Zhang X, Harmon KE, Keller RS, Matrougui K, Bennett JA, et al. Orai3 is an estrogen receptor alpha-regulated Ca(2)(+) channel that promotes tumorigenesis. FASEB J. 2013;27(1):63-75.

199. Nelson LR, Bulun SE. Estrogen production and action. Journal of the American Academy of Dermatology. 2001;45(3, Supplement):S116-S24.

200. Flourakis M, Lehen'kyi V, Beck B, Raphael M, Vandenberghe M, Abeele FV, et al. Orai1 contributes to the establishment of an apoptosis-resistant phenotype in prostate cancer cells. Cell Death Dis. 2010;1:e75.

201. Slatnik CLP, Duff E. Ovarian cancer: Ensuring early diagnosis. The Nurse Practitioner. 2015;40(9).

202. Stewart C, Ralyea C, Lockwood S. Ovarian Cancer: An Integrated Review. Seminars in Oncology Nursing. 2019;35(2):151-6.

203. Matulonis UA, Sood AK, Fallowfield L, Howitt BE, Sehouli J, Karlan BY. Ovarian cancer. Nature Reviews Disease Primers. 2016;2:16061.

204. Mallen A, Soong TR, Townsend MK, Wenham RM, Crum CP, Tworoger SS. Surgical prevention strategies in ovarian cancer. Gynecologic Oncology. 2018;151(1):166-75.

205. Schmidt S, Liu G, Liu G, Yang W, Honisch S, Pantelakos S, et al. Enhanced Orai1 and STIM1 expression as well as store operated Ca2+ entry in therapy resistant ovary carcinoma cells. Oncotarget. 2014;5(13):4799-810.

206. Abdelazeem KNM, Droppova B, Sukkar B, al-Maghout T, Pelzl L, Zacharopoulou N, et al. Upregulation of Orai1 and STIM1 expression as well as store-operated Ca2+ entry in ovary carcinoma cells by placental growth factor. Biochemical and Biophysical Research Communications. 2019;512(3):467-72.

207. Wang Y-W, Zhang J-H, Yu Y, Yu J, Huang L. Inhibition of Store-Operated Calcium Entry Protects Endothelial Progenitor Cells from H₂O₂-Induced Apoptosis. Biomol Ther (Seoul). 2016;24(4):371-9.

208. Cheng JC, Chang HM, Leung PC. Epidermal growth factor induces human oviductal epithelial cell invasion by down-regulating E-cadherin expression. J Clin Endocrinol Metab. 2012;97(8):E1380-9.

209. Yan W, Chen J, Chen Z, Chen H. Deregulated miR-296/S100A4 axis promotes tumor invasion by inducing epithelial-mesenchymal transition in human ovarian cancer. American journal of cancer research. 2016;6(2):260-9.

210. He J, Yu JJ, Xu Q, Wang L, Zheng JZ, Liu LZ, et al. Downregulation of ATG14 by EGR1-MIR152 sensitizes ovarian cancer cells to cisplatin-induced apoptosis by inhibiting cyto-protective autophagy. Autophagy. 2015;11(2):373-84.

211. He J, Yu J-J, Xu Q, Wang L, Zheng JZ, Liu L-Z, et al. Downregulation of ATG14 by EGR1-MIR152 sensitizes ovarian cancer cells to cisplatin-induced apoptosis by inhibiting cyto-protective autophagy. Autophagy. 2015;11(2):373-84.

212. Hylander B, Repasky E, Shrikant P, Intengan M, Beck A, Driscoll D, et al. Expression of Wilms tumor gene (WT1) in epithelial ovarian cancer. Gynecol Oncol. 2006;101(1):12-7.

213. Miller-Hodges E, Hohenstein P. WT1 in disease: shifting the epithelial-mesenchymal balance. The Journal of pathology. 2012;226(2):229-40.

214. Andersson C, Oji Y, Ohlson N, Wang S, Li X, Ottander U, et al. Prognostic significance of specific anti-WT1 IgG antibody level in plasma in patients with ovarian carcinoma. Cancer medicine. 2014;3(4):909-18.

215. Bonnefond M-L, Florent R, Lenoir S, Lambert B, Abeilard E, Giffard F, et al. Inhibition of store-operated channels by carboxyamidotriazole sensitizes ovarian carcinoma cells to anti-Bclx(L) strategies through Mcl-1 down-regulation. Oncotarget. 2018;9(74):33896-911.

216. Mignen O, Brink C, Enfissi A, Nadkarni A, Shuttleworth TJ, Giovannucci DR, et al. Carboxyamidotriazole-induced inhibition of mitochondrial calcium import blocks capacitative calcium entry and cell proliferation in HEK-293 cells. Journal of Cell Science. 2005;118(23):5615.

217. Hussain MM, Kotz H, Minasian L, Premkumar A, Sarosy G, Reed E, et al. Phase II Trial of Carboxyamidotriazole in Patients With Relapsed Epithelial Ovarian Cancer. Journal of Clinical Oncology. 2003;21(23):4356-63.

218. Thomas LW, Lam C, Edwards SW. Mcl-1; the molecular regulation of protein function. FEBS Letters. 2010;584(14):2981-9.

219. Morciano G, Giorgi C, Balestra D, Marchi S, Perrone D, Pinotti M, et al. Mcl-1 involvement in mitochondrial dynamics is associated with apoptotic cell death. Mol Biol Cell. 2016;27(1):20-34.

220. Shigemasa K, Katoh O, Shiroyama Y, Mihara S, Mukai K, Nagai N, et al. Increased MCL-1 expression is associated with poor prognosis in ovarian carcinomas. Jpn J Cancer Res. 2002;93(5):542-50.

221. Hsieh AC, Costa M, Zollo O, Davis C, Feldman ME, Testa JR, et al. Genetic dissection of the oncogenic mTOR pathway reveals druggable addiction to translational control via 4EBP-eIF4E. Cancer cell. 2010;17(3):249-61.

222. Li R-J, Xu J, Fu C, Zhang J, Zheng YG, Jia H, et al. Regulation of mTORC1 by lysosomal calcium and calmodulin. eLife. 2016;5:e19360.

223. Lonergan PE, Tindall DJ. Androgen receptor signaling in prostate cancer development and progression. J Carcinog. 2011;10:20-.

224. Lin B, Ferguson C, White JT, Wang S, Vessella R, True LD, et al. Prostate-localized and Androgen-regulated Expression of the Membrane-bound Serine Protease <em>TMPRSS2</em&gt. Cancer Research. 1999;59(17):4180.

225. Pezaro C, Woo HH, Davis ID. Prostate cancer: measuring PSA. Internal Medicine Journal. 2014;44(5):433-40.

226. Attard G, Parker C, Eeles RA, Schröder F, Tomlins SA, Tannock I, et al. Prostate cancer. The Lancet. 2016;387(10013):70-82.

227. Tomlins SA, Laxman B, Varambally S, Cao X, Yu J, Helgeson BE, et al. Role of the TMPRSS2-ERG gene fusion in prostate cancer. Neoplasia (New York, NY). 2008;10(2):177-88.

228. Geybels MS, McCloskey KD, Mills IG, Stanford JL. Calcium Channel Blocker Use and Risk of Prostate Cancer by TMPRSS2:ERG Gene Fusion Status. The Prostate. 2017;77(3):282-90.

229. Chen R, Zeng X, Zhang R, Huang J, Kuang X, Yang J, et al. Cav1.3 channel α1D protein is overexpressed and modulates androgen receptor transactivation in prostate cancers11This work was partially supported by grants from DoD PCRP program (W81XWH-09-1-0455) and KUMC Valk Foundation to Dr Benyi Li, and grants from China Natural Science Foundation to Dr Benyi Li (NSFC #81172427) and Dr Jun Yang (NSFC #81101927). This project was also supported by the “Chutian Scholar” program funded by Hubei Province of China dedicated to China Three Gorges University. Urologic Oncology: Seminars and Original Investigations. 2014;32(5):524-36.

230. Wen S, Niu Y, Lee SO, Chang C. Androgen receptor (AR) positive vs negative roles in prostate cancer cell deaths including apoptosis, anoikis, entosis, necrosis and autophagic cell death. Cancer treatment reviews. 2014;40(1):31-40.

231. Eisenberger MA, Blumenstein BA, Crawford ED, Miller G, McLeod DG, Loehrer PJ, et al. Bilateral Orchiectomy with or without Flutamide for Metastatic Prostate Cancer. New England Journal of Medicine. 1998;339(15):1036-42.

232. Pagliarulo V, Bracarda S, Eisenberger MA, Mottet N, Schröder FH, Sternberg CN, et al. Contemporary role of androgen deprivation therapy for prostate cancer. European urology. 2012;61(1):11-25.

233. Schröder F, Crawford ED, Axcrona K, Payne H, Keane TE. Androgen deprivation therapy: past, present and future. BJU International. 2012;109(s6):1-12.

234. Niu Y, Altuwaijri S, Lai K-P, Wu C-T, Ricke WA, Messing EM, et al. Androgen receptor is a tumor suppressor and proliferator in prostate cancer. Proceedings of the National Academy of Sciences of the United States of America. 2008;105(34):12182-7.

235. Niu Y, Altuwaijri S, Yeh S, Lai K-P, Yu S, Chuang K-H, et al. Targeting the stromal androgen receptor in primary prostate tumors at earlier stages. Proceedings of

the National Academy of Sciences of the United States of America. 2008;105(34):12188-93.

236. Niu Y, Chang TM, Yeh S, Ma WL, Wang YZ, Chang C. Differential androgen receptor signals in different cells explain why androgen-deprivation therapy of prostate cancer fails. Oncogene. 2010;29:3593.

237. Sun Y, Wang B-E, Leong KG, Yue P, Li L, Jhunjhunwala S, et al. Androgen Deprivation Causes Epithelial–Mesenchymal Transition in the Prostate: Implications for Androgen-Deprivation Therapy. Cancer Research. 2012;72(2):527.

238. Mulholland DJ. PSA-negative/low prostate cancer cells: the true villains of CRPC? Asian journal of andrology. 2012;14(5):663-4.

239. Hoang DT, Iczkowski KA, Kilari D, See W, Nevalainen MT. Androgen receptor-dependent and -independent mechanisms driving prostate cancer progression: Opportunities for therapeutic targeting from multiple angles. Oncotarget. 2016;8(2):3724-45.

240. Tan S-H, Dagvadorj A, Shen F, Gu L, Liao Z, Abdulghani J, et al. Transcription Factor Stat5 Synergizes with Androgen Receptor in Prostate Cancer Cells. Cancer Research. 2008;68(1):236.

241. Sharma Naomi L, Massie Charlie E, Ramos-Montoya A, Zecchini V, Scott Helen E, Lamb Alastair D, et al. The Androgen Receptor Induces a Distinct Transcriptional Program in Castration-Resistant Prostate Cancer in Man. Cancer Cell. 2013;23(1):35-47.

242. Whitworth H, Bhadel S, Ivey M, Conaway M, Spencer A, Hernan R, et al. Identification of kinases regulating prostate cancer cell growth using an RNAi phenotypic screen. PloS one. 2012;7(6):e38950-e.

243. Arora VK, Schenkein E, Murali R, Subudhi SK, Wongvipat J, Balbas MD, et al. Glucocorticoid receptor confers resistance to antiandrogens by bypassing androgen receptor blockade. Cell. 2013;155(6):1309-22.

244. Saraon P, Jarvi K, Diamandis EP. Molecular Alterations during Progression of Prostate Cancer to Androgen Independence. Clinical Chemistry. 2011;57(10):1366.

245. Sahu B, Laakso M, Pihlajamaa P, Ovaska K, Sinielnikov I, Hautaniemi S, et al. FoxA1 Specifies Unique Androgen and Glucocorticoid Receptor Binding Events in Prostate Cancer Cells. Cancer Research. 2013;73(5):1570.

246. Isikbay M, Otto K, Kregel S, Kach J, Cai Y, Vander Griend DJ, et al. Glucocorticoid receptor activity contributes to resistance to androgen-targeted therapy in prostate cancer. Hormones & cancer. 2014;5(2):72-89.

247. Bossi A, Escudier B, Massard C, Serrate C, Gross-Goupil M, De La Motte Rouge T, et al. Diethylstilbestrol (DES) retains activity and is a reasonable option in patients previously treated with docetaxel for castration-resistant prostate cancer. Annals of Oncology. 2009;20(5):965-.

248. Maly IV, Hofmann WA. Calcium and Nuclear Signaling in Prostate Cancer. International journal of molecular sciences. 2018;19(4).

249. Perrouin Verbe M-A, Bruyere F, Rozet F, Vandier C, Fromont G. Expression of store-operated channel components in prostate cancer: the prognostic paradox. Human Pathology. 2016;49:77-82.

250. Kappel S, Marques IJ, Zoni E, Stokłosa P, Peinelt C, Mercader N, et al. Store-Operated Ca(2+) Entry as a Prostate Cancer Biomarker - a Riddle with Perspectives. Current molecular biology reports. 2017;3(4):208-17.

251. Berry PA, Birnie R, Droop AP, Maitland NJ, Collins AT. The calcium sensor STIM1 is regulated by androgens in prostate stromal cells. The Prostate. 2011;71(15):1646-55.

252. Edlind MP, Hsieh AC. PI3K-AKT-mTOR signaling in prostate cancer progression and androgen deprivation therapy resistance. Asian journal of andrology. 2014;16(3):378-86.

253. Taylor BS, Schultz N, Hieronymus H, Gopalan A, Xiao Y, Carver BS, et al. Integrative genomic profiling of human prostate cancer. Cancer cell. 2010;18(1):11-22.

254. Zhou Y, Gu P, Li J, Li F, Zhu J, Gao P, et al. Suppression of STIM1 inhibits the migration and invasion of human prostate cancer cells and is associated with PI3K/Akt signaling inactivation. Oncol Rep. 2017;38(5):2629-36.

255. Crumbaker M, Khoja L, Joshua AM. AR Signaling and the PI3K Pathway in Prostate Cancer. Cancers. 2017;9(4):34.

256. Carver BS, Tran J, Gopalan A, Chen Z, Shaikh S, Carracedo A, et al. Aberrant ERG expression cooperates with loss of PTEN to promote cancer progression in the prostate. Nature Genetics. 2009;41:619.

257. King JC, Xu J, Wongvipat J, Hieronymus H, Carver BS, Leung DH, et al. Cooperativity of TMPRSS2-ERG with PI3-kinase pathway activation in prostate oncogenesis. Nature Genetics. 2009;41:524.

258. Jamaspishvili T, Berman DM, Ross AE, Scher HI, De Marzo AM, Squire JA, et al. Clinical implications of PTEN loss in prostate cancer. Nature Reviews Urology. 2018;15:222.

259. Boosani CS, Agrawal DK. PTEN modulators: a patent review. Expert opinion on therapeutic patents. 2013;23(5):569-80.

260. Gregg JL, Brown KE, Mintz EM, Piontkivska H, Fraizer GC. Analysis of gene expression in prostate cancer epithelial and interstitial stromal cells using laser capture microdissection. BMC Cancer. 2010;10:165.

261. Abdulkadir SA, Carbone JM, Naughton CK, Humphrey PA, Catalona WJ, Milbrandt J. Frequent and early loss of the EGR1 corepressor NAB2 in human prostate carcinoma. Hum Pathol. 2001;32(9):935-9.

262. Abdulkadir SA, Qu Z, Garabedian E, Song SK, Peters TJ, Svaren J, et al. Impaired prostate tumorigenesis in Egr1-deficient mice. Nat Med. 2001;7(1):101-7.

263. Brett A, Pandey S, Fraizer G. The Wilms' tumor gene (WT1) regulates E-cadherin expression and migration of prostate cancer cells. Molecular cancer. 2013;12:3.

264. Fraizer GC, Eisermann K, Pandey S, Brett-Morris A, Bazarov A, Nock S, et al. Functional Role of WT1 in Prostate Cancer. In: van den Heuvel-Eibrink MM, editor. Wilms Tumor. Brisbane (AU)2016.

265. Lin P-C, Giannopoulou EG, Park K, Mosquera JM, Sboner A, Tewari AK, et al. Epigenomic alterations in localized and advanced prostate cancer. Neoplasia (New York, NY). 2013;15(4):373-83.

266. Xu Y, Zhang S, Niu H, Ye Y, Hu F, Chen S, et al. STIM1 accelerates cell senescence in a remodeled microenvironment but enhances the epithelial-to-mesenchymal transition in prostate cancer. Scientific reports. 2015;5:11754.

267. Dart AE, Worth DC, Muir G, Chandra A, Morris JD, McKee C, et al. The drebrin/EB3 pathway drives invasive activity in prostate cancer. Oncogene. 2017;36:4111.

268. Ohga K, Takezawa R, Arakida Y, Shimizu Y, Ishikawa J. Characterization of YM-58483/BTP2, a novel store-operated Ca2+ entry blocker, on T cell-mediated immune responses in vivo. International Immunopharmacology. 2008;8(13):1787-92.

269. Ritchie MF, Samakai E, Soboloff J. STIM1 is required for attenuation of PMCA-mediated Ca^{2+} clearance during T-cell activation. EMBO J. 2012;31(5):1123-33.

270. Xu S-Q, Buraschi S, Morcavallo A, Genua M, Shirao T, Peiper SC, et al. A novel role for drebrin in regulating progranulin bioactivity in bladder cancer. Oncotarget. 2015;6(13):10825-39.

271. Mercer JC, Qi Q, Mottram LF, Law M, Bruce D, Iyer A, et al. Chemico-genetic identification of drebrin as a regulator of calcium responses. The international journal of biochemistry & cell biology. 2010;42(2):337-45.

272. Brawer MK. Prostatic intraepithelial neoplasia: an overview. Reviews in urology. 2005;7 Suppl 3(Suppl 3):S11-S8.

273. Mahalingam D, Wilding G, Denmeade S, Sarantopoulas J, Cosgrove D, Cetnar J, et al. Mipsagargin, a novel thapsigargin-based PSMA-activated prodrug: results of a first-in-man phase I clinical trial in patients with refractory, advanced or metastatic solid tumours. British journal of cancer. 2016;114(9):986-94.

274. Hanif F, Muzaffar K, Perveen K, Malhi SM, Simjee SU. Glioblastoma Multiforme: A Review of its Epidemiology and Pathogenesis through Clinical Presentation and Treatment. Asian Pacific journal of cancer prevention : APJCP.18(1):3-9.

275. Jäkel S, Dimou L. Glial Cells and Their Function in the Adult Brain: A Journey through the History of Their Ablation. Frontiers in cellular neuroscience. 2017;11:24-.

276. Alcantara Llaguno SR, Parada LF. Cell of origin of glioma: biological and clinical implications. British journal of cancer. 2016;115(12):1445-50.

277. Shergalis A, Bankhead A, Luesakul U, Muangsin N, Neamati N. Current Challenges and Opportunities in Treating Glioblastoma. Pharmacological Reviews. 2018;70(3):412.

278. Fletcher JI, Williams RT, Henderson MJ, Norris MD, Haber M. ABC transporters as mediators of drug resistance and contributors to cancer cell biology. Drug Resistance Updates. 2016;26:1-9.

279. Kelly K, Sacapano MR, Prosolovich K, Ong J, Black K. Blood brain barrier permeability to temozolomide. Cancer Research. 2005;65(9 Supplement):330.

280. Stupp R, Mason WP, van den Bent MJ, Weller M, Fisher B, Taphoorn MJB, et al. Radiotherapy plus Concomitant and Adjuvant Temozolomide for Glioblastoma. New England Journal of Medicine. 2005;352(10):987-96.

281. R. Perry J, Laperriere N, J. O'Callaghan C, A. Brandes A, Menten J, Phillips C, et al. Short-Course Radiation plus Temozolomide in Elderly Patients with Glioblastoma2017. 1027-37 p.

282. Davis ME. Glioblastoma: Overview of Disease and Treatment. Clinical journal of oncology nursing. 2016;20(5 Suppl):S2-S8.

283. Fernandes C CA, Osório L, Lago RC, Linhares P, Carvalho B, and Caeiro C. Current Standards of Care in Glioblastoma Therapy. 2017. In: Glioblastoma [Internet]. Brisbane, AU: Codon Publications. Available from: https://www.ncbi.nlm.nih.gov/books/NBK469987/

284. Cheng SY, Huang HJ, Nagane M, Ji XD, Wang D, Shih CC, et al. Suppression of glioblastoma angiogenicity and tumorigenicity by inhibition of endogenous expression of vascular endothelial growth factor. Proceedings of the National Academy of Sciences. 1996;93(16):8502.

285. Stark-Vance V. Bevacizumab and CPT-11 in the treatment of relapsed malignant glioma. Neuro-oncology. 2005;7(342):369.

286. Gilbert MR, Dignam JJ, Armstrong TS, Wefel JS, Blumenthal DT, Vogelbaum MA, et al. A Randomized Trial of Bevacizumab for Newly Diagnosed Glioblastoma. New England Journal of Medicine. 2014;370(8):699-708.

287. Motiani RK, Hyzinski-Garcia MC, Zhang X, Henkel MM, Abdullaev IF, Kuo YH, et al. STIM1 and Orai1 mediate CRAC channel activity and are essential for human glioblastoma invasion. Pflugers Arch. 2013;465(9):1249-60.

288. Liu C, Yao J, Mercola D, Adamson E. The transcription factor EGR-1 directly transactivates the fibronectin gene and enhances attachment of human glioblastoma cell line U251. J Biol Chem. 2000;275(27):20315-23.

289. Liu H, Hughes JD, Rollins S, Chen B, Perkins E. Calcium entry via ORAI1 regulates glioblastoma cell proliferation and apoptosis. Exp Mol Pathol. 2011;91(3):753-60.

290. Scrideli CA, Carlotti CG, Jr., Okamoto OK, Andrade VS, Cortez MA, Motta FJ, et al. Gene expression profile analysis of primary glioblastomas and non-neoplastic brain tissue: identification of potential target genes by oligonucleotide microarray and real-time quantitative PCR. J Neurooncol. 2008;88(3):281-91.

291. Ruano Y, Mollejo M, Ribalta T, Fiano C, Camacho FI, Gomez E, et al. Identification of novel candidate target genes in amplicons of Glioblastoma multiforme tumors detected by expression and CGH microarray profiling. Mol Cancer. 2006;5:39.

292. Chen D-G, Zhu B, Lv S-Q, Zhu H, Tang J, Huang C, et al. Inhibition of EGR1 inhibits glioma proliferation by targeting CCND1 promoter. Journal of experimental & clinical cancer research : CR. 2017;36(1):186-.

293. Li G, Zhang Z, Wang R, Ma W, Yang Y, Wei J, et al. Suppression of STIM1 inhibits human glioblastoma cell proliferation and induces G0/G1 phase arrest. J Exp Clin Cancer Res. 2013;32:20.

294. Chen Y-W, Chen Y-F, Chen Y-T, Chiu W-T, Shen M-R. The STIM1-Orai1 pathway of store-operated Ca2+ entry controls the checkpoint in cell cycle G1/S transition. Scientific Reports. 2016;6:22142.

295. Mittelbronn M, Harter P, Warth A, Lupescu A, Schilbach K, Vollmann H, et al. EGR-1 is regulated by N-methyl-D-aspartate-receptor stimulation and associated with patient survival in human high grade astrocytomas. Brain pathology (Zurich, Switzerland). 2009;19(2):195-204.

296. Hashiba T, Izumoto S, Kagawa N, Suzuki T, Hashimoto N, Maruno M, et al. Expression of WT1 protein and correlation with cellular proliferation in glial tumors. Neurol Med Chir (Tokyo). 2007;47(4):165-70; discussion 70.

297. Schittenhelm J, Mittelbronn M, Nguyen TD, Meyermann R, Beschorner R. WT1 expression distinguishes astrocytic tumor cells from normal and reactive astrocytes. Brain Pathol. 2008;18(3):344-53.

298. Calogero A, Arcella A, De Gregorio G, Porcellini A, Mercola D, Liu C, et al. The Early Growth Response Gene EGR-1 Behaves as a Suppressor Gene That Is Down-Regulated Independent of ARF/Mdm2 but not p53 Alterations in Fresh Human Gliomas. Clinical Cancer Research. 2001;7(9):2788.

299. Rauscher J, Beschorner R, Gierke M, Bisdas S, Braun C, Ebner FH, et al. WT1 expression increases with malignancy and indicates unfavourable outcome in astrocytoma. Journal of Clinical Pathology. 2014;67(7):556.

300. Chung SC, McDonald TV, Gardner P. Inhibition by SK&F 96365 of Ca2+ current, IL-2 production and activation in T lymphocytes. British journal of pharmacology. 1994;113(3):861-8.

301. Song M, Chen D, Yu SP. The TRPC channel blocker SKF 96365 inhibits glioblastoma cell growth by enhancing reverse mode of the Na(+) /Ca(2+) exchanger and increasing intracellular Ca(2+). British journal of pharmacology. 2014;171(14):3432-47.

302. Brown Rachel C, Davis Thomas P. Calcium Modulation of Adherens and Tight Junction Function. Stroke. 2002;33(6):1706-11.

303. Brown RC, Wu L, Hicks K, O'Neil RG. Regulation of blood-brain barrier permeability by transient receptor potential type C and type v calcium-permeable channels. Microcirculation (New York, NY : 1994). 2008;15(4):359-71.

304. Kawamoto H, Minato N. Myeloid cells. The International Journal of Biochemistry & Cell Biology. 2004;36(8):1374-9.

305. Kondo M. Lymphoid and myeloid lineage commitment in multipotent hematopoietic progenitors. Immunological reviews. 2010;238(1):37-46.

306. Lai AY, Kondo M. T and B lymphocyte differentiation from hematopoietic stem cell. Seminars in immunology. 2008;20(4):207-12.

307. Morrison SJ, Wandycz AM, Hemmati HD, Wright DE, Weissman IL. Identification of a lineage of multipotent hematopoietic progenitors. Development. 1997;124(10):1929.

308. Lai AY, Lin SM, Kondo M. Heterogeneity of Flt3-Expressing Multipotent Progenitors in Mouse Bone Marrow. The Journal of Immunology. 2005;175(8):5016.

309. Lai AY, Kondo M. Asymmetrical lymphoid and myeloid lineage commitment in multipotent hematopoietic progenitors. The Journal of experimental medicine. 2006;203(8):1867-73.

310. Small D. FLT3 Mutations: Biology and Treatment. ASH Education Program Book. 2006;2006(1):178-84.

311. Daver N, Schlenk RF, Russell NH, Levis MJ. Targeting FLT3 mutations in AML: review of current knowledge and evidence. Leukemia. 2019;33(2):299-312.

312. Meshinchi S, Woods WG, Stirewalt DL, Sweetser DA, Buckley JD, Tjoa TK, et al. Prevalence and prognostic significance of Flt3 internal tandem duplication in pediatric acute myeloid leukemia. Blood. 2001;97(1):89.

313. De Kouchkovsky I, Abdul-Hay M. 'Acute myeloid leukemia: a comprehensive review and 2016 update'. Blood Cancer Journal. 2016;6:e441.

314. Fathi AT, Chen Y-B. Treatment of FLT3-ITD acute myeloid leukemia. Am J Blood Res. 2011;1(2):175-89.

315. Kabarowski JHS, Witte ON. Consequences of BCR-ABL Expression within the Hematopoietic Stem Cell in Chronic Myeloid Leukemia. STEM CELLS. 2000;18(6):399-408.

316. Jabbour E, Kantarjian H. Chronic myeloid leukemia: 2018 update on diagnosis, therapy and monitoring. American Journal of Hematology. 2018;93(3):442-59.

317. Arrigoni E, Del Re M, Galimberti S, Restante G, Rofi E, Crucitta S, et al. Concise Review: Chronic Myeloid Leukemia: Stem Cell Niche and Response to Pharmacologic Treatment. STEM CELLS Translational Medicine. 2018;7(3):305-14.

318. Sacha T. Imatinib in chronic myeloid leukemia: an overview. Mediterranean journal of hematology and infectious diseases. 2014;6(1):e2014007-e.

319. Soboloff J, Zhang Y, Minden M, Berger SA. Sensitivity of myeloid leukemia cells to calcium influx blockade: application to bone marrow purging. Exp Hematol. 2002;30(10):1219-26.

320. Rossi G, Minervini MM, Carella AM, Melillo L, Cascavilla N. Wilms' Tumor Gene (WT1) Expression and Minimal Residual Disease in Acute Myeloid Leukemia. In: van den Heuvel-Eibrink MM, editor. Wilms Tumor. Brisbane (AU)2016.

321. Owen C, Fitzgibbon J, Paschka P. The clinical relevance of Wilms Tumour 1 (WT1) gene mutations in acute leukaemia. Hematol Oncol. 2010;28(1):13-9.

322. Rampal R, Figueroa ME. Wilms tumor 1 mutations in the pathogenesis of acute myeloid leukemia. Haematologica. 2016;101(6):672-9.

323. Rampal R, Figueroa ME. Wilms tumor 1 mutations in the pathogenesis of acute myeloid leukemia. Haematologica. 2016;101(6):672-9.

324. Tian J, Li Z, Han Y, Jiang T, Song X, Jiang G. The progress of early growth response factor 1 and leukemia. Intractable & rare diseases research. 2016;5(2):76-82.

325. Saeed H, Abdallah BM, Ditzel N, Catala-Lehnen P, Qiu W, Amling M, et al. Telomerase-deficient mice exhibit bone loss owing to defects in osteoblasts and increased osteoclastogenesis by inflammatory microenvironment. J Bone Miner Res. 2011;26(7):1494-505.

326. Gibbs JD, Liebermann DA, Hoffman B. Egr-1 abrogates the E2F-1 block in terminal myeloid differentiation and suppresses leukemia. Oncogene. 2008;27(1):98-106.

327. Shafarenko M, Liebermann DA, Hoffman B. Egr-1 abrogates the block imparted by c-Myc on terminal M1 myeloid differentiation. Blood. 2005;106(3):871-8.

328. Gardner JP, Balasubramanyam M, Studzinski GP. Up-regulation of Ca^{2+} influx mediated by store-operated channels in HL60 cells induced to differentiate by 1 alpha,25-dihydroxyvitamin D3. J Cell Physiol. 1997;172(3):284-95.

329. Wang Q, Salman H, Danilenko M, Studzinski GP. Cooperation between antioxidants and 1,25-dihydroxyvitamin D3 in induction of leukemia HL60 cell differentiation through the JNK/AP-1/Egr-1 pathway. J Cell Physiol. 2005;204(3):964-74.

330. Chen F, Wang Q, Wang X, Studzinski GP. Up-regulation of Egr1 by 1,25-dihydroxyvitamin D3 contributes to increased expression of p35 activator of cyclin-dependent kinase 5 and consequent onset of the terminal phase of HL60 cell differentiation. Cancer Res. 2004;64(15):5425-33.

331. Cabanas H, Harnois T, Magaud C, Cousin L, Constantin B, Bourmeyster N, et al. Deregulation of calcium homeostasis in Bcr-Abl-dependent chronic myeloid leukemia. Oncotarget; Vol 9, No 41. 2018.

332. Hoover PJ, Lewis RS. Stoichiometric requirements for trapping and gating of Ca2+ release-activated Ca2+ (CRAC) channels by stromal interaction molecule 1 (STIM1). Proceedings of the National Academy of Sciences of the United States of America. 2011;108(32):13299-304.

333. Li Z, Liu L, Deng Y, Ji W, Du W, Xu P, et al. Graded activation of CRAC channel by binding of different numbers of STIM1 to Orai1 subunits. Cell Res. 2011;21(2):305-15.

334. Scrimgeour N, Litjens T, Ma L, Barritt GJ, Rychkov GY. Properties of Orai1 mediated store-operated current depend on the expression levels of STIM1 and Orai1 proteins. J Physiol. 2009;587(Pt 12):2903-18.

335. Soboloff J, Spassova MA, Tang XD, Hewavitharana T, Xu W, Gill DL. Orai1 and STIM reconstitute store-operated calcium channel function. J Biol Chem. 2006;281(30):20661-5.

336. Diez-Bello R, Jardin I, Salido GM, Rosado JA. Orai1 and Orai2 mediate store-operated calcium entry that regulates HL60 cell migration and FAK phosphorylation. Biochimica et Biophysica Acta (BBA) - Molecular Cell Research. 2017;1864(6):1064-70.

337. Di Marcantonio D, Martinez E, Sidoli S, Vadaketh J, Nieborowska-Skorska M, Gupta A, et al. PKC epsilon is a Key Regulator of Mitochondrial Redox Homeostasis in Acute Myeloid Leukemia. Clinical Cancer Research. 2017:clincanres.2684.017.

338. Clemens RA, Lowell CA. Store-operated calcium signaling in neutrophils. J Leukoc Biol. 2015;98(4):497-502.

339. Apalla Z, Nashan D, Weller RB, Castellsagué X. Skin Cancer: Epidemiology, Disease Burden, Pathophysiology, Diagnosis, and Therapeutic Approaches. Dermatology and therapy. 2017;7(Suppl 1):5-19.

340. Bradford PT, Anderson WF, Purdue MP, Goldstein AM, Tucker MA. Rising melanoma incidence rates of the trunk among younger women in the United States. Cancer Epidemiol Biomarkers Prev. 2010;19(9):2401-6.

341. Leonardi GC, Falzone L, Salemi R, Zanghì A, Spandidos DA, McCubrey JA, et al. Cutaneous melanoma: From pathogenesis to therapy (Review). International journal of oncology. 2018;52(4):1071-80.

342. Schadendorf D, van Akkooi ACJ, Berking C, Griewank KG, Gutzmer R, Hauschild A, et al. Melanoma. The Lancet. 2018;392(10151):971-84.

343. Rastrelli M, Tropea S, Rossi CR, Alaibac M. Melanoma: Epidemiology, Risk Factors, Pathogenesis, Diagnosis and Classification. In Vivo. 2014;28(6):1005-11.

344. Miller SA, Hamilton SL, Wester UG, Cyr WH. An Analysis of UVA Emissions from Sunlamps and the Potential Importance for Melanoma. Photochemistry and Photobiology. 1998;68(1):63-70.

345. Roh MR, Eliades P, Gupta S, Grant-Kels JM, Tsao H. Cutaneous melanoma in women. International journal of women's dermatology. 2017;3(1 Suppl):S11-S5.

346. de Giorgi V, Mavilia C, Massi D, Gozzini A, Aragona P, Tanini A, et al. Estrogen Receptor Expression in Cutaneous Melanoma: A Real-Time Reverse Transcriptase–Polymerase Chain Reaction and Immunohistochemical Study. Archives of Dermatology. 2009;145(1):30-6.

347. Marzagalli M, Montagnani Marelli M, Casati L, Fontana F, Moretti RM, Limonta P. Estrogen Receptor β in Melanoma: From Molecular Insights to Potential Clinical Utility. Frontiers in endocrinology. 2016;7:140-.

348. Verdier-Sevrain S, Yaar M, Cantatore J, Traish A, Gilchrest BA. Estradiol induces proliferation of keratinocytes via a receptor mediated mechanism. The FASEB Journal. 2004;18(11):1252-4.

349. Kelsey TW, Li LQ, Mitchell RT, Whelan A, Anderson RA, Wallace WHB. A validated age-related normative model for male total testosterone shows increasing variance but no decline after age 40 years. PloS one. 2014;9(10):e109346-e.

350. Bokov AF, Ko D, Richardson A. The Effect Of Gonadectomy And Estradiol On Sensitivity To Oxidative Stress. Endocrine Research. 2009;34(1-2):43-58.

351. Wang Y, Ou Z, Sun Y, Yeh S, Wang X, Long J, et al. Androgen receptor promotes melanoma metastasis via altering the miRNA-539-3p/USP13/MITF/AXL signals. Oncogene. 2016;36:1644.

352. D'Orazio J, Jarrett S, Amaro-Ortiz A, Scott T. UV radiation and the skin. International journal of molecular sciences. 2013;14(6):12222-48.

353. Dale Wilson B, Moon S, Armstrong F. Comprehensive review of ultraviolet radiation and the current status on sunscreens. The Journal of clinical and aesthetic dermatology. 2012;5(9):18-23.

354. Brenner M, Hearing VJ. The protective role of melanin against UV damage in human skin. Photochemistry and photobiology. 2008;84(3):539-49.

355. Schadendorf D, Fisher DE, Garbe C, Gershenwald JE, Grob JJ, Halpern A, et al. Melanoma. Nat Rev Dis Primers. 2015;1:15003.

356. Raimondi S, Sera F, Gandini S, Iodice S, Caini S, Maisonneuve P, et al. MC1R variants, melanoma and red hair color phenotype: A meta-analysis. International Journal of Cancer. 2008;122(12):2753-60.

357. Garcia-Borron JC, Sanchez-Laorden BL, Jimenez-Cervantes C. Melanocortin-1 receptor structure and functional regulation. Pigment Cell Res. 2005;18(6):393-410.

358. Schadendorf D, Fisher DE, Garbe C, Gershenwald JE, Grob J-J, Halpern A, et al. Melanoma. Nature Reviews Disease Primers. 2015;1:15003.

359. Hodis E, Watson Ian R, Kryukov Gregory V, Arold Stefan T, Imielinski M, Theurillat J-P, et al. A Landscape of Driver Mutations in Melanoma. Cell. 2012;150(2):251-63.

360. Ascierto PA, Kirkwood JM, Grob J-J, Simeone E, Grimaldi AM, Maio M, et al. The role of BRAF V600 mutation in melanoma. Journal of translational medicine. 2012;10:85-

.

361. Muñoz-Couselo E, Adelantado EZ, Ortiz C, García JS, Perez-Garcia J. NRAS-mutant melanoma: current challenges and future prospect. OncoTargets and therapy. 2017;10:3941-7.

362. Heppt MV, Siepmann T, Engel J, Schubert-Fritschle G, Eckel R, Mirlach L, et al. Prognostic significance of BRAF and NRAS mutations in melanoma: a German study from routine care. BMC Cancer. 2017;17(1):536.

363. Thomas NE, Edmiston SN, Kanetsky PA, Busam KJ, Kricker A, Armstrong BK, et al. Associations of MC1R Genotype and Patient Phenotypes with BRAF and NRAS Mutations in Melanoma. The Journal of investigative dermatology. 2017;137(12):2588-98.

364. Hooper R, Zaidi MR, Soboloff J. The heterogeneity of store-operated calcium entry in melanoma. Sci China Life Sci. 2016;59(8):764-9.

365. Vashisht A, Trebak M, Motiani RK. STIM and Orai proteins as novel targets for cancer therapy. A Review in the Theme: Cell and Molecular Processes in Cancer Metastasis. American journal of physiology Cell physiology. 2015;309(7):C457-C69.

366. Stanisz H, Saul S, Muller CS, Kappl R, Niemeyer BA, Vogt T, et al. Inverse regulation of melanoma growth and migration by Orai1/STIM2-dependent calcium entry. Pigment Cell Melanoma Res. 2014;27(3):442-53.

367. Feldman B, Fedida-Metula S, Nita J, Sekler I, Fishman D. Coupling of mitochondria to store-operated Ca(2+)-signaling sustains constitutive activation of protein kinase B/Akt and augments survival of malignant melanoma cells. Cell Calcium. 2010;47(6):525-37.

368. Ben-Kasus Nissim T, Zhang X, Elazar A, Roy S, Stolwijk JA, Zhou Y, et al. Mitochondria control store-operated Ca2+ entry through Na+ and redox signals. The EMBO Journal. 2017;36(6):797-815.

369. Bogeski I, Kummerow C, Al-Ansary D, Schwarz EC, Koehler R, Kozai D, et al. Differential redox regulation of ORAI ion channels: a mechanism to tune cellular calcium signaling. Sci Signal. 2010;3(115):ra24.

370. Fedida-Metula S, Feldman B, Koshelev V, Levin-Gromiko U, Voronov E, Fishman D. Lipid rafts couple store-operated Ca^{2+} entry to constitutive activation of PKB/Akt in a Ca^{2+}/calmodulin-, Src- and PP2A-mediated pathway and promote melanoma tumor growth. Carcinogenesis. 2012;33(4):740-50.

371. Chen R, Kim O, Yang J, Sato K, Eisenmann KM, McCarthy J, et al. Regulation of Akt/PKB Activation by Tyrosine Phosphorylation. Journal of Biological Chemistry. 2001;276(34):31858-62.

372. Umemura M, Baljinnyam E, Feske S, De Lorenzo MS, Xie LH, Feng X, et al. Store-operated Ca^{2+} entry (SOCE) regulates melanoma proliferation and cell migration. PLoS One. 2014;9(2):e89292.

373. Schleifer H, Doleschal B, Lichtenegger M, Oppenrieder R, Derler I, Frischauf I, et al. Novel pyrazole compounds for pharmacological discrimination between receptor-operated and store-operated Ca(2+) entry pathways. British journal of pharmacology. 2012;167(8):1712-22.

374. Zitt C, Strauss B, Schwarz EC, Spaeth N, Rast G, Hatzelmann A, et al. Potent inhibition of Ca^{2+} release-activated Ca^{2+} channels and T-lymphocyte activation by the pyrazole derivative BTP2. J Biol Chem. 2004;279(13):12427-37.

375. He LP, Hewavitharana T, Soboloff J, Spassova MA, Gill DL. A functional link between store-operated and TRPC channels revealed by the 3,5-bis(trifluoromethyl)pyrazole derivative, BTP2. J Biol Chem. 2005;280(12):10997-1006.

376. Umemura M, Baljinnyam E, Feske S, De Lorenzo MS, Xie L-H, Feng X, et al. Store-Operated Ca(2) (+) Entry (SOCE) Regulates Melanoma Proliferation and Cell Migration. PLoS ONE. 2014;9(2):e89292.

377. Mackiewicz J, Mackiewicz A. BRAF and MEK inhibitors in the era of immunotherapy in melanoma patients. Contemporary oncology (Poznan, Poland). 2018;22(1A):68-72.

378. Girotti MR, Lopes F, Preece N, Niculescu-Duvaz D, Zambon A, Davies L, et al. Paradox-breaking RAF inhibitors that also target SRC are effective in drug-resistant BRAF mutant melanoma. Cancer cell. 2015;27(1):85-96.

379. Homsi J, Cubitt CL, Zhang S, Munster PN, Yu H, Sullivan DM, et al. Src activation in melanoma and Src inhibitors as therapeutic agents in melanoma. Melanoma Research. 2009;19(3).

380. Elias D, Ditzel HJ. The potential of Src inhibitors. Aging. 2015;7(10):734-5.

381. Halaban R, Bacchiocchi A, Straub R, Cao J, Sznol M, Narayan D, et al. A novel anti-melanoma SRC-family kinase inhibitor. Oncotarget. 2019;10(23):2237-51.

382. Weeraratna AT, Jiang Y, Hostetter G, Rosenblatt K, Duray P, Bittner M, et al. Wnt5a signaling directly affects cell motility and invasion of metastatic melanoma. Cancer Cell. 2002;1(3):279-88.

383. Webster MR, Xu M, Kinzler KA, Kaur A, Appleton J, O'Connell MP, et al. Wnt5A promotes an adaptive, senescent-like stress response, while continuing to drive invasion in melanoma cells. Pigment Cell Melanoma Res. 2015;28(2):184-95.

384. Asem MS, Buechler S, Wates RB, Miller DL, Stack MS. Wnt5a Signaling in Cancer. Cancers. 2016;8(9):79.

385. Hooper R, Zhang X, Webster M, Go C, Kedra J, Marchbank K, et al. Novel Protein Kinase C-Mediated Control of Orai1 Function in Invasive Melanoma. Mol Cell Biol. 2015;35(16):2790-8.

386. Kawasaki T, Ueyama T, Lange I, Feske S, Saito N. Protein kinase C-induced phosphorylation of Orai1 regulates the intracellular Ca^{2+} level via the store-operated Ca^{2+} channel. J Biol Chem. 2010;285(33):25720-30.

387. Denning MF. Specifying protein kinase C functions in melanoma. Pigment Cell Melanoma Res. 2012;25(4):466-76.

388. Doornbos R, Theelen M, van der Hoeven PC, van Blitterswijk W, Verkleij AJ, Bergen en Henegouwen PMP. Protein Kinase C Is a Negative Regulator of Protein Kinase B Activity1999. 8589-96 p.

389. Takashima A, English B, Chen Z, Cao J, Cui R, Williams RM, et al. Protein Kinase Cδ Is a Therapeutic Target in Malignant Melanoma with NRAS Mutation. ACS Chemical Biology. 2014;9(4):1003-14.

390. Jenei V, Sherwood V, Howlin J, Linnskog R, Säfholm A, Axelsson L, et al. A t-butyloxycarbonyl-modified Wnt5a-derived hexapeptide functions as a potent antagonist of Wnt5a-dependent melanoma cell invasion. Proceedings of the National Academy of Sciences of the United States of America. 2009;106(46):19473-8.

391. Blagodatski A, Poteryaev D, Katanaev VL. Targeting the Wnt pathways for therapies. Molecular and cellular therapies. 2014;2:28-.

392. Takada R, Satomi Y, Kurata T, Ueno N, Norioka S, Kondoh H, et al. Monounsaturated Fatty Acid Modification of Wnt Protein: Its Role in Wnt Secretion. Developmental Cell. 2006;11(6):791-801.

393. Pierro C, Zhang X, Kankeu C, Trebak M, Bootman MD, Roderick HL. Oncogenic KRAS suppresses store-operated Ca(2+) entry and I(CRAC) through ERK pathway-dependent remodelling of STIM expression in colorectal cancer cell lines. Cell calcium. 2018;72:70-80.

394. Bhatia P, Friedlander P, Zakaria EA, Kandil E. Impact of BRAF mutation status in the prognosis of cutaneous melanoma: an area of ongoing research. Ann Transl Med. 2015;3(2):24-.

395. Dhillon AS, Hagan S, Rath O, Kolch W. MAP kinase signalling pathways in cancer. Oncogene. 2007;26(22):3279-90.

396. Braicu C, Buse M, Busuioc C, Drula R, Gulei D, Raduly L, et al. A Comprehensive Review on MAPK: A Promising Therapeutic Target in Cancer. Cancers. 2019;11(10):1618.

397. Esteves GNN, Ferraz LS, Alvarez MMP, Costa CAd, Lopes RdM, Tersariol ILdS, et al. BRAF and NRAS mutated melanoma: Different Ca2+ responses, Na+/Ca2+ exchanger expression, and sensitivity to inhibitors. Cell Calcium. 2020;90:102241.

398. Anastas JN, Kulikauskas RM, Tamir T, Rizos H, Long GV, von Euw EM, et al. WNT5A enhances resistance of melanoma cells to targeted BRAF inhibitors. The Journal of clinical investigation. 2014;124(7):2877-90.

399. Lopez-Guerrero AM, Pascual-Caro C, Martin-Romero FJ, Pozo-Guisado E. Store-operated calcium entry is dispensable for the activation of ERK1/2 pathway in prostate cancer cells. Cellular Signalling. 2017;40:44-52.

400. Johnson DB, Smalley KSM, Sosman JA. Molecular pathways: targeting NRAS in melanoma and acute myelogenous leukemia. Clinical cancer research : an official journal of the American Association for Cancer Research. 2014;20(16):4186-92.

401. Bae C, Jara-Oseguera A, Swartz KJ. TRPM channels come into focus. Science. 2018;359(6372):160.

402. Duncan LM, Deeds J, Hunter J, Shao J, Holmgren LM, Woolf EA, et al. Down-regulation of the novel gene melastatin correlates with potential for melanoma metastasis. Cancer Res. 1998;58(7):1515-20.

403. Xu XZ, Moebius F, Gill DL, Montell C. Regulation of melastatin, a TRP-related protein, through interaction with a cytoplasmic isoform. Proceedings of the National Academy of Sciences of the United States of America. 2001;98(19):10692-7.

404. Guo H, Carlson JA, Slominski A. Role of TRPM in melanocytes and melanoma. Experimental dermatology. 2012;21(9):650-4.

405. Devi S, Kedlaya R, Maddodi N, Bhat KMR, Weber CS, Valdivia H, et al. Calcium homeostasis in human melanocytes: role of transient receptor potential melastatin 1 (TRPM1) and its regulation by ultraviolet light. American journal of physiology Cell physiology. 2009;297(3):C679-C87.

406. Zholos A. Pharmacology of transient receptor potential melastatin channels in the vasculature. British journal of pharmacology. 2010;159(8):1559-71.

407. Xu Y, Orlandi C, Cao Y, Yang S, Choi C-I, Pagadala V, et al. The TRPM1 channel in ON-bipolar cells is gated by both the α and the βγ subunits of the G-protein Go. Scientific Reports. 2016;6:20940.

408. Badheka D, Yudin Y, Borbiro I, Hartle CM, Yazici A, Mirshahi T, et al. Inhibition of Transient Receptor Potential Melastatin 3 ion channels by G-protein βγ subunits. eLife. 2017;6:e26147.

409. Morgans CW, Brown RL, Duvoisin RM. TRPM1: the endpoint of the mGluR6 signal transduction cascade in retinal ON-bipolar cells. BioEssays : news and reviews in molecular, cellular and developmental biology. 2010;32(7):609-14.

410. Shen Y, Rampino MAF, Carroll RC, Nawy S. G-protein-mediated inhibition of the Trp channel TRPM1 requires the Gβγ dimer. Proceedings of the National Academy of Sciences of the United States of America. 2012;109(22):8752-7.

411. McNeill MS, Paulsen J, Bonde G, Burnight E, Hsu M-Y, Cornell RA. Cell Death of Melanophores in Zebrafish trpm7 Mutant Embryos Depends on Melanin Synthesis. Journal of Investigative Dermatology. 2007;127(8):2020-30.

412. Chen J, Luan Y, Yu R, Zhang Z, Zhang J, Wang W. Transient receptor potential (TRP) channels, promising potential diagnostic and therapeutic tools for cancer. BioScience Trends. 2014;8(1):1-10.

413. Su L-T, Agapito MA, Li M, Simonson WTN, Huttenlocher A, Habas R, et al. TRPM7 Regulates Cell Adhesion by Controlling the Calcium-dependent Protease Calpain. Journal of Biological Chemistry. 2006;281(16):11260-70.

414. Chubanov V, Schäfer S, Ferioli S, Gudermann T. Natural and Synthetic Modulators of the TRPM7 Channel. Cells. 2014;3(4):1089-101.

415. Hofmann T, Schäfer S, Linseisen M, Sytik L, Gudermann T, Chubanov V. Activation of TRPM7 channels by small molecules under physiological conditions. Pflügers Archiv - European Journal of Physiology. 2014;466(12):2177-89.

416. Yamamura H, Ugawa S, Ueda T, Morita A, Shimada S. TRPM8 activation suppresses cellular viability in human melanoma. American Journal of Physiology-Cell Physiology. 2008;295(2):C296-C301.

417. Kijpornyongpan T, Sereemaspun A, Chanchao C. Dose-Dependent Cytotoxic Effects of Menthol on Human Malignant Melanoma A-375 Cells: Correlation with TRPM8 Transcript Expression2014. 1551-6 p.

418. Yang Y, Guo W, Ma J, Xu P, Zhang W, Guo S, et al. Downregulated TRPV1 Expression Contributes to Melanoma Growth via the Calcineurin-ATF3-p53 Pathway. Journal of Investigative Dermatology. 2018;138(10):2205-15.

419. Szallasi A. TRP Channels as Therapeutic Targets: From Basic Science to Clinical Use Elsevier Science and Technology; 2015.

420. Neves de Oliveira BH, Dalmaz C, Zeidan-Chulia F. Network-Based Identification of Altered Stem Cell Pluripotency and Calcium Signaling Pathways in Metastatic Melanoma. Med Sci (Basel). 2018;6(1).

421. Greene M, Young T, Clark WJR. MALIGNANT MELANOMA IN RENAL-TRANSPLANT RECIPIENTS. The Lancet. 1981;317(8231):1196-9.

422. Ryu S, Youn C, Moon AR, Howland A, Armstrong CA, Song PI. Therapeutic Inhibitors against Mutated BRAF and MEK for the Treatment of Metastatic Melanoma. Chonnam Med J. 2017;53(3):173-7.

423. Yang H, Higgins B, Kolinsky K, Packman K, Go Z, Iyer R, et al. RG7204 (PLX4032), a Selective BRAF^{V600E} Inhibitor, Displays Potent Antitumor Activity in Preclinical Melanoma Models. Cancer Research. 2010;70(13):5518.

424. Kakadia S, Yarlagadda N, Awad R, Kundranda M, Niu J, Naraev B, et al. Mechanisms of resistance to BRAF and MEK inhibitors and clinical update of US Food

and Drug Administration-approved targeted therapy in advanced melanoma. OncoTargets and therapy. 2018;11:7095-107.

425. Bald T, Quast T, Landsberg J, Rogava M, Glodde N, Lopez-Ramos D, et al. Ultraviolet-radiation-induced inflammation promotes angiotropism and metastasis in melanoma. Nature. 2014;507(7490):109-13.

426. Mayengbam SS, Singh A, Pillai AD, Bhat MK. Influence of cholesterol on cancer progression and therapy. Translational Oncology. 2021;14(6):101043.

427. Luden G. The Blood Cholesterol-Its Importance, and the Value of its Determination in Cancer Research. Can Med Assoc J. 1922;12(3):147-52.

428. Kuzu OF, Noory MA, Robertson GP. The Role of Cholesterol in Cancer. Cancer Research. 2016;76(8):2063.

429. Ding X, Zhang W, Li S, Yang H. The role of cholesterol metabolism in cancer. Am J Cancer Res. 2019;9(2):219-27.

430. Pencheva N, Buss CG, Posada J, Merghoub T, Tavazoie SF. Broad-spectrum therapeutic suppression of metastatic melanoma through nuclear hormone receptor activation. Cell. 2014;156(5):986-1001.

431. Guerra B, Recio C, Aranda-Tavío H, Guerra-Rodríguez M, García-Castellano JM, Fernández-Pérez L. The Mevalonate Pathway, a Metabolic Target in Cancer Therapy. Frontiers in Oncology. 2021;11:209.

432. Lee HJ, Jo SY, Hwang JS, Chang SE. Mevastatin suppresses melanogenesis by lowering the levels of cyclic adenosine monophosphate and cholesterol. Experimental Dermatology. 2016;25(10):820-2.

433. Pich C, Teiti I, Rochaix P, Mariamé B, Couderc B, Favre G, et al. Statins Reduce Melanoma Development and Metastasis through MICA Overexpression. Frontiers in Immunology. 2013;4:62.

434. Pencheva N, Buss, CG, Posada, J, Merghoub, T, Tavazoie, S. LXR Agonism Inhibits Metastatic Melanoma through Activation of ApoE. Cancer Discovery. 2014;4(5):OF16.

435. Bilen O, Kamal A, Virani SS. Lipoprotein abnormalities in South Asians and its association with cardiovascular disease: Current state and future directions. World J Cardiol. 2016;8(3):247-57.

436. Pu J, Romanelli R, Zhao B, Azar KMJ, Hastings KG, Nimbal V, et al. Dyslipidemia in special ethnic populations. Cardiol Clin. 2015;33(2):325-33.

437. Goldenberg A, Vujic I, Sanlorenzo M, Ortiz-Urda S. Melanoma risk perception and prevention behavior among African-Americans: the minority melanoma paradox. Clin Cosmet Investig Dermatol. 2015;8:423-9.

438. Bradford PT. Skin cancer in skin of color. Dermatol Nurs. 2009;21(4):170-8.

439. Derler I, Jardin I, Stathopulos PB, Muik M, Fahrner M, Zayats V, et al. Cholesterol modulates Orai1 channel function. Sci Signal. 2016;9(412):ra10.

440. Derler I, Plenk P, Fahrner M, Muik M, Jardin I, Schindl R, et al. The extended transmembrane Orai1 N-terminal (ETON) region combines binding interface and gate for Orai1 activation by STIM1. J Biol Chem. 2013;288(40):29025-34.

441. Pacheco J, Dominguez L, Bohorquez-Hernandez A, Asanov A, Vaca L. A cholesterol-binding domain in STIM1 modulates STIM1-Orai1 physical and functional interactions. Sci Rep. 2016;6:29634.

442. Buhaescu I, Izzedine H. Mevalonate pathway: A review of clinical and therapeutical implications. Clinical Biochemistry. 2007;40(9):575-84.

443. Ward NC, Watts GF, Eckel RH. Statin Toxicity. Circulation Research. 2019;124(2):328-50.

444. Karlic H, Varga F. Mevalonate Pathway. In: Boffetta P, Hainaut P, editors. Encyclopedia of Cancer (Third Edition). Oxford: Academic Press; 2019. p. 445-57.

445. Ernster L, Dallner G. Biochemical, physiological and medical aspects of ubiquinone function. Biochimica et Biophysica Acta (BBA) - Molecular Basis of Disease. 1995;1271(1):195-204.

446. Burda P, Aebi M. The dolichol pathway of N-linked glycosylation. Biochimica et Biophysica Acta (BBA) - General Subjects. 1999;1426(2):239-57.

447. Shimano H, Sato R. SREBP-regulated lipid metabolism: convergent physiology - divergent pathophysiology. Nat Rev Endocrinol. 2017;13(12):710-30.

448. Dorotea D, Koya D, Ha H. Recent Insights Into SREBP as a Direct Mediator of Kidney Fibrosis via Lipid-Independent Pathways. Frontiers in Pharmacology. 2020;11:265.

449. Lee SJ, Sekimoto T, Yamashita E, Nagoshi E, Nakagawa A, Imamoto N, et al. The Structure of Importin-ß Bound to SREBP-2: Nuclear Import of a Transcription Factor. Science. 2003;302(5650):1571.

450. Mullen PJ, Yu R, Longo J, Archer MC, Penn LZ. The interplay between cell signalling and the mevalonate pathway in cancer. Nature reviews Cancer. 2016;16(11):718-31.

451. Li HY, Appelbaum FR, Willman CL, Zager RA, Banker DE. Cholesterol-modulating agents kill acute myeloid leukemia cells and sensitize them to therapeutics by blocking adaptive cholesterol responses. Blood. 2003;101(9):3628-34.

452. Novak A, Binnington B, Ngan B, Chadwick K, Fleshner N, Lingwood CA. Cholesterol masks membrane glycosphingolipid tumor-associated antigens to reduce their immunodetection in human cancer biopsies. Glycobiology. 2013;23(11):1230-9.

453. Freed-Pastor William A, Mizuno H, Zhao X, Langerød A, Moon S-H, Rodriguez-Barrueco R, et al. Mutant p53 Disrupts Mammary Tissue Architecture via the Mevalonate Pathway. Cell. 2012;148(1):244-58.

454. Hong X, Roh W, Sullivan RJ, Wong KHK, Wittner BS, Guo H, et al. The Lipogenic Regulator SREBP2 Induces Transferrin in Circulating Melanoma Cells and Suppresses Ferroptosis. Cancer Discovery. 2021;11(3):678.

455. Geng L, Cuneo KC, Cooper MK, Wang H, Sekhar K, Fu A, et al. Hedgehog signaling in the murine melanoma microenvironment. Angiogenesis. 2007;10(4):259-67.

456. Pietrobono S, Santini R, Gagliardi S, Dapporto F, Colecchia D, Chiariello M, et al. Targeted inhibition of Hedgehog-GLI signaling by novel acylguanidine derivatives inhibits melanoma cell growth by inducing replication stress and mitotic catastrophe. Cell Death & Disease. 2018;9(2):142.

457. Stecca B, Mas C, Clement V, Zbinden M, Correa R, Piguet V, et al. Melanomas require HEDGEHOG-GLI signaling regulated by interactions between GLI1 and the RAS-MEK/AKT pathways. Proceedings of the National Academy of Sciences. 2007;104(14):5895.

458. Maxfield FR, van Meer G. Cholesterol, the central lipid of mammalian cells. Current opinion in cell biology. 2010;22(4):422-9.

459. Hevonoja T, Pentikäinen MO, Hyvönen MT, Kovanen PT, Ala-Korpela M. Structure of low density lipoprotein (LDL) particles: basis for understanding molecular changes in modified LDL. Biochim Biophys Acta. 2000;1488(3):189-210.

460. Go G-W, Mani A. Low-density lipoprotein receptor (LDLR) family orchestrates cholesterol homeostasis. Yale J Biol Med. 2012;85(1):19-28.

461. Ogedegbe H, Brown DW. Lipids, Lipoproteins, and Apolipoproteins and Their Disease Associations. Labmedicine. 2001;32:384-9.

462. Jeon H, Blacklow SC. STRUCTURE AND PHYSIOLOGIC FUNCTION OF THE LOW-DENSITY LIPOPROTEIN RECEPTOR. Annual Review of Biochemistry. 2005;74(1):535-62.

463. Gu H-M, Zhang D-W. Hypercholesterolemia, low density lipoprotein receptor and proprotein convertase subtilisin/kexin-type 9. J Biomed Res. 2015;29(5):356-61.

464. Ma Y, Wang W, Zhang J, Lu Y, Wu W, Yan H, et al. Hyperlipidemia and Atherosclerotic Lesion Development in Ldlr-Deficient Mice on a Long-Term High-Fat Diet. PLOS ONE. 2012;7(4):e35835.

465. Huff MW, Daugherty A, Lu H. Chapter 18 - Atherosclerosis. In: Ridgway ND, McLeod RS, editors. Biochemistry of Lipids, Lipoproteins and Membranes (Sixth Edition). Boston: Elsevier; 2016. p. 519-48.

466. Tapia-Vieyra JV, Delgado-Coello B, Mas-Oliva J. Atherosclerosis and Cancer; A Resemblance with Far-reaching Implications. Archives of Medical Research. 2017;48(1):12-26.

467. Reily C, Stewart TJ, Renfrow MB, Novak J. Glycosylation in health and disease. Nature Reviews Nephrology. 2019;15(6):346-66.

468. Eichler J. Protein glycosylation. Current Biology. 2019;29(7):R229-R31.

469. Hart GW, Housley MP, Slawson C. Cycling of O-linked beta-N-acetylglucosamine on nucleocytoplasmic proteins. Nature. 2007;446(7139):1017-22.

470. Williams RT, Senior PV, Van Stekelenburg L, Layton JE, Smith PJ, Dziadek MA. Stromal interaction molecule 1 (STIM1), a transmembrane protein with growth suppressor activity, contains an extracellular SAM domain modified by N-linked glycosylation. Biochim Biophys Acta. 2002;1596(1):131-7.

471. Choi YJ, Zhao Y, Bhattacharya M, Stathopulos PB. Structural perturbations induced by Asn131 and Asn171 glycosylation converge within the EFSAM core and enhance stromal interaction molecule-1 mediated store operated calcium entry. Biochim Biophys Acta Mol Cell Res. 2017;1864(6):1054-63.

472. Akella NM, Ciraku L, Reginato MJ. Fueling the fire: emerging role of the hexosamine biosynthetic pathway in cancer. BMC Biology. 2019;17(1):52.

473. Nishikawa T, Adachi M, Isobe M. C-Glycosylation. In: Fraser-Reid BO, Tatsuta K, Thiem J, editors. Glycoscience: Chemistry and Chemical Biology. Berlin, Heidelberg: Springer Berlin Heidelberg; 2008. p. 755-811.

474. Breitling J, Aebi M. N-linked protein glycosylation in the endoplasmic reticulum. Cold Spring Harb Perspect Biol. 2013;5(8):a013359.

475. Mohanty S, Chaudhary BP, Zoetewey D. Structural Insight into the Mechanism of. Biomolecules. 2020;10(4).

476. Harada Y, Ohkawa Y, Kizuka Y, Taniguchi N. Oligosaccharyltransferase: A Gatekeeper of Health and Tumor Progression. International journal of molecular sciences. 2019;20(23):6074.

477. Mohorko E, Glockshuber R, Aebi M. Oligosaccharyltransferase: the central enzyme of N-linked protein glycosylation. Journal of Inherited Metabolic Disease. 2011;34(4):869-78.

478. Torres CR, Hart GW. Topography and polypeptide distribution of terminal N-acetylglucosamine residues on the surfaces of intact lymphocytes. Evidence for O-linked GlcNAc. J Biol Chem. 1984;259(5):3308-17.

479. Zhu-Mauldin X, Marsh SA, Zou L, Marchase RB, Chatham JC. Modification of STIM1 by O-linked N-acetylglucosamine (O-GlcNAc) attenuates store-operated calcium entry in neonatal cardiomyocytes. J Biol Chem. 2012;287(46):39094-106.

480. Zachara NE, O'Donnell N, Cheung WD, Mercer JJ, Marth JD, Hart GW. Dynamic O-GlcNAc modification of nucleocytoplasmic proteins in response to stress. A survival response of mammalian cells. J Biol Chem. 2004;279(29):30133-42.

481. Yang X, Qian K. Protein O-GlcNAcylation: emerging mechanisms and functions. Nat Rev Mol Cell Biol. 2017;18(7):452-65.

482. Marshall S, Bacote V, Traxinger RR. Discovery of a metabolic pathway mediating glucose-induced desensitization of the glucose transport system. Role of hexosamine biosynthesis in the induction of insulin resistance. J Biol Chem. 1991;266(8):4706-12.

483. Akella NM, Ciraku L, Reginato MJ. Fueling the fire: emerging role of the hexosamine biosynthetic pathway in cancer. BMC Biol. 2019;17(1):52.

484. GRYDER RM, POGELL BM. Further studies on glucosamine 6-phosphate synthesis by rat liver enzymes. J Biol Chem. 1960;235:558-62.

485. Wells L, Gao Y, Mahoney JA, Vosseller K, Chen C, Rosen A, et al. Dynamic O-glycosylation of nuclear and cytosolic proteins: further characterization of the

nucleocytoplasmic beta-N-acetylglucosaminidase, O-GlcNAcase. J Biol Chem. 2002;277(3):1755-61.

486. Iyer SP, Hart GW. Dynamic nuclear and cytoplasmic glycosylation: enzymes of O-GlcNAc cycling. Biochemistry. 2003;42(9):2493-9.

487. Ong Q, Han W, Yang X. O-GlcNAc as an Integrator of Signaling Pathways. Front Endocrinol (Lausanne). 2018;9:599.

488. Williams RT, Manji SS, Parker NJ, Hancock MS, Van Stekelenburg L, Eid JP, et al. Identification and characterization of the STIM (stromal interaction molecule) gene family: coding for a novel class of transmembrane proteins. Biochem J. 2001;357(Pt 3):673-85.

489. Shuttleworth TJ. STIM and Orai proteins and the non-capacitative ARC channels. Front Biosci. 2012;17:847-60.

490. Mignen O, Thompson JL, Shuttleworth TJ. STIM1 regulates Ca^{2+} entry via arachidonate-regulated Ca^{2+}-selective (ARC) channels without store depletion or translocation to the plasma membrane. J Physiol. 2007;579(Pt 3):703-15.

491. Mignen O, Shuttleworth TJ. I(ARC), a novel arachidonate-regulated, noncapacitative Ca(2+) entry channel. J Biol Chem. 2000;275(13):9114-9.

492. Mignen O, Thompson JL, Shuttleworth TJ. Ca^{2+} selectivity and fatty acid specificity of the noncapacitative, arachidonate-regulated Ca^{2+} (ARC) channels. J Biol Chem. 2003;278(12):10174-81.

493. Soboloff J, Spassova MA, Hewavitharana T, He L-P, Xu W, Johnstone LS, et al. STIM2 is an inhibitor of STIM1-mediated store-operated Ca2+ entry. Current Biology. 2006;16(14):1465-70.

494. Spassova MA, Soboloff J, He LP, Xu W, Dziadek MA, Gill DL. STIM1 has a plasma membrane role in the activation of store-operated Ca(2+) channels. Proc Natl Acad Sci U S A. 2006;103(11):4040-5.

495. Ercan E, Chung SH, Bhardwaj R, Seedorf M. Di-arginine signals and the K-rich domain retain the Ca(2)(+) sensor STIM1 in the endoplasmic reticulum. Traffic. 2012;13(7):992-1003.

496. Ercan E, Momburg F, Engel U, Temmerman K, Nickel W, Seedorf M. A conserved, lipid-mediated sorting mechanism of yeast Ist2 and mammalian STIM proteins to the peripheral ER. Traffic. 2009;10(12):1802-18.

497. Shuttleworth TJ, Thompson JL, Mignen O. STIM1 and the noncapacitative ARC channels. Cell Calcium. 2007;42(2):183-91.

498. Kilch T, Alansary D, Peglow M, Dorr K, Rychkov G, Rieger H, et al. Mutations of the Ca2+-sensing stromal interaction molecule STIM1 regulate Ca2+ influx by altered oligomerization of STIM1 and by destabilization of the Ca2+ channel Orai1. J Biol Chem. 2013;288(3):1653-64.

499. Csutora P, Peter K, Kilic H, Park KM, Zarayskiy V, Gwozdz T, et al. Novel role for STIM1 as a trigger for calcium influx factor production. J Biol Chem. 2008;283(21):14524-31.

500. Imperiali B, Hendrickson TL. Asparagine-linked glycosylation: specificity and function of oligosaccharyl transferase. Bioorg Med Chem. 1995;3(12):1565-78.

501. Prakriya M, Feske S, Gwack Y, Srikanth S, Rao A, Hogan PG. Orai1 is an essential pore subunit of the CRAC channel. Nature. 2006;443(7108):230-3.

502. Gwack Y, Srikanth S, Feske S, Cruz-Guilloty F, Oh-hora M, Neems DS, et al. Biochemical and functional characterization of Orai proteins. J Biol Chem. 2007;282(22):16232-43.

503. Niemeyer BA. Changing calcium: CRAC channel (STIM and Orai) expression, splicing, and posttranslational modifiers. Am J Physiol Cell Physiol. 2016;310(9):C701-9.

504. Kappel S, Borgström A, Stokłosa P, Dörr K, Peinelt C. Store-operated calcium entry in disease: Beyond STIM/Orai expression levels. Semin Cell Dev Biol. 2019;94:66-73.

505. Dörr K, Kilch T, Kappel S, Alansary D, Schwär G, Niemeyer BA, et al. Cell type-specific glycosylation of Orai1 modulates store-operated Ca2+ entry. Sci Signal. 2016;9(418):ra25.

506. Zhang SL, Yu Y, Roos J, Kozak JA, Deerinck TJ, Ellisman MH, et al. STIM1 is a Ca^{2+} sensor that activates CRAC channels and migrates from the Ca^{2+} store to the plasma membrane. Nature. 2005;437(7060):902-5.

507. Liou J, Kim ML, Heo WD, Jones JT, Myers JW, Ferrell JE, Jr., et al. STIM is a Ca^{2+} sensor essential for Ca^{2+}-store-depletion-triggered Ca^{2+} influx. Curr Biol. 2005;15(13):1235-41.

508. Arruda AP, Pers BM, Parlakgul G, Güney E, Goh T, Cagampan E, et al. Defective STIM-mediated store operated Ca2+ entry in hepatocytes leads to metabolic dysfunction in obesity. Elife. 2017;6.

509. Baldini SF, Wavelet C, Hainault I, Guinez C, Lefebvre T. The Nutrient-Dependent O-GlcNAc Modification Controls the Expression of Liver Fatty Acid Synthase. J Mol Biol. 2016;428(16):3295-304.

510. Nagy T, Champattanachai V, Marchase RB, Chatham JC. Glucosamine inhibits angiotensin II-induced cytoplasmic Ca2+ elevation in neonatal cardiomyocytes via protein-associated O-linked N-acetylglucosamine. Am J Physiol Cell Physiol. 2006;290(1):C57-65.

511. Hunton DL, Lucchesi PA, Pang Y, Cheng X, Dell'Italia LJ, Marchase RB. Capacitative calcium entry contributes to nuclear factor of activated T-cells nuclear translocation and hypertrophy in cardiomyocytes. J Biol Chem. 2002;277(16):14266-73.

512. Pang Y, Hunton DL, Bounelis P, Marchase RB. Hyperglycemia inhibits capacitative calcium entry and hypertrophy in neonatal cardiomyocytes. Diabetes. 2002;51(12):3461-7.

513. Banerjee PS, Ma J, Hart GW. Diabetes-associated dysregulation of O-GlcNAcylation in rat cardiac mitochondria. Proceedings of the National Academy of Sciences of the United States of America. 2015;112(19):6050-5.

514. Wells L, Vosseller K, Hart GW. Glycosylation of nucleocytoplasmic proteins: signal transduction and O-GlcNAc. Science. 2001;291(5512):2376-8.

515. Novello MJ, Zhu J, Feng Q, Ikura M, Stathopulos PB. Structural elements of stromal interaction molecule function. Cell Calcium. 2018;73:88-94.

516. Rechsteiner M, Rogers SW. PEST sequences and regulation by proteolysis. Trends Biochem Sci. 1996;21(7):267-71.

517. Amino acid sequences common to rapidly degrade proteins: the PEST hypothesis [Internet]. American Association for the Advancement of Science. 1986.

518. Nomura A, Yokoe S, Tomoda K, Nakagawa T, Martin-Romero FJ, Asahi M. Fluctuation in O-GlcNAcylation inactivates STIM1 to reduce store-operated calcium ion entry via downregulation of Ser621 phosphorylation. J Biol Chem. 2020.

519. Yu F, Sun L, Machaca K. Orai1 internalization and STIM1 clustering inhibition modulate SOCE inactivation during meiosis. Proc Natl Acad Sci U S A. 2009;106(41):17401-6.

520. Ladenson RP, Schwartz SO, Ivy AC. Incidence of the blood groups and the secretor factor in patients with pernicious anemia and stomach carcinoma. Am J Med Sci. 1949;217(2):194-7.

521. Hakomori SI, Murakami WT. Glycolipids of hamster fibroblasts and derived malignant-transformed cell lines. Proc Natl Acad Sci U S A. 1968;59(1):254-61.

522. Pinho SS, Reis CA. Glycosylation in cancer: mechanisms and clinical implications. Nature Reviews Cancer. 2015;15(9):540-55.

523. Ying H, Kimmelman AC, Lyssiotis CA, Hua S, Chu GC, Fletcher-Sananikone E, et al. Oncogenic Kras maintains pancreatic tumors through regulation of anabolic glucose metabolism. Cell. 2012;149(3):656-70.

524. Moloughney JG, Kim PK, Vega-Cotto NM, Wu CC, Zhang S, Adlam M, et al. mTORC2 Responds to Glutamine Catabolite Levels to Modulate the Hexosamine Biosynthesis Enzyme GFAT1. Mol Cell. 2016;63(5):811-26.

525. Moloughney JG, Vega-Cotto NM, Liu S, Patel C, Kim PK, Wu CC, et al. mTORC2 modulates the amplitude and duration of GFAT1 Ser-243 phosphorylation to maintain flux through the hexosamine pathway during starvation. J Biol Chem. 2018;293(42):16464-78.

526. Lucena MC, Carvalho-Cruz P, Donadio JL, Oliveira IA, de Queiroz RM, Marinho-Carvalho MM, et al. Epithelial Mesenchymal Transition Induces Aberrant Glycosylation through Hexosamine Biosynthetic Pathway Activation. J Biol Chem. 2016;291(25):12917-29.

527. Gélinas R, Dontaine J, Horman S, Beauloye C, Bultot L, Bertrand L. AMP-Activated Protein Kinase and O-GlcNAcylation, Two Partners Tightly Connected to Regulate Key Cellular Processes. Frontiers in endocrinology. 2018;9:519-.

528. Sodi VL, Khaku S, Krutilina R, Schwab LP, Vocadlo DJ, Seagroves TN, et al. mTOR/MYC Axis Regulates O-GlcNAc Transferase Expression and O-GlcNAcylation in Breast Cancer. Mol Cancer Res. 2015;13(5):923-33.

529. Very N, Steenackers A, Dubuquoy C, Vermuse J, Dubuquoy L, Lefebvre T, et al. Cross regulation between mTOR signaling and O-GlcNAcylation. J Bioenerg Biomembr. 2018;50(3):213-22.

530. Freire-de-Lima L, Gelfenbeyn K, Ding Y, Mandel U, Clausen H, Handa K, et al. Involvement of O-glycosylation defining oncofetal fibronectin in epithelial-mesenchymal transition process. Proc Natl Acad Sci U S A. 2011;108(43):17690-5.

531. Ge X, Peng X, Li M, Ji F, Chen J, Zhang D. OGT regulated O-GlcNacylation promotes migration and invasion by activating IL-6/STAT3 signaling in NSCLC cells. Pathology - Research and Practice. 2021;225:153580.

532. Pinho SS, Figueiredo J, Cabral J, Carvalho S, Dourado J, Magalhães A, et al. E-cadherin and adherens-junctions stability in gastric carcinoma: functional implications of glycosyltransferases involving N-glycan branching biosynthesis, N-acetylglucosaminyltransferases III and V. Biochim Biophys Acta. 2013;1830(3):2690-700.

533. Carvalho-cruz P, Alisson-Silva F, Todeschini AR, Dias WB. Cellular glycosylation senses metabolic changes and modulates cell plasticity during epithelial to mesenchymal transition. Developmental Dynamics. 2018;247(3):481-91.

534. Kim J, Lee HM, Cai F, Ko B, Yang C, Lieu EL, et al. The hexosamine biosynthesis pathway is a targetable liability in KRAS/LKB1 mutant lung cancer. Nature Metabolism. 2020;2(12):1401-12.

535. Pham LV, Bryant JL, Mendez R, Chen J, Tamayo AT, Xu-Monette ZY, et al. Targeting the hexosamine biosynthetic pathway and O-linked N-acetylglucosamine cycling for therapeutic and imaging capabilities in diffuse large B-cell lymphoma. Oncotarget. 2016;7(49):80599-611.

536. Trapannone R, Rafie K, van Aalten DM. O-GlcNAc transferase inhibitors: current tools and future challenges. Biochem Soc Trans. 2016;44(1):88-93.

537. Ortiz-Meoz RF, Jiang J, Lazarus MB, Orman M, Janetzko J, Fan C, et al. A small molecule that inhibits OGT activity in cells. ACS chemical biology. 2015;10(6):1392-7.

538. Stanisz H, Vultur A, Herlyn M, Roesch A, Bogeski I. The role of Orai–STIM calcium channels in melanocytes and melanoma. The Journal of Physiology. 2016;594(11):2825-35.

539. Pourfarhangi KE, Bergman A, Gligorijevic B. ECM Cross-Linking Regulates Invadopodia Dynamics. Biophysical journal. 2018;114(6):1455-66.

540. Leslie M. Melanoma cells travel on calcium cycles. The Journal of Cell Biology. 2014;207(4):434-.

541. Sun J, Lin S, Keeley T, Yang S. Disseminating melanoma cells surf on calcium waves. Molecular & Cellular Oncology. 2015;2(4):e1002714.

542. Gaffal E, Landsberg J, Bald T, Sporleder A, Kohlmeyer J, Tuting T. Neonatal UVB exposure accelerates melanoma growth and enhances distant metastases in Hgf-Cdk4(R24C) C57BL/6 mice. Int J Cancer. 2011;129(2):285-94.

543. De Fabo EC, Noonan FP, Fears T, Merlino G. Ultraviolet B but not ultraviolet A radiation initiates melanoma. Cancer Res. 2004;64(18):6372-6.

544. Go CK, Hooper R, Aronson MR, Schultz B, Cangoz T, Nemani N, et al. The Ca(2+) export pump PMCA clears near-membrane Ca(2+) to facilitate store-operated Ca(2+) entry and NFAT activation. Sci Signal. 2019;12(602).

545. Liao Y, Smyth GK, Shi W. featureCounts: an efficient general purpose program for assigning sequence reads to genomic features. Bioinformatics. 2014;30(7):923-30.

546. Liao Y, Smyth GK, Shi W. The R package Rsubread is easier, faster, cheaper and better for alignment and quantification of RNA sequencing reads. Nucleic acids research. 2019;47(8):e47-e.

547. Anders S, Huber W. Differential expression analysis for sequence count data. Genome Biol. 2010;11(10):R106-R.

548. Bairoch A. Cellosaurus https://web.expasy.org/cellosaurus: SIB Swiss Institute of Bioinformatics; 2021 [

549. Herlyn M. Melanoma Research Center https://wistar.org/our-scientists/meenhard-herlyn: The Wistar Institute; 2021 [

550. Garay T, Juhász É, Molnár E, Eisenbauer M, Czirók A, Dekan B, et al. Cell migration or cytokinesis and proliferation? – Revisiting the “go or grow” hypothesis in cancer cells in vitro. Experimental Cell Research. 2013;319(20):3094-103.

551. Valle EF, Zalka Ad Fau - Groszek L, Groszek L Fau - Stackpole CW, Stackpole CW. Patterning of B16 melanoma metastasis and colonization generally relates to tumor cell growth-stimulating or growth-inhibiting effects of organs and tissues. Clin Exp Metastasis. 1992;10(6):419-29.

552. Overwijk WW, Restifo NP. B16 as a mouse model for human melanoma. Curr Protoc Immunol. 2001;Chapter 20:Unit-20.1.

553. Thomsen SK, Raimondo A, Hastoy B, Sengupta S, Dai X-Q, Bautista A, et al. Type 2 diabetes risk alleles in PAM impact insulin release from human pancreatic β-cells. Nature genetics. 2018;50(8):1122-31.

554. Huang J, Hsia SH, Imamura T, Usui I, Olefsky JM. Annexin II Is a Thiazolidinedione-Responsive Gene Involved in Insulin-Induced Glucose Transporter Isoform 4 Translocation in 3T3-L1 Adipocytes. Endocrinology. 2004;145(4):1579-86.

555. van Wijk JPH, Dreijerink KMA, Pieterman CRC, Lips CJM, Zelissen PMJ, Valk GD. Increased prevalence of impaired fasting glucose in MEN1 gene mutation carriers. Clinical Endocrinology. 2012;76(1):67-71.

556. Liu X, Liu M, Zhang J, Bai X, Ramos F, Van Remmen H, et al. Downregulation of Grb2 contributes to the insulin-sensitizing effect of calorie restriction. Am J Physiol Endocrinol Metab. 2009;296(5):E1067-E75.

557. Liu C-C, Hu J, Tsai C-W, Yue M, Melrose HL, Kanekiyo T, et al. Neuronal LRP1 regulates glucose metabolism and insulin signaling in the brain. The Journal of neuroscience : the official journal of the Society for Neuroscience. 2015;35(14):5851-9.

558. Actis Dato V, Chiabrando GA. The Role of Low-Density Lipoprotein Receptor-Related Protein 1 in Lipid Metabolism, Glucose Homeostasis and Inflammation. International journal of molecular sciences. 2018;19(6):1780.

559. Lorenzo DN, Bennett V. Cell-autonomous adiposity through increased cell surface GLUT4 due to ankyrin-B deficiency. Proceedings of the National Academy of Sciences of the United States of America. 2017;114(48):12743-8.

560. Alogaili F, Chinnarasu S, Jaeschke A, Kranias EG, Hui DY. Hepatic HAX-1 inactivation prevents metabolic diseases by enhancing mitochondrial activity and bile salt export. Journal of Biological Chemistry. 2020;295(14):4631-46.

561. Valencia A, Rajadurai A Fau - Carle AB, Carle Ab Fau - Kochevar IE, Kochevar IE. 7-Dehydrocholesterol enhances ultraviolet A-induced oxidative stress in keratinocytes: roles of NADPH oxidase, mitochondria, and lipid rafts. 2006(0891-5849 (Print)).

562. Gniadecki R, Christoffersen N, Wulf HC. Cholesterol-Rich Plasma Membrane Domains (Lipid Rafts) in Keratinocytes: Importance in the Baseline and UVA-Induced Generation of Reactive Oxygen Species. Journal of Investigative Dermatology. 2002;118(4):582-8.

563. van Weelden H, de Gruijl Fr Fau - van der Putte SC, van der Putte Sc Fau - Toonstra J, Toonstra J Fau - van der Leun JC, van der Leun JC. The carcinogenic risks of modern tanning equipment: is UV-A safer than UV-B? (0340-3696 (Print)).

564. Bruls Wa Fau - Slaper H, Slaper H Fau - van der Leun JC, van der Leun Jc Fau - Berrens L, Berrens L. Transmission of human epidermis and stratum corneum as a function of thickness in the ultraviolet and visible wavelengths. (0031-8655 (Print)).

565. de Gruijl FR. Photocarcinogenesis: UVA vs. UVB radiation. (1422-2868 (Print)).

566. Sample A, He YY. Mechanisms and prevention of UV-induced melanoma. Photodermatol Photoimmunol Photomed. 2018;34(1):13-24.

567. Cadet J, Douki T, Ravanat J-L. Oxidatively Generated Damage to Cellular DNA by UVB and UVA Radiation. Photochemistry and Photobiology. 2015;91(1):140-55.

568. Brash DE. UV-induced Melanin Chemiexcitation: A New Mode of Melanoma Pathogenesis. Toxicologic Pathology. 2016;44(4):552-4.

569. Shah P, He Y-Y. Molecular regulation of UV-induced DNA repair. Photochemistry and photobiology. 2015;91(2):254-64.

570. Yokoyama H, Mizutani R. Structural biology of DNA (6-4) photoproducts formed by ultraviolet radiation and interactions with their binding proteins. International journal of molecular sciences. 2014;15(11):20321-38.

571. Hung K-F, Sidorova Julia M, Nghiem P, Kawasumi M. The 6-4 photoproduct is the trigger of UV-induced replication blockage and ATR activation. Proceedings of the National Academy of Sciences. 2020;117(23):12806-16.

572. Anna B, Blazej Z, Jacqueline G, Andrew CJ, Jeffrey R, Andrzej S. Mechanism of UV-related carcinogenesis and its contribution to nevi/melanoma. Expert Rev Dermatol. 2007;2(4):451-69.

573. Sample A, He Y-Y. Mechanisms and prevention of UV-induced melanoma. Photodermatol Photoimmunol Photomed. 2018;34(1):13-24.

574. Lahtz C, Kim S-I, Bates SE, Li AX, Wu X, Pfeifer GP. UVB irradiation does not directly induce detectable changes of DNA methylation in human keratinocytes. F1000Res. 2013;2:45-.

575. Wang P-W, Hung Y-C, Lin T-Y, Fang J-Y, Yang P-M, Chen M-H, et al. Comparison of the Biological Impact of UVA and UVB upon the Skin with Functional Proteomics and Immunohistochemistry. Antioxidants (Basel). 2019;8(12):569.

576. Tilburg J, Slieker RC, Suchiman H ED, Heath A, Heemst Dv, Slagboom P E, et al. Repeat UVA exposure of human skin fibroblasts induces both a transitionary and recovery DNA methylation response. Epigenomics. 2020;12(7):563-73.

577. Chen IP, Henning S Fau - Faust A, Faust A Fau - Boukamp P, Boukamp P Fau - Volkmer B, Volkmer B Fau - Greinert R, Greinert R. UVA-induced epigenetic regulation

of P16(INK4a) in human epidermal keratinocytes and skin tumor derived cells. (1474-9092 (Electronic)).

578. Ueoka H, Sasaki K, Miyawaki T, Ichino T, Tatsumi K, Suzuki S, et al. A Cytosol-Localized Geranyl Diphosphate Synthase from Lithospermum erythrorhizon and Its Molecular Evolution1 [OPEN]. Plant Physiology. 2020;182(4):1933-45.

579. Fu Y, Zou T, Shen X, Nelson PJ, Li J, Wu C, et al. Lipid metabolism in cancer progression and therapeutic strategies. MedComm (2020). 2020;2(1):27-59.

580. Lin L, Sabnis AJ, Chan E, Olivas V, Cade L, Pazarentzos E, et al. The Hippo effector YAP promotes resistance to RAF- and MEK-targeted cancer therapies. Nature genetics. 2015;47(3):250-6.

581. Hentschel A, Zahedi RP, Ahrends R. Protein lipid modifications--More than just a greasy ballast. Proteomics. 2016;16(5):759-82.

582. Liang J, Guo L, Li K, Xiao X, Zhu W, Zheng X, et al. Inhibition of the mevalonate pathway enhances cancer cell oncolysis mediated by M1 virus. Nature Communications. 2018;9(1):1524.

583. Zhu L, Liu F, Hao Q, Feng T, Chen Z, Luo S, et al. Dietary Geranylgeranyl Pyrophosphate Counteracts the Benefits of Statin Therapy in Experimental Pulmonary Hypertension. Circulation. 2021;143(18):1775-92.

APPENDIX

Abbreviations

ANOVA: Analysis of Variance

BTP2: 3,5-Bis(Trifluoromethyl)pyrazole

CHL: Cholesterol

DN: Dominant Negative

ECAR: Extracellular Acidification Rate

ER: Endoplasmic Reticulum IA65: 4-((5-Phenyl-4-(trifluoromethyl)thiazol-2-yl)amino)benzoic acid

LDLR-/-: Low Density Lipoprotein Receptor knockout

LN: Lymph Node

MAPK: Mitogen Associated Protein Kinase

PCA: Principal Component Analysis

PFO: Perfringolysin-O

PM: Plasma Membrane

O1C44: Orai1WT overexpressing clone 44

O1C78: Orai1WT overexpressing clone 78

O1o/e: Orai1WT overexpressed

OCR: Oxygen Consumption Rate

OGT: O-GlcNAc Transferase

s.c.: subcutaneous injection

SOCE: Store-Operated Ca^{2+} Entry

SS: Squalene Synthase

STIM: Stromal Interaction Molecule

Tg: Thapsigargin

UV: Ultraviolet

UV2: Cells UV exposed 2 weeks prior to measurement

UV5: Cells UV exposed 5 weeks prior to measurement